

DISSERTATION

SYNTHESIS AND CHARACTERIZATION OF URANIUM(IV) COMPOUNDS:  
FROM MONONUCLEAR COMPLEXES TO MULTINUCLEAR ASSEMBLIES

Submitted by

Brian S. Newell

Department of Chemistry

In partial fulfillment of the requirements

For the Degree of Doctor of Philosophy

Colorado State University

Fort Collins, Colorado

Fall 2011

Doctoral Committee:

Advisor: Matthew P. Shores

Co-Advisor: Oren P. Anderson

Eugene Y. Chen

Nancy E. Levinger

Mingzhong Wu

Copyright by Brian Scott Newell 2011

All Rights Reserved

## ABSTRACT

### SYNTHESIS AND CHARACTERIZATION OF URANIUM(IV) COMPOUNDS: FROM MONONUCLEAR COMPLEXES TO MULTINUCLEAR ASSEMBLIES

This dissertation describes the synthesis of multinuclear compounds that possess magnetically-coupled actinide, namely uranium-238, clusters. These assemblies are supported by both acetylide-type ligands as well as triamidoamine or softer phosphine ligands.

Synthetic inorganic chemists have been able to synthesize molecules and clusters with increased spin,  $S$ , or axial anisotropy,  $D$ , in an effort to augment the spin-reversal barriers and create better single-molecule magnets (SMMs). However, efforts to simultaneously increase these parameters are complicated. One potential route utilizes heavy atoms as a result of their larger single-ion anisotropy and believed ability to modulate the magnetism of other systems. My research is placed in this context in Chapter 1, where recent efforts to incorporate heavy atoms into expanded clusters are discussed.

In Chapter 2, the preparation and magnetic property investigations of a structurally related family of mono-, di- and trinuclear U(IV) aryl acetylide complexes are presented. The reaction between  $[(NN'_3)UCl]$  and lithiated aryl acetylides leads to the formation of hexacoordinate compounds. In contrast, combining the uranacycle  $[(bit-NN'_3)U]$  (*bit-*

$\text{NN}'_3 = [\text{N}(\text{CH}_2\text{CH}_2\text{NSi}^i\text{BuMe}_2)_2(\text{CH}_2\text{CH}_2\text{Si}^i\text{BuMeCH}_2)]$  with stoichiometric amounts of mono-, bis-, and tris(ethynyl) benzenes affords pentacoordinate arylacetylide complexes, where  $\text{NN}'_3 = [\text{N}(\text{CH}_2\text{CH}_2\text{NSi}^i\text{BuMe}_2)_3]$ . The measured magnetic susceptibilities for these compounds trend toward non-magnetic ground states at low temperatures. Nevertheless, the di- and trinuclear pentacoordinate compounds appear to display weak magnetic communication between the uranium centers. This communication is modeled by fitting of the DC magnetic susceptibility data, using the spin Hamiltonian  $\hat{H} = -2J(\hat{S}_i \cdot \hat{S}_j)$ . Geometry-optimized Stuttgart/6-31g\* B3LYP hybrid DFT calculations were carried out (spin-orbit coupling omitted) on model complexes and the electrochemistry of the monomeric phenylacetylide complex exhibits a reversible redox couple at  $-1.02$  V versus  $[\text{Cp}_2\text{Fe}]^{+/0}$ , assignable to an oxidation of U(IV) to U(V).

Efforts to study the magnetic correlations as a result of cubic ligands fields are presented in Chapter 3, whereby a neutral bidentate phosphine ligand was utilized. In the course of structurally characterizing previously reported complexes based on the 1,2-bis(dimethylphosphino)ethane)) (dmpe) ligand ( $[(\text{dmpe})_2\text{UCl}_4]$  (**3.1**) and  $[(\text{dmpe})_2\text{UMe}_4]$  (**3.2**)), we found that adjusting the U:dmpe ratio leads to an unprecedented species. Whereas the use of two or three equivalents of dmpe relative to  $\text{UCl}_4$  produces **3.1** as a blue-green solid, use of a 1:1 dmpe: $\text{UCl}_4$  stoichiometry yields  $[(\text{dmpe})_4\text{U}_4\text{Cl}_{16}] \cdot 2\text{CH}_2\text{Cl}_2$  (**3.3**· $2\text{CH}_2\text{Cl}_2$ ) as a green solid. In turn, **3.3** is used to prepare a mixed-chelating ligand complex featuring the bidentate ligand 4,4'-dimethyl-2,2'-bipyridine (dmbpy),  $[(\text{dmpe})(\text{dmbpy})\text{UCl}_4]$  (**3.4**). The measured magnetic susceptibilities for **3.1–3.4** trend toward non-magnetic ground states at low temperatures.

In Chapter 4, we hypothesized that preparing complexes that contain U(IV) in a cubic ligand field environment, using acetylide ligands, might allow for the isolation of compounds exhibiting enhanced magnetic coupling. In that vein, we report the synthesis and characterization of  $[(\text{dmpe})_2\text{U}(\text{CCPh})_4]$  (**4.1**) (CCPh = phenylacetylide) and  $[(\text{dmpe})_2\text{U}(\text{CCPh})_5(\text{Li}\cdot\text{Et}_2\text{O})]$  (**4.2**). No reproducible magnetic susceptibility data were obtained and a discussion about these difficulties is presented.

In the course of studying the crystal structure of the mixed-chelating ligand complex  $[(\text{dmpe})(\text{dmbpy})\text{UCl}_4]$  (**3.4**) an interesting effect on the  $\text{U}-\text{Cl}\cdots\text{H}$  was observed. Several computation methods were utilized to determine that the  $\text{M}-\text{Cl}\cdots\text{HC}$  distance based on approach angles is suggestive that Cl is acting more like chlorine and less like chloride. This provides a route to study U–L bonding and is presented in Chapter 5.

Finally, in Chapter 6, efforts to synthesize a mixed-metal complex are discussed and preliminary characterization of a dinuclear ethynylbenzene *5f-3d* complex (**6.3**) is presented. While an unambiguously paramagnetic metal-complex was not isolated, initial electrochemical studies indicate a redox process takes place. A short discussion about the temperature dependence of the magnetic susceptibility is given.

## ACKNOWLEDGEMENTS

This dissertation and the work presented herein would not have been possible without the help of several people throughout my journey of graduate school and, in general, life. First and foremost I would like to thank my parents, Tony and Kathleen Newell for their continued support through the good times and bad. I cannot express to them enough how much I appreciate all they have done for me. I would also like to thank my sister, Stacey, who has been an important part of my life and has supported me wholeheartedly through all my endeavors. Their endless love and support has kept me going and I hope they know what it means to me.

I would also like to thank my advisor, Professor Matthew Shores for his guidance and support throughout my time in his group. He is very dedicated to his work and even though we did not see eye-to-eye at times, my tenure with his group has made me the scientist that I am today. I know that great things will continue to come out of his lab in the future as a result of his tireless dedication.

To my lab mates, Wesley Hoffert, Ashley McDaniel, Stephanie Fiedler, and Christina Klug, Thank you for all your support throughout this process. The proofreading and insight into my experiments has been very beneficial. The staff of the CIF also deserves thanks for training me and troubleshooting instrument issues. Susie Miller and Professor Oren Anderson deserve credit for nurturing my love of X-ray crystallography and were especially helpful in showing me how single crystals should be selected, mounted, and

analyzed with the SMART and APEX2 diffractometers. I know that these skills will continue to be valuable even after I leave CSU.

## AUTOBIOGRAPHY

Brian Scott Newell was born on April 13<sup>th</sup>, 1980 in Manassas, Virginia, to parents Tony and Kathleen Newell. He moved with his family to Austin, TX in 1985 and attended high school in Pflugerville, TX, graduating in 1998. After attending Texas A&M University for one year, he attended Blinn College in College Station, TX, earning an A.S. in Science in 2002. He earned his B.S. in chemistry in 2004 from Texas State University–San Marcos in San Marcos, TX. In 2005, he began his Ph.D. work at Colorado State University, where he studied inorganic chemistry with Prof. Matthew P. Shores. Brian earned his doctorate in 2011, and will be doing Postdoctoral research at Colorado State University with a focus in X-ray crystallography.

Brian loves the outdoors and anything associated including: Biking, hiking, climbing, snowboarding, Frisbee golf, and camping just to name a few.

## TABLE OF CONTENTS

<b>Chapter 1. Actinide-Containing Compounds: Routes to Increased Coupling and Magnetic Anisotropy.....</b>	<b>1</b>
1.1 Introduction .....	1
1.2 Why Lanthanides? .....	4
1.3 3 <i>d</i> -4 <i>f</i> Mixed-Metal Complexes.....	6
1.4 Why Actinides? .....	7
1.5 Coupling in a Dinuclear U(V) Complex.....	9
1.6 3 <i>d</i> -5 <i>f</i> Mixed Metal Complexes: Ferromagnetic Exchange Coupling in the Linear, Chloride-Bridged Cluster (cyclam)Co(II)[(μ-Cl)U(IV)(Me <sub>2</sub> Pz) <sub>4</sub> ] <sub>2</sub> .....	13
1.7 A Uranium(III) Complex Exhibiting Properties Consistent with a SMM.....	18
1.8 A Delocalized Arene-Bridged Diuranium Single-Molecule Magnet .....	21
1.9 Conclusions .....	23
1.10 Overview of Work to be Presented.....	24
1.11 References .....	25
<b>Chapter 2. Experimental Evidence for Magnetic Exchange in Di- and Trinuclear Uranium(IV) Ethynylbenzene Complexes .....</b>	<b>31</b>
2.1 Introduction .....	31
2.2 Division of Labor Section.....	34
2.3 Experimental Section.....	34
2.3.1 Preparation of Compounds. ....	34
[(NN' <sub>3</sub> )U(CcPh) <sub>2</sub> (Li·THF)] (2.1).....	35
[(NN' <sub>3</sub> ) <sub>2</sub> U <sub>2</sub> ( <i>p</i> -DEB)(THF)] (2.2) .....	35
[(NN' <sub>3</sub> )U(CcPh)] (2.3) .....	36
[(NN' <sub>3</sub> ) <sub>2</sub> U <sub>2</sub> ( <i>m</i> -DEB)] (2.4) .....	37
[(NN' <sub>3</sub> ) <sub>2</sub> U <sub>2</sub> ( <i>p</i> -DEB)] (2.5) .....	37
[(NN' <sub>3</sub> ) <sub>3</sub> U <sub>3</sub> (TEB)] (2.6).....	38

2.3.2 X-ray Structure Determination. ....	39
2.3.3 Magnetic Susceptibility Measurements.....	40
2.3.4 Other Physical Measurements. ....	41
2.3.5 Electronic Structure Calculations. ....	42
2.4 Results and Discussion .....	46
2.4.1 Synthesis and characterization of [(NN' <sub>3</sub> )U] acetylide complexes. ....	46
2.4.2 Oxidation of the pentacoordinate U(IV) arylacetylide complexes. ....	53
2.4.3 Magnetic properties of the U(IV) complexes. ....	55
2.4.4 Theoretical Consideration. ....	63
2.5 Summary and Outlook .....	66
2.6 Acknowledgments. ....	68
2.7 References .....	69
<b>Chapter 3. Synthesis and Characterization of a Novel Tetranuclear 5f Compound: Stable Synthons for Exploring U(IV) Chemistry .....</b>	<b>78</b>
3.1 Introduction .....	78
3.2 Division of Labor Section .....	79
3.3 Experimental Section .....	80
3.3.1 Preparation of Compounds. ....	80
[(dmpe) <sub>2</sub> UCl <sub>4</sub> ] (3.1) .....	80
[(dmpe) <sub>2</sub> UMe <sub>4</sub> ] (3.2).....	81
[(dmpe) <sub>4</sub> U <sub>4</sub> Cl <sub>16</sub> ]·2CH <sub>2</sub> Cl <sub>2</sub> (3.3·2CH <sub>2</sub> Cl <sub>2</sub> ) .....	82
[(dmpe)(dmbpy)UCl <sub>4</sub> ] (3.4) .....	83
3.3.2 X-ray Structure Determinations. ....	84
3.3.3 Magnetic Susceptibility Measurements.....	86
3.3.4 Other Physical Measurements. ....	87
3.4 Results and Discussion .....	87
3.4.1 Syntheses and Characterizations of [(dmpe) <sub>2</sub> UX <sub>4</sub> ] (X = Cl, Me).....	87
3.4.2 A New Tetranuclear U(IV) Species as “(dmpe)UX <sub>4</sub> ” Synthons. ....	90
3.4.3 Structural Comparisons. ....	93
3.4.4 Magnetic Properties. ....	95
3.5 Summary and Outlook .....	99

3.6 Acknowledgments. ....	99
3.7 References: .....	101
<b>Chapter 4. Preparation and Attempt at the Magnetic Characterization of Eight- and Nine Coordinate Uranium(IV) Arylacetylide Complexes Based on 1,2-Bis(dimethylphosphino)ethane .....</b>	<b>106</b>
4.1 Introduction .....	106
4.2 Division of Labor Section .....	107
4.3 Experimental Section .....	107
4.3.1 Preparation of Compounds. ....	107
[(dmpe) <sub>2</sub> U(CCPh) <sub>4</sub> ] (4.1) .....	108
[(dmpe) <sub>2</sub> U(CCPh) <sub>5</sub> (Li·Et <sub>2</sub> O)] (4.2) .....	110
4.3.2 X-ray Structure Determinations. ....	111
4.3.3 Magnetic Susceptibility Measurements.....	114
4.3.4 Other Physical Measurements. ....	115
4.4 Results and Discussion .....	115
4.4.1 Syntheses and Characterization of Eight- and Nine-Coordinate [(dmpe) <sub>2</sub> U]-Acetylide Complexes.....	115
4.4.2 Structural Comparisons. ....	116
4.4.3 Magnetic Properties. ....	119
4.5 Summary and Outlook .....	124
4.6 Acknowledgments. ....	124
4.7 Crystallographic Information Formatted (cif) files for crystals 4.1 and 4.2 .....	125
4.8 References .....	146
<b>Chapter 5. Evidence for Interesting U-Cl··HC Interactions in the Mixed Chelating Ligand Complex [(dmpe)(dmbpy)UCl<sub>4</sub>].....</b>	<b>148</b>
5.1 Introduction .....	148
5.2 Division of Labor Section .....	150
5.3 Experimental Section .....	150
5.3.1 Details of CCDC Search.....	150
5.4 Results and Discussion .....	151
5.5 Summary and Outlook .....	157
5.6 Acknowledgments. ....	158

5.7 References .....	159
<b>Chapter 6. Synthesis and Characterization of a Linear 5f-3d Arylacetylide-Bridged U<sup>IV</sup>-Fe<sup>II</sup> Complex .....</b>	<b>161</b>
6.1 Introduction .....	161
6.2 Division of Labor Section .....	162
6.3 Experimental Section .....	162
6.3.1 Preparation of Compounds. ....	162
[(dmpe) <sub>2</sub> FeCl( <i>i</i> Pr <sub>3</sub> SiDEB)] (6.1) .....	163
[(dmpe) <sub>2</sub> FeCl( <i>p</i> -DEBH)] (6.2) .....	163
[(NN' <sub>3</sub> )U( <i>p</i> -DEB)FeCl(dmpe) <sub>2</sub> ] (6.3) .....	164
6.3.2 X-ray Structure Determination. ....	166
6.3.3 Magnetic Susceptibility Measurements.....	168
6.3.4 Other Physical Measurements. ....	168
6.4 Results and Discussion .....	169
6.4.1 Syntheses and Characterizations of.....	169
6.4.2 X-ray Crystallography.....	170
6.4.3 Magnetic Properties. ....	173
6.4.4 Oxidation of the dinuclear 5f-3d arylacetylide complex. ....	174
6.5 Summary and Outlook .....	175
6.6 Acknowledgments. ....	176
6.7 Crystallographic Information Formatted (cif) files for crystal 6.3 .....	176
6.8 References .....	186
<b>Appendix 190</b>	
A.1 Supporting Information for Chapter 2 .....	190
A.2 Supporting Information for Chapter 3 .....	214

## LISTS OF TABLES

Table 2.1. Crystallographic data for compounds [(NN' <sub>3</sub> )U(CCPh) <sub>2</sub> (Li·THF)] (2.1), [(NN' <sub>3</sub> ) <sub>2</sub> U <sub>2</sub> ( <i>p</i> -DEB)(THF) <sub>2</sub> ]·C <sub>5</sub> H <sub>12</sub> (2.2·THF·C <sub>5</sub> H <sub>12</sub> ), [(NN' <sub>3</sub> )U(CCPh)] (2.3), [(NN' <sub>3</sub> ) <sub>2</sub> U <sub>2</sub> ( <i>m</i> -DEB)]·C <sub>5</sub> H <sub>12</sub> (2.4·C <sub>5</sub> H <sub>12</sub> ), and [(NN' <sub>3</sub> ) <sub>2</sub> U <sub>2</sub> ( <i>p</i> -DEB)]·C <sub>5</sub> H <sub>12</sub> (2.5·C <sub>5</sub> H <sub>12</sub> )...44	
Table 2.2. Selected bond distances (Å) and angles (°) for crystallographically (2.1–2.5) and computationally determined (2.3–2.5) structures of the new mono- and dinuclear U(IV) complexes .....	45
Table 2.3. Tabulated MAGFIT results for compounds [(NN' <sub>3</sub> ) <sub>2</sub> U <sub>2</sub> ( <i>p</i> -DEB)(THF)] (2.2), [(NN' <sub>3</sub> ) <sub>2</sub> U <sub>2</sub> ( <i>m</i> -DEB)] (2.4), [(NN' <sub>3</sub> ) <sub>2</sub> U <sub>2</sub> ( <i>p</i> -DEB)] (2.5), and [(NN' <sub>3</sub> ) <sub>3</sub> U <sub>3</sub> (TEB)] (2.6).....	62
Table 3.1. Crystallographic data for compounds [(dmpe) <sub>2</sub> UCl <sub>4</sub> ] (3.1), [(dmpe) <sub>2</sub> UMe <sub>4</sub> ] (3.2), [(dmpe) <sub>4</sub> U <sub>4</sub> Cl <sub>16</sub> ]·2CH <sub>2</sub> Cl <sub>2</sub> (3.3·2CH <sub>2</sub> Cl <sub>2</sub> ), and [(dmpe)(dmbpy)UCl <sub>4</sub> ] (3.4).....	86
Table 3.2. Selected bond distances (Å) and angles (°) for the crystallographically-determined structures [(dmpe) <sub>2</sub> UCl <sub>4</sub> ] (3.1), [(dmpe) <sub>2</sub> UMe <sub>4</sub> ] (3.2), [(dmpe)(dmbpy)UCl <sub>4</sub> ] (3.4) and [(dmpe) <sub>2</sub> U(OPh) <sub>4</sub> ].....	93
Table 3.3. Selected bond distances (Å) and angles (°) for the structure of [(dmpe) <sub>4</sub> U <sub>4</sub> Cl <sub>16</sub> ]·2CH <sub>2</sub> Cl <sub>2</sub> (3.3·2CH <sub>2</sub> Cl <sub>2</sub> ).....	94
Table 3.4. SHAPE analyses for compounds 3.1–3.4. The smallest number indicates the most closely related polyhedron shape .....	95
Table 4.1. Crystallographic data for compounds [(dmpe) <sub>2</sub> U(CCPh) <sub>4</sub> ] (4.1) and [(dmpe) <sub>2</sub> U(CCPh) <sub>5</sub> (Li·Et <sub>2</sub> O)] (4.2).....	113
ellipsoids .....	113

Table 4.2. Selected bond distances (Å) and angles (°) for crystallographically-determined structures [(dmpe) <sub>2</sub> U(CCPPh) <sub>4</sub> ] (4.1) and [(dmpe) <sub>2</sub> U(CCPPh) <sub>5</sub> (Li·Et <sub>2</sub> O)] (4.2).....	118
Table 5.1. Selected bond distances (Å) and angles (°) for the crystallographically-determined structures [(dmpe) <sub>2</sub> UCl <sub>4</sub> ] (3.1) and [(dmpe)(dmbpy)UCl <sub>4</sub> ] (3.4). This data is originally presented in Chapter 3. ....	152
Table 5.2. Selected bond distances (Å) and angles (°) for the halogen bonds in the crystallographically-determined structure [(dmpe) <sub>2</sub> UCl <sub>4</sub> ] (3.1) .....	152
Table 5.3. Selected bond distances (Å) and angles (°) for the halogen bonds in the crystallographically-determined structure [(dmpe)(dmbpy)UCl <sub>4</sub> ] (3.4).....	152
.....	166
Table 6.1. Crystallographic data for compound [(NN') <sub>3</sub> U( <i>p</i> -DEB)FeCl(dmpe) <sub>2</sub> ] (6.3)..	167
Table 6.2. Selected bond distances (Å) and angles (°) for crystallographically determined structures (6.3) of the 5 <i>f</i> -3 <i>d</i> complex.....	172
Table A1.1. Cartesian coordinates for the calculated complex [N(CH <sub>2</sub> CH <sub>2</sub> NH) <sub>3</sub> U(CCH)], a model for the mononuclear U(IV) complex 2.3 .....	200
Table A1.2. Cartesian coordinates for the calculated complex 2.4, a model for the <i>m</i> -DEB-bridged dinuclear U(IV) complex 2.4.....	201
Table A1.2 continued.....	202
Table A1.3. Cartesian coordinates for the calculated complex 2.5, a model for the <i>p</i> -DEB-bridged dinuclear U(IV) complex 2.5.....	203
Table A1.3 continued.....	204
Table A2.1. Cross referenced collection of notebook and crystal structure data sets for relevant compounds	228

## LISTS OF FIGURES

Figure 1.1. Energy diagram for a SMM with negative axial anisotropy .....	3
Figure 1.2. Two different isomers of $[(\text{MeC}_5\text{H}_4)_3\text{U}]_2(\mu\text{-N}_2\text{C}_6\text{H}_4)$ .....	10
Figure 1.3. Experimental (symbols) versus calculated (lines) molar magnetic susceptibility for $[(\text{MeC}_5\text{H}_4)_3\text{U}]_2(\mu\text{-1,4-N}_2\text{C}_6\text{H}_4)$ .....	10
Figure 1.4. Resonance structures of $[(\text{MeC}_5\text{H}_4)_3\text{U}]_2(\mu\text{-1,4-N}_2\text{C}_6\text{H}_4)$ that indicate a viable superexchange pathway for the observed antiferromagnetic coupling .....	12
Figure 1.5. Structure of the linear cluster $(\text{cyclam})\text{Co}[(\mu\text{-Cl})\text{U}(\text{Me}_2\text{Pz})_4]_2$ .....	13
Figure 1.6. Variable-temperature magnetic susceptibility data for the trinuclear cluster $(\text{cyclam})\text{Co}[(\mu\text{-Cl})\text{U}(\text{Me}_2\text{Pz})_4]_2$ and its previously published analogue, $(\text{cyclam})\text{Zn}[(\mu\text{-Cl})\text{U}(\text{Me}_2\text{Pz})_4]_2$ .....	14
Figure 1.7. Empirical $\chi_{MT}$ data arising upon subtraction of the $\text{ZnU}_2$ cluster data from the $\text{CoU}_2$ (blue diamonds) and $\text{NiU}_2$ (red circles) cluster data .....	16
Figure 1.8. Plots of $\chi_{MT}$ data for the $\text{CoU}_2$ (blue diamonds) and $\text{NiU}_2$ (red circles) clusters upon modification to account for the loss of spin of the U(IV) centers at low temperatures. Calculated fits to the data are shown as black lines ( $J_{\text{max}}(\text{Co}) = 48 \text{ cm}^{-1}$ , $J_{\text{max}}(\text{Ni}) = 19 \text{ cm}^{-1}$ ). Figure taken from reference .....	17
Figure 1.9. Structure of the trigonal prismatic complex $\text{U}(\text{Ph}_2\text{BPz}_2)_3$ .....	19
Figure 1.10. Temperature dependence of the in-phase ( $\chi_M'$ , inset) and out-of-phase ( $\chi_M''$ ) components of the AC susceptibility of $\text{U}(\text{Ph}_2\text{BPz}_2)_3$ .....	19

Figure 1.11. Arrhenius plot of $U(\text{Ph}_2\text{BPz}_2)_3$ in the presence of applied DC fields of 0, 100, and 1000 Oe.....	20
Figure 1.12. Solid-state structure of $[\text{U}(\text{BIPM}^{\text{TMS}}\text{H})(\text{I})_2(\mu\text{-}\eta^6\text{:}\eta^6\text{-C}_6\text{H}_5\text{CH}_3)]$ as determined by X-ray crystallography, depicted with 30% probability ellipsoids; for clarity, hydrogen atoms, disorder components and lattice solvent are omitted. ....	21
Figure 1.13. (Top left): Temperature dependence of the DC magnetic susceptibility of $[(\text{U}(\text{BIPM}^{\text{TMS}}\text{H})(\text{I})_2(\mu\text{-}\eta^6\text{:}\eta^6\text{-C}_6\text{H}_5\text{CH}_3)]$ at applied fields of 0.1 T ( $T < 50$ K) and 1 T ( $T > 40$ K). (Top right): Magnetic hysteresis at 1.8 K at a sweep rate of $26 \text{ Oe}\cdot\text{s}^{-1}$ . (Bottom left and right): (Bottom left and right):.....	23
Figure 2.1. Crystal structures of the U(IV) arylacetylide complexes in compounds 2.1 (left) and 2.3 (right), rendered with 40% ellipsoids .....	48
Figure 2.2. Crystal structure of the dinuclear complex in compound $2.2\cdot\text{THF}\cdot\text{C}_5\text{H}_{12}$ , rendered with 40% ellipsoids .....	49
Figure 2.3. Crystal structures of the dinuclear complexes in compounds $2.4\cdot\text{C}_5\text{H}_{12}$ (top) and $2.5\cdot\text{C}_5\text{H}_{12}$ (bottom), rendered with 40% ellipsoids .....	52
Figure 2.4. Electrochemical behavior for 2.3 in static solution recorded in 0.1 M solution of $[\text{TBA}][\text{BAr}^{\text{F}}_4]$ in <i>o</i> -difluorobenzene.....	54
Figure 2.5. Temperature dependence of the magnetic susceptibility for compounds $[(\text{NN}'_3)\text{U}(\text{CCPh})_2(\text{Li}\cdot\text{THF})]$ (2.1) and $[(\text{NN}'_3)\text{U}(\text{CCPh})]$ (2.3), obtained at a measuring field of 1000 G .....	57
Figure 2.6. Top: temperature dependence of the magnetic susceptibility for compounds 2.3 and 2.4, obtained at a measuring field of 1000 G; and fit of the data obtained from the subtraction method for 2.4, see text for details of the fitting procedures. Bottom: solid	

lines give best fits to the data obtained from the subtraction method for complexes 2.2, 2.4, 2.5, and 2.6 .....	61
Figure 2.7. (a) Average field fragment molecular orbital diagram for $[(NN'_3)U^{IV}(CCH)]$ , relative energies are provided on an eV scale. (b) Net spin density plot of the ground state triplet. (c) Net spin density plot of the lowest “singlet” broken symmetry state .....	65
Figure 2.8. Net spin density plots for <i>m</i> - and <i>p</i> -DEB-bridged dinuclear species based on 2.4 and 2.5.....	66
Figure 3.1. Molecular structures of the U(IV) phosphine complexes in compounds 3.1 (left) and 3.2 (right), rendered with 40% ellipsoids .....	89
Figure 3.2. Crystal structure of the U(IV) phosphine complex in $3.3 \cdot 2CH_2Cl_2$ , rendered with 40% ellipsoids .....	91
Figure 3.3. Left: crystal structure of the U(IV) phosphine complex in 3.4, rendered with 40% ellipsoids .....	93
Figure 3.4. Temperature dependence of the magnetic susceptibility for compounds 3.1–3.4, obtained at a measuring field of 1000 Oe .....	96
Figure 4.1. Energy diagram representing the crystal field splittings of an $f^2$ configuration in octahedral (left), cubic (middle), and trigonal bipyramidal (right) ligand fields .....	107
Figure 4.2. Full IR spectrum of 4.1 taken as a mineral oil mull .....	109
Figure 4.3. Electronic absorption spectrum of 4.1 .....	109
Figure 4.4. $^1H$ NMR spectrum of $[(dmpe)_2U(CCPPh)_4]$ (4.1) obtained in $C_6D_6$ .....	109
Figure 4.5. Full IR spectrum of 4.2 taken as a mineral oil mull .....	111
Figure 4.6. Electronic absorption spectrum of 4.2 .....	111

Figure 4.7. The U-containing complex in the crystal structure of 4.1, rendered with 40% ellipsoids .....	113
Figure 4.8. The U-containing complex in the crystal structure of 4.2, rendered with 40% ellipsoids .....	114
Figure 4.9. Crystal structure of the U(IV) arylacetylide complex in compound 4.1 rendered with 40% ellipsoids .....	117
Figure 4.10. Crystal structure of the U(IV) arylacetylide complex in compound 4.2 rendered with 40% ellipsoids .....	119
Figure 4.11. Temperature dependence of the magnetic susceptibility for [(dmpe) <sub>2</sub> U(CCPh) <sub>4</sub> ] (4.1, notebook reference: 534-bsn_chiquartz_eicosane2) and [(dmpe) <sub>2</sub> U(CCPh) <sub>5</sub> (Li·Et <sub>2</sub> O)] (4.2, notebook reference: 537-bsn_chiquartz_eicosane1) .....	122
Figure 4.12. Temperature dependence of the inverse susceptibility for compounds 4.1 (notebook reference: 534-bsn_chiquartz_eicosane2) and 4.2 (notebook reference: 537-bsn_chiquartz_eicosane1) obtained at a measuring field of 1000 G .....	122
Figure 4.13. Several attempts at collecting reproducible data for the temperature dependence of the magnetic susceptibility for compound 4.2 obtained at a measuring field of 1000 G. The plot on the left represents several attempts from the batch 537-bsn. The plot on the right represents several attempts from the batch 551-bsn .....	123
Figure 4.14. Several attempts at collecting reproducible data for the temperature dependence of the magnetic susceptibility for compound 4.1 obtained at a measuring field of 1000 G .....	123

Figure 4.15. Temperature dependence of the in-phase ( $\chi'$ , left) and out-of-phase ( $\chi''$ , right) components of the AC susceptibility for 4.2.....	124
Figure 5.1. Comparison of hydrogen bond and halogen bond geometries .....	149
Figure 5.2. A typical construction of CCDC searches, in this case any metal-chloride (4M–Cl) interactions.....	150
Figure 5.3. Overlay of representative U(IV) complexes in compounds 3.1 (red) and 3.4 (blue); two different orientations are show for clarity.....	151
Figure 5.4. Plot of the U(IV) phosphine complex in 3.1, rendered with 20% ellipsoids showing the parallel U–Cl···H–C interactions .....	153
Figure 5.5. Plot of the U(IV) phosphine complex in 3.4, rendered with 40% ellipsoids showing both parallel and perpendicular U–Cl···H–C interactions .....	153
Figure 5.6. (Left) Illustration of 3.4 showing a sigma hole (designated with a black arrow) that is formed by the approach of the H–C group.....	155
Figure 5.7. Results of search through the CCDC showing the M–Cl .....	155
Figure 5.8. Schematic showing the interaction of Cl <sub>2</sub> + CH <sub>4</sub> as perpendicular approach of a C–H bond to Cl <sub>2</sub> (90° Cl–Cl–H angle, left) and a co-linear approach of a C–H bond to Cl <sub>2</sub> (right) .....	156
Figure 5.9. Results of calculations showing the interaction energy of Cl <sub>2</sub> + CH <sub>4</sub> as a co-linear approach of a C–H bond to Cl <sub>2</sub> and perpendicular approach of a C–H bond to Cl <sub>2</sub> (90° Cl–Cl–H angle).....	157
Figure 6.1. Full IR spectrum of 6.3 taken as a mineral oil mull .....	165
Figure 6.2. Electronic absorption spectrum of 6.3, collected in toluene solution.....	165

Figure 6.3. $^1\text{H}$ NMR spectrum of $[(\text{NN}'_3)\text{U}(p\text{-DEB})\text{FeCl}(\text{dmpe})_2]$ (6.3) obtained in $\text{C}_6\text{D}_6$ .....	166
Figure 6.4. All the atoms in the crystal structure of 6.3, rendered with 40% ellipsoids .	168
Figure 6.5. Crystal structure of the $5f\text{-}3d$ arylacetylide bridged complex (6.3) rendered with 40% ellipsoids .....	172
Figure 6.6. Temperature dependence of the magnetic susceptibility for compound 6.3, obtained at a measuring field of 1000 G from 2-300 K.....	174
Figure 6.7. Electrochemical behavior for compound 6.3 in static solution (left) and while stirring (right) recorded in 0.1 M solution of $[\text{Bu}_4\text{N}][\text{BAR}^{\text{F}}_4]$ .....	175
Figure A1.1. Full IR spectrum of 2.1 (left) and expanded (right) taken as mineral oil mulls .....	190
Figure A1.2. Expanded IR spectrum of 2.2 taken as a mineral oil mull .....	191
Figure A1.3. Expanded IR spectrum of 2.3 taken as a mineral oil mull .....	191
Figure A1.5. Expanded IR spectrum of 2.5 taken as a mineral oil mull .....	191
Figure A1.4. Expanded IR spectrum of 2.4 taken as a mineral oil mull .....	191
Figure A1.6. Expanded IR spectrum of 2.6 taken as a mineral oil mull .....	191
Figure A1.8. Quantitative UV-visible spectrum of 2.2 taken in pentane .....	192
Figure A1.9. Quantitative UV-visible spectrum of 2.3 taken in toluene .....	192
Figure A1.11. Quantitative UV-visible spectrum of 2.5 taken in toluene .....	192
Figure A1.10. Quantitative UV-visible spectrum of 2.4 taken in pentane .....	192
Figure A1.12. Quantitative UV-visible spectrum of 2.6 taken in pentane .....	192
Figure A1.13. Electrochemical behavior for 2.3 in static solution (top) and while stirring (bottom) recorded in 0.1 M solution of $[\text{TBA}][\text{BAR}^{\text{F}}_4]$ in <i>o</i> -difluorobenzene .....	193

Figure A1.14. Electrochemical behavior for 2.2, 2.4, 2.5, and 2.6 in static solution recorded in 0.1 M solution of [TBA][BAr <sup>F</sup> <sub>4</sub> ] in <i>o</i> -difluorobenzene .....	194
Figure A1.15. Temperature dependence of the magnetic susceptibility and fit for compound 2.2 obtained at a measuring field of 1000 G.....	194
Figure A1.16. Temperature dependence of the magnetic susceptibility and fit for compound 2.5 obtained at a measuring field of 1000 G.....	195
Figure A1.17. Temperature dependence of the magnetic susceptibility and fit for compound 2.6 obtained at a measuring field of 1000 G.....	195
Figure A1.18. Temperature dependence of the inverse susceptibility for compounds 2.2 and 2.4–2.6 obtained at a measuring field of 1000 G.....	195
Figure A1.19. <sup>1</sup> H NMR spectrum of [(NN' <sub>3</sub> )U(CCPh) <sub>2</sub> (Li·THF)] (2.1) obtained in C <sub>6</sub> D <sub>6</sub> at ambient temperature with a 500 MHz spectrometer.....	196
Figure A1.20. <sup>1</sup> H NMR spectrum of [(NN' <sub>3</sub> )U(CCPh)] (2.3) obtained in C <sub>6</sub> D <sub>6</sub> at ambient temperature with a 500 MHz spectrometer.....	196
Figure A1.21. <sup>1</sup> H NMR spectrum of [(NN' <sub>3</sub> ) <sub>2</sub> U <sub>2</sub> ( <i>m</i> -DEB)] (2.4) obtained in C <sub>6</sub> D <sub>6</sub> at ambient temperature with a 500 MHz spectrometer .....	197
Figure A1.22. <sup>1</sup> H NMR spectrum of [(NN' <sub>3</sub> ) <sub>2</sub> U <sub>2</sub> ( <i>p</i> -DEB)] (2.5) obtained in C <sub>6</sub> D <sub>6</sub> at ambient temperature with a 500 MHz spectrometer .....	197
Figure A1.23. DFT results for U–CC bending in model complex of 2.3 .....	198
Figure A1.24. The U-containing complex in the crystal structure of 2.4·C <sub>5</sub> H <sub>12</sub> at 100 K rendered with 40% ellipsoids.....	198
Figure A1.25. The U-containing complex in the crystal structure of 2.5·C <sub>5</sub> H <sub>12</sub> at 100 K rendered with 40% ellipsoids.....	199

Figure A1.26. Temperature dependence of the in-phase ( $\chi'$ , top) and out-of-phase ( $\chi''$ , bottom) components of the AC susceptibility under 1000 Oe applied DC field collected at various AC frequencies for 2.4 encased in Eicosane .....	199
Figure A2.1. Full IR spectrum of 3.1 taken as mineral oil mulls.....	214
Figure A2.2. Full IR spectrum of 3.2 taken as a mineral oil mull.....	214
Figure A2.3. Full IR spectrum of 3.3 taken as a mineral oil mull.....	214
Figure A2.4. Full IR spectrum of 3.4 taken as a mineral oil mull.....	214
Figure A2.5. Electronic absorption spectrum of 3.1 taken in dichloromethane .....	215
Figure A2.7. Electronic absorption spectrum of 3.3 taken in dimethyl sulfoxide .....	215
Figure A2.6. Electronic absorption spectrum of 3.1 taken in dimethyl sulfoxide .....	215
Figure A2.8. Electronic absorption spectrum of 3.3 taken in dichloromethane .....	215
Figure A2.9. Electronic absorption spectrum of 3.4 taken in acetonitrile .....	215
Figure A2.10. Temperature dependence of the inverse susceptibility for compounds 3.1–3.4 obtained at a measuring field of 1000 G.....	216
Figure A2.11. $^1\text{H}$ NMR spectrum of 3.1 obtained in toluene- $d_8$ at ambient temperature with a 500 MHz spectrometer.....	216
Figure A2.12. $^1\text{H}$ NMR spectrum of 3.1 obtained in $(\text{CD}_3)_2\text{SO}$ at ambient temperature with a 500 MHz spectrometer.....	217
Figure A2.13. $\{^1\text{H}\}^{31}\text{P}$ NMR spectrum of 3.1 obtained in $(\text{CD}_3)_2\text{SO}$ at ambient temperature with a 500 MHz spectrometer.....	217
Figure A2.14. $^1\text{H}$ NMR spectrum of 3.1 obtained in $\text{CD}_2\text{Cl}_2$ at ambient temperature with a 500 MHz spectrometer.....	218

Figure A2.15. $\{^1\text{H}\}^{31}\text{P}$ NMR spectrum of 3.1 obtained in $\text{CD}_2\text{Cl}_2$ at ambient temperature with a 500 MHz spectrometer .....	218
Figure A2.16. (Top) $^1\text{H}$ NMR spectrum of 3.2 obtained in toluene- $d_8$ at $-80^\circ\text{C}$ with a 500 MHz spectrometer .....	219
Figure A2.17. $^1\text{H}$ NMR spectrum of 3.3 obtained in $(\text{CD}_3)_2\text{SO}$ at ambient temperature with a 500 MHz spectrometer .....	220
Figure A2.18. $\{^1\text{H}\}^{31}\text{P}$ NMR spectrum of 3.3 obtained in $(\text{CD}_3)_2\text{SO}$ at ambient temperature with a 500 MHz spectrometer .....	220
Figure A2.19. $^1\text{H}$ NMR spectrum of 3.3 obtained in $\text{CD}_2\text{Cl}_2$ at ambient temperature with a 500 MHz spectrometer .....	221
Figure A2.20. $\{^1\text{H}\}^{31}\text{P}$ NMR spectrum of 3.3 obtained in $\text{CD}_2\text{Cl}_2$ at ambient temperature with a 500 MHz spectrometer .....	221
Figure A2.21. $^1\text{H}$ NMR spectrum of 3.4 obtained in $\text{CD}_3\text{CN}$ at ambient temperature with a 500 MHz spectrometer .....	222
Figure A2.22. The U-containing complexes in the crystal structure of 3.1, rendered with 40% ellipsoids .....	223
Figure A2.23. The U-containing complex in the crystal structure of 3.2, rendered with 40% ellipsoids .....	223
Figure A2.24. The U-containing complex in the crystal structure of 3.3· $2\text{CH}_2\text{Cl}_2$ at 120 K rendered with 40% ellipsoids .....	224
Figure A2.25. The U-containing complex in the crystal structure of 3.4, rendered with 40% ellipsoids .....	224

Figure A2.26. Electronic absorption spectrum for the product of mixing 3.1 with one equivalent of dmbpy (547-bsn) .....	225
Figure A2.27. Temperature dependence of $\chi_M T$ for compound 3.3 assuming various amounts of $\text{CH}_2\text{Cl}_2$ solvate (considering scenarios with 0, 2, and 7.75 equivalents of $\text{CH}_2\text{Cl}_2$ ) .....	225
Figure A2.28. Magnetization for compounds 3.1 (left) and 3.3 (right), obtained at measuring fields of 1, 2, 3, 4, and 5 T from 2-35 K.....	226
Figure A2.29. Temperature dependence of the in-phase ( $\chi'$ , left) and out-of-phase ( $\chi''$ , right) components of the AC susceptibility under 0 or 1000 Oe applied DC field collected at various AC frequencies for 3.3 encased in Eicosane.....	226
Figure A2.30. Temperature dependence of $\mu_{\text{eff}}$ for compounds 3.1–3.4; B.M. = Bohr magneton.....	227

## LISTS OF SCHEMES

Scheme 2.1. Synthesis of complexes 2.3-2.6.....	50
Scheme 3.1. Syntheses of chelating phosphine complexes of U(IV).....	88
Scheme 4.1. Syntheses of chelating phosphine complexes of U(IV).....	116
Scheme 6.1. Synthesis of chelating <i>5f-3d</i> complex of U(IV)–Fe(II) .....	170

## **Chapter 1. Actinide-Containing Compounds: Routes to Increased Coupling and Magnetic Anisotropy**

### **1.1 Introduction**

As our society advances, a push for ever smaller and more powerful data storage devices is at the forefront. Areal density has steadily been on the rise since the introduction of the first magnetic storage drive in 1956.<sup>1</sup> Initially at a growth rate of about 25% per year, this has grown drastically since the early 1990s at a rate of about 60% per year, translating to an increase factor in areal density of more than 17 million.<sup>2</sup> In 2010, the Seagate Corporation announced its new data storage drive, which is capable of storing 541 GBit/in<sup>2</sup>.<sup>3</sup> As the technological revolution continues we, as a society, will need a better and more reliable way to store large amounts of magnetic data. One might expect that with this rapid expansion in areal storage density, drive manufacturers are fast approaching the superparamagnetic limit.<sup>1</sup> Researchers are finding new methods for recording and sensing the bit, ultimately pushing the areal density past previous predictions of the superparamagnetic limit.<sup>4,5</sup> The superparamagnetic limit is defined as the maximum number of bits/unit area that is feasible to fit on a magnetic storage device while allowing the bit to still be able to retain magnetic information. The superparamagnetic effect becomes an issue as magnetic bits get smaller and as a result, there is a point at which thermal fluctuations reduce the signal strength such that they will no longer retain their magnetic information.

Since the discovery of magnetic bistability displayed by certain high-nuclearity *molecular* species in the 1990s, the field of molecular magnetism has flourished.<sup>6</sup> These single-molecule magnets (SMMs) could serve to store massive amounts of data; on the order of 200,000 GBit/in<sup>2</sup> or 1.1 petabytes (PB) of information could be stored on a 3.5” hard drive as a result of the minute size of these clusters (~1 nm). A SMM is a molecule which behaves as a superparamagnet. The prerequisites for such a system are depicted in an energy plot shown in Figure 1.1.<sup>7</sup> The ideal characteristics of a SMM include a strong coupling (large  $J$ ) to isolate the ground state. Other ideal characteristic of SMMs include a large ground state spin,  $S$ , and large overall *negative* axial anisotropy,  $D$ . Easy-axis anisotropy or a negative  $D$  is required for SMMs to produce a “double-well” potential as depicted in Figure 1.1. By combining these properties, an energy barrier can be formed such that the system can be trapped in one of the high-spin energy wells. This energy barrier is manifested as a barrier to spin reorientation,  $U$ , where the “height” of this barrier is defined by  $U = S^2|D|$  (for integer spin systems) and  $U = (S^2 - 1/4)|D|$  (for half-integer spin systems). In order for SMMs to be considered for real applications they must have the highest possible working temperature (i.e.,  $U$  significantly greater than  $k_B T$ ). The working temperature is defined as the temperature below which the relaxation of the magnetization becomes slow compared to the time scale of a particular investigation technique.<sup>8</sup>

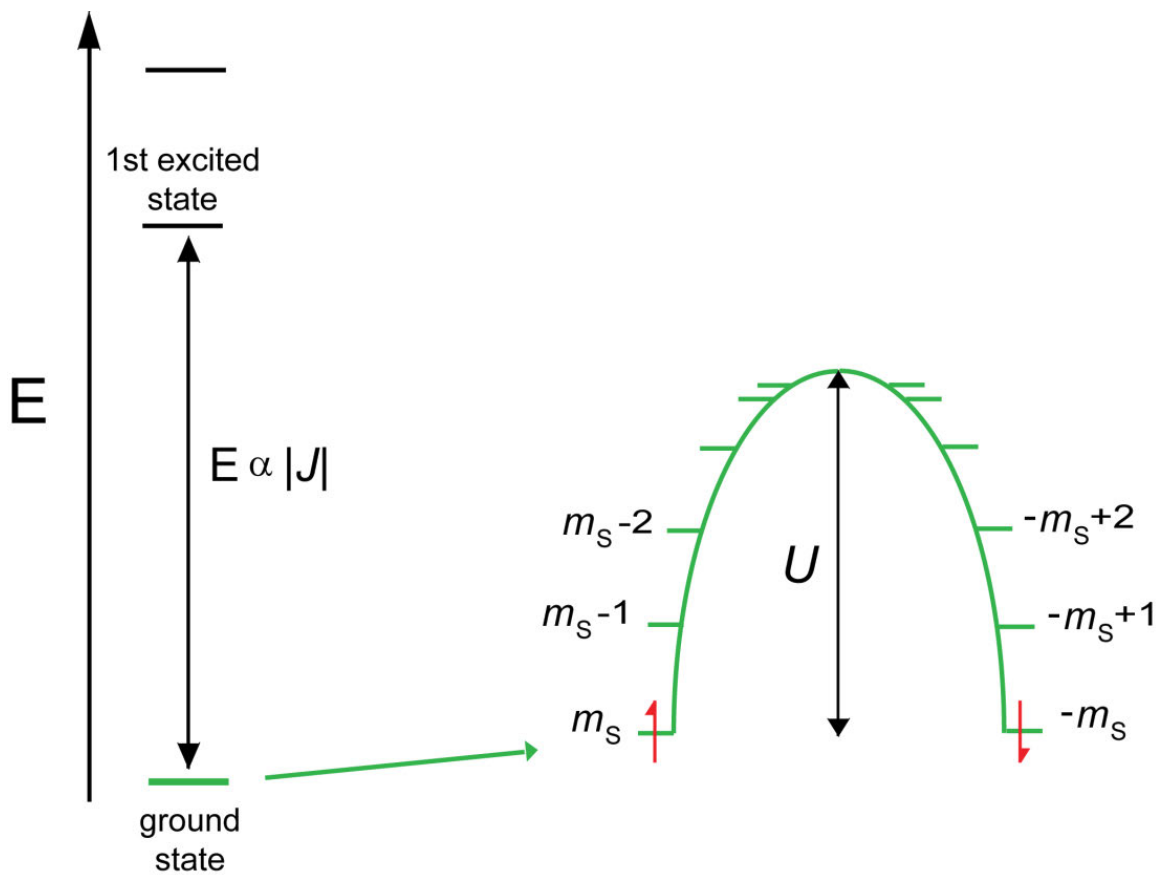


**Figure 1.1.** Energy diagram for a SMM with negative axial anisotropy. The arrows in the  $\pm m_s$  levels represent the orientation of the spin ( $S$ ) relative to the easy-axis of the cluster. Figure taken from reference 9.

The effect of this working temperature becomes evident for the original SMM,  $[\text{Mn}_{12}\text{O}_{12}(\text{MeCO}_2)_{16}(\text{H}_2\text{O})_4]$  or  $\text{Mn}_{12}\text{Ac}$ , which at low temperature relaxes so slowly that the behavior of individual molecules resembles that of bulk magnets.<sup>10</sup> In fact, if a molecule is magnetized at 2 K the magnetization is still *ca.* 40% of the saturation value after two months. At 1.5 K it would be necessary to wait for *ca.* 40 years to lose “the memory.” The resulting bistability leads many to believe that SMMs may allow for the realization of the smallest practical unit for magnetic memory.

However, under non-ideal conditions (intermediate to low  $J$  coupling), thermal energy allows for excited states to mix with the ground state, thereby providing a route

for electrons to “relax” into non-SMM manifolds. Chemists are able to make molecules with large spins,  $S$ , but the difficulty lies in synthetic control of the molecular anisotropy,  $D$ . The record working temperature originally set in the 1990s was  $\sim 4$  K.<sup>10</sup> Magnetic hysteresis is observed, but only upon cooling the material to liquid helium temperatures. Most recently, researchers have set a new record working temperature of  $\sim 8$  K.<sup>11</sup> Again, magnetic hysteresis is observed, but the working temperature has only been doubled in two decades. Therefore, before SMMs can be realized as the next magnetic generation of information storage bits, chemists must find a way to raise the working temperatures.

Since slow relaxation was observed in a molecule, much attention has focused on developing the magnetic properties of large polynuclear compounds containing transition metal and/or rare earth ions.<sup>12</sup> Several attempts to synthesize molecules that exhibit more desirable properties (*i.e.*, larger  $S$ ,  $J$ , and  $|D|$ ) have been undertaken, and have been reviewed recently.<sup>13-15</sup> In this chapter, my focus will be on mixed-metal ( $3d-4f$  and  $3d-5f$ ) complexes, and several interesting uranium complexes in various oxidation states. The examples presented herein are not meant to be comprehensive but rather to give the reader insight into the current research pertaining to the use of heavy elements in the design of SMMs. Compounds that contain  $f$ -block elements are able to display large single-ion anisotropy. This offers a direct route to synthetic control of  $D$ , which as noted above is the most difficult parameter to control synthetically.

## 1.2 Why Lanthanides?

People are becoming increasingly more interested in studying molecules built around lanthanide ions. Although the  $4f$  orbitals are not known for participating in bonding interactions with the ligand sets, many of these complexes exhibit properties consistent

with SMMs like slow magnetic relaxation.<sup>11,16-31</sup> Despite the report of multiple compounds that display properties consistent with SMMs, only a handful display magnetic hysteresis, the defining characteristic of a SMM.<sup>11,16,31</sup> Only a few specific examples are mentioned in this work, for a more comprehensive review in this area the reader is referred to the literature.<sup>22-27</sup> Murugesu and coworkers have recently used a compartmental Schiff base ligand based on the *o*-vanillin motif to synthesize and fully characterize a family of centrosymmetric dinuclear lanthanide complexes.<sup>16</sup> For all complexes, antiferromagnetic interactions between the lanthanide ions are observed. Simulations based on *ab initio* calculations predict that the strength of the interaction increases with the decrease of the intramolecular Ln(III)–Ln(III) distances as well as the increase in the bridging Ln(III)–O–Ln(III) angle.<sup>16</sup> Due to the fast relaxation of the magnetization for Tb(III) and Ho(III) analogues, only the Dy(III) analogue exhibits a slow relaxation of the magnetization associated with SMM behavior. In general, due to the reduced quantum tunneling of the magnetization in the free Dy(III) ion, that element has yielded the largest number of pure 4*f* SMMs of the lanthanides.<sup>16,32,33</sup>

Until recently it was believed that despite these promising results a setback to using lanthanide ions lies in the limitations of bonding interactions of the 4*f* orbitals. However, Long and coworkers have shown that strong magnetic coupling does exist in lanthanide complexes with the recent publication of a N<sub>2</sub><sup>3-</sup> radical-bridged Dy(III) complex, which is the current record holder with a working temperature of 8 K.<sup>11</sup> These results represent a breakthrough in the design of SMMs.

### 1.3 3d-4f Mixed-Metal Complexes

The purpose of 3d-4f assemblies is to take advantage of the single-ion anisotropy of the lanthanides in addition to the enhanced magnetic coupling associated with transition metals.<sup>34</sup> The first mixed-metal 3d-4f complex to exhibit magnetic hysteresis was reported by Christou and coworkers in 2004 with  $U = 6.3$  K ( $[\text{Mn}_{11}\text{Dy}_4\text{O}_8(\text{OH})_6(\text{OMe})_2(\text{O}_2\text{CPh})_{16}]^{5+}$ ).<sup>35</sup> This complex represents the first mixed-metal 3d-4f SMM to exhibit hysteresis loops and quantum tunneling of the magnetization.

Christou and coworkers recently reported the synthesis, structure, and magnetic properties of  $[\text{Ce}_4\text{Mn}_{10}\text{O}_{10}(\text{OMe})_6(\text{O}_2\text{CPh})_{16}]^{2+}$  which contains two Ce(III), two Ce(IV) and ten Mn(IV) ions and has a ground state spin of  $S = 4$ .<sup>36</sup> Variable temperature magnetic susceptibility measurements indicated the presence of antiferromagnetic exchange interactions within the molecule while the magnetization data was indicative of a magnetically anisotropic ground state. The authors observed minor hysteresis but with a very narrow coercivity that showed no noticeable temperature or frequency dependence, clearly not the superparamagnet-like behavior expected of an SMM. The authors attribute the tiny hysteresis at 0.04 K to weak intermolecular interactions caused by the intermolecular hydrogen bonding between the MeOH and chelating nitrate groups.

There have been a number of publications detailing the results of mixed-metal 3d-4f complexes.<sup>34-52</sup> Recently, Andruh and coworkers reported the synthesis and characterization of a dinuclear  $[\text{Ni}(\text{II})\text{Ln}(\text{III})]$  Schiff-base complexes that demonstrates slow magnetic relaxation.<sup>34</sup> In cases where magnetic coupling is observed it is not clear whether it is due to coupling of the *f* and *d* orbitals or rather a modulation of the transition metal orbitals by the lanthanide. However, these examples demonstrate the great promise

of  $f$  elements in the future of SMM chemistry, especially if their single-ion properties could be incorporated into high-nuclearity clusters where the spin and axial anisotropy of many metals could contribute to the energy barrier to spin reversal. However, it is difficult to envision high-nuclearity lanthanide clusters with concerted spin behavior because the  $4f$  valence orbitals typically lack the radial extension and energetic proximity required for significant overlap with bridging ligand orbitals.<sup>14,53-55</sup> This results in small covalent interactions and weak pathways for magnetic superexchange through diamagnetic bridging ligands although as described above, superexchange through radical ligands has been shown to be quite strong in one purely  $4f$  system.<sup>11</sup>

#### 1.4 Why Actinides?

The actinide ions that contain  $f$  electrons are of interest because of the possibility of magnetic communication through  $5f$  orbitals, which would favor a stronger ground state coupling,  $J$ . The greater radial extension of the  $5f$  valence orbitals of actinides can potentially provide increased overlap with bridging ligand orbitals, thereby enhancing the concerted magnetic behavior between bridged metal centers within a single cluster unit.<sup>15,53,56</sup> Thus far, efforts have focused exclusively on species incorporating uranium because this actinide element offers minimal radioactivity (in depleted form) with accessible oxidation states allowing for zero, one, two, or three unpaired electrons. The complexity of understanding the magnetic properties grows moving from  $f^0$ - $f^3$  (U(VI)-U(III)) and researchers have confronted the intricacies of the magnetic exchange in a number of interesting ways. Often, the goal is identifying and, to the extent possible, quantifying ferro- or antiferromagnetic exchange coupling. Understanding these exchange interactions is not only essential to the development of models for the basic

electronic structure of the  $5f$  elements but also may represent the key to producing better actinide-based SMMs.

Although the electronic structure of the early actinides contains features of both lanthanides (dominated by spin-orbit coupling) and transition metals (dominated by ligand field effects), the dynamic magnetic properties of actinide complexes have been much less explored.<sup>57</sup> Despite a growing number of varied synthetic systems incorporating paramagnetic uranium centers, unraveling actinide magnetic behavior remains a challenge because of the lack of a theoretical foundation for accurately modeling the complex interactions that govern actinide magnetic susceptibility.<sup>15</sup> In transition metal ions, it is usually possible to treat the magnetic susceptibility as being due to the unpaired spins, with minimal effects from the orbital components. The “spin-only” approximation, which works reasonably well for most first-row transition metal species, loses its validity with the actinide ions where spin-orbit interactions dominate the ligand field interactions.

In heavier elements with a larger effective nuclear charge ( $Z$ ), spin-orbit interactions dominate the interactions between individual spins or orbital angular momenta. As a result, the spin tends to couple with the orbital angular momenta of individual electrons to form individual electron angular momenta. This  $j-j$  coupling scheme describes the lanthanides well but breaks down when applied to actinides. Instead, it becomes appropriate to invoke an intermediate coupling scheme whereby spin-spin repulsions are considered before the spin and orbital angular momenta are coupled to then allow for the  $J$  states to mix. This intermediate coupling scheme is required since neither the Russell-

Saunders or *j-j* coupling method can describe the electronic structure of actinides to any accuracy.

Christou and coworkers reported the synthesis, structure, and magnetic properties of  $[\text{Th}_6\text{Mn}_{10}\text{O}_{22}(\text{OH})_2(\text{O}_2\text{CPh})_{16}]^{2+}$  which contains six Th(IV) and ten Mn(IV) ions and has a ground state spin of  $S = 3$ , but no hysteresis is observed. This compound is the largest transition-metal/actinide complex known to date and is an example of utilizing a heavy atom to modulate the molecular anisotropy although it is interesting to note the use of Th(IV) which contains no *f* electrons.

A recent review by Long and coworkers shows the importance of studying actinide-containing systems.<sup>15</sup> The possibility of molecular systems that incorporate the single-ion anisotropy of the actinides along with possible enhanced magnetic coupling through *5f* orbitals is greatly intriguing.

### 1.5 Coupling in a Dinuclear U(V) Complex

Over two decades ago the first observation of magnetic exchange coupling was reported in an actinide-containing molecule for the binuclear 1,4-diimidobenzene-bridged complex  $[(\text{MeC}_5\text{H}_4)_3\text{U}]_2(\mu\text{-}1,4\text{-N}_2\text{C}_6\text{H}_4)$ .<sup>58</sup> In this *JACS* communication, Andersen and coworkers demonstrated the viability of electronic coupling between two U(V) centers (Figure 1.2) by comparison of the variable temperature magnetic susceptibility data of structurally related compounds.<sup>58</sup> As the temperature is decreased from 300 K down to *ca.* 140 K the *meta*-isomer,  $[(\text{MeC}_5\text{H}_4)_3\text{U}]_2(\mu\text{-}1,3\text{-N}_2\text{C}_6\text{H}_4)$ , displays essentially constant magnetic susceptibility (Figure 1.3). As the temperature is decreased further, down to 5 K, the magnetic susceptibility begins to rise monotonically. This behavior is consistent with an isolated  $5f^1$  spin-center and is essentially the sum of that observed for two

(MeC<sub>5</sub>H<sub>4</sub>)<sub>3</sub>U(NPh) units, which indicates a lack of any magnetic exchange between the two U(V) centers.<sup>58,59</sup> Similar behavior is observed with the magnetic susceptibility data obtained for the *para*-isomer, [(MeC<sub>5</sub>H<sub>4</sub>)<sub>3</sub>U]<sub>2</sub>(μ-1,4-N<sub>2</sub>C<sub>6</sub>H<sub>4</sub>), down to *ca.* 75 K. However, at lower temperatures a downturn is exhibited (Figure 1.3).

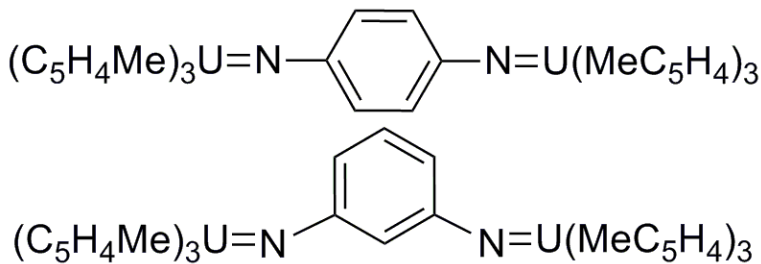


**Figure 1.2.** Two different isomers of [(MeC<sub>5</sub>H<sub>4</sub>)<sub>3</sub>U]<sub>2</sub>(μ-N<sub>2</sub>C<sub>6</sub>H<sub>4</sub>). Top: depiction of the antiferromagnetically coupled isomer. Bottom: depiction of the *para*- isomer with no magnetic coupling. Figure adapted from reference 58.

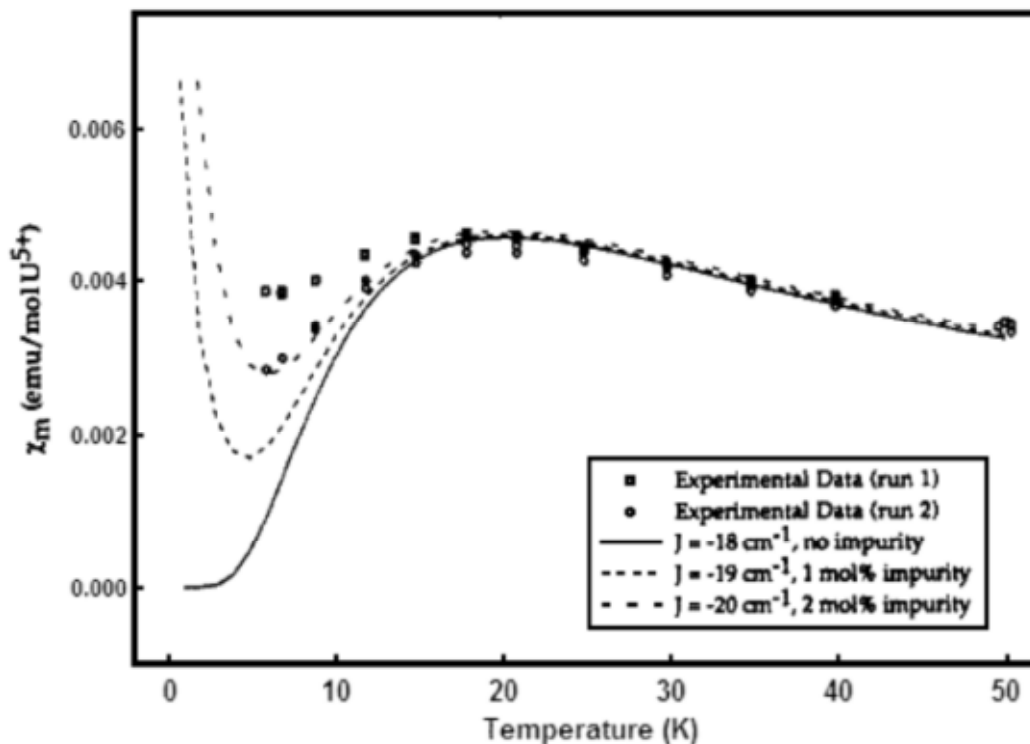


**Figure 1.3.** Experimental (symbols) versus calculated (lines) molar magnetic susceptibility for [(MeC<sub>5</sub>H<sub>4</sub>)<sub>3</sub>U]<sub>2</sub>(μ-1,4-N<sub>2</sub>C<sub>6</sub>H<sub>4</sub>). Each calculated curve is modeled with a different amount of the paramagnetic impurity, (MeC<sub>5</sub>H<sub>4</sub>)<sub>3</sub>U(THF). Figure taken from reference 58.

The local symmetry about the uranium centers in these compounds is approximately  $C_{3v}$ . The ground state term for a U(V)  $5f^4$  ion is  ${}^2F_{5/2}$  and under  $C_{3v}$  symmetry, the  $J = 5/2$  ground state is split by the ligand field into three magnetic doublets or Stark sublevels, two  $\mu = 1/2$  states and one  $\mu = 3/2$  state, where  $\mu$  is the crystal quantum number.<sup>60</sup> According to the selection rules of EPR, a spectrum is expected for a sublevel with crystal quantum number  $\mu = 1/2$ , while no spectrum is expected for a sublevel with crystal quantum number  $\mu = 3/2$ . The lack of an EPR spectrum in the *meta*-bridged dinuclear complex,  $[(\text{MeC}_5\text{H}_4)_3\text{U}]_2(\mu\text{-}1,3\text{-N}_2\text{C}_6\text{H}_4)$ , at 4 K is suggestive that only the lowest energy Stark sublevel ( $\mu = 3/2$ ) is populated.

Andersen and coworkers attempted to quantify the coupling in  $[(\text{MeC}_5\text{H}_4)_3\text{U}]_2(\mu\text{-}1,4\text{-N}_2\text{C}_6\text{H}_4)$  by comparing the experimental  $\chi_M T$  vs  $T$  data to calculated susceptibilities. To model the magnetic interaction between the U(V) metal centers, the authors utilized the Hamiltonian for an isolated dinuclear complex shown in Eq 1.1:

$$H = -2J(\hat{S}_{z1} \cdot \hat{S}_{z2}) + g_{\parallel}\mu_B\hat{H}_z \cdot (\hat{S}_{z1} \cdot \hat{S}_{z2}) \quad (1.1)$$

The effective spin operator for each  $S = 1/2$  U(V) ion is  $\hat{S}_{z1}$  where the  $z$  direction is defined along the U...U axis,  $J$  is the magnetic exchange constant,  $g_{\parallel}$  is the Landé  $g$  factor,  $\mu_B$  is the Bohr magneton, and  $\hat{H}_z$  is the magnetic field vector. It is important to note however, that with decreasing temperature the deviations in the magnetic susceptibility as a result of the depopulation of the uranium Stark sublevels is not accounted for by this Hamiltonian. Rather, it assumes these deviations are a result of the exchange between two  $S = 1/2$  ions.<sup>58</sup> As a result, the authors claim that the observed drop in the magnetic susceptibility of the *para*-bridged complex,  $[(\text{MeC}_5\text{H}_4)_3\text{U}]_2(\mu\text{-}1,4\text{-N}_2\text{C}_6\text{H}_4)$ , can be explained by magnetic exchange interactions rather than the usual

depopulation of the Stark sublevels.<sup>58</sup> The resulting calculated and experimental susceptibility data are presented in Figure 1.3. The differences between the two experimental data sets were attributed to sample impurity and the susceptibilities were calculated with varying amounts of paramagnetic impurity. Employment of these parameters affords a best fit with an exchange constant of  $J = -19 \text{ cm}^{-1}$  and an estimated paramagnetic impurity of 1 mol %.<sup>58</sup> Although this coupling was observed to be antiferromagnetic in nature, it demonstrates the viability of  $f$  orbital communication.

The observation that the spins on each uranium center in the *para*-bridged complex,  $[(\text{MeC}_5\text{H}_4)_3\text{U}]_2(\mu\text{-}1,4\text{-N}_2\text{C}_6\text{H}_4)$ , couple antiferromagnetically can be rationalized by a superexchange pathway whereby the uranium centers can communicate across the conjugated ligand via resonance as depicted in Figure 1.4. This exchange pathway does not exist for the *meta*-bridged complex. Note that others have shown through theoretical<sup>61</sup> and experimental work<sup>62</sup> with transition metal complexes that ferromagnetic coupling is observed through *meta*-bridged species whereas antiferromagnetic coupling is observed through *para*-bridged species.

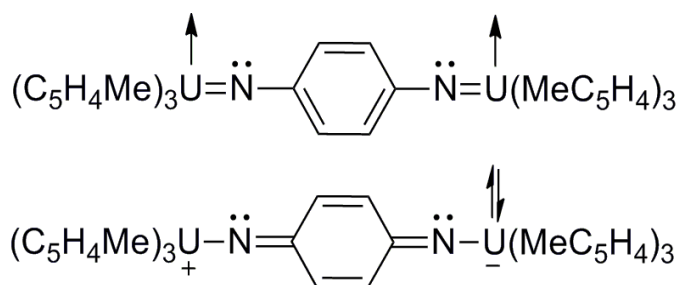


**Figure 1.4.** Resonance structures of  $[(\text{MeC}_5\text{H}_4)_3\text{U}]_2(\mu\text{-}1,4\text{-N}_2\text{C}_6\text{H}_4)$  that indicate a viable superexchange pathway for the observed antiferromagnetic coupling. Figure adapted from reference 58.

### 1.6 3d-5f Mixed Metal Complexes: Ferromagnetic Exchange Coupling in the Linear, Chloride-Bridged Cluster (cyclam)Co(II)[( $\mu$ -Cl)U(IV)(Me<sub>2</sub>Pz)<sub>4</sub>]<sub>2</sub>

Long and coworkers have shown that cleavage of a [U(Me<sub>2</sub>Pz)<sub>4</sub>]<sub>2</sub> dimer by (cyclam)CoCl<sub>2</sub> affords the trinuclear cluster (cyclam)Co[( $\mu$ -Cl)U(Me<sub>2</sub>Pz)<sub>4</sub>]<sub>2</sub> (cyclam = 1,4,8,11-tetraazacyclotetradecane in moderate yield.<sup>63</sup> The structure is shown in Figure 1.5 and is centrosymmetric with an inversion center located on the central cobalt atom.

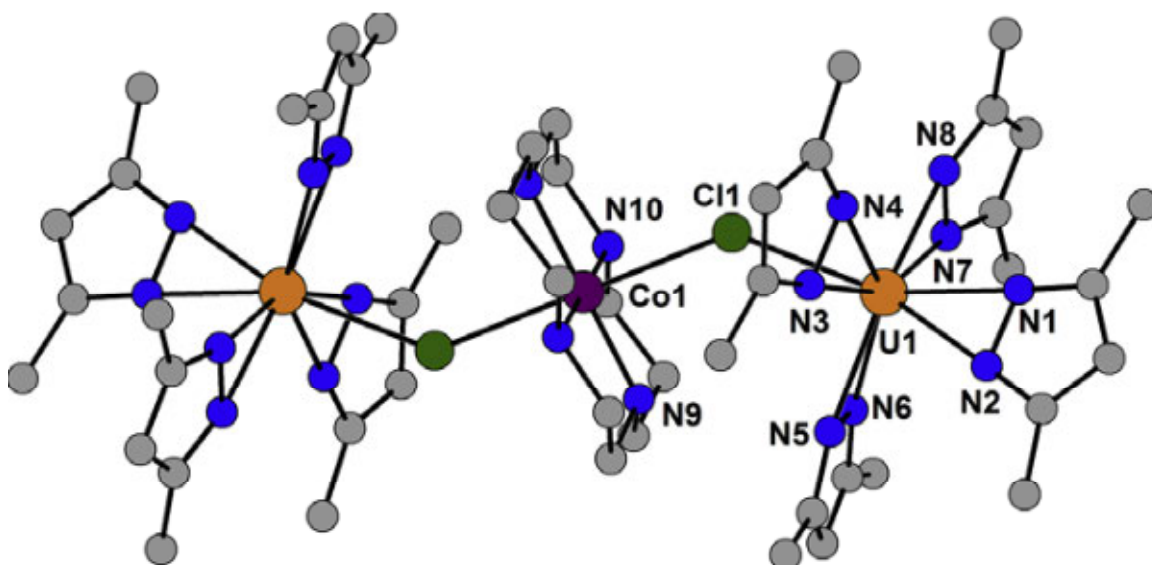


**Figure 1.5.** Structure of the linear cluster (cyclam)Co[( $\mu$ -Cl)U(Me<sub>2</sub>Pz)<sub>4</sub>]<sub>2</sub>. Orange, purple, green, gray and blue spheres represent U, Co, Cl, C, and N atoms, respectively. Hydrogen atoms are omitted for clarity. The cluster resides on an inversion center within the crystal. Figure taken from reference 63.

Temperature-dependent magnetic susceptibility data were collected on the precursor complex (cyclam)CoCl<sub>2</sub> and appears in Figure 1.6. This complex displayed temperature invariant behavior with a value of 0.41 emu·K·mol<sup>-1</sup> which is indicative of an  $S = \frac{1}{2}$  compound.<sup>63</sup> The temperature-dependent magnetic susceptibility data for CoU<sub>2</sub> and ZnU<sub>2</sub> is shown in Figure 1.6. Both compounds showed similar behavior. At 300 K, the  $\chi_M T$  values for ZnU<sub>2</sub> and CoU<sub>2</sub> of 2.06 and 2.47 emu·K·mol<sup>-1</sup>, respectively, correlate well

with the expected spin-only values suggestive of two uncoupled U(IV) ions and, in the latter case, one low-spin Co(II) ion. The magnetic susceptibilities of both compounds are dominated by a reduction in the effective spin of the  $5f^2$  configuration of U(IV) as the temperature decreases.<sup>63</sup> As the temperature is lowered the differences in the two compounds is more pronounced. The  $\chi_M T$  value decays less rapidly for  $\text{CoU}_2$  and since the structures are similar, ligand field differences alone cannot account for the variation about the uranium centers. This is suggestive of magnetic exchange coupling between the Co(II) and U(IV) centers in the  $\text{CoU}_2$  cluster.

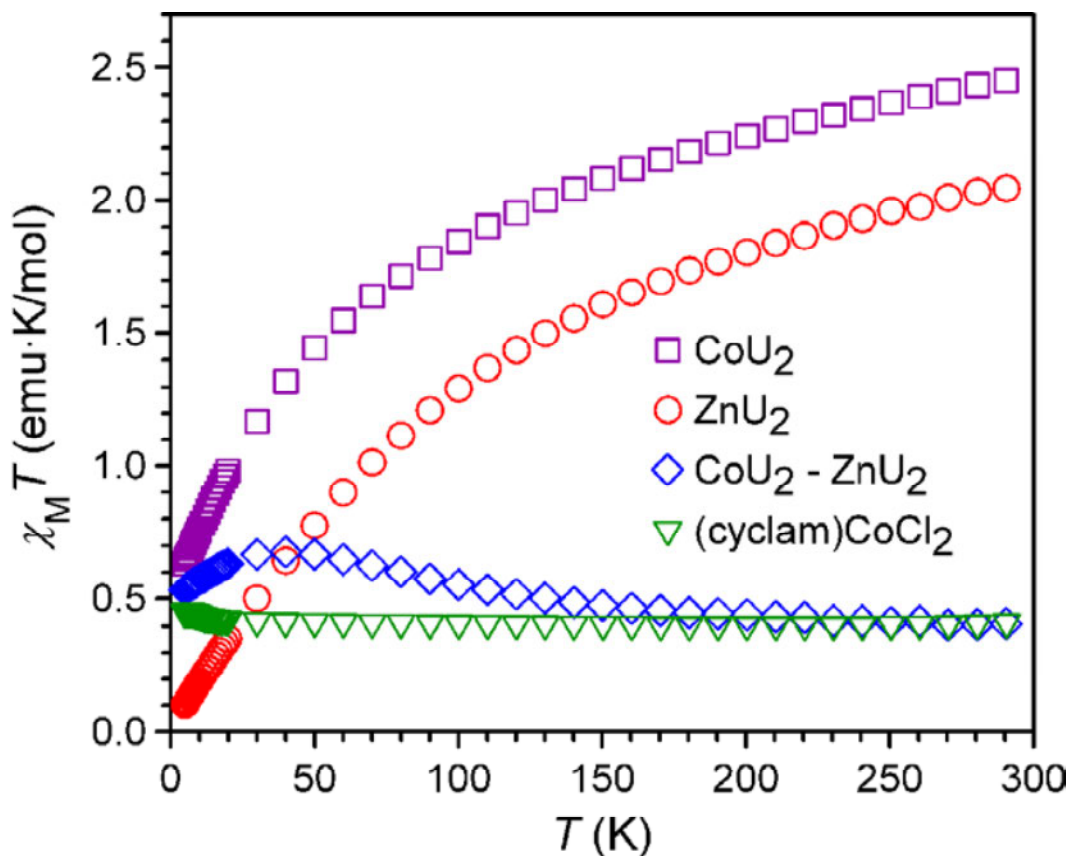


**Figure 1.6.** Variable-temperature magnetic susceptibility data for the trinuclear cluster  $(\text{cyclam})\text{Co}[(\mu\text{-Cl})\text{U}(\text{Me}_2\text{Pz})_4]_2$  and its previously published analogue,  $(\text{cyclam})\text{Zn}[(\mu\text{-Cl})\text{U}(\text{Me}_2\text{Pz})_4]_2$ . Blue diamonds correspond to a subtraction of the  $\text{ZnU}_2$  data from the  $\text{CoU}_2$  data. Magnetic data for the precursor complex  $(\text{cyclam})\text{CoCl}_2$  are depicted as green triangles. Figure taken from reference 63.

To probe the magnitude of this interaction the authors subtracted the raw magnetic susceptibility data for ZnU<sub>2</sub> from CoU<sub>2</sub> to yield a corrected  $\chi_M T$  for an isolated  $d^7$  Co(II) ion along with any residual moment due to exchange coupling. The plot of this subtraction technique appears in Figure 1.6 (blue diamonds) and is consistent with an isolated Co(II) center at high temperature. The results of the subtraction technique corresponded to the  $\chi_M T$  value measured for (cyclam)CoCl<sub>2</sub>. However, as the temperature is lowered,  $\chi_M T$  displayed an upturn and reaches a maximum of 0.68 emu·K·mol<sup>-1</sup> at 40 K, suggestive of ferromagnetic exchange between the U(IV) and Co(II) metal centers. To estimate the strength of the exchange coupling the authors employed MAGFIT 3.1 to fit the subtracted magnetic susceptibility data above 70 K using a spin Hamiltonian of the form  $\hat{H} = -2J[\hat{S}_{Co} \cdot (\hat{S}_{U(1)} + \hat{S}_{U(2)})] + g_{\mu_B} S \cdot B$ . To account for a spin-only contribution from the two U<sup>IV</sup> ions to the total spin, a temperature-invariant value of 2.00 emu·K·mol<sup>-1</sup> was added back into the data. Optimizing the fit parameters, the authors obtain values of  $J = 15 \text{ cm}^{-1}$ ,  $g = 1.92$ , and TIP =  $3.16 \times 10^{-4} \text{ emu} \cdot \text{mol}^{-1}$ . The adjusted data as well as the optimized fit for the CoU<sub>2</sub> cluster are shown in Figure 1.7 (blue diamonds). Reoptimization of the data for the previously reported NiU<sub>2</sub> cluster leads to  $J = 2.8 \text{ cm}^{-1}$ ,  $g = 1.96$ , and TIP =  $5.15 \times 10^{-4} \text{ emu} \cdot \text{mol}^{-1}$  (Figure 1.7, red circles).<sup>63,64</sup> Since this method of data treatment eliminates the effects of spin-orbital contributions and ligand field effects, these results represent a lower bound to the exchange energy.

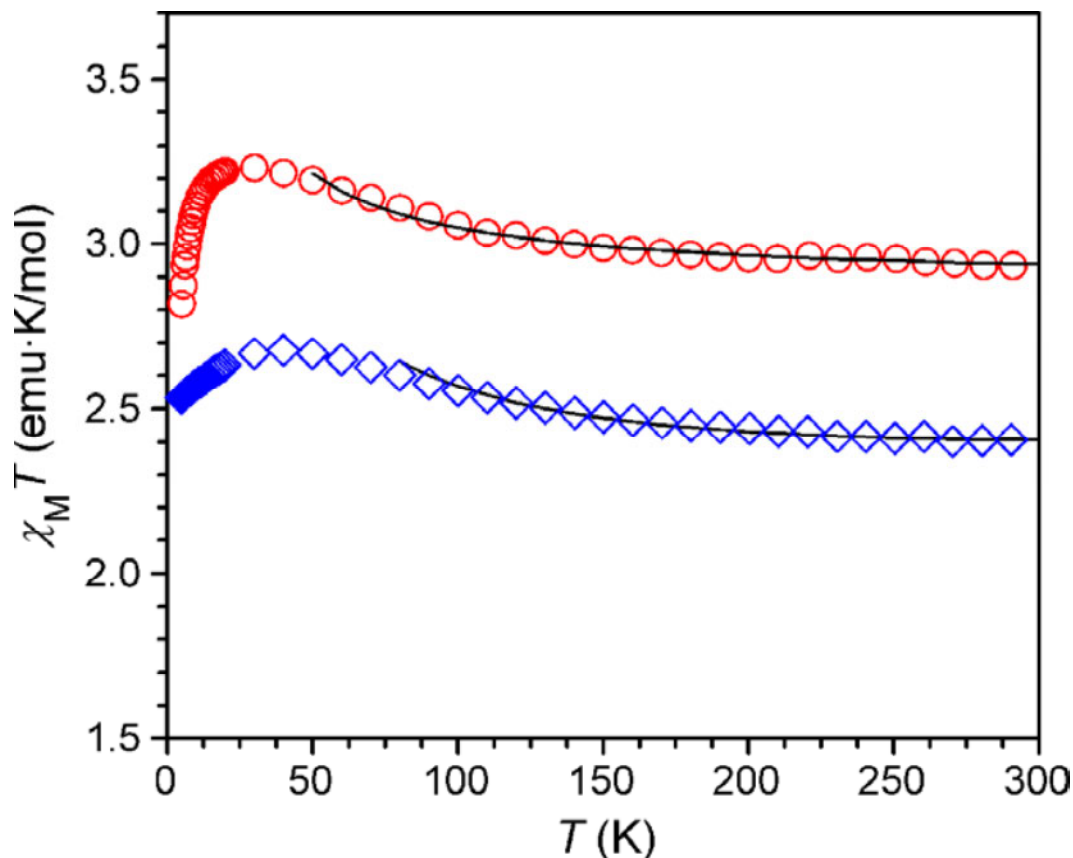


**Figure 1.7.** Empirical  $\chi_M T$  data arising upon subtraction of the  $\text{ZnU}_2$  cluster data from the  $\text{CoU}_2$  (blue diamonds) and  $\text{NiU}_2$  (red circles) cluster data. A calculated value of  $2.00 \text{ emu}\cdot\text{K}\cdot\text{mol}^{-1}$  has been added to represent a spin-only contribution from two  $\text{U(IV)}$  centers. Best calculated fits to the data are shown as black lines ( $J_{\min}(\text{Co}) = 15 \text{ cm}^{-1}$ ,  $J_{\min}(\text{Ni}) = 2.8 \text{ cm}^{-1}$ ). Figure taken from reference 63.

To provide an upper bound for the exchange coupling the authors proposed a second model in which they assumed that the reduction in  $\chi_M T$  in the  $\text{ZnU}_2$  and  $\text{CoU}_2$  data sets with temperature could be modeled by combining the effects of spin-orbit coupling and ligand field perturbations into a single empirical factor based on the magnetic susceptibility of the  $\text{ZnU}_2$  cluster. Using this method, the authors were able to fit the corrected data for the  $\text{CoU}_2$  cluster with the Hamiltonian discussed previously to give  $J = 48 \text{ cm}^{-1}$ ,  $g = 1.80$ , and  $\text{TIP} = 1.67 \times 10^{-4} \text{ emu}\cdot\text{mol}^{-1}$  (Figure 1.8, blue diamonds) and  $J = 19 \text{ cm}^{-1}$ ,  $g = 1.85$ , and  $\text{TIP} = 5.15 \times 10^{-4}$  for the  $\text{NiU}_2$  cluster (Figure 1.8, red circles).<sup>63</sup>

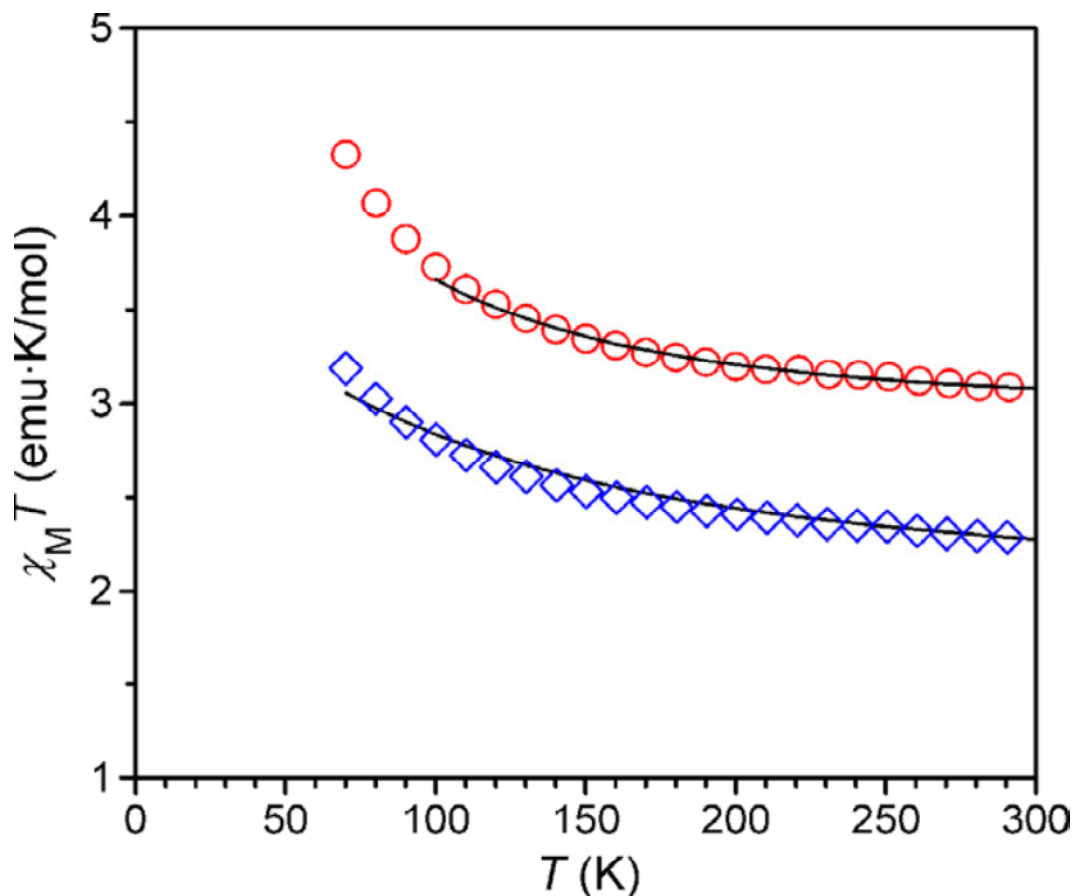


**Figure 1.8.** Plots of  $\chi_M T$  data for the CoU<sub>2</sub> (blue diamonds) and NiU<sub>2</sub> (red circles) clusters upon modification to account for the loss of spin of the U(IV) centers at low temperatures. Calculated fits to the data are shown as black lines ( $J_{\max}(\text{Co}) = 48 \text{ cm}^{-1}$ ,  $J_{\max}(\text{Ni}) = 19 \text{ cm}^{-1}$ ). Figure taken from reference 63.

Variable-field magnetization data for the CoU<sub>2</sub> cluster showed a significant separation of the isofield lines at low temperatures, consistent with large axial anisotropy. Quantitative fitting of these data have not produced reasonable results. Despite the presence of zero-field splitting, AC magnetic susceptibility measurements performed between 1.8 K and 10 K with oscillating frequencies of up to 1500 Hz showed no out-of-phase signal indicative of SMM behavior.<sup>63</sup>

## 1.7 A Uranium(III) Complex Exhibiting Properties Consistent with a SMM

The previously reported trigonal prismatic U(III) complex,  $\text{U}(\text{Ph}_2\text{BPz}_2)_3$  (Figure 1.9),<sup>65</sup> has been shown to display slow magnetic relaxation as evidenced by the AC magnetic susceptibility data.<sup>66</sup> The temperature dependence of the in-phase ( $\chi'_M$ ) and out-of-phase ( $\chi''_M$ ) AC susceptibility under zero applied DC field is shown in the top of Figure 1.10. The frequency dependent peaks observed for the  $\chi''_M$  signal are characteristic of slow relaxation of the magnetic susceptibility in discrete molecules. As observed in previous lanthanide systems,  $\chi''_M$  represents only a small component of the total susceptibility under zero field.<sup>67,68</sup> The authors recognized that the  $5f^3$  configuration of U(III) can deliver an oblate single-ion anisotropy as described by Skomski.<sup>69</sup> When strong spin-orbit coupling is present for an axial ligand environment, the spin can be preferentially aligned along the unique molecular axis. This acts to minimize the crystal-field energy by reducing contacts between the equatorial  $f$ -element charge cloud and the ligand donor atom charges.<sup>66,69</sup> As a result, the authors showed that the application of a small DC magnetic field can change the relaxation and increase the  $\chi''_M$  to  $\chi'_M$  ratio.<sup>66</sup>

Under zero applied magnetic field it is possible to observe quantum tunneling between opposite orientations of the ground-state spin as a result of mixing of the near-degenerate levels in Kramers ions by transverse components of the internal magnetic field.<sup>70</sup> To test whether this occurs in  $\text{U}(\text{Ph}_2\text{BPz}_2)_3$ , the authors collected variable-frequency AC susceptibility data at a number of applied DC fields in the range 0-500 Oe. All of the data were acquired at 1.8 K, where deviations from Arrhenius behavior suggested that quantum tunneling is the dominant process (see Figure 1.11).

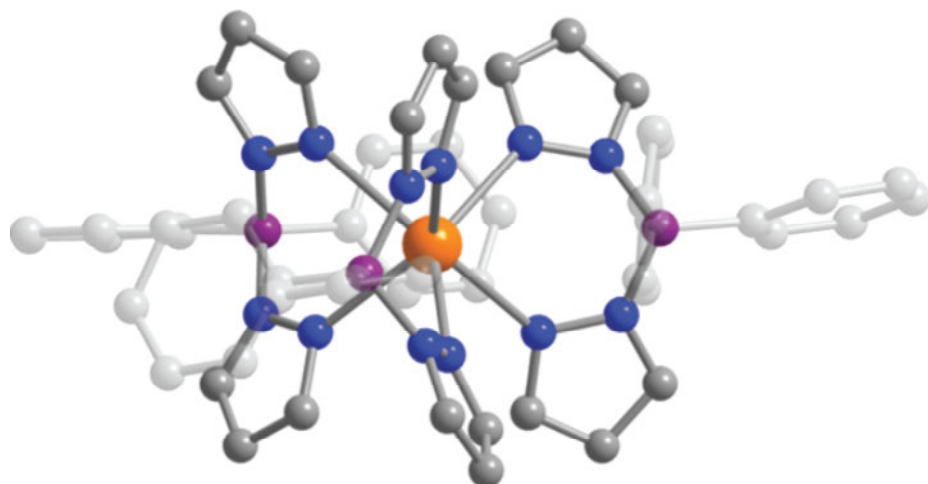


**Figure 1.9.** Structure of the trigonal prismatic complex  $\text{U}(\text{Ph}_2\text{BPz}_2)_3$ .<sup>65</sup> Orange, purple, gray, and blue spheres represent U, B, C, and N atoms, respectively; Hydrogen atoms have been omitted for clarity. The coordination at the  $\text{U}^{\text{III}}$  center approximates  $D_{3h}$  symmetry, with U–N distances of 2.487(7)–2.568(7) Å and N–U–N angles of 73.2(2)–73.6(3) and 83.0(2)–95.1(2)°. The shortest intermolecular U···U distance is 10.791(2) Å. Figure taken from reference 66.

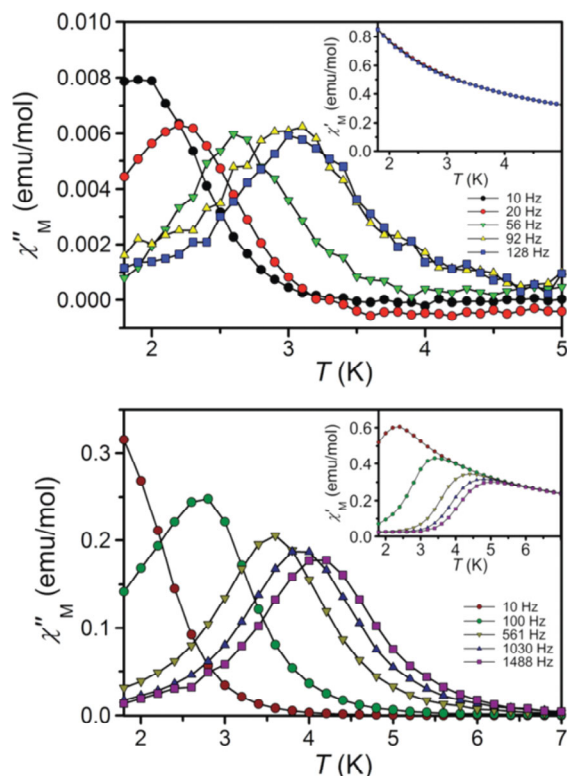


**Figure 1.10.** Temperature dependence of the in-phase ( $\chi'_M$ , inset) and out-of-phase ( $\chi''_M$ ) components of the AC susceptibility of  $\text{U}(\text{Ph}_2\text{BPz}_2)_3$  under (top) zero and (bottom) 1000 Oe applied DC fields, collected at various AC frequencies. Figure taken from reference 66.

Arrhenius plots obtained under applied DC fields of 0, 100, and 1000 Oe are shown in Figure 1.11. Although the three sets of relaxation data shown in Figure 1.11 follow the same line at high temperatures, the deviation from linearity at low temperature is DC-field-dependent which is indicative of several relaxation regimes and can be used to describe the onset of a regime where quantum tunneling of the magnetization is the dominant process.<sup>6</sup> Fitting the linear region, the authors extracted an effective relaxation barrier of  $U_{\text{eff}} = 20 \text{ cm}^{-1}$  (lifetime of  $\tau_0 = 1 \times 10^{-9} \text{ s}$ ), consistent with SMM behavior.<sup>66</sup> These results demonstrated the ability of a simple  $U^{\text{III}}$  complex to display SMM behavior.

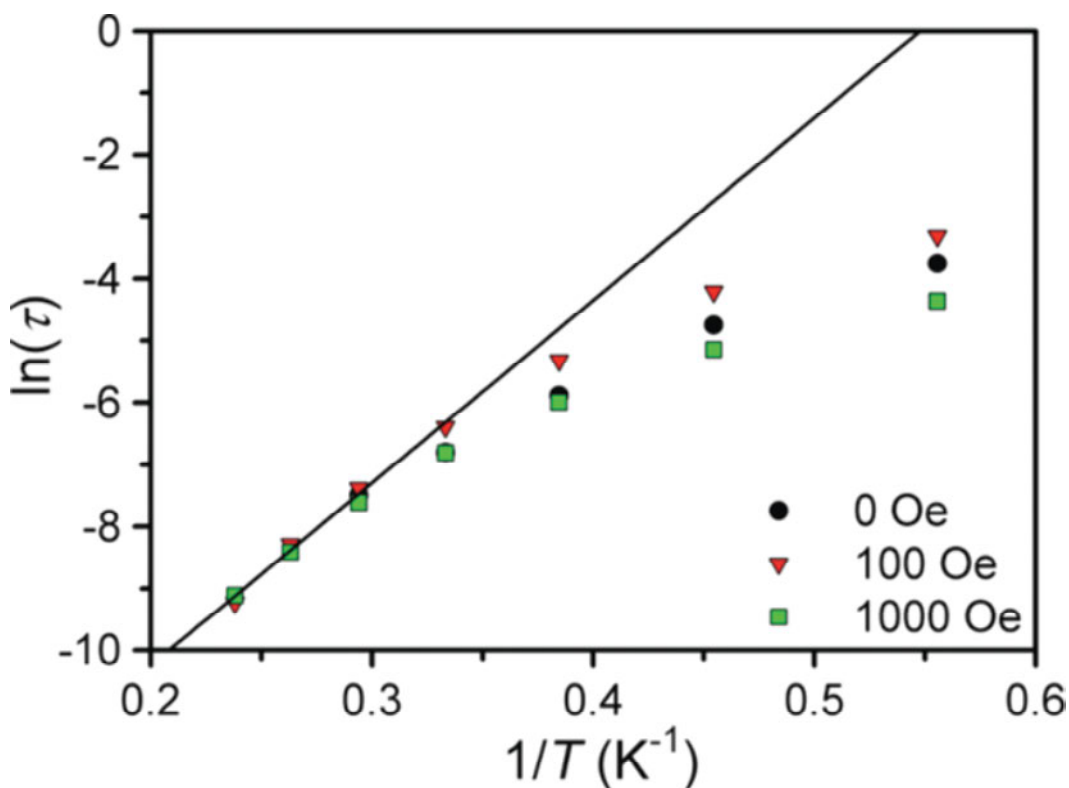


**Figure 1.11.** Arrhenius plot of  $U(\text{Ph}_2\text{BPz}_2)_3$  in the presence of applied DC fields of 0, 100, and 1000 Oe. The solid line represents an Arrhenius fit to the data in the thermally activated regime. Figure taken from reference 66. The deviation from linearity at low temperature can be used to describe the onset of a regime where quantum tunneling of the magnetization is the dominant process.<sup>6,66</sup>

## 1.8 A Delocalized Arene-Bridged Diuranium Single-Molecule Magnet

Recently, Liddle and coworkers reported the synthesis and characterization of the inverted sandwich arene-bridged diuranium complex  $[(U(BIPM^{TMS}H)(I))_2(\mu-\eta^6:\eta^6-C_6H_5CH_3)]$ .<sup>71</sup> The structure of  $[(U(BIPM^{TMS}H)(I))_2(\mu-\eta^6:\eta^6-C_6H_5CH_3)]$  is shown in Figure 1.12.

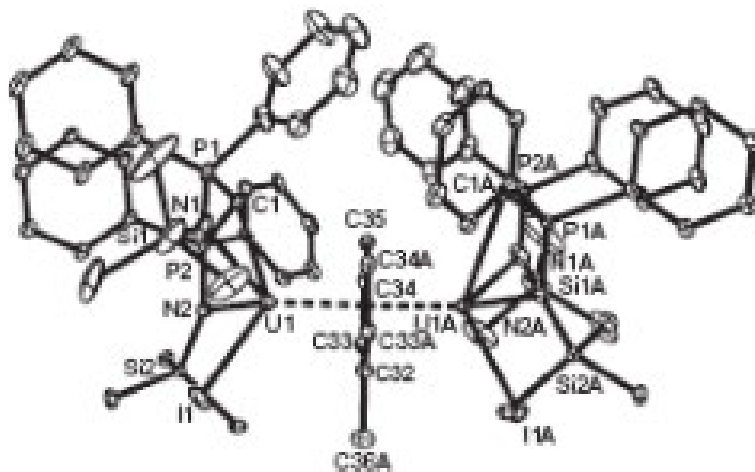


**Figure 1.12.** Solid-state structure of  $[U(BIPM^{TMS}H)(I))_2(\mu-\eta^6:\eta^6-C_6H_5CH_3)]$  as determined by X-ray crystallography, depicted with 30% probability ellipsoids; for clarity, hydrogen atoms, disorder components and lattice solvent are omitted. Figure adapted from reference 71.

The temperature dependence of  $[U(BIPM^{TMS}H)(I))_2(\mu-\eta^6:\eta^6-C_6H_5CH_3)]$  at 298 K, in benzene-*d*<sup>6</sup>, was measured to be  $1.80 \text{ emu}\cdot\text{K}\cdot\text{mol}^{-1}$  which decreases gradually with temperature to  $0.59 \text{ emu}\cdot\text{K}\cdot\text{mol}^{-1}$  at 1.8 K as shown in Figure 1.13 (top left). The room temperature  $\chi_M T$  value is significantly lower than expected for two uncoupled U(III) ions ( $3.28 \text{ emu}\cdot\text{K}\cdot\text{mol}^{-1}$ ), assuming a fully unquenched orbital moment.<sup>71,72</sup> As the temperature is lowered the value of  $\chi_M T$  does not approach zero, which suggests that no strong antiferromagnetic exchange interactions are present. However, it does appear that

there is a noticeable downturn of the measured  $\chi_M T$  at low temperature and if data were collected at extremely low temperature ( $< 1.8$  K) the  $\chi_M T$  value may indeed approach zero.

A magnetic hysteresis measurement was performed at low temperature (1.8 K, Figure 1.13 (top right)) to characterize the ground state further. Hysteresis behavior was observed, suggesting that  $[(U(BIPM^{TMS}H)(I))_2(\mu-\eta^6:\eta^6-C_6H_5CH_3)]$  acts as a SMM.<sup>73</sup> The absence of coercivity at zero field suggests that efficient quantum tunneling of the magnetization is occurring.<sup>74</sup> Since depleted  $^{238}U$  has no net nuclear spin this cannot be induced by hyperfine interactions but is more likely caused by low-symmetry components of the crystal field. To further probe the slow relaxation of  $[(U(BIPM^{TMS}H)(I))_2(\mu-\eta^6:\eta^6-C_6H_5CH_3)]$ , the temperature dependence of the in-phase ( $\chi'_M$ ) and out-of-phase ( $\chi''_M$ ) AC susceptibility was measured (Figure 1.13, bottom left and right, respectively), with the application of an external DC field of 0.1 T. Under these conditions the authors observed frequency-dependent out-of-phase signals, consistent with SMM behavior.

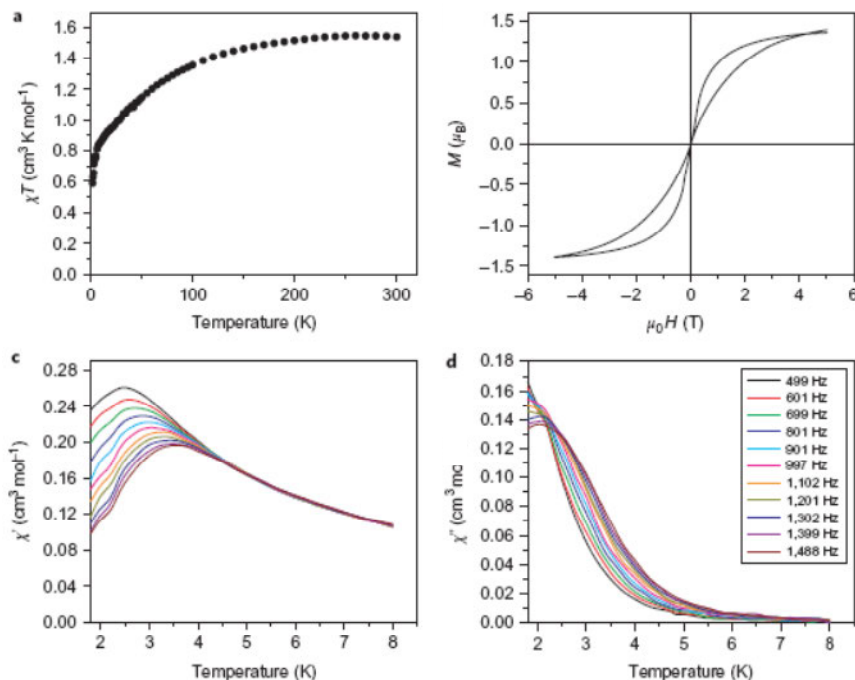


**Figure 1.13.** (Top left): Temperature dependence of the DC magnetic susceptibility of  $[(\text{U}(\text{BIPM}^{\text{TMS}}\text{H})(\text{I}))_2(\mu\text{-}\eta^6\text{:}\eta^6\text{-C}_6\text{H}_5\text{CH}_3)]$  at applied fields of 0.1 T ( $T < 50$  K) and 1 T ( $T > 40$  K). (Top right): Magnetic hysteresis at 1.8 K at a sweep rate of  $26 \text{ Oe}\cdot\text{s}^{-1}$ . (Bottom left and right): (Bottom left and right): Frequency dependence of the in-phase ( $\chi'_M$ ) and out-of-phase ( $\chi''_M$ ) AC susceptibility, respectively, measured with an applied DC field of 0.1 T at the indicated frequencies. Figure taken from reference 71.

## 1.9 Conclusions

These results demonstrate that magnetically characterized  $f$ -electron-containing species can display magnetic exchange coupling interactions in polymetallic clusters. Also, the utilization of uranium-containing compounds allows for isolation of discrete molecules possessing large(r) magnetic anisotropy. This is of utmost importance to improving the working temperatures of SMMs. From these examples it seems clear that simple low-nuclearity clusters may serve as the key to unraveling the complex interactions that give rise to magnetic exchange coupling in actinide-containing molecules.

Magnetic investigations of complexes of U(III) and U(IV) ions indicate that ligand-field effects impart perturbations on the spin-orbit coupling present in actinide systems. As a result, the magnetic properties of these systems are extremely complex. However, when magnetic data can be fit, the combined presence of magnetic anisotropy and magnetic exchange interactions suggests that actinide-containing compounds may be ripe for application and further studies are warranted.

### **1.10 Overview of Work to be Presented**

Described herein are further research efforts relating to the synthesis and characterization of novel uranium-containing complexes that display increased magnetic anisotropy. The main focus of this work is to develop the methodology needed to prepare paramagnetic uranium-containing compounds supported by ethynylbenzene bridging ligands. In Chapter 2, the preparation and magnetic property investigations of a structurally related family of mono-, di- and trinuclear U(IV) aryl acetylide complexes are presented. Efforts to study the magnetic correlations as a result of cubic ligands fields on [(dmpe)<sub>2</sub>U]-containing complexes that may serve as interesting starting materials for other U-containing complexes are presented in Chapter 3. In Chapter 4, eight- and nine-coordinate [(dmpe)<sub>2</sub>U]-arylacetylide complexes are presented for use as potential building blocks for larger topologies. In Chapter 5 an interesting effect of the angular dependence of U–Cl···H interactions was observed. As in most synthetic chemistry, inorganic synthesis is incredibly challenging. During my tenure at Colorado State University I have explored additional synthetic routes that deserve additional attention by future group members. In this regard, some preliminary results and suggestions for future research are presented in Chapter 6.

## 1.11 References

- (1) Areal Density.  
[http://www.pcmag.com/encyclopedia\\_term/0,2542,t=areal+density&i=37970,00.asp](http://www.pcmag.com/encyclopedia_term/0,2542,t=areal+density&i=37970,00.asp) (accessed July 30, 2011).
- (2) Mueller, S., *Upgrading and Repairing PCs, 15th Anniversary Edition*. Que: 2003; p 1608.
- (3) Toshiba Introduces Industry's Highest Areal Density 2.5-inch 750GB Hard Disk Drives. [http://www.toshiba.co.jp/about/press/2010\\_03/pr2501.htm](http://www.toshiba.co.jp/about/press/2010_03/pr2501.htm) (accessed June 30, 2011).
- (4) Eschenfe.Ah, *J. Appl. Phys.* **1970**, *41*, 1372.
- (5) Wildmann, M., *IEEE Trans. Mag.* **1974**, *10*, 509.
- (6) Sessoli, R.; Tsai, H. L.; Schake, A. R.; Wang, S. Y.; Vincent, J. B.; Folting, K.; Gatteschi, D.; Christou, G.; Hendrickson, D. N., *J. Am. Chem. Soc.* **1993**, *115*, 1804.
- (7) Marvaud, V.; Herrera, J. M.; Barilero, T.; Tuyeras, F.; Garde, R.; Sculler, A.; Decroix, C.; Cantuel, M.; Desplanches, C., *Mon. Chem.* **2003**, *134*, 149.
- (8) Gatteschi, D.; Sessoli, R.; Cornia, A., *Chem. Commun.* **2000**, 725.
- (9) Hoffert, W. A. Synthesis and Characterization of Low-Dimensional Paramagnetic Acetylide Complexes. Colorado State University, Fort Collins, 2011.
- (10) Sessoli, R.; Gatteschi, D.; Caneschi, A.; Novak, M. A., *Nature* **1993**, *365*, 141.
- (11) Rinehart, J. D.; Fang, M.; Evans, W. J.; Long, J. R., *Nat. Chem.* **2011**, *3*, 538.
- (12) Muller, A.; Peters, F.; Pope, M. T.; Gatteschi, D., *Chem. Rev.* **1998**, *98*, 239.
- (13) Buznli, J. C. G.; Piguet, C., *Chem. Rev.* **2002**, *102*, 1897.

- (14) Benelli, C.; Gatteschi, D., *Chem. Rev.* **2002**, *102*, 2369.
- (15) Rinehart, J. D.; Harris, T. D.; Kozimor, S. A.; Bartlett, B. M.; Long, J. R., *Inorg. Chem.* **2009**, *48*, 3382.
- (16) Long, J.; Habib, F.; Lin, P. H.; Korobkov, I.; Enright, G.; Ungur, L.; Wernsdorfer, W.; Chibotaru, L. F.; Murugesu, M., *J. Am. Chem. Soc.* **2011**, *133*, 5319.
- (17) Guo, F. S.; Liu, J. L.; Leng, J. D.; Meng, Z. S.; Lin, Z. J.; Tong, M. L.; Gao, S.; Ungur, L. V.; Chibotaru, L. F., *Chem. Eur. J.* **2011**, *17*, 2458.
- (18) Li, D. P.; Zhang, X. P.; Wang, T. W.; Ma, B. B.; Li, C. H.; Li, Y. Z.; You, X. Z., *Chem. Commun.* **2011**, *47*, 6867.
- (19) Hewitt, I. J.; Tang, J.; Madhu, N. T.; Anson, C. E.; Lan, Y.; Luzon, J.; Etienne, M.; Sessoli, R.; Powell, A. K., *Angew. Chem. Int. Ed.* **2010**, *49*, 6352.
- (20) Ke, H. S.; Xu, G. F.; Guo, Y. N.; Gamez, P.; Beavers, C. M.; Teat, S. J.; Tang, J. K., *Chem. Commun.* **2010**, *46*, 6057.
- (21) Gao, Y. J.; Xu, G. F.; Zhao, L.; Tang, J. K.; Llu, Z. L., *Inorg. Chem.* **2009**, *48*, 11495.
- (22) Andruh, M.; Costes, J. P.; Diaz, C.; Gao, S., *Inorg. Chem.* **2009**, *48*, 3342.
- (23) Huang, Y. G.; Jiang, F. L.; Hong, M. C., *Coord. Chem. Rev.* **2009**, *253*, 2814.
- (24) Ishikawa, N., Phthalocyanine-Based Magnets. In *Functional Phthalocyanine Molecular Materials*, Jiang, J., Ed. 2010; Vol. 135, pp 211.
- (25) Reinoso, S., *Dalton Trans.* **2011**, *40*, 6610.
- (26) Sessoli, R.; Powell, A. K., *Coord. Chem. Rev.* **2009**, *253*, 2328.
- (27) Zhang, X. H.; Wang, S. P., *Progress in Chemistry* **2010**, *22*, 1709.

- (28) Ishikawa, N.; Sugita, M.; Ishikawa, T.; Koshihara, S.; Kaizu, Y., *J. Phys. Chem. B* **2004**, *108*, 11265.
- (29) AlDamen, M. A.; Cardona-Serra, S.; Clemente-Juan, J. M.; Coronado, E.; Gaita-Arino, A.; Marti-Gastaldo, C.; Luis, F.; Montero, O., *Inorg. Chem.* **2009**, *48*, 3467.
- (30) Lemaire, M. T., *Pure Appl. Chem.* **2011**, *83*, 141.
- (31) Gonidec, M.; Biagi, R.; Corradini, V.; Moro, F.; De Renzi, V.; del Pennino, U.; Summa, D.; Muccioli, L.; Zannoni, C.; Amabilino, D. B.; Veciana, J., *J. Am. Chem. Soc.* **2011**, *133*, 6603.
- (32) Caldeira, A. O.; Leggett, A. J., *Phys. Rev. Lett.* **1981**, *46*, 211.
- (33) Leggett, A. J.; Chakravarty, S.; Dorsey, A. T.; Fisher, M. P. A.; Garg, A.; Zwerger, W., *Rev. Mod. Phys.* **1987**, *59*, 1.
- (34) Pasatoiu, T. D.; Sutter, J. P.; Madalan, A. M.; Fella, F. Z. C.; Duhayon, C.; Andruh, M., *Inorg. Chem.* **2011**, *50*, 5890.
- (35) Mishra, A.; Wernsdorfer, W.; Abboud, K. A.; Christou, G., *J. Am. Chem. Soc.* **2004**, *126*, 15648.
- (36) Mishra, A.; Tasiopoulos, A. J.; Wernsdorfer, W.; Abboud, K. A.; Christou, G., *Inorg. Chem.* **2007**, *46*, 3105.
- (37) Shiga, T.; Ohba, M.; Okawa, H., *Inorg. Chem. Commun.* **2003**, *6*, 15.
- (38) Yuan, Y. P.; Wang, R. Y.; Kong, D. Y.; Mao, J. G.; Clearfield, A., *J. Solid State Chem.* **2005**, *178*, 2030.
- (39) He, F.; Tong, M. L.; Chen, X. M., *Inorg. Chem.* **2005**, *44*, 8285.
- (40) Shi, W.; Chen, X. Y.; Zhao, B.; Yu, A.; Song, H. B.; Cheng, P.; Wang, H. G.; Liao, D. Z.; Yan, S. P., *Inorg. Chem.* **2006**, *45*, 3949.

- (41) Mereacre, V. M.; Ako, A. M.; Clerac, R.; Wernsdorfer, W.; Filoti, G.; Bartolome, J.; Anson, C. E.; Powell, A. K., *J. Am. Chem. Soc.* **2007**, *129*, 9248.
- (42) Ako, A. M.; Mereacre, V.; Clerac, R.; Hewitt, I. J.; Lan, Y. H.; Anson, C. E.; Powell, A. K., *Dalton Trans.* **2007**, 5245.
- (43) Gheorghe, R.; Costes, J. P.; Shova, S.; Andruh, M., *Rev. Roum. Chim.* **2007**, *52*, 753.
- (44) Li, P. X.; Mao, J. G., *Cryst. Growth Des.* **2008**, *8*, 3385.
- (45) Chandrasekhar, V.; Pandian, B. M.; Boomishankar, R.; Steiner, A.; Viftal, J. J.; Hourri, A.; Clerac, R., *Inorg. Chem.* **2008**, *47*, 4918.
- (46) Wang, M.; Yuan, D. Q.; Ma, C. B.; Yuan, M. J.; Hu, M. Q.; Li, N.; Chen, H.; Chen, C. N.; Liu, Q. T., *Dalton Trans.* **2010**, *39*, 7276.
- (47) Mori, F.; Nyui, T.; Ishida, T.; Nogami, T.; Choi, K. y.; Nojiri, H., *J. Am. Chem. Soc.* **2006**, *128*, 1440.
- (48) Peristeraki, T.; Samios, M.; Siczek, M.; Lis, T.; Milios, C. J., *Inorg. Chem.* **2011**, *50*, 5175.
- (49) Gu, Z. G.; Fang, H. C.; Yin, P. Y.; Tong, L.; Ying, Y.; Hu, S. J.; Li, W. S.; Cai, Y. P., *Cryst. Growth Des.* **2011**, *11*, 2220.
- (50) Papatriantafyllopoulou, C.; Wernsdorfer, W.; Abboud, K. A.; Christou, G., *Inorg. Chem.* **2011**, *50*, 421.
- (51) Rigaux, G.; Inglis, R.; Morrison, S.; Prescimone, A.; Cadiou, C.; Evangelisti, M.; Brechin, E. K., *Dalton Trans.* **2011**, *40*, 4797.
- (52) Feltham, H. L. C.; Clérac, R.; Powell, A. K.; Brooker, S., *Inorg. Chem.* **2011**, *50*, 4232.
- (53) Crosswhite, H. M.; Crosswhite, H.; Carnall, W. T.; Paszek, A. P., *J. Chem. Phys.* **1980**, *72*, 5103.

- (54) Costes, J. P.; Dahan, F.; Dupuis, A.; Laurent, J. P., *Chem. Eur. J.* **1998**, *4*, 1616.
- (55) Kahn, M. L.; Mathoniere, C.; Kahn, O., *Inorg. Chem.* **1999**, *38*, 3692.
- (56) Gaunt, A. J.; Reilly, S. D.; Enriquez, A. E.; Scott, B. L.; Ibers, J. A.; Sekar, P.; Ingram, K. I. M.; Kaltsoyannis, N.; Neu, M. P., *Inorg. Chem.* **2008**, *47*, 29.
- (57) Schelter, E. J.; Veauthier, J. M.; Thompson, J. D.; Scott, B. L.; John, K. D.; Morris, D. E.; Kiplinger, J. L., *J. Am. Chem. Soc.* **2006**, *128*, 2198.
- (58) Rosen, R. K.; Andersen, R. A.; Edelstein, N. M., *J. Am. Chem. Soc.* **1990**, *112*, 4588.
- (59) Graves, C. R.; Yang, P.; Kozimor, S. A.; Vaughn, A. E.; Clark, D. L.; Conradson, S. D.; Schelter, E. J.; Scott, B. L.; Thompson, J. D.; Hay, P. J.; Morris, D. E.; Kiplinger, J. L., *J. Am. Chem. Soc.* **2008**, *130*, 5272.
- (60) Wybourne, B. G., *Spectroscopic Properties of Rare Earths*. Interscience Publishers: New York, 1965.
- (61) Ovchinnikov, A. A., *Theor. Chim. Acta* **1978**, *47*, 297.
- (62) Weyland, T.; Lapinte, C.; Frapper, G.; Calhorda, M. J.; Halet, J. F.; Toupet, L., *Organometallics* **1997**, *16*, 2024.
- (63) Rinehart, J. D.; Bartlett, B. M.; Kozimor, S. A.; Long, J. R., *Inorg. Chimi. Acta* **2008**, *361*, 3534.
- (64) Kozimor, S. A.; Bartlett, B. M.; Rinehart, J. D.; Long, J. R., *J. Am. Chem. Soc.* **2007**, *129*, 10672.
- (65) Maria, L.; Campello, M. P.; Domingos, A.; Santos, I.; Andersen, R., *J. Chem. Soc., Dalton Trans.* **1999**, 2015.
- (66) Rinehart, J. D.; Long, J. R., *J. Am. Chem. Soc.* **2009**, *131*, 12558.

- (67) Ishikawa, N.; Sugita, M.; Ishikawa, T.; Koshihara, S.; Kaizu, Y., *J. Am. Chem. Soc.* **2003**, *125*, 8694.
- (68) Lin, P. H.; Burchell, T. J.; Cleÿrac, R.; Murugesu, M., *Angew. Chem. Int. Ed.* **2008**, *47*, 8848.
- (69) Skomski, R., *Simple Models of Magnetism*. Oxford University Press: Oxford, 2008.
- (70) Sugita, M.; Ishikawa, N.; Ishikawa, T.; Koshihara, S.; Kaizu, Y., *Inorg. Chem.* **2006**, *45*, 1299.
- (71) Mills, D. P.; Moro, F.; McMaster, J.; van Slageren, J.; Lewis, W.; Blake, A. J.; Liddle, S. T., *Nat. Chem.* **2011**, *3*, 454.
- (72) Jones, E. R.; Hendrick, M.; Stone, J. A.; Karraker, D. G., *J. Chem. Phys.* **1974**, *60*, 2088.
- (73) Gatteschi, D.; Sessoli, R.; Villain, J., *Molecular nanomagnets*. Oxford University Press: Oxford, 2006.
- (74) Yang, E. C.; Wernsdorfer, W.; Zakharov, L. N.; Karaki, Y.; Yamaguchi, A.; Isidro, R. M.; Lu, G. D.; Wilson, S. A.; Rheingold, A. L.; Ishimoto, H.; Hendrickson, D. N., *Inorg. Chem.* **2006**, *45*, 529.

## Chapter 2. Experimental Evidence for Magnetic Exchange in Di- and Trinuclear Uranium(IV) Ethynylbenzene Complexes

### 2.1 Introduction

The electronic structures of actinide-containing complexes feature a rich interplay of orbital interactions, spin-orbit coupling and electron correlation; the understanding of which is critical to using actinides in fuels or catalysis, and to settle longstanding questions about the role of *f* orbitals in metal-ligand bonding.<sup>1-10</sup> The magnetic properties of actinide complexes represent a mixing of characteristics normally associated with transition metal ions (e.g. superexchange) and lanthanides (e.g. spin-orbit coupling),<sup>11</sup> and can be used to probe electronic structure in detail. Thus, combining magnetochemical studies with high level calculations offers a pathway for understanding this unique group of compounds.

In addition to fundamental interest in electronic structure, recent work in *f*-element magnetochemistry is motivated by the potential for these species to contribute to the development of single-molecule magnets (SMMs).<sup>12-15</sup> These monodisperse superparamagnetic particles exhibit a thermal barrier to magnetic spin reorientation, and may eventually find use in data storage,<sup>16,17</sup> quantum computing<sup>18-23</sup> or refrigeration applications.<sup>24,25</sup> However, their exploitation awaits variants that can display magnetic bistability at more practical temperatures than the ~4.5 K currently observed.<sup>15</sup> Here, incorporation of paramagnetic lanthanide ions have received attention, since spin-orbit coupling and relativistic effects common to those ions can engender the large single-ion

anisotropies necessary for slow magnetization relaxation behavior.<sup>26-36</sup> Several complexes have properties consistent with SMMs, such as the observation of frequency-dependent out-of-phase AC susceptibility signals.<sup>37-42</sup> A drawback to the approach is that the “buried”  $4f$  orbitals in lanthanides participate only weakly in bonding interactions, leading to marginal exchange coupling with neighboring spin centers;<sup>43-45</sup> this ultimately limits the maximum temperature at which the magnetic bistability occurs.

Alternatively, all of the abovementioned attributes can be found in the early actinides, with the added benefit of larger, more diffuse  $5f$  orbitals capable of stronger bonding and exchange interactions.<sup>46-51</sup> However, the dynamic magnetic properties of actinide complexes are less well known, in part due to difficulties in determining ligand field parameters and the complications arising from relativistic effects as well as  $d$  and  $f$  electron correlations.<sup>38,52</sup> Nevertheless, recent reports indicate that synthetic efforts toward paramagnetic actinide-containing assemblies offer diverse and interesting magnetism. A  $\text{Th}_6\text{Mn}_{10}$  cluster shows that even  $f^0$  species may contribute to the observation of frequency-dependent out-of-phase susceptibility signals.<sup>26</sup> Coupling between uranium and transition metal ions has been investigated, and ferromagnetic communication between transition metal ions and cubic U(IV) centers has been demonstrated in molecular species.<sup>11,47-50,53-56</sup> Also relevant to the work to be presented here, Andersen’s dinuclear complex  $[\text{((MeC}_5\text{H}_4)_3\text{U)}_2(\mu\text{-1,4-N}_2\text{C}_6\text{H}_4)]$  illustrates the viability of U(V)-U(V) magnetic exchange via  $f$  orbitals.<sup>57</sup> Further advancement in this area hinges on improving synthetic control over paramagnetic uranium ligand field and spin-orbit parameters, so as to optimize exchange coupling between uranium and transition-metal species, and ultimately to control molecular magnetic anisotropy.

The purpose of the present study is to investigate coordination geometry effects on U(IV) magnetic properties. It is well known that the  $5f^2$  electronic configuration gives diamagnetic ground states when the U(IV) coordination geometry is octahedral, but exhibits paramagnetic ground states ( $S = 1$ ) when the U(IV) ion is surrounded by a cubic ligand field.<sup>48-50,52-56,58,59</sup> We wondered if a trigonal bipyramidal (tbp) coordination geometry may offer another way for U(IV) to show paramagnetic ground states. Here, group theory predicts a doubly degenerate  $e''$  ground state, which should result in an  $S = 1$  species.<sup>58</sup> We note that predicting the level of splitting of the  $f$  orbitals due to ligand field effects alone is complicated by the substantial spin-orbit coupling present in the actinides.<sup>60</sup> It is also known that many low symmetry U(IV) complexes give “non-magnetic” ground states.<sup>61</sup> Nevertheless, monomeric tbp U(IV) phenylacetylide complexes in which triamidoamine ( $NN'_3$ ) ligands occupy the other coordination sites offer synthetic precedent for enforcing 5-coordinate geometries,<sup>62-66</sup> and to our knowledge the magnetic properties of these species have not been studied in detail. In addition, ethynylbenzene ligands have been demonstrated to be efficient communicators of spin information between paramagnetic transition metal species.<sup>67,68</sup> Thus, the combination of  $[(NN'_3)U]$  species with bridging aryl acetylide ligands may be expected to give rise to di- and trinuclear assemblies by which uranium magnetochemistry may be tuned structurally.

Herein, we describe the preparation and (magneto)structural characterization of di- and trinuclear penta- and hexacoordinate U(IV) species bridged by aryl acetylides. The experimental and theoretical assessment of exchange coupling in these species provides evidence for weak exchange coupling operative between pentacoordinate U(IV) centers.

## 2.2 Division of Labor Section

All experimental work and characterization was performed by Brian S. Newell. Density functional theory calculations were done by Anthony K. Rappé. *Inorg. Chem.* **2010**, *49*, 1595–1605.

## 2.3 Experimental Section

**2.3.1 Preparation of Compounds.** All manipulations were carried out either inside a dinitrogen-filled glove box (MBRAUN Labmaster 130) or via standard Schlenk techniques on a N<sub>2</sub> manifold. Pentane was distilled over sodium metal, degassed (freeze-pump-thawed 3 × 20 min) and stored under an atmosphere of dinitrogen. All other solvents were reagent grade, passed through alumina, degassed and stored under dinitrogen. The compounds UCl<sub>4</sub>,<sup>69</sup> [Li<sub>3</sub>(NN′<sub>3</sub>)(THF)<sub>3</sub>] (where NN′<sub>3</sub> = [N(CH<sub>2</sub>CH<sub>2</sub>NSi<sup>i</sup>BuMe<sub>2</sub>)<sub>3</sub>]),<sup>70</sup> [(NN′<sub>3</sub>)UCl],<sup>71</sup> [(*bit*-NN′<sub>3</sub>)U] (where *bit*-NN′<sub>3</sub> = [N(CH<sub>2</sub>CH<sub>2</sub>NSi<sup>i</sup>BuMe<sub>2</sub>)<sub>2</sub>(CH<sub>2</sub>CH<sub>2</sub>Si<sup>i</sup>BuMeCH<sub>2</sub>)])<sup>63</sup>, [(NN′<sub>3</sub>)U(CCPH)] (**2.3**),<sup>63</sup> and 1,3,5-triethynylbenzene<sup>72</sup> (H<sub>3</sub>TEB) were prepared according to the literature, except that sublimation was not carried out on the [(NN′<sub>3</sub>)UCl] complex. The acetylene ligands 1,4- and 1,3-diethynylbenzene (*p*-H<sub>2</sub>DEB and *m*-H<sub>2</sub>DEB, respectively) were purchased from Sigma and were sublimed or distilled, respectively, before use. The lithiated acetylides, lithium phenylacetylide and Li<sub>2</sub>(*p*-DEB), were synthesized by reacting the appropriate stoichiometric amount of *n*-BuLi with the corresponding free acetylene in pentane. The solids were collected, dried in vacuo, and used without further characterization. All other reagents were obtained from commercial vendors and used without further purification.

**Caution!** Depleted uranium (primary isotope <sup>238</sup>U) is a weak α emitter (4.197 MeV) with a half-life of 4.47 × 10<sup>9</sup> years; manipulations and reactions should be carried out in

monitored fume hoods or in an inert atmosphere glove box in a radiation laboratory equipped with  $\alpha$ - and  $\beta$ -counting equipment.

**[(NN')<sub>3</sub>U(CPh)<sub>2</sub>(Li·THF)] (2.1).** Solid, recrystallized [(NN')<sub>3</sub>UCl] (0.198 g, 0.261 mmol) was combined with lithium phenylacetylide (0.057 g, 0.53 mmol) and 15 mL of pentane. The yellow-green mixture was stirred at room temperature for 1 h. Subsequent addition of 2 mL of THF resulted in a color change to red-brown. The mixture was stirred at room temperature for 1 h, and then filtered to remove LiCl. Volatiles were removed from the filtrate in vacuo to afford a red-brown residue. This was extracted into 10 mL of pentane, concentrated to ca. 5 mL under reduced pressure, and left at ambient temperature for 8 h, at which point several red-brown crystals were observed. The product was collected by filtration, dried in vacuo, and recrystallized from hot pentane to afford a deep red crystalline solid (0.121 g, 46 % yield based on [(NN')<sub>3</sub>UCl]). Single crystals suitable for X-ray analysis were grown from a concentrated pentane solution maintained at -34 °C for 8 h. Absorption spectrum (pentane)  $\lambda_{\max}$  ( $\epsilon_M$ ): 686 nm (95 L·mol<sup>-1</sup>·cm<sup>-1</sup>). <sup>1</sup>H NMR (293 K, C<sub>6</sub>D<sub>6</sub>):  $\delta$  8.09 (br, 6H, CH<sub>2</sub>), 7.39 (d, 4H, THF), 7.06 (br, 4H, Ar-H), 6.90 (m, 6H, Ar-H), 5.22 (s, 27H, <sup>t</sup>Bu), 4.01 (s, 18H, SiCH<sub>2</sub>), 3.66 (br, 8H, THF), 1.50 (d, 4H, THF), 1.42 (br, 8H, THF) -16.39 ppm (br, 6H, CH<sub>2</sub>). IR (mineral oil):  $\nu_{C\equiv C}$  2044 cm<sup>-1</sup>. Magnetic susceptibility (SQUID, 300 K):  $\mu_{\text{eff}} = 2.14 \mu_B$ . Anal. Calcd for C<sub>44</sub>H<sub>75</sub>N<sub>4</sub>OSi<sub>3</sub>ULi: C, 52.57; H, 7.52; N, 5.57. Found: C, 52.38; H, 7.76; N, 5.52.

**[(NN')<sub>3</sub>U<sub>2</sub>(p-DEB)(THF)] (2.2).** Solid [(NN')<sub>3</sub>UCl] (0.500 g, 0.659 mmol) was combined with Li<sub>2</sub>(p-DEB) (0.045 g, 0.330 mmol) and 5 mL of toluene. The resulting brown-green mixture was stirred at ambient temperature for 8 h, filtered to remove LiCl, concentrated to ca. 2 mL under reduced pressure, and then cooled to -34 °C. After 8 h, a

yellow-green crystalline precipitate was observed. The crude product was collected by filtration, dried in vacuo, and recrystallized from hot pentane to afford a yellow crystalline solid (0.152 g, 28 % yield based on  $[(\text{NN}'_3)\text{UCl}]$ ). Single crystals of  $[(\text{NN}'_3)_2\text{U}_2(p\text{-DEB})(\text{THF})_2]\cdot\text{C}_5\text{H}_{12}$  (**2.2**·THF·C<sub>5</sub>H<sub>12</sub>) suitable for X-ray analysis were grown from a concentrated pentane solution maintained at  $-34\text{ }^\circ\text{C}$  for 8 h. Absorption spectrum (pentane)  $\lambda_{\text{max}}$  ( $\epsilon_{\text{M}}$ ): 501 (406) 528 (326), 587 (212), 606 (176), 687 nm (320 L·mol<sup>-1</sup>·cm<sup>-1</sup>). IR (mineral oil):  $\nu_{\text{C}=\text{C}}$  2061 cm<sup>-1</sup>. Magnetic susceptibility (SQUID, 300 K):  $\mu_{\text{eff}} = 4.73\ \mu_{\text{B}}$ . Anal. Calcd for C<sub>62</sub>H<sub>126</sub>N<sub>8</sub>OSi<sub>6</sub>U<sub>2</sub>: C, 45.29; H, 7.72; N, 6.81. Found: C, 45.07; H, 7.22; N, 6.81.

**$[(\text{NN}'_3)\text{U}(\text{CCPh})]$  (2.3).** A solution of phenylacetylene in 1 mL of pentane (80  $\mu\text{L}$ , 0.73 mmol) was added dropwise to a stirred solution of  $[(\text{bit-NN}'_3)\text{U}]$  (0.539 g, 0.745 mmol) in 10 mL of pentane at  $-78\text{ }^\circ\text{C}$ , and the resulting yellow-green solution was warmed to room temperature and stirred for 3 h. The solution was filtered, concentrated to ca. 2 mL under reduced pressure, and then cooled to  $-34\text{ }^\circ\text{C}$ . After 8 h, a yellow-green microcrystalline precipitate was observed. The crude product was collected by filtration, dried in vacuo, and recrystallized from hot pentane to afford a yellow-green crystalline solid (0.400 g, 65 % based on  $[(\text{bit-NN}'_3)\text{U}]$ ) Single crystals suitable for X-ray analysis were grown from a concentrated pentane solution maintained at  $-34\text{ }^\circ\text{C}$  for 8 h. Absorption spectrum (pentane)  $\lambda_{\text{max}}$  ( $\epsilon_{\text{M}}$ ): 281 (4800), 485 (42), 503 (44), 529 (48), 587 (26), 614 (19), 621 (19), 629 (18), 650 (16), 654 (16), 658 (17), 687 (75), 691 (70), 719 (20), 803 (12), 828 (13), 880 (12), 924 (12), 961 nm (10 L·mol<sup>-1</sup>·cm<sup>-1</sup>). <sup>1</sup>H NMR (293 K, C<sub>6</sub>D<sub>6</sub>):  $\delta$  8.09 (s, 6H, CH<sub>2</sub>), 5.23 (s, 27H, <sup>t</sup>Bu), 4.02 (s, 18H, SiCH<sub>2</sub>), 3.37 (m, 2H, Ar-H), 1.52 (d, 2H, Ar-H), 1.51 (s, 1H, Ar-H),  $-16.35$  ppm (s, 6H, CH<sub>2</sub>). IR (mineral oil):  $\nu_{\text{C}=\text{C}}$

2054  $\text{cm}^{-1}$ . Magnetic susceptibility (SQUID, 300 K):  $\mu_{\text{eff}} = 3.12 \mu_{\text{B}}$ . Anal. Calcd for  $\text{C}_{32}\text{H}_{62}\text{N}_4\text{Si}_3\text{U}$ : C, 46.58; H, 7.57; N, 6.79. Found: C, 46.50; H, 7.21; N, 6.83.

**[( $\text{NN}'_3$ ) $_2\text{U}_2(m\text{-DEB})$ ] (2.4).** A solution of *m*-H<sub>2</sub>DEB in 1 mL of pentane (37  $\mu\text{L}$ , 0.28 mmol) was added dropwise to a stirred solution of [(*bit*- $\text{NN}'_3$ )U] (0.407 g, 0.563 mmol) in 10 mL of pentane at  $-78\text{ }^\circ\text{C}$ , and the resulting yellow-green solution was warmed to room temperature and stirred for 3 h. The solution was filtered, concentrated to ca. 2 mL under reduced pressure, and then cooled to  $-34\text{ }^\circ\text{C}$ . After 8 h, a yellow-green microcrystalline precipitate was observed. The crude product was collected by filtration, dried in vacuo, and recrystallized from hot pentane to afford a yellow-green crystalline solid (0.336 g, 76 % based on *m*-H<sub>2</sub>DEB). Single crystals suitable for X-ray analysis were grown from a concentrated pentane solution maintained at  $-34\text{ }^\circ\text{C}$  for 8 h. Absorption spectrum (pentane)  $\lambda_{\text{max}}$  ( $\epsilon_{\text{M}}$ ): 281 (11400) 485 (73), 503 (74), 529 (78), 587 (35), 614 (21), 629 (20), 650 (17), 658 (18), 687 (138), 691 (124), 719 (26), 803 (11), 828 (14), 881 (13), 925 (14), 961 nm ( $11\text{ L}\cdot\text{mol}^{-1}\cdot\text{cm}^{-1}$ ).  $^1\text{H}$  NMR (293 K,  $\text{C}_6\text{D}_6$ ):  $\delta$  7.90 (s, 12H,  $\text{CH}_2$ ), 4.77 (s, 54H,  $^t\text{Bu}$ ), 4.62 (br, 2H, Ar-*H*), 3.44 (s, 36H,  $\text{SiCH}_2$ ),  $-0.52$  (t, 1H, Ar-*H*),  $-3.96$  (s, 1H, Ar-*H*),  $-16.36$  ppm (s, 12H,  $\text{CH}_2$ ). IR (mineral oil):  $\nu_{\text{C}=\text{C}}$  2053  $\text{cm}^{-1}$ . Magnetic susceptibility (SQUID, 300 K):  $\mu_{\text{eff}} = 4.49 \mu_{\text{B}}$ . Anal. Calcd for  $\text{C}_{58}\text{H}_{118}\text{N}_8\text{Si}_6\text{U}_2$ : C, 44.31; H, 7.57; N, 7.12. Found: C, 44.72; H, 7.65; N, 6.69.

**[( $\text{NN}'_3$ ) $_2\text{U}_2(p\text{-DEB})$ ] (2.5).** A solution of *p*-H<sub>2</sub>DEB in pentane (0.033 g, 0.26 mmol) was added dropwise to a stirred solution of [(*bit*- $\text{NN}'_3$ )U] (0.402 g, 0.556 mmol) in 10 mL pentane at  $-78\text{ }^\circ\text{C}$ , resulting in the precipitation of a yellow solid. This mixture was warmed to room temperature and stirred for 3 h. The yellow precipitate was collected by filtration, dried in vacuo, and recrystallized from hot toluene to afford a yellow-green

crystalline solid (0.362 g, 89 % based on *p*-H<sub>2</sub>DEB). Single crystals suitable for X-ray analysis were grown from a concentrated toluene solution maintained at -34 °C for 8 h. Absorption spectrum (toluene)  $\lambda_{\max}$  ( $\epsilon_M$ ): 312 (20700), 329 (15800), 363 (4200), 503 (77), 529 (116), 587 (47), 614 (30), 621 (31), 629 (28), 650 (24), 658 (25), 687 (150), 691 (135), 719 (34), 803 (13), 828 (16), 880 (15), 924 (15), 961 nm (12 L·mol<sup>-1</sup>·cm<sup>-1</sup>). <sup>1</sup>H NMR (293 K, C<sub>6</sub>D<sub>6</sub>):  $\delta$  8.07 (s, 12H, CH<sub>2</sub>), 7.70 (br, 2H, Ar-H), 5.54 (s, 54H, <sup>t</sup>Bu), 4.65 (s, 36H, SiCH<sub>2</sub>), 2.70 (br, 2H, Ar-H), -16.45 (br, 2H, Ar-H), -18.04 ppm (s, 12H, CH<sub>2</sub>). IR (mineral oil)  $\nu_{C=C}$  2060 cm<sup>-1</sup>. Magnetic susceptibility (SQUID, 300 K):  $\mu_{\text{eff}} = 4.45 \mu_B$ . Anal. Calcd for C<sub>58</sub>H<sub>118</sub>N<sub>8</sub>Si<sub>6</sub>U<sub>2</sub>: C, 44.31; H, 7.57; N, 7.12. Found: C, 44.24; H, 7.53; N, 6.96.

**[(NN')<sub>3</sub>U<sub>3</sub>(TEB)] (2.6).** A solution of H<sub>3</sub>TEB in 1 mL of pentane (0.020 g, 0.13 mmol) was added dropwise to a stirred solution of [(*bit*-NN')<sub>3</sub>U] (0.306 g, 0.423 mmol) in 10 mL of pentane at -78 °C, and the resulting yellow-green solution was warmed to room temperature and stirred for 3 h. The solution was filtered, concentrated to ca. 2 mL under reduced pressure, and then cooled to -34 °C. After 8 h, a yellow-green microcrystalline precipitate was observed. The crude product was collected by filtration, dried in vacuo, and recrystallized from hot pentane to afford a yellow-green crystalline solid (0.243 g, 79 %, based on H<sub>3</sub>TEB). Single crystals suitable for X-ray analysis were grown from a concentrated pentane solution maintained at -34 °C for 8 h. Absorption spectrum (pentane)  $\lambda_{\max}$  ( $\epsilon_M$ ): 292 (21000), 503 (11), 529 (114), 587 (44), 614 (23), 621 (23), 629 (20), 650 (16), 658 (17), 687 (198), 691 (177), 719 (33), 803 (8), 828 (13), 880 (12), 924 (13), 961 nm (9 L·mol<sup>-1</sup>·cm<sup>-1</sup>). IR (mineral oil):  $\nu_{C=C}$  2054 cm<sup>-1</sup>. Magnetic

susceptibility (SQUID, 300 K):  $\mu_{\text{eff}} = 5.45 \mu_{\text{B}}$ . Anal. Calcd for  $\text{C}_{84}\text{H}_{184}\text{N}_{12}\text{Si}_9\text{U}_3$ : C, 43.50; H, 7.56; N, 7.22. Found: C, 43.14; H, 7.44; N, 6.82.

**2.3.2 X-ray Structure Determination.** Structures were determined for the compounds listed in Table 2.1. Single crystals were coated with Paratone-N oil in the glove box and mounted under a cold stream of dinitrogen gas. Single crystal X-ray diffraction data were acquired on a Bruker Kappa APEX II CCD diffractometer with  $\text{MoK}\alpha$  radiation ( $\lambda = 0.71073 \text{ \AA}$ ) and a graphite monochromator. Initial lattice parameters were obtained from a least-squares analysis of more than 100 reflections; these parameters were later refined against all data. None of the crystals showed significant decay during data collection. Data were integrated and corrected for Lorentz and polarization effects using SAINT, and semiempirical absorption corrections were applied using SADABS.<sup>73</sup> Space group assignments were based on systematic absences,  $E$  statistics, and successful refinement of the structures. Structures were solved by direct methods or Patterson maps and were refined with the aid of successive Fourier difference maps against all data using the SHELXTL 6.14 software package.<sup>74</sup> Thermal parameters for all atoms with  $Z > 3$  were refined anisotropically, except for those disordered over multiple partially occupied sites in the structures of **2.4**· $\text{C}_5\text{H}_{12}$  and **2.5**· $\text{C}_5\text{H}_{12}$  and solvate molecules in **2.5**· $\text{C}_5\text{H}_{12}$ . All hydrogen atoms were assigned to ideal positions and refined using a riding model with an isotropic thermal parameter 1.2 times that of the attached carbon atom (1.5 times for methyl hydrogens).

Data for **2.4**· $\text{C}_5\text{H}_{12}$  were truncated to 1.0  $\text{\AA}$  resolution during integration due to weak scattering. In the structure of **2.4**· $\text{C}_5\text{H}_{12}$ , one of the  $\text{Si}^i\text{BuMe}_2$  groups is disordered over two positions and refined to a 71:29 ratio. The methylene carbons (C29 and C30) of the

ligand with the disordered Si group as well as all of the carbon atoms of the pentane solvate molecule were refined anisotropically but restrained to have the same  $U_{ij}$  parameters.

Data for **2.5**·C<sub>5</sub>H<sub>12</sub> were truncated to 0.9 Å resolution during integration due to weak scattering. In the structure of **2.5**·C<sub>5</sub>H<sub>12</sub>, two of the Si(Me<sub>2</sub>)<sup>t</sup>Bu groups are disordered over two positions and refined to 65:35 and 73:27 site occupancy ratios. All chemically equivalent atoms were restrained to have the same  $U_{ij}$  parameters. The space between the uranium complexes shows severe solvent disorder. One pentane solvate molecule was found in Fourier difference maps and the thermal parameters of the carbon atoms were refined isotropically. SQUEEZE<sup>75</sup> was used to remove the remaining disordered components; approximately 0.25 equivalents of pentane (per formula unit) are estimated to be present in the void space. The final residual structure factors for the structure of **2.5**·C<sub>5</sub>H<sub>12</sub> are high owing to the relatively poor quality of the data.

Refinement of matrix scans for crystals of **2.6** give a primitive orthorhombic cell with the following unit cell parameters:  $a = 18.5219(7)$ ,  $b = 22.2851(8)$ ,  $c = 28.0242(10)$  Å and  $V = 11567(1)$  Å<sup>3</sup>. A preliminary refinement of **6** confirms the expected cluster connectivity, but the diffraction data are not of sufficient quality to afford a complete X-ray analysis. Selected bond distances and angles for crystals of compounds **2.1–2.5** are collected in Table 2.1. All other metric parameters can be found in Appendix 1.

**2.3.3 Magnetic Susceptibility Measurements.** Magnetic susceptibility measurements were collected using a Quantum Design MPMS XL SQUID magnetometer. DC magnetic susceptibility data were collected at temperatures ranging from 2 to 300 K at an applied field of 0.1 T. Powdered microcrystalline samples (**2.1**

(19.36 mg, 0.01926 mmol), **2.2** (21.60 mg, 0.01258 mmol), **2.3** (23.88 mg, 0.2894 mmol), **2.4** (10.41 mg, 0.006621 mmol), **2.5** (18.35 mg, 0.01167 mmol), **2.6** (15.85 mg, 0.006834 mmol)). were loaded into gelatin capsules in the glove box, inserted into a straw and transported to the SQUID instrument under dinitrogen. AC magnetic susceptibility data were collected at temperatures ranging from 2 to 5 K at an applied field of 0.1 T with various AC frequencies. Powdered microcrystalline samples were loaded into gelatin capsules in the glove box and suspended in Eicosane to prevent crystallite torqueing at high magnetic fields. Contributions to the magnetization from the gelatin capsule and the straw were measured independently and subtracted from the total measured signal. Data were corrected for diamagnetic contributions using Pascal's constants. Susceptibility data were fit with theoretical models using a relative error minimization routine (MAGFIT 3.1).<sup>76</sup> Reported coupling constants are based on exchange Hamiltonians of the form  $\hat{H} = -2J(\hat{S}_i \cdot \hat{S}_j)$ .

**2.3.4 Other Physical Measurements.** UV-visible absorption spectra were obtained in pentane or toluene solutions in an airtight glass cell of path length 1 cm on an Agilent 8453 spectrometer. <sup>1</sup>H NMR spectra were recorded using a Varian INOVA 500 MHz instrument, and the spectra were referenced internally using residual protio solvent resonances relative to tetramethylsilane ( $\delta = 0$  ppm). Infrared spectra were collected on a Thermo Nicolet 380 FTIR spectrometer as mineral oil mulls pressed between sodium chloride plates. EPR spectra were obtained using a continuous wave X-band Bruker EMX 200U instrument. Electrochemical measurements were conducted with a CH Instruments 1232A potentiostat/galvanostat, and the data were processed with CHI software (version 7.20). All experiments were performed in a glove box using a 20 mL

glass scintillation vial as the cell. The electrodes consisted of platinum wire microelectrode (0.250 mm diameter), platinum wire mesh counter, and Ag/Ag<sup>+</sup> reference electrodes. Solution concentrations employed during CV studies were typically 3 mM for the uranium complex and 0.1 M for the [TBA][B(Ar<sup>F</sup>)<sub>4</sub>] electrolyte. All potentials are reported versus the [Cp<sub>2</sub>Fe]<sup>+0</sup> couple. Elemental analyses were performed by Columbia Analytical Services, Tucson, AZ (compounds **2.2-2.6**) or by the Micro-Mass facility at the University of California, Berkeley (compound **2.1**).

**2.3.5 Electronic Structure Calculations.** Spin unrestricted B3LYP hybrid density functional studies<sup>77</sup> were carried out on model complexes of **2.3**, **2.4** and **2.5** where the <sup>t</sup>BuMe<sub>2</sub>Si substituents are replaced by H atoms and geometries optimized. Singlet states were described with broken symmetry representations. In a broken symmetry treatment  $\alpha$  and  $\beta$  orbitals of a given molecular orbital are allowed to be different, permitting the differential localization of  $\alpha$  and  $\beta$  spin sets.<sup>61</sup> For  $M_S = 0$  “singlet” states this model is not an eigenfunction of spin but is an admixture of spin states. The standard Noodleman spin projection formula ( $J = (E_{HS} - E_{BS}) / \langle S^2 \rangle$ ) can be used to estimate spin–spin coupling constants,  $J$ .<sup>78</sup> This treatment has been demonstrated to reproduce spin-spin ( $J$ ) coupling in transition metal complexes within a factor of two.<sup>79</sup> The Stuttgart RSC 1997 basis and effective core potential was employed for U, which incorporates scalar relativistic effects and replaces 60 core electrons.<sup>78-81</sup> Linear dependency issues and SCF convergence was improved by deletion of the outermost zeta=0.05 S, P, D, and F exponents. The 6-31g\* basis sets were used for C, H, and N atoms.<sup>82-84</sup> All calculations were carried out in the G03 suite of electronic structure codes.<sup>85</sup> Selected bond distances and angles for the

calculated structures are presented in Table 2.1. Coordinates for the calculated structures are provided in Appendix 1.

**Table 2.1.** Crystallographic data for compounds [(NN<sub>3</sub>)U(CCPPh)<sub>2</sub>(Li·THF)] (**2.1**), [(NN<sub>3</sub>)<sub>2</sub>U<sub>2</sub>(*p*-DEB)(THF)<sub>2</sub>]·C<sub>5</sub>H<sub>12</sub> (**2.2**·THF·C<sub>5</sub>H<sub>12</sub>), [(NN<sub>3</sub>)U(CCPPh)] (**2.3**), [(NN<sub>3</sub>)<sub>2</sub>U<sub>2</sub>(*m*-DEB)]·C<sub>5</sub>H<sub>12</sub> (**2.4**·C<sub>5</sub>H<sub>12</sub>), and [(NN<sub>3</sub>)<sub>2</sub>U<sub>2</sub>(*p*-DEB)]·C<sub>5</sub>H<sub>12</sub> (**2.5**·C<sub>5</sub>H<sub>12</sub>).

	<b>2.1</b>	<b>2.2</b> ·THF·C <sub>5</sub> H <sub>12</sub>	<b>2.3</b>	<b>2.4</b> ·C <sub>5</sub> H <sub>12</sub>	<b>2.5</b> ·C <sub>5</sub> H <sub>12</sub>
formula	C <sub>44</sub> H <sub>75</sub> N <sub>4</sub> O <sub>5</sub> Si <sub>3</sub> ULi	C <sub>66</sub> H <sub>134</sub> N <sub>8</sub> O <sub>2</sub> Si <sub>6</sub> U <sub>2</sub>	C <sub>32</sub> H <sub>62</sub> N <sub>4</sub> Si <sub>3</sub> U	C <sub>63</sub> H <sub>130</sub> N <sub>8</sub> Si <sub>6</sub> U <sub>2</sub>	C <sub>63</sub> H <sub>130</sub> N <sub>8</sub> Si <sub>6</sub> U <sub>2</sub>
formula wt	1005.32	1788.56	825.16	1644.35	1644.35
color, habit	red/brown needle	yellow/green block	yellow/green rod	yellow/green rod	yellow/green cube
<i>T</i> , K	100(2)	100(2)	100(2)	100(2)	100(2)
space group	<i>P</i> 2 <sub>1</sub> / <i>c</i>	<i>P</i> $\bar{1}$	<i>P</i> $\bar{1}$	<i>P</i> 2 <sub>1</sub> / <i>c</i>	<i>P</i> 2 <sub>1</sub> 2 <sub>1</sub> 2
<i>Z</i>	4	2	4	4	4
<i>a</i> , Å	14.6808(3)	16.6289(5)	12.4841(16)	21.6288(13)	23.2529(10)
<i>b</i> , Å	18.0721(4)	16.8054(4)	17.7695(8)	17.3104(10)	18.4727(8)
<i>c</i> , Å	18.8132(3)	17.4480(4)	18.0989(9)	22.1171(13)	19.1547(8)
$\alpha$ , deg	90	75.127(2)	89.375(3)	90	90
$\beta$ , deg	96.3540(10)	78.361(2)	89.013(3)	107.924(4)	90
$\gamma$ , deg	90	67.296(2)	77.136(3)	90	90
<i>V</i> , Å <sup>3</sup>	4960.72(17)	4317.19(19)	3913.5(3)	7878.8(8)	8227.8(6)
<i>d</i> <sub>calc</sub> , g/cm <sup>3</sup>	1.346	1.376	1.401	1.386	1.269
GOF	0.99	1.06	1.01	1.06	1.22
<i>R</i> <sub>1</sub> ( <i>wR</i> <sub>2</sub> ) <sup>b</sup> , %	3.36(6.29)	4.35(10.17)	3.42(9.38)	3.17(6.70)	10.54(25.78)

<sup>a</sup> Obtained with graphite-monochromated Mo K $\alpha$  ( $\lambda = 0.71073$  Å) radiation.

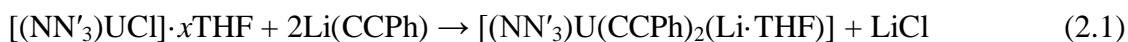
<sup>b</sup>  $R_1 = \sum||F_o| - |F_c||/\sum|F_o|$ ,  $wR_2 = \{\sum[w(F_o^2 - F_c^2)^2]/\sum[w(F_o^2)^2]\}^{1/2}$  for all data.

**Table 2.2.** Selected bond distances (Å) and angles (°) for crystallographically (**2.1–2.5**) and computationally determined (**2.3–2.5**) structures of the new mono- and dinuclear U(IV) complexes.

	<b>2.1</b>	<b>2.2</b>	<b>2.3</b>	<b>2.3(calc)</b>	<b>2.4</b>	<b>2.4 (calc)</b>	<b>2.5</b>	<b>2.5 (calc)</b>
U–C	2.604(3) 2.562(2)	2.479(7) 2.475(7)	2.480(4)		2.490(9) 2.443(9)		2.31(2) 2.48(2)	
U–N <sub>ax</sub> (amino)	2.6597(19)	2.668(5) 2.653(5) 2.285(5)	2.702(3)		2.693(6) 2.673(6) 2.207(6)		2.64(2) 2.73(2) 2.26(2)	
U–N <sub>eq</sub> (amido)	2.2799(19) 2.293(2) 2.2437(19)	2.260(5) 2.257(5) 2.284(5) 2.254(5) 2.263(5)	2.214(3) 2.220(3) 2.245(3)		2.214(6) 2.230(6) 2.211(6) 2.223(6) 2.229(6)		2.24(2) 2.26(2) 2.18(2) 2.12(2) 2.28(2)	
C≡C	1.219(3) 1.222(3)	1.210(9) 1.219(9)	1.212(5)		1.215(10) 1.210(11)		1.22(3) 1.42(3)	
U–C–C	177.8(2) 169.1(2)	176.6(6) 173.0(6)	160.9(4)		158.2(7) 170.2(7)		177(2) 161(2)	
N <sub>ax</sub> –U–C	109.81(7) 167.32(7)	165.06(19) 161.08(19) 68.03(17)	174.92(12)		174.7(2) 177.4(2) 69.5(2)		178.2(10) 177.4(8) 69.5(7)	
N <sub>ax</sub> –U–N <sub>eq</sub>	70.03(6) 70.06(6) 69.43(7)	70.19(17) 69.86(17) 70.20(16) 68.70(16) 69.89(17) 100.7(2)	69.06(11) 69.26(11) 68.90(11)		69.41(12) 69.4(2) 69.7(2) 70.2(2) 69.9(2) 107.0(2)		72.0(8) 68.1(8) 69.5(7) 69.4(7) 66.5(7) 111.4(8)	
N <sub>eq</sub> –U–N <sub>eq</sub>	94.80(7) 129.65(7) 98.30(7)	96.71(18) 124.96(19) 105.16(18) 121.86(19) 97.16(19)	108.42(12) 106.64(12) 108.87(12)		107.1(2) 111.0(2) 107.2(2) 111.6(2) 107.8(2)		107.4(8) 107.7(8) 105.7(8) 106.2(7) 110.2(8)	
U...U	n/a	13.0415(5)	n/a	n/a	9.2837(9)		12.9499(11)	
U–O	n/a	2.503(4) 2.571(4)	n/a	n/a	n/a	n/a	n/a	n/a

## 2.4 Results and Discussion

**2.4.1 Synthesis and characterization of [(NN'<sub>3</sub>)U] acetylide complexes.** Several monomeric synthons avail themselves for the preparation of pentacoordinate U(IV) species. Scott and coworkers have shown that the [(NN'<sub>3</sub>)UCl] complex can undergo ligand substitution with a variety of lithiated ligands via salt metathesis.<sup>66</sup> However, in our hands the apparent 1:1 combination of [(NN'<sub>3</sub>)UCl] with lithium phenylacetylide does not yield the expected pentacoordinate complex, but instead produces a hexacoordinate species, [(NN'<sub>3</sub>)U(CCPh)<sub>2</sub>(Li·THF)] (**2.1**) as the only isolable product (equation 1).



Adventitious tetrahydrofuran present in the unsublimed U(IV) starting material changes the stoichiometry of the reaction, and lithium ion coordination to the phenyl acetylide ligands likely drives formation of **2.1** over the expected mono-arylacetylide compound. Rationalization of the reaction conditions by doubling the amount of added lithium phenylacetylide and performing the reaction with an excess of THF allows for a greater isolated yield of the hexacoordinate U(IV) bis-arylacetylide complex.

The X-ray analyses of single crystals of **2.1** reveal two different polymorphs depending on the reaction conditions (*P* $\bar{1}$  from 1:1 and *P*2<sub>1</sub>/*c* from 1:2 stoichiometry). Metric parameters for the complexes in both polymorphs are essentially identical; the structures differ only in the relative orientation of the complexes within the unit cells. The thermal ellipsoid representation of the monoclinic polymorph of **2.1** is shown in Figure 2.1; see Appendix 1 for the triclinic structure. The uranium is ligated by three amido nitrogens, one amine nitrogen, and two phenylacetylide carbon atoms in  $\eta^1$

fashion. The (NN'<sub>3</sub>) fragment is unsymmetrically oriented with respect to the metal center, resulting in a wider range of 'flap' dihedral angles N<sub>ax</sub>-U-N<sub>eq</sub>-Si (137–163°) than is normally observed for virtually all other compounds containing the [(NN'<sub>3</sub>)U] fragment (131–137°).<sup>63</sup> However, the range of dihedral angles in **2.1** is similar to that reported by Scott and coworkers for the U(V) oxo-bridged dimer [(*bit*-NN'<sub>3</sub>)<sub>2</sub>U<sub>2</sub>(μ-O)] (132–177°).<sup>63</sup> The ligands form a distorted octahedral first coordination sphere about the metal center, as evidenced by the Σ parameter (177.71), which is the sum of the deviations from 90° of the twelve *cis* φ angles in the coordination sphere ( $\Sigma = \sum_{i=1}^{12} |90 - \varphi_i|$ ).<sup>86</sup> The two acetylide bridges are nearly linear, with U–C–C angles of 169.1(2) and 177.8(2)°. This contrasts with the only other structurally characterized U(IV) aryl acetylide complex, [(NN'<sub>3</sub>)U(CCPHMe)], a pentacoordinate U(IV) complex that shows a U–C–C angle of 156.4°.<sup>63</sup> In the structure of **2.1**, the lithium ion is coordinated by tetrahydrofuran in an η<sup>1</sup> mode, and by the acetylides in a π fashion; the latter coordination mode may help explain the observed linearity of the U–C–C linkages.

The absorption spectrum of **2.1** (Figure A1.1) contains only one feature at 686 nm. While spectral features which would normally mark the presence of a U(IV) ion in solution are absent, the position (686 nm) and molar absorptivity (95 L·mol<sup>-1</sup>·cm<sup>-1</sup>) of the singular absorption maximum observed are similar to other pentacoordinate U(IV) complexes containing the (NN'<sub>3</sub>) ligand.<sup>66,71,87</sup>

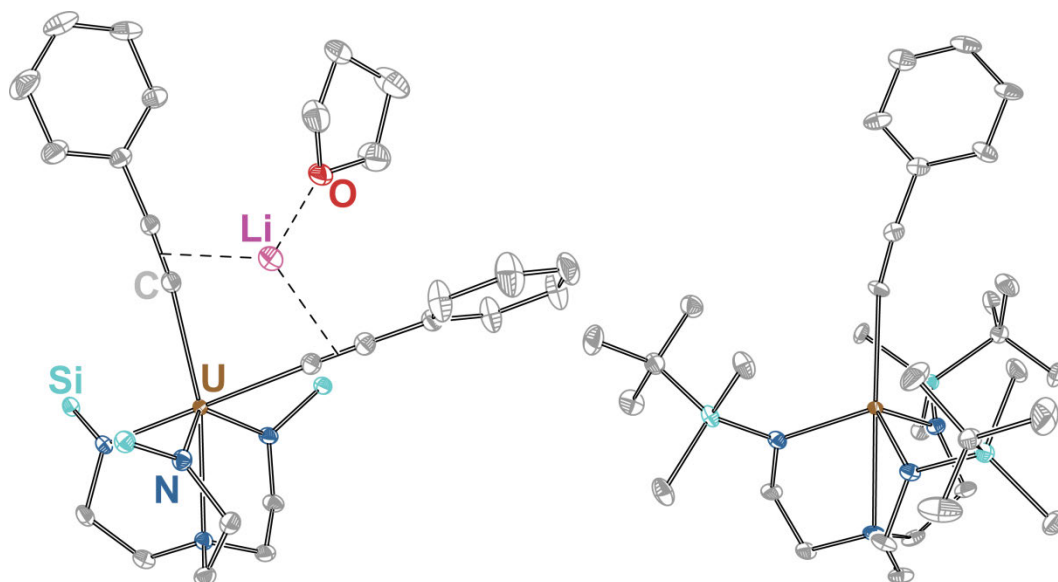


**Figure 2.1.** Crystal structures of the U(IV) arylacetylide complexes in compounds **2.1** (left) and **2.3** (right), rendered with 40% ellipsoids. Brown, dark blue, light blue, red, purple, and gray ellipsoids represent U, N, Si, O, Li and C atoms, respectively. Hydrogen atoms are omitted for clarity and the Me<sub>2</sub><sup>t</sup>Bu groups have been removed from the Si atoms in **2.1** for a clearer display of the coordination geometry about the uranium center.

Whereas the reaction of [(NN'<sub>3</sub>)UCl] with lithium phenylacetylide yields a bis-phenylacetylide complex, its combination with 0.5 equivalents of a ditopic aryl acetylide such as Li<sub>2</sub>(*p*-DEB) results in the formation of dinuclear U(IV) complexes. Unlike the formation of **2.1**, only one acetylide interacts with each U(IV) ion, however the presence of adventitious tetrahydrofuran nevertheless provides a hexacoordinate U(IV) complex [(NN'<sub>3</sub>)<sub>2</sub>U<sub>2</sub>(*p*-DEB)(THF)] (**2.2**) via equation 2.2:



Uranium complexes are quite oxophilic,<sup>88</sup> and consistent with the formation of complex **2.1**, the triamidoamine groups are not sufficiently sterically encumbering to prevent the coordination of a sixth ligand. Thus, hexacoordinate geometry is observed in the solid state structure of [(NN'<sub>3</sub>)<sub>2</sub>U<sub>2</sub>(*p*-DEB)(THF)<sub>2</sub>] (**2.2**·THF), as determined by X-ray analysis (Figure 2.2). Again, the [(NN'<sub>3</sub>)U] fragment is asymmetrically oriented, as measured by

the dihedral angles  $N_{ax}-U-N_{eq}-Si$  ranging from 132 to 176°. The U–O distances (2.583(4) and 2.571(4) Å for U1–O1 and U2–O2, respectively) are similar to those reported for other crystallographically characterized U(IV) tetrahydrofuran adducts.<sup>87,89-92</sup> The THF solvent molecules are rotated by approximately 90° with respect to each other. The  $\eta^1$ -bound acetylide in **2.2** links the uranium centers in a nearly linear fashion with U–C–C angles of 173.0(6) and 176.6(6)°. The uranium centers in **2.2**·THF sit in distorted octahedrons as measured by their respective  $\Sigma$  parameters (175.21° for U1 and 191.78° for U2).<sup>86</sup> The (NN'<sub>3</sub>) fragments in **2.2**·THF are rotated by approximately 90° with respect to each other.

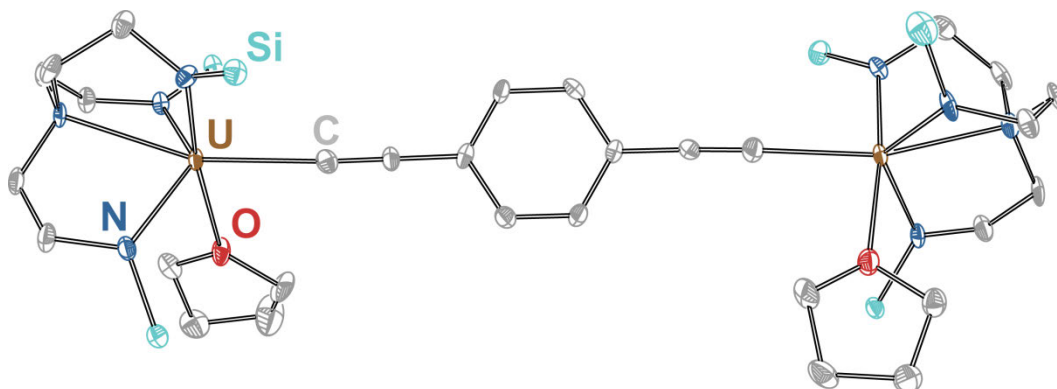
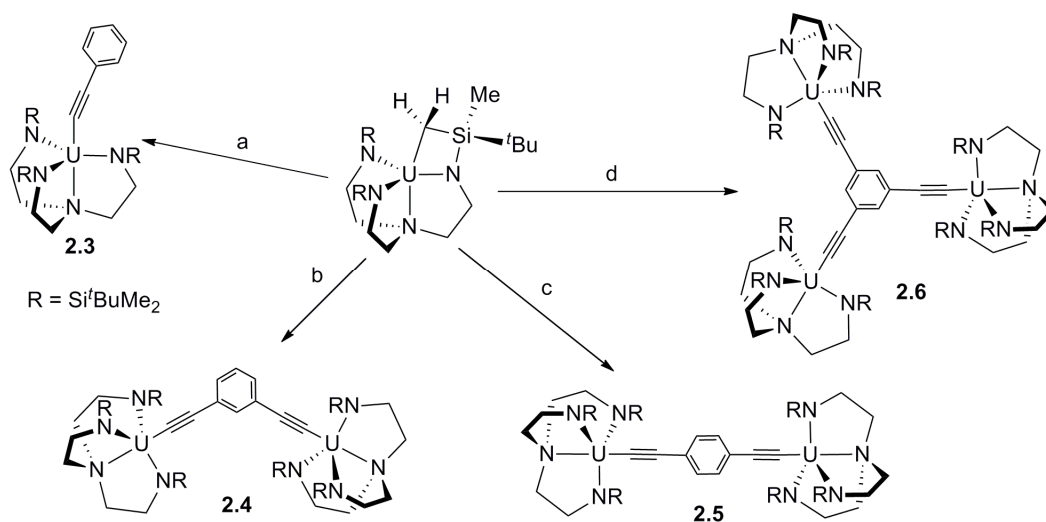


**Figure 2.2.** Crystal structure of the dinuclear complex in compound **2.2**·THF·C<sub>5</sub>H<sub>12</sub>, rendered with 40% ellipsoids. Brown, dark blue, light blue, red, and gray ellipsoids represent U, N, Si, O, and C atoms, respectively. Me<sub>2</sub><sup>t</sup>Bu groups have been removed from the Si atoms for a clearer display of the coordination geometry about the uranium center. Hydrogen atoms and solvent molecules are omitted for clarity.

Whereas the crystal structure of **2.2**·THF·C<sub>5</sub>H<sub>12</sub> clearly shows two tetrahydrofuran molecules per complex, the elemental analysis data obtained for bulk **2.2** indicate that approximately one tetrahydrofuran molecule is absent in the bulk samples. As will be

discussed in more detail below, the “hexacoordinate” **2.2** and the pentacoordinate **2.5** are found to have virtually identical spectroscopic properties.

Alternatively, the mono-deprotonated complex  $[(bit-NN'_3)U]$  can serve as an excellent precursor for reactions with free acetylenes, also previously demonstrated by Scott and coworkers.<sup>63</sup> As shown in Scheme 2.1, the triamidoamine ligand can be reprotonated by the acetylene, and the acetylide anion formed in situ can bind to the cationic U(IV) center. In our hands, the combination of the orange-brown  $[(bit-NN'_3)U]$  with one equivalent of phenylacetylene allows for the preparation of the yellow-green pentacoordinate U(IV) monoacetylide complex (**2.3**) in good yield.



**Scheme 2.1.** Synthesis of complexes **2.3-2.6** (a = phenylacetylene, b = *m*-H<sub>2</sub>DEB, c = *p*-H<sub>2</sub>DEB, and d = H<sub>3</sub>TEB. All reactions were carried out in pentane at  $-78$  °C.

The crystal structure of monomeric **2.3**, determined from crystals grown at  $-34$  °C from a saturated pentane solution (Figure 2.1), is very similar to the previously reported  $[(NN'_3)U(CCPhMe)]$  complex.<sup>93</sup> The triamidoamine ligand adopts a typical trigonal pyramidal geometry around the uranium center in **2.3**. Although not imposed

crystallographically, the ligand is essentially three-fold symmetric about the U center, as measured by the dihedral angles  $N_{ax}-U-N_{eq}-Si$  ( $131-137^\circ$ ). The acetylide ligand binds the U(IV) ion in an  $\eta^1$  fashion, but shows a bent configuration unlike those of the nearly linear acetylides in the hexacoordinate complex **2.2** (U–C–C angle  $160.9(4)^\circ$ ). This bending is similar to Scott's pentacoordinate complex, where it was suggested that the alkynyl uranium fragment bends in order to allow for increased U–C  $\pi$ -overlap.<sup>63</sup> DFT calculations (discussed below) reveal that bending the U–C–C bond angle from  $180^\circ$  to  $160^\circ$  only slightly perturbs the energy of the complex, implying that intermolecular packing forces may represent significant contributors to the observed bond angles.

Utilizing the same revision to the synthetic procedure as described in the synthesis of **2.3**, we find that mixing [*bit*- $NN'_3$ ]U with the appropriate acetylenes leads to di- and trinuclear complexes in which the U(IV) center is pentacoordinate (Scheme 2.1). In this manner, we have prepared the di- and trinuclear U(IV) ethynylbenzene complexes [ $(NN'_3)_2U_2(m-DEB)$ ] (**2.4**), [ $(NN'_3)_2U_2(p-DEB)$ ] (**2.5**), and [ $(NN'_3)_3U_3(TEB)$ ] (**2.6**) in good yields. Crystal structures for the dinuclear compounds **2.4** and **2.5** are depicted in Figure 2.3. Crystals of trinuclear **2.6** diffract sufficiently to confirm the expected cluster connectivity, but the diffraction data are not of sufficient quality to provide a complete X-ray analysis. As with compound **2.3**, the [ $(NN'_3)U$ ] adopts its usual orientation, with dihedral angles of  $132-142^\circ$  and  $136-145^\circ$  for **2.4** and **2.5**, respectively. Interestingly, one of the U–acetylide linkages in *meta*-bridged **2.4** is significantly more linear than the other (U–C–C angle of  $158.2(7)^\circ$  versus  $170.2(7)^\circ$ ). Fourier difference maps do not indicate any evidence for crystallographic disorder present in the structure of **2.4**. Rather, the different U–C–C bond angles observed could be due to a competition between ( $NN'_3$ )

sterics, which would favor linear U–C–C linkages, and  $\pi$ -overlap of the acetylide and U(IV) ion, similar to that observed in the structure of the monomeric complex **2.3**. The (NN'<sub>3</sub>) fragments in *meta*-bridged **2.4** are rotated by approximately 60° with respect to each other. In *para*-bridged **2.5**, the (NN'<sub>3</sub>) fragments are not rotated with respect to each other and can be related by a non-crystallographic mirror plane.

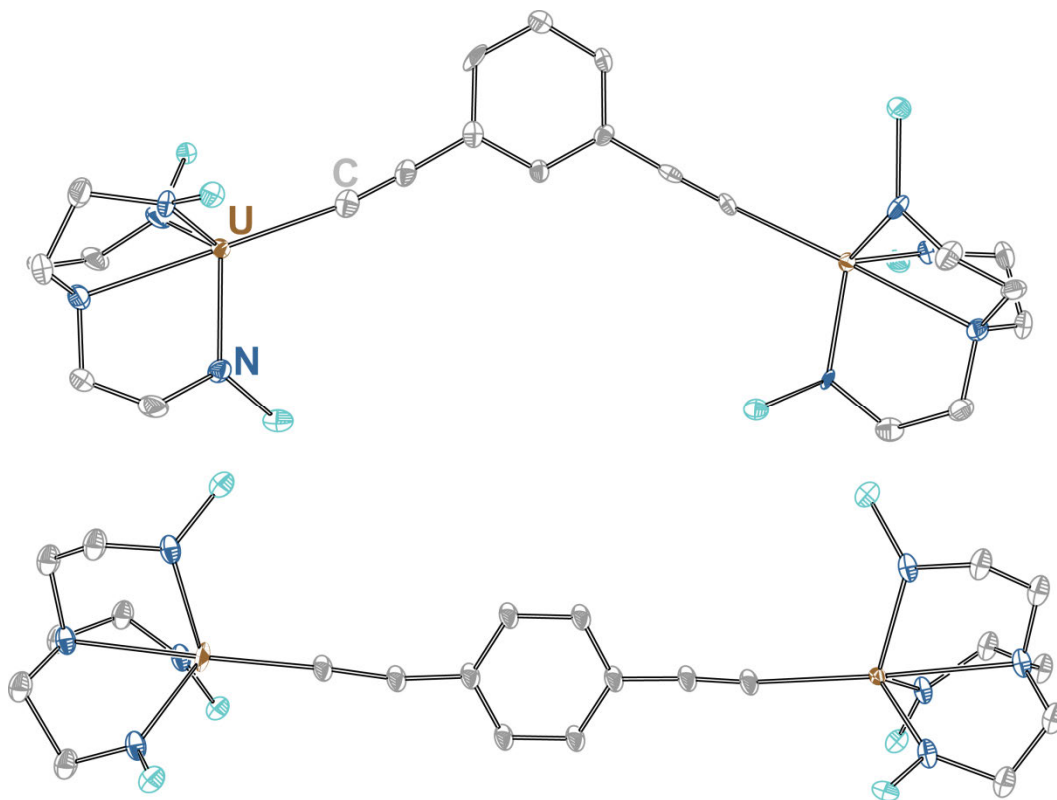


**Figure 2.3.** Crystal structures of the dinuclear complexes in compounds **2.4**·C<sub>5</sub>H<sub>12</sub> (top) and **2.5**·C<sub>5</sub>H<sub>12</sub> (bottom), rendered with 40% ellipsoids. Brown, dark blue, light blue, and gray ellipsoids represent U, N, Si, and C atoms, respectively. Me<sub>2</sub><sup>t</sup>Bu groups have been removed from the Si atoms for a clearer display of the coordination geometry about the uranium center. Hydrogen atoms and solvent molecules are omitted for clarity. One and two of the SiMe<sub>2</sub><sup>t</sup>Bu groups are disordered over two positions for **2.4**·C<sub>5</sub>H<sub>12</sub> and **2.5**·C<sub>5</sub>H<sub>12</sub>, respectively; only one orientation is shown for clarity. See Figures A1.24 and A1.25 for disordered components.

We have characterized all the ethynylbenzene-bridged species by FT-IR and UV-Visible spectroscopic techniques (Figures A1.1–A1.12). The fingerprint region of the IR is nearly identical to those reported for most of the structurally characterized compounds containing the  $[(NN'_3)U]$  fragment.<sup>63,64,66,94</sup> The electronic absorption spectra of uranium compounds represent a good indicator for the oxidation state of the metal ion; and the spectra of complex **2.2** and compounds **2.4–2.6** are consistent with an assignment of U(IV), in agreement with other reported  $[(NN'_3)U]$ -containing compounds.<sup>95</sup> Interestingly, the UV-visible spectra of **2.2** and **2.5** in toluene are similar; they also display similar infrared spectra. While these could indicate that the coordination environment of the uranium center does not have a discernable effect on electronic properties, more likely these results point to tetrahydrofuran solvate loss in solution. Thus, crystals of **2.2**·THF·C<sub>5</sub>H<sub>12</sub> show two tetrahydrofuran molecules, but bulk **2.2** contains only one, and dissolved **2.2** is spectroscopically identical to **2.5**, which contains no THF solvate.

**2.4.2 Oxidation of the pentacoordinate U(IV) arylyacetylide complexes.** Efforts to produce unambiguously paramagnetic assemblies from **2.2**, and **2.4–2.6**, either by oxidations or reductions that may lead to U(V) or U(III) species, respectively, yield mixed results. Cyclic voltammetry experiments performed on the monomeric phenylacetylide complex **2.3** in *o*-difluorobenzene show a well-defined, reversible wave centered at  $-1.02$  V versus  $Fc^+/Fc$  (Figure 2.4). This process is assignable to an oxidation of the neutral compound to a formally U(V) species, and is supported by an agitation experiment whereby the voltammogram is collected while stirring the sample (Figure A1.13). This is comparable to results reported by Kiplinger and coworkers for

$[(C_5Me_5)_2U(=N-Ar)(X)]$  ( $X = F, Cl, Br, I$ ), where reversible redox couples ranging between  $-1.21$  and  $-1.84$  V versus  $Fc^+/Fc$  are observed.<sup>96</sup> While the cyclic voltammograms suggest a reversible  $U(IV/V)$  redox couple on the time scale of the experiment (scan rate of  $50$  mV/s), initial attempts to isolate oxidized complexes by chemical oxidation with  $[FeCp^*_2](BAr^F_4)$  have not been successful. Infrared spectra obtained on the products of oxidation attempts show no shift in the acetylide resonance, contrary to what would be expected if a change in uranium oxidation state occurred. In addition, crystals isolated from the oxidation attempts were determined to be  $[(C_5Me_5)Fe(C_5Me_4CH_2)](BAr^F_4)$ .<sup>97</sup>

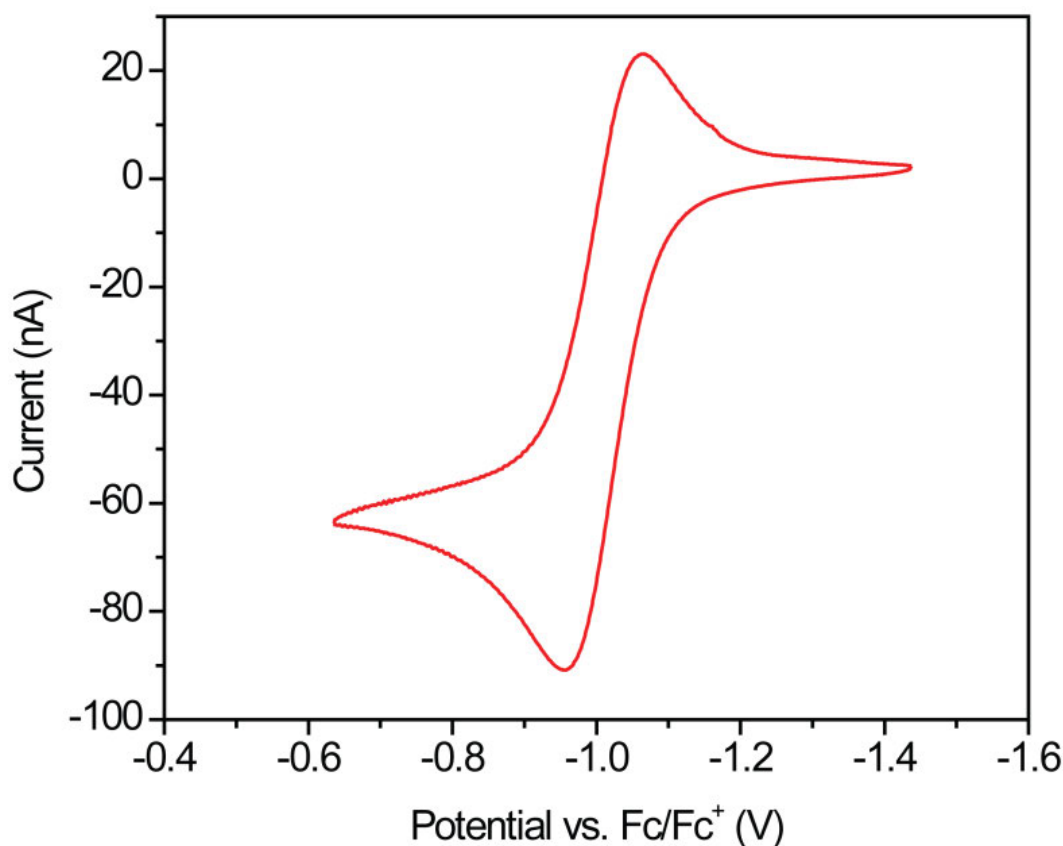


**Figure 2.4.** Electrochemical behavior for **2.3** in static solution recorded in  $0.1$  M solution of  $[TBA][BAr^F_4]$  in *o*-difluorobenzene at ambient temperature with a  $0.250$  mm diameter platinum wire microelectrode.

Attempts to obtain cyclic voltammograms on compounds **2.2**, **2.4**, **2.5**, and **2.6** under similar conditions have proven more difficult. Although experimental conditions have been systematically varied (including solvents, scan rates, and working electrodes), in all instances, only ill-defined waves are observed (Figure A1.14), suggesting the occurrence of multi-electron processes and/or the decomposition of the original species. It is also possible that the complicated nature of the cyclic voltammograms could be due to electronic communication between the uranium centers via the bridging ligand.

**2.4.3 Magnetic properties of the U(IV) complexes.** The temperature dependence of the magnetic susceptibility (2–300 K) for each uranium-acetylide complex was characterized by SQUID magnetometry (Figures 2.5 and 2.6, also Figures A1.15–A1.17), and MAGFIT<sup>76</sup> was used to fit the subtracted paramagnetic susceptibility data (vide infra) to a simple spin Hamiltonian with one exchange parameter  $J$  (black traces in Figure 2.6 and Figures A1.15–A1.17). Fitted parameters are listed in Table 2.3.

*Magnetic susceptibilities of monomeric complexes 2.1 and 2.3.* The temperature dependencies of the magnetic susceptibility,  $\chi_M T$ , for the monomeric U(IV) arylacetylide complexes **2.1** and **2.3** are shown in Figure 2.5. The room temperature  $\chi_M T$  values for **2.1** and **2.3** (1.37 and 1.18 emu·K·mol<sup>-1</sup>, respectively) are comparable to those of other reported complexes containing U(IV) in a low symmetry ligand field and are consistent with the presence of a paramagnetic ground state at room temperature.<sup>49,94,98</sup> Upon decreasing the temperature, higher-energy Stark sublevels begin to depopulate, resulting in a subsequent decrease in the magnitude of the total angular momentum vector. This phenomenon leads to a variation in the thermal population of the many states that are

energetically comparable to the ground state.<sup>11</sup> The physical manifestation of this decrease in the angular momentum is evident by the decrease in the observed magnetic susceptibility. As can be seen in a plot of  $\chi_{\text{M}}T$  versus  $T$  for **2.1**, a gradual decrease to 0.93  $\text{emu}\cdot\text{K}\cdot\text{mol}^{-1}$  at 120 K occurs, followed by a sharper decrease to 0.13  $\text{emu}\cdot\text{K}\cdot\text{mol}^{-1}$  at 8 K. Similarly, as the temperature is reduced to 160 K,  $\chi_{\text{M}}T$  for **2.3** reveals a gradual decrease to 0.99  $\text{emu}\cdot\text{K}\cdot\text{mol}^{-1}$ , followed by a sharper decrease to 0.03  $\text{emu}\cdot\text{K}\cdot\text{mol}^{-1}$  at 2 K. The behavior of the hexacoordinate **2.1** can be interpreted as a ground state diamagnetic  $f^2$  species, which is paramagnetic at room temperature due to spin-orbit coupling, temperature-independent paramagnetism (TIP), and thermal population of paramagnetic excited states. A poorly isolated singlet ground state is not atypical for complexes with  $5f^2$  valence configurations;<sup>99-101</sup> further, it is well known that an octahedral ligand field will produce a diamagnetic ground state for a  $5f^2$  electronic configuration.<sup>59</sup> Although the pentacoordinate species **2.3** displays magnetic properties which appear to be consistent with a non-magnetic ground state,<sup>102-104</sup> there seems to be less influence from TIP than observed for **2.1**. Overall, the foregoing results imply that coordination geometry differences impart only minor impacts on the magnetic properties of these  $[(\text{NN}'_3)\text{U}]$ -containing complexes.

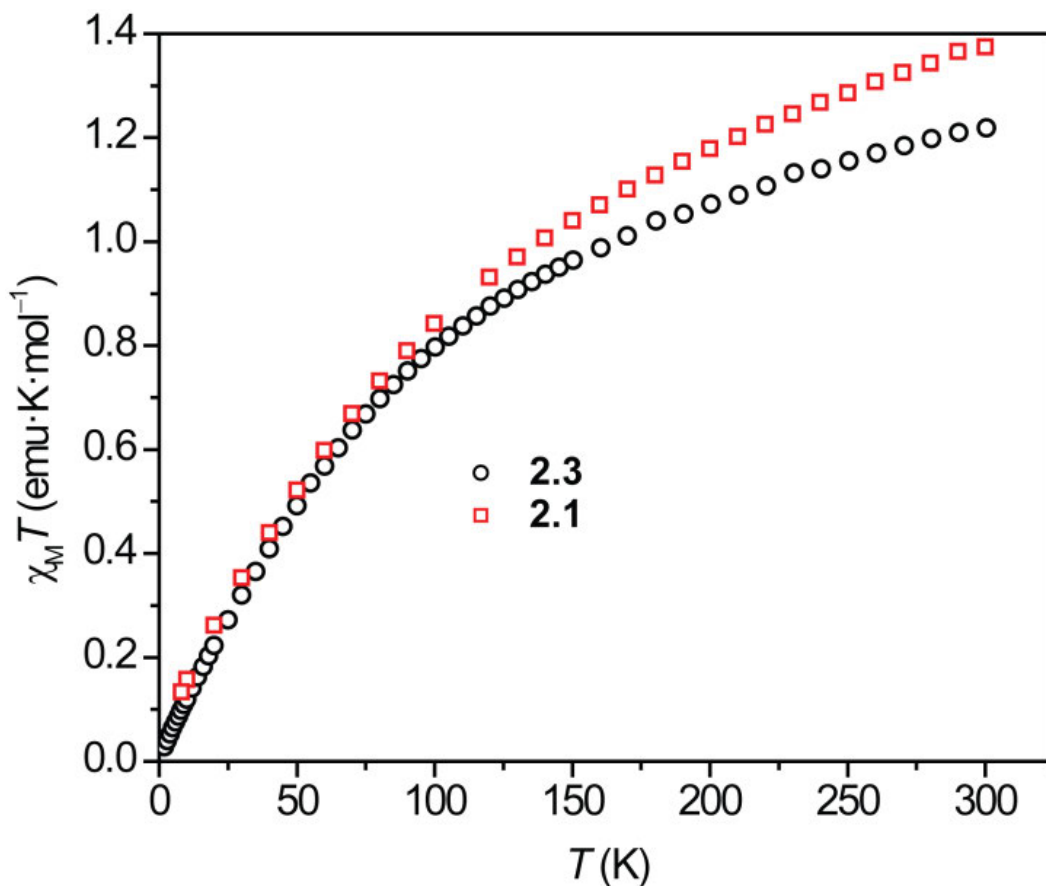


**Figure 2.5.** Temperature dependence of the magnetic susceptibility for compounds  $[(\text{NN}'_3)\text{U}(\text{CCPh})_2(\text{Li}\cdot\text{THF})]$  (**2.1**) and  $[(\text{NN}'_3)\text{U}(\text{CCPh})]$  (**2.3**), obtained at a measuring field of 1000 G.

*Magnetism of di- and trinuclear species 2.2, 2.4–2.6.* The temperature dependence of the magnetic susceptibility for dinuclear “hexacoordinate” complex **2.2** is shown in Figure A1.15. The room temperature  $\chi_M T$  value for **2.2** ( $1.40 \text{ emu}\cdot\text{K}\cdot\text{mol}^{-1}$  per U(IV) ion) is comparable to that of other reported complexes with U(IV) in a low symmetry ligand field.<sup>49,94,98</sup> It is important to note that  $\chi_M T$  drops as the temperature approaches zero to a minimum of  $0.04 \text{ emu}\cdot\text{K}\cdot\text{mol}^{-1}$  at 2 K. Again, this may be due to “octahedral” geometry, similar to the description of the magnetic properties of **2.1**. However, the drop is not linear like **2.1**, perhaps related to the fact that the 6-coordinate geometry is quite distorted from a perfect octahedron. The construction of a Weiss plot for **2.2** (Figure A1.18) yields

a  $\theta$  value of  $-180$  K with a Curie constant ( $C$ ) of  $4.44 \text{ cm}^3 \cdot \text{K} \cdot \text{mol}^{-1}$ . Another complicating factor is the potential loss of some THF from ground up bulk samples of this compound. In fact, if the mass of one equivalent of THF is removed from **2.2**, the resulting susceptibility data virtually overlay the data for **2.5** (vide infra).

Although complexes **2.4–2.6** display quite different coordination geometries from the crystal of **2.2**·THF, their magnetic properties appear to be quite similar on a per U(IV) basis. The temperature dependence of the magnetic susceptibility,  $\chi_M T$ , for the *meta*-bridged dinuclear complex **2.4** is shown in Figure 2.6; those for *para*-bridged **2.5** and TEB-bound **2.6** can be found in the Appendix (Figures A1.16, and A1.17, respectively; figure A1.18 reveals Weiss constant determinations). The room temperature  $\chi_M T$  value for **2.4** ( $1.26 \text{ emu} \cdot \text{K} \cdot \text{mol}^{-1}$  per U(IV) ion) is in the range of other literature values for paramagnetic U(IV) ions in low symmetry ligand fields.<sup>49,94,98</sup> Similar to the behavior of **2.2**,  $\chi_M T$  approaches zero as the temperature is reduced, which appears to be consistent with a non-magnetic ground state.<sup>102-104</sup> This is inconsistent with the simple ligand-field diagram for an  $f^2$  ion in trigonal bipyramidal complex geometries, however it must be noted that spin-orbit coupling was not been included in the group theoretical analysis.

However, when we perform a precedented subtraction scheme<sup>11</sup> on the susceptibility data for complexes **2.2**, **2.4**, **2.5** and **2.6**, the adjusted data reveal evidence of net intramolecular exchange interactions.<sup>50,105</sup> Here, the discussion is focused on the data interpretation for *meta*-bridged **2.4**, but is applicable to the magnetic interpretations for the other multinuclear complexes **2.2**, **2.5** and **2.6**. At each temperature, two times the paramagnetic susceptibility of the monoacetylide species **2.3** (three times the paramagnetic susceptibility of **2.3** in the case of trinuclear **2.6**) are subtracted from the

corresponding paramagnetic susceptibility of the dinuclear *meta*-bridged complex **2.4** to remove any contribution from the spin-orbit coupling of the U(IV) ions. To this value is added the contribution expected for two  $S = 1$  ions (i.e.  $\chi_{MT} = 1.00$  for  $g = 2.00$ ). In the case where no communication between the metal centers is occurring, a plot of the obtained values versus temperature is expected to form a line with zero slope at a  $\chi_{MT}$  value of  $2.00 \text{ emu}\cdot\text{K}\cdot\text{mol}^{-1}$  (assuming  $g = 2.00$ ).<sup>50,53,65,101</sup> However, the resulting blue traces (Figure 2.6, A1.15, A1.16, and A1.17) do possess some curvature, suggesting the presence of U-U magnetic interactions. While this method of data treatment only allows an estimation of the lower limit to any exchange interactions (since spin-orbit interactions have been removed), MAGFIT estimates the magnetic exchange in *meta*-bridged **2.4** to be weakly *ferromagnetic*, with  $J = 4.76 \text{ cm}^{-1}$ . There are scant comparisons available in the literature. The coupling in  $[(\text{MeC}_5\text{H}_4)_6\text{U}_2(\mu\text{-}1,4\text{-N}_2\text{C}_6\text{H}_4)]$  was reported by Andersen and coworkers to be significantly stronger and *antiferromagnetic*, ( $J = -19 \text{ cm}^{-1}$ );<sup>57</sup> however it must be noted that this represents coupling between U(V) centers. Coupling between U(IV) and Ni(II) in  $(\text{cyclam})\text{Ni}[(\mu\text{-Cl})\text{U}(\text{Me}_2\text{Pz})_4]_2$  using the abovementioned subtraction scheme yields a  $J$  value of  $2.8 \text{ cm}^{-1}$ .<sup>50</sup> Meanwhile, coupling of Fe(III) ions through the *m*-DEB bridge is *ferromagnetic*, albeit significantly stronger than that observed in the *meta*-bridged dinuclear complex **2.4** ( $J = 65 \text{ cm}^{-1}$ ).<sup>67</sup>

Interestingly, fits to the data for para-bridged **2.5** and trinuclear complex **2.6** (Table 2.3) also indicate weak *ferromagnetic* coupling, although the  $J$  couplings are weaker ( $2.75$  and  $1.11 \text{ cm}^{-1}$ , respectively) than that determined for **2.4**. Note that  $g$  values determined from the fitting procedure are consistent with other reported U(IV) complexes.<sup>49,50</sup> In an attempt to compare experimental  $g$  values with calculated  $g$  values,

room temperature EPR data was collected on **2.4** although, the compound was EPR silent. Data derived from best fits for “hexacoordinate” dinuclear complex **2.2** are also presented in Table 2.3, but the determined parameters are less reliable owing to the lack of a suitable monomeric hexacoordinate U(IV) complex for use in the data adjustment scheme as well as some uncertainty about the coordination geometry in bulk samples of **2.2**.

Indeed, this exemplifies a general concern about the potential for measurement errors to propagate in the course of applying the subtraction scheme. Regarding the reproducibility of data, we have analyzed multiple samples of the mono- and multi-nuclear complexes, both within a batch and between different preparations, and obtain the same raw data in all cases. With respect to electronic differences between the mono- and multi-nuclear complexes (**2.3** and **2.4–2.6**, respectively) it is possible that the observed curvature in the  $\chi_M T$  versus  $T$  plots represent artifacts, but the structural similarities argues against this. Finally, fits to the corrected data give the same values, even when the initial guesses for  $J$  and  $g$  are varied significantly. Thus, we argue that the temperature dependence of the corrected susceptibilities represent real albeit qualitative evidence of magnetic coupling operative between U(IV) centers.

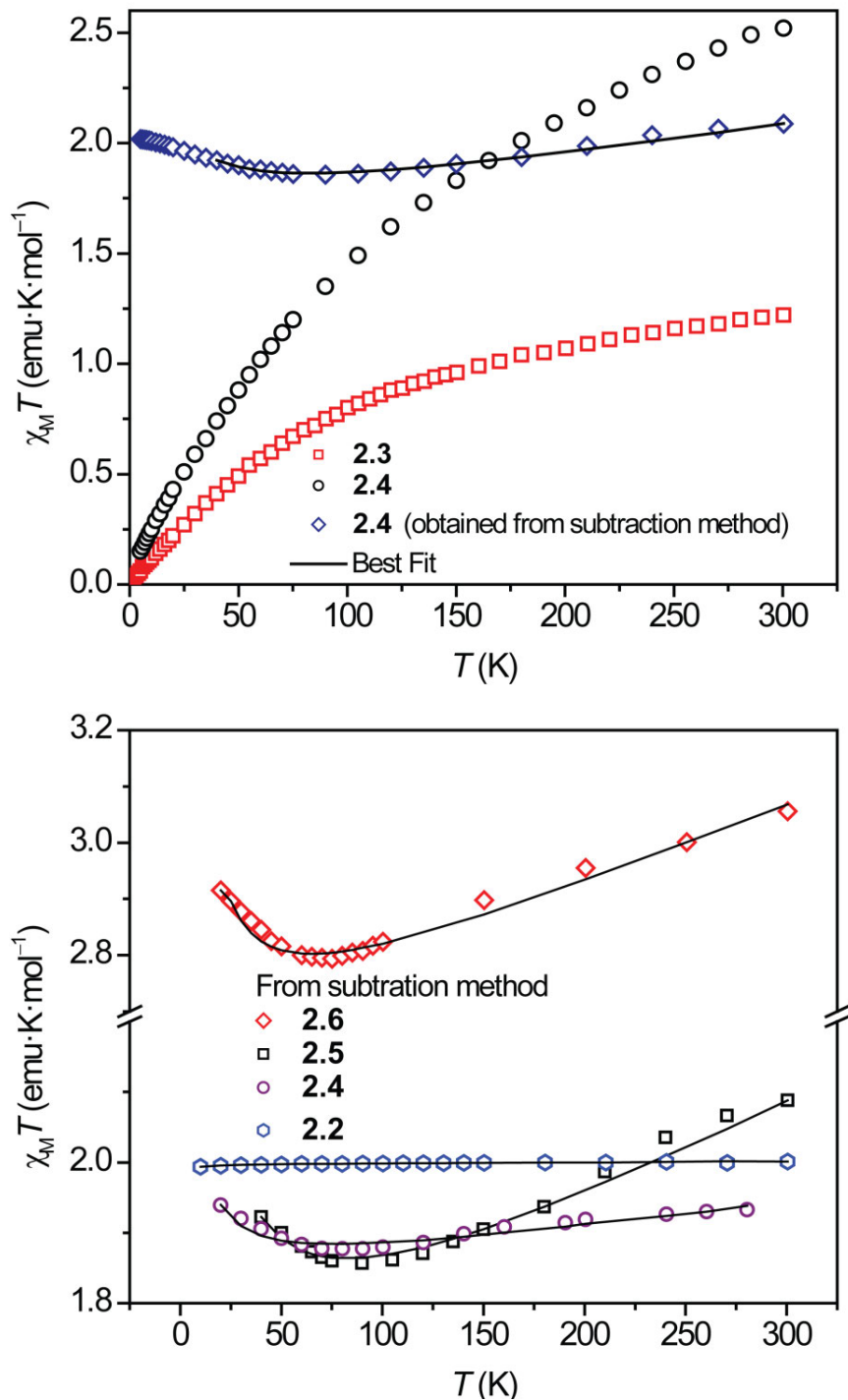


**Figure 2.6.** Top: temperature dependence of the magnetic susceptibility for compounds **2.3** and **2.4**, obtained at a measuring field of 1000 G; and fit of the data obtained from the subtraction method for **2.4**, see text for details of the fitting procedures. Bottom: solid lines give best fits to the data obtained from the subtraction method for complexes **2.2**, **2.4**, **2.5**, and **2.6**; see text for details of the data correction procedures.

**Table 2.3.** Tabulated MAGFIT results for compounds [(NN'3)<sub>2</sub>U<sub>2</sub>(*p*-DEB)(THF)] (**2.2**), [(NN'3)<sub>2</sub>U<sub>2</sub>(*m*-DEB)] (**2.4**), [(NN'3)<sub>2</sub>U<sub>2</sub>(*p*-DEB)] (**2.5**), and [(NN'3)<sub>3</sub>U<sub>3</sub>(TEB)] (**2.6**).

	<b>2.2</b>	<b>2.4</b>	<b>2.5</b>	<b>2.6</b>
$J$ (cm <sup>-1</sup> )	-0.05	4.76	2.75	1.11
$g$	1.99	1.80	1.89	1.84
TIP (×10 <sup>-6</sup> emu)	5	1435	860	1473
relative error	0.19	0.18	0.08	0.17

Based on analogy with transition metal analogues,<sup>67,106</sup> we would expect antiferromagnetic coupling for paramagnetic species bridged by *p*-DEB and ferromagnetic exchange for di- and trinuclear complexes bridged by *m*-DEB and TEB, respectively. In addition, antiferromagnetic coupling is observed in Andersen's *para*-substituted U(V) bridged imido species, although the fact that the bridging ligand is not an acetylide may be significant.<sup>57</sup> Thus, while the results of the subtraction procedure may appear reasonable for the *meta*-linked complexes **2.4** and **2.6**, we might expect *antiferromagnetic* coupling for the *p*-DEB-bridged **2.5**. That this is not operative suggests that the particular bridging geometry may only have a small effect on the type of coupling in these U(IV) complexes. We note, however, that the geometry and nuclearity do appear to have an effect on the strength of the coupling (Table 2.3). First, the *meta*-linked **2.4** exhibits a  $J$  value twice as large as that determined for **2.5**. Second, comparison of the magnetic data for **2.4** and **2.6** shows that increasing the number of uranium centers results in a smaller coupling constant. Similar effects have been observed in cyanide-bridged transition metal complexes, where increased nuclearity distributes spin density over a larger area, resulting in weaker coupling.<sup>106</sup>

An important part of this discussion is that we must fully consider the possibilities that intermolecular pathways (H-bonding, U-U interactions, and close contacts) could

contribute to the observed magnetic properties, and confirm that they are not significant contributors. There were no significant contacts in compounds **2.1–2.6**, other than weak van der Waals interactions, that would allow for any obvious pathways for magnetic communication to occur (see Appendix 1) In compounds **2.1–2.6**, the shortest intermolecular U...U distance was found in **2.4** with a distance of 8.9261(5) Å. The shortest intramolecular U...U interaction was also found in **2.4** with a distance of 9.2837(9) Å. None of these contacts portend significant contributions to the observed magnetism, thus lending further support to our assertion that any residual magnetism in these complexes is due to intramolecular communication between the uranium centers.

**2.4.4 Theoretical Consideration.** To gain deeper insight into the complex magnetic behavior, we carried out geometry-optimized Stuttgart/6-31g\* B3LYP hybrid DFT calculations on model systems where the <sup>t</sup>BuMe<sub>2</sub>Si substituents in the NN'<sub>3</sub> ligand are replaced by H atoms and relativistic effects are included in the uranium effective core potential. The structure obtained from the geometry optimization of a mononuclear model of **2.3**, [N(CH<sub>2</sub>CH<sub>2</sub>NH)<sub>3</sub>U(CCH)], compares well with the crystal structure of **2.3**, although one difference is that the U–C–C linkage is linear in the model complex. Computations carried out as a function of the U–C–C angle (Figure A1.23) address the observation of both bent and linear U–C–C linkages in the isolated complexes **2.1–2.6**. The calculations show that bending the U–C–C angle from 180° to 160° only increases the energy by 0.5 kcal/mol for both the ground state triplet and lowest energy excited state singlet. The harmonic curve in Figure A1.23 demonstrates that, as is typical of *sp* hybridized carbon, the bending potential is more quartic than harmonic in character.

A conventional (spin-orbit coupling omitted) study on the model for **2.3** yields a triplet ground state with two electrons in singly occupied  $f$   $\pi$ -type orbitals—consistent with the group theoretic analysis.<sup>58</sup> The calculated  $f$  orbitals are mixtures of the  $5f$  general set;<sup>107</sup> the occupied orbitals that would have  $\pi$  overlap with the acetylide ligand most closely resemble  $f_{xz^2}$  and  $f_{yz^2}$  (Figure 2.7). The lowest  $M_S=0$  “singlet” state is one wherein the two singly occupied orbitals are “singlet coupled” via a broken symmetry solution. In order to obtain the relative energies of the set of 7  $f$  orbitals as well obtain the character of these frontier orbitals an average field computation was carried out wherein the two triplet-coupled electrons are evenly distributed over the 7  $f$  orbitals. Only the two lowest energy orbitals, the ones occupied in the conventional triplet study, show net orbital overlap with the  $\pi$ -type orbitals on the bound acetylide. Nevertheless, net spin density plots for the ground state triplet and lowest excited state singlet (Figure 2.7b and c) show that negligible spin density is found on the acetylide. As is visually evident in Figure 2.7 the 7 frontier orbitals are dominantly  $5f$  in character. The largest d coefficient in any of the 7 frontier orbitals was only 0.118.

The triplet state is lower in energy than the broken symmetry solution by 8.4 kcal/mol. Given a U(IV) spin-orbit coupling parameter of roughly 6.3 kcal/mol,<sup>58</sup> however, the triplet and singlet states should strongly mix, resulting in a  $j = 0$  ground state. This is consistent with the observed magnetic properties of **2.3**, where a paramagnetic complex at room temperature becomes “non-magnetic” as the temperature is reduced.

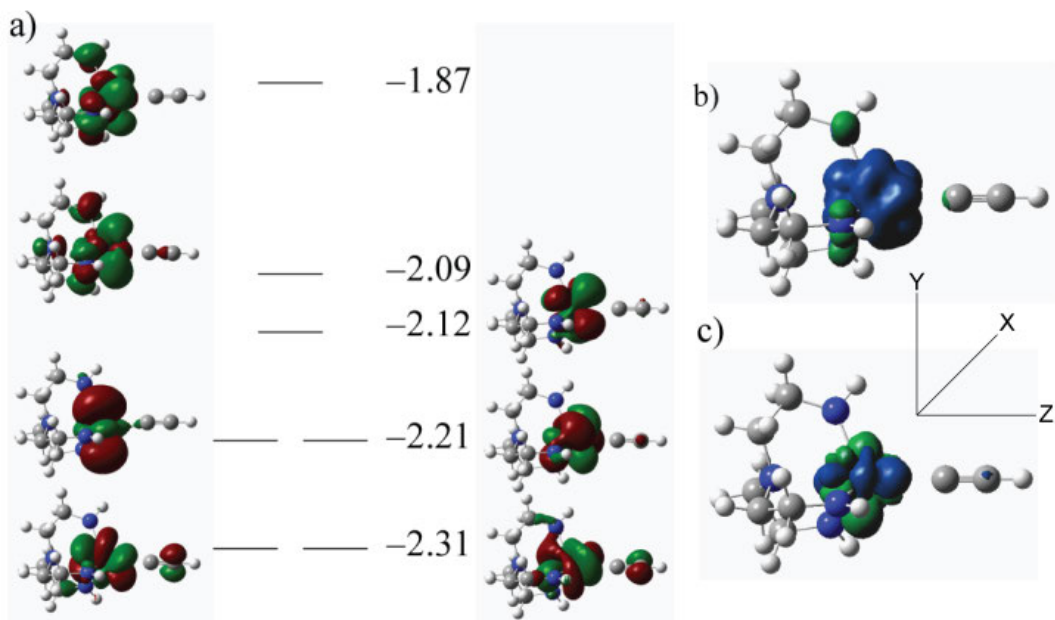


**Figure 2.7.** (a) Average field fragment molecular orbital diagram for  $[(NN'_3)U^{IV}(CCH)]$ , relative energies are provided on an eV scale. (b) Net spin density plot of the ground state triplet. (c) Net spin density plot of the lowest “singlet” broken symmetry state. Blue surfaces correspond to net  $\alpha$  spin density and green to net  $\beta$  spin density.

For model species based on the dinuclear complexes **2.4** and **2.5**, a broken symmetry model was used to construct the antiferromagnetically coupled low spin state, and  $J$  was computed to be 1.6 and  $-0.1 \text{ cm}^{-1}$  for the *meta*- and *para*-bridged complexes, respectively. The signs of the computed coupling constants are not consistent with the observed magnetic properties, but do conform to what is expected in ethynylbenzene-bridged systems:<sup>108,109</sup> ferromagnetic coupling for *meta*-bridged **2.4** and antiferromagnetic coupling for *para*-bridged **2.5**. We note that the magnitudes of the calculated coupling constants for models of **2.4** and **2.5** are much smaller than those computed for similar transition-metal based systems.<sup>109</sup> As with the model mononuclear complex calculation, net spin density ( $\rho_\alpha - \rho_\beta$ ) plots generated for models of **2.4** and **2.5** (Figure 2.8) show very little bridging-ligand density, no matter what spin states are used

for the U(IV) constituent ions. We conclude that ethynylbenzene ligands such as DEB and TEB are generally competent for mediating  $J$ -coupling in transition metal complexes, but not for U(IV) with the NN<sub>3</sub> ancillary ligand set in the t<sub>bp</sub> coordination geometry.

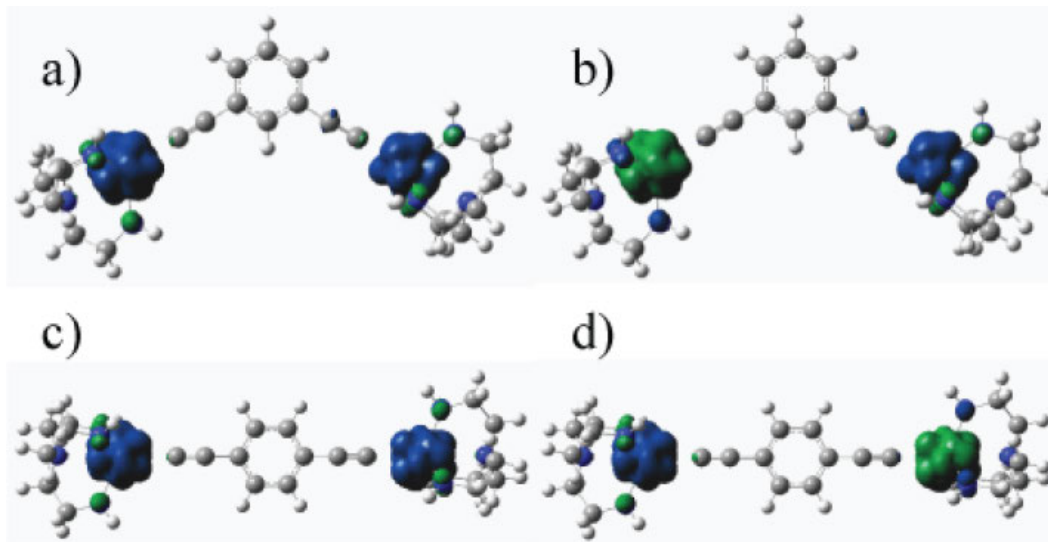


**Figure 2.8.** Net spin density plots for *m*- and *p*-DEB-bridged dinuclear species based on **2.4** and **2.5**. Blue surfaces correspond to net  $\alpha$  spin density and green to net  $\beta$  spin density. Triplets are displayed in a and c, and singlet (broken symmetry) wavefunctions are shown in b and d.

## 2.5 Summary and Outlook

We have prepared a structurally related family of penta- and hexacoordinate U(IV) complexes bridged by anionic ethynylbenzene ligands, and have used multiple techniques to characterize them. Despite the fact that all the compounds in this study give non-magnetic ground states at low temperature, consistent with those described elsewhere in the literature,<sup>94-98,100-105,110-112</sup> we have shown that the di- and trinuclear pentacoordinate U(IV)-containing compounds **2.4**, **2.5**, and **2.6** appear to display weak ferromagnetic communication between the uranium centers, as evidenced by fits to the magnetic data.

This is promising for future work utilizing actinide elements in the generation of new SMMs.

The observed and calculated magnetic properties of this family of U(IV)-containing complexes can be rationalized in the following way. First, a trigonal bipyramidal ligand field provides the potential to observe a triplet ground state for a U(IV) ion, but spin-orbit coupling causes admixture of excited singlet states, reducing paramagnetic contributions. Second, although calculations point to  $\pi$ -type orbital overlap between acetylide ligands and the  $5f$  orbitals of the U(IV) ion, negligible spin density from the metal leaks onto the bridging ligands, leading to weak ferromagnetic coupling via application of Hund's rule.

The lack of delocalization for U(IV) is likely due to a metal-bridging ligand energy mismatch. Andersen's bis-diazenylbenzene ligand<sup>59</sup> or a bis-cyanylbenzene species is hypothesized to provide a better energy match. In addition, because the  $f$  orbitals that can interact with acetylide  $\pi$  orbitals also have  $\sigma$  interactions with the  $\text{NN}'_3$  ligand, substituent changes on the tetradentate ligand may also give rise to significant changes in magnetism. Computational studies focusing on *meta* and *para* substituted uranium complexes with modified bridging ligands are planned, and the results will be compared with transition-metal based systems, both experimentally and computationally.

We have also shown that the monomeric arylacetylide complex, **2.3**, undergoes a reversible redox couple assignable to a U(IV/V) process. This offers a route toward half integer actinide-containing spin systems where the DEB ligand may enjoy more substantial orbital overlap with U(III) or U(V) ions. Efforts to find chemically accessible reductions or oxidations of **2.1**, **2.4–2.6**, and related compounds to U(III) or U(V) are

underway. Precedent for this possibility is given by the recent report of organometallic U(IV) complex oxidation by Cu(I) phenylacetylide.<sup>113</sup>

**2.6 Acknowledgments.** This research was supported by Colorado State University and the ACS Petroleum Research Fund (44691-G3). We thank Ms. Susie Miller and Prof. Oren Anderson for advice on crystal structure refinements, Dr. Christopher Rithner for assistance with NMR data collection, and Dr. J. Hay and Prof. C. M. Elliott for helpful conversations.

## 2.7 References

- (1) Andrea, T.; Eisen, M. S., *Chem. Soc. Rev.* **2008**, *37*, 550.
- (2) Ephritikhine, M., *Dalton Trans.* **2006**, 2501.
- (3) Fox, A. R.; Bart, S. C.; Meyer, K.; Cummins, C. C., *Nature* **2008**, *455*, 341.
- (4) Schnaars, D. D.; Wu, G.; Hayton, T. W., *Dalton Trans.* **2008**, 6121.
- (5) Denning, R. G., *J. Phys. Chem. A* **2007**, *111*, 4125.
- (6) Gaunt, A. J.; Reilly, S. D.; Enriquez, A. E.; Scott, B. L.; Ibers, J. A.; Sekar, P.; Ingram, K. I. M.; Kaltsoyannis, N.; Neu, M. P., *Inorg. Chem.* **2008**, *47*, 29.
- (7) Jensen, M. P.; Bond, A. H., *J. Am. Chem. Soc.* **2002**, *124*, 9870.
- (8) Choppin, G. R., *J. Alloy* **2002**, *344*, 55.
- (9) Mazzanti, M.; Wietzke, R. L.; Pecaut, J.; Latour, J. M.; Maldivi, P.; Remy, M., *Inorg. Chem.* **2002**, *41*, 2389.
- (10) Miguirditchian, M.; Guillaneux, D.; Guillaumont, D.; Moisy, P.; Madic, C.; Jensen, M. P.; Nash, K. L., *Inorg. Chem.* **2005**, *44*, 1404.
- (11) Rinehart, J. D.; Harris, T. D.; Kozimor, S. A.; Bartlett, B. M.; Long, J. R., *Inorg. Chem.* **2009**, *48*, 3382.
- (12) Sessoli, R.; Tsai, H. L.; Schake, A. R.; Wang, S. Y.; Vincent, J. B.; Folting, K.; Gatteschi, D.; Christou, G.; Hendrickson, D. N., *J. Am. Chem. Soc.* **1993**, *115*, 1804.
- (13) Sessoli, R.; Gatteschi, D.; Caneschi, A.; Novak, M. A., *Nature* **1993**, *365*, 141.
- (14) Aromi, G.; Brechin, E. K., Synthesis of 3d metallic single-molecule magnets. In *Single-Molecule Magnets and Related Phenomena*, 2006; Vol. 122, pp 1.

- (15) Milios, C. J.; Inglis, R.; Vinslava, A.; Bagai, R.; Wernsdorfer, W.; Parsons, S.; Perlepes, S. P.; Christou, G.; Brechin, E. K., *J. Am. Chem. Soc.* **2007**, *129*, 12505.
- (16) Long, J. R., *Chemistry of Nanostructured Materials*. World Scientific: Hong Kong, 2003.
- (17) Bogani, L.; Wernsdorfer, W., *Nature Mat.* **2008**, *7*, 179.
- (18) Friedman, J. R.; Sarachik, M. P.; Tejada, J.; Ziolo, R., *Phys. Rev. Lett.* **1996**, *76*, 3830.
- (19) Thomas, L.; Lioni, F.; Ballou, R.; Gatteschi, D.; Sessoli, R.; Barbara, B., *Nature* **1996**, *383*, 145.
- (20) Gatteschi, D.; Sessoli, R., *Angew. Chem.-Int. Edit.* **2003**, *42*, 268.
- (21) Wernsdorfer, W.; Sessoli, R., *Science* **1999**, *284*, 133.
- (22) Leuenberger, M. N.; Loss, D., *Nature* **2001**, *410*, 789.
- (23) Affronte, M.; Troiani, F.; Ghirri, A.; Carretta, S.; Santini, P.; Corradini, V.; Schuecker, R.; Murn, C.; Timco, G.; Winpenny, R. E., *Dalton Trans.* **2006**, 2810.
- (24) Ciasca, G.; De Seta, M.; Capellini, G.; Evangelisti, F.; Ortolani, M.; Virgilio, M.; Grosso, G.; Nucara, A.; Calvani, P., *Phys. Rev. B* **2009**, *79*, 7.
- (25) Evangelisti, M.; Candini, A.; Ghirri, A.; Affronte, M.; Brechin, E. K.; McInnes, E. J. L., *Appl. Phys. Lett.* **2005**, *87*, 3.
- (26) Mishra, A.; Tasiopoulos, A. J.; Wernsdorfer, W.; Abboud, K. A.; Christou, G., *Inorg. Chem.* **2007**, *46*, 3105.
- (27) Costes, J. P.; Auchel, M.; Dahan, F.; Peyrou, V.; Shova, S.; Wernsdorfer, W., *Inorg. Chem.* **2006**, *45*, 1924.

- (28) Hamamatsu, T.; Yabe, K.; Towatari, M.; Osa, S.; Matsumoto, N.; Re, N.; Pochaba, A.; Mrozinski, J.; Gallani, J. L.; Barla, A.; Imperia, P.; Paulsen, C.; Kappler, J. P., *Inorg. Chem.* **2007**, *46*, 4458.
- (29) Mishra, A.; Wernsdorfer, W.; Abboud, K. A.; Christou, G., *J. Am. Chem. Soc.* **2004**, *126*, 15648.
- (30) Zaleski, C. M.; Depperman, E. C.; Kampf, J. W.; Kirk, M. L.; Pecoraro, V. L., *Angew. Chem. Int. Ed.* **2004**, *43*, 3912.
- (31) Gao, S.; Su, G.; Yi, T.; Ma, B. Q., *Phys. Rev. B* **2001**, *63*, 054431.
- (32) Mereacre, V. M.; Ako, A. M.; Clerac, R.; Wernsdorfer, W.; Filoti, G.; Bartolome, J.; Anson, C. E.; Powell, A. K., *J. Am. Chem. Soc.* **2007**, *129*, 9248.
- (33) Papatriantafyllopoulou, C.; Estrader, M.; Efthymiou, C. G.; Dermitzaki, D.; Gkotsis, K.; Terzis, A.; Diaz, C.; Perlepes, S. P., *Polyhedron* **2009**, *28*, 1652.
- (34) Klokishner, S. I.; Ostrovsky, S. M.; Reu, O. S.; Palii, A. V.; Tregenna-Piggott, P. L. W.; Brock-Nannestad, T.; Bendix, J.; Mutka, H., *J. Phys. Chem. C* **2009**, *113*, 8573.
- (35) Mereacre, V.; Prodius, D.; Ako, A. M.; Kaur, N.; Lipkowski, J.; Simmons, C.; Dalal, N.; Geru, I.; Anson, C. E.; Powell, A. K.; Turta, C., *Polyhedron* **2008**, *27*, 2459.
- (36) Sorace, L.; Sangregorio, C.; Figuerola, A.; Benelli, C.; Gatteschi, D., *Chem. Eur. J.* **2009**, *15*, 1377.
- (37) Ishikawa, N.; Sugita, M.; Ishikawa, T.; Koshihara, S.; Kaizu, Y., *J. Am. Chem. Soc.* **2003**, *125*, 8694.
- (38) Ishikawa, N.; Sugita, M.; Ishikawa, T.; Koshihara, S.; Kaizu, Y., *J. Phys. Chem. B* **2004**, *108*, 11265.
- (39) Ishikawa, N.; Sugita, M.; Wernsdorfer, W., *J. Am. Chem. Soc.* **2005**, *127*, 3650.

- (40) Ishikawa, N.; Sugita, M.; Wernsdorfer, W., *Angew. Chem. Int. Ed.* **2005**, *44*, 2931.
- (41) AlDamen, M. A.; Clemente-Juan, J. M.; Coronado, E.; Martí-Gastaldo, C.; Gaita-Ariño, A., *J. Am. Chem. Soc.* **2008**, *130*, 8874.
- (42) Gamer, M. T.; Lan, Y.; Roesky, P. W.; Powell, A. K.; Clérac, R., *Inorg. Chem.* **2008**, *47*, 6518.
- (43) Kahn, M. L.; Mathoniere, C.; Kahn, O., *Inorg. Chem.* **1999**, *38*, 3692.
- (44) Benelli, C.; Gatteschi, D., *Chem. Rev.* **2002**, *102*, 2369.
- (45) Costes, J. P.; Dahan, F.; Dupuis, A.; Laurent, J. P., *Chem. Eur. J.* **1998**, *4*, 1616.
- (46) Kaltsoyannis, N.; Scott, P., *The f Elements*. Oxford University Press: New York, 1999; p 46.
- (47) Monreal, M. J.; Diaconescu, P. L., *Organometallics* **2008**, *27*, 1702.
- (48) Diaconescu, P. L.; Arnold, P. L.; Baker, T. A.; Mindiola, D. J.; Cummins, C. C., *J. Am. Chem. Soc.* **2000**, *122*, 6108.
- (49) Kozimor, S. A.; Bartlett, B. M.; Rinehart, J. D.; Long, J. R., *J. Am. Chem. Soc.* **2007**, *129*, 10672.
- (50) Rinehart, J. D.; Bartlett, B. M.; Kozimor, S. A.; Long, J. R., *Inorg. Chem. Acta* **2008**, *361*, 3534.
- (51) Gaunt, A. J.; Reilly, S. D.; Enriquez, A. E.; Scott, B. L.; Ibers, J. A.; Sekar, P.; Ingram, K. I. M.; Kaltsoyannis, N.; Neu, M. P., *Inorg. Chem.* **2008**, *47*, 29.
- (52) Schelter, E. J.; Veauthier, J. M.; Thompson, J. D.; Scott, B. L.; John, K. D.; Morris, D. E.; Kiplinger, J. L., *J. Am. Chem. Soc.* **2006**, *128*, 2198.
- (53) Salmon, L.; Thuery, P.; Riviere, E.; Ephritikhine, M., *Inorg. Chem.* **2006**, *45*, 83.

- (54) Graves, C. R.; Yang, P.; Kozimor, S. A.; Vaughn, A. E.; Clark, D. L.; Conradson, S. D.; Schelter, E. J.; Scott, B. L.; Thompson, J. D.; Hay, P. J.; Morris, D. E.; Kiplinger, J. L., *J. Am. Chem. Soc.* **2008**, *130*, 5272.
- (55) Schelter, E. J.; Wu, R. L.; Scott, B. L.; Thompson, J. D.; Morris, D. E.; Kiplinger, J. L., *Angew. Chem.-Int. Edit.* **2008**, *47*, 2993.
- (56) Kiplinger, J. L.; Scott, B. L.; Schelter, E. J.; Tourneir, J., *J. Alloy* **2007**, *444*, 477.
- (57) Rosen, R. K.; Andersen, R. A.; Edelstein, N. M., *J. Am. Chem. Soc.* **1990**, *112*, 4588.
- (58) Figgis, B. N.; Hitchman, M. A., *Ligand Field Theory and Its Applications*. Wiley-VCH: 2000; p 354.
- (59) Edwards, P. G.; Andersen, R. A.; Zalkin, A., *J. Am. Chem. Soc.* **1981**, *103*, 7792.
- (60) Cotton, S., *Lanthanide and Actinide Chemistry*. Wiley: West Sussex, 2006; p 263.
- (61) Schelter, E. J.; Yang, P.; Scott, B. L.; Thompson, J. D.; Martin, R. L.; Hay, P. J.; Morris, D. E.; Kiplinger, J. L., *Inorg. Chem.* **2007**, *46*, 7477.
- (62) Gebala, A. E.; Tsutsui, M., *J. Am. Chem. Soc.* **1973**, *95*, 91.
- (63) Boaretto, R.; Roussel, P.; Alcock, N. W.; Kingsley, A. J.; Munslow, I. J.; Sanders, C. J.; Scott, P., *J. Organomet. Chem.* **1999**, *591*, 174.
- (64) Roussel, P.; Hitchcock, P. B.; Tinker, N.; Scott, P., *Chem. Commun.* **1996**, 2053.
- (65) Le Borgne, T.; Riviere, E.; Marrot, J.; Thuery, P.; Girerd, J. J.; Ephritikhine, M., *Chem. Eur. J.* **2002**, *8*, 774.
- (66) Roussel, P.; Hitchcock, P. B.; Tinker, N. D.; Scott, P., *Inorg. Chem.* **1997**, *36*, 5716.
- (67) Weyland, T.; Costuas, K.; Mari, A.; Halet, J. F.; Lapinte, C., *Organometallics* **1998**, *17*, 5569.

- (68) Zimmerman, P. M.; Paul, A.; Zhang, Z. Y.; Musgrave, C. B., *Inorg. Chem.* **2009**, *48*, 1069.
- (69) Hermann, J. A.; Suttle, J. F., *Inorg. Synth.* **1957**, *5*, 143.
- (70) Roussel, P.; Alcock, N. W.; Scott, P., *Inorg. Chem.* **1998**, *37*, 3435.
- (71) Roussel, P.; Alcock, N. W.; Boaretto, R.; Kingsley, A. J.; Munslow, I. J.; Sanders, C. J.; Scott, P., *Inorg. Chem.* **1999**, *38*, 3651.
- (72) Royles, B. J. L.; Smith, D. M., *J. Chem. Soc.-Perkin Trans. 1* **1994**, 355.
- (73) Sheldrick, G. M. *SADABS*, Bruker AXS: Madison, WI.
- (74) Sheldrick, G. M. *SHELXTL*, Bruker AXS: Madison, WI, 2004.
- (75) Spek, A. L., *J. Appl. Cryst.* **2003**, *36*, 7.
- (76) Schmitt, E. A. Characterization of Tetranuclear Manganese Complexes and Thermochromic Cu(II) and Ni(II) Complexes. Ph.D. Thesis, University of Illinois at Urbana-Champaign, 1995.
- (77) Becke, A. D., *J. Chem. Phys.* **1993**, *98*, 5648.
- (78) Noodleman, L.; Davidson, E. R., *Chem. Phys.* **1986**, *109*, 131.
- (79) Hart, J. R.; Rappe, A. K.; Gorun, S. M.; Upton, T. H., *J. Phys. Chem.* **1992**, *96*, 6255.
- (80) Noodleman, L., *J. Chem. Phys.* **1981**, *74*, 5737.
- (81) Kuechle, W.; Dolg, M.; Stoll, H.; Preuss, H., *Mol. Phys.* **1991**, *74*, 1245.
- (82) Ditchfield, R.; Hehre, W. J.; Pople, J. A., *J. Chem. Phys.* **1971**, *54*, 724.

- (83) Hehre, W. J.; Ditchfie.R; Pople, J. A., *J. Chem. Phys.* **1972**, *56*, 2257.
- (84) Binkley, J. S.; Pople, J. A.; Hehre, W. J., *J. Am. Chem. Soc.* **1980**, *102*, 939.
- (85) Frisch, M. J. *Gaussian 03*, Gaussian, Inc.: Wallingford, CT, 2004.
- (86) Guionneau, P.; Marchivie, M.; Bravic, G.; Letard, J. F.; Chasseau, D., *J. Mater. Chem.* **2002**, *12*, 2546.
- (87) Ball, R. G.; Edelman, F.; Matisons, J. G.; Takats, J.; Marques, N.; Marcalo, J.; Dematos, A. P.; Bagnall, K. W., *Inorg. Chem. Acta* **1987**, *132*, 137.
- (88) Gorden, A. E. V.; Xu, J. D.; Raymond, K. N.; Durbin, P., *Chem. Rev.* **2003**, *103*, 4207.
- (89) Charpin, P.; Nierlich, M.; Vigner, D.; Lance, M.; Baudin, C., *Acta Cryst.* **1988**, *44*, 255.
- (90) Gaunt, A. J.; Scott, B. L.; Neu, M. P., *Inorg. Chem.* **2006**, *45*, 7401.
- (91) Salmon, L.; Thuery, P.; Asfari, Z.; Ephritikhine, M., *Dalton Trans.* **2006**, 3006.
- (92) Salmon, L.; Thuery, P.; Ephritikhine, M., *Chem. Comm.* **2006**, 856.
- (93) Boaretto, R.; Roussel, P.; Kingsley, A. J.; Munslow, I. J.; Sanders, C. J.; Alcock, N. W.; Scott, P., *Chem. Comm.* **1999**, 1701.
- (94) Roussel, P.; Boaretto, R.; Kingsley, A. J.; Alcock, N. W.; Scott, P., *J. Chem. Soc.-Dalton Trans.* **2002**, 1423.
- (95) Schelter, E. J.; Veauthier, J. M.; Graves, C. R.; John, K. D.; Scott, B. L.; Thompson, J. D.; Pool-Davis-Tournear, J. A.; Morris, D. E.; Kiplinger, J. L., *Chem. Eur. J.* **2008**, *14*, 7782.
- (96) Graves, C. R.; Vaughn, A. E.; Schelter, E. J.; Scott, B. L.; Thompson, J. D.; Morris, D. E.; Kiplinger, J. L., *Inorg. Chem.* **2008**, *47*, 11879.

- (97) Kreindlin, A. Z.; Dolgushin, F. M.; Yanovsky, A. I.; Kerzina, Z. A.; Petrovskii, P. V.; Rybinskaya, M. I., *J. Organomet. Chem.* **2000**, *616*, 106.
- (98) Spirlet, M. R.; Rebizant, J.; Apostolidis, C.; Dornberger, E.; Kanellakopulos, B.; Powietzka, B., *Poly* **1996**, *15*, 1503.
- (99) Siddall, T. H., *Theory and Applications of Molecular Paramagnetism*. Wiley: New York, 1976.
- (100) Kanellakopulos, B., *Organometallics of the f-Elements*. Dordrecht, Netherlands, 1978.
- (101) Edelstein, N. M.; Lander, G. H., *The Chemistry of the Actinide and Transactinide Elements*. Springer: 2006; Vol. 4, Ch. 20.
- (102) Almond, P. M.; Deakin, L.; Porter, M. J.; Mar, A.; Albrecht-Schmitt, T. E., *Chem. Mat.* **2000**, *12*, 3208.
- (103) Kiplinger, J. L.; Pool, J. A.; Schelter, E. J.; Thompson, J. D.; Scott, B. L.; Morris, D. E., *Angew. Chem.-Int. Edit.* **2006**, *45*, 2036.
- (104) Schelter, E. J.; Morris, D. E.; Scott, B. L.; Thompson, J. D.; Kiplinger, J. L., *Inorg. Chem.* **2007**, *46*, 5528.
- (105) Salmon, L.; Thuery, P.; Riviere, E.; Girerd, J. J.; Ephritikhine, M., *Chem. Commun.* **2003**, 762.
- (106) Shores, M. P.; Sokol, J. J.; Long, J. R., *J. Am. Chem. Soc.* **2002**, *124*, 2279.
- (107) Chiu, Y. N.; Wang, F. E., *Theor. Chim. Acta* **1985**, *68*, 179.
- (108) Ovchinnikov, A. A., *Theor. Chim. Acta* **1978**, *47*, 297.
- (109) Hoffert, W. A.; Rappe, A. K.; Shores, M. P., *Manuscript in preparation*, Using a LANL2/6.

- (110) Boudreaux, E. M., L. N., *Theory and Application of Molecular Paramagnetism*. John Wiley & Sons: New York, 1976; p 510.
- (111) Suski, W.; Baran, A.; Folcik, L.; Wochowski, K.; Mydlarz, T., *J. Alloy* **1992**, *181*, 249.
- (112) Karbowski, M.; Drozdowski, J., *J. Alloy* **1998**, *271*, 863.
- (113) Graves, C. R.; Scott, B. L.; Morris, D. E.; Kiplinger, J. L., *Organometallics* **2008**, *27*, 3335.

## Chapter 3. Synthesis and Characterization of a Novel Tetranuclear 5f

### Compound: Stable Synthons for Exploring U(IV) Chemistry

#### 3.1 Introduction

Burgeoning interest in organouranium complexes stems from their potential to impart unusual and/or catalytic reactivity on organic substrates as well as to offer insight into actinide electronic structure.<sup>1-6</sup> The preparation of stable mixed ligand uranium compounds is of importance to realize these goals, as evidenced by recent efforts.<sup>3,5,7-15</sup> Such complexes also aid understanding of actinide magnetochemistry. The magnetic properties of actinides represent a mixing of properties normally associated with transition metal (magnetic exchange coupling) and lanthanide ions (e.g. spin-orbit coupling).<sup>4</sup> Large spin-orbit coupling may be anticipated to generate anisotropy, relevant to maximizing single-molecule magnet (SMM) blocking temperatures, provided that paramagnetic ground states are achieved. Slow relaxation of magnetization has been observed recently in certain uranium complexes.<sup>4,15,16</sup> A recent effort in our group to control U(IV) paramagnetism and magnetic communication via trigonal bipyramidal coordination of the ion shows some promise in terms of magnetic coupling, but is countered by relatively weak overlap of bridging ligand and metal orbitals attributable to the hardness of the ancillary triamidoamine ligand set.<sup>17</sup>

To improve U-L-M communication, we are pursuing “new” U(IV) building blocks, and have become interested in precedent surrounding octacoordinate [(dmpe)<sub>2</sub>UX<sub>4</sub>] (dmpe = 1,2-bis(dimethylphosphino)ethane, X = Cl or Me) complexes. First reported by

Andersen in 1981, these species display cubic-like geometries, which in principle allow for paramagnetic  $f^2$  ground states.<sup>18</sup> In addition, the softer dmpe ligands may increase U-ligand orbital overlap and afford greater spin density on acetylide bridging ligands. Finally, fruitful substitution chemistry has been demonstrated, with the chloride ligands replaceable by alkyl and ultimately alkoxide ligands. Similar to our work, and following Scott's precedent,<sup>17,19</sup> these complexes appear suitable for substitution with acetylide-type ligands. From here, elaboration to  $UM_4$  molecular species and/or network solids is envisioned, wherein interesting magnetic properties may be present in the new compounds.

In the process of reproducing Andersen's chemistry for production of  $[(dmpe)_2UX_4]$  starting materials, we have obtained X-ray quality crystals of  $[(dmpe)_2UCl_4]$  (**3.1**) and  $[(dmpe)_2UMe_4]$  (**3.2**), structural data for which have not been reported previously. More significantly, we have found that variation of U:dmpe stoichiometry leads to a previously unknown tetranuclear complex,  $[(dmpe)_4U_4Cl_{16}] \cdot 2CH_2Cl_2$  (**3.3**· $2CH_2Cl_2$ ). This novel tetranuclear complex acts as a “(dmpe)UCl<sub>4</sub>” synthon, allowing the preparation of U(IV) complexes with mixed-chelating ligands; synthetic utility is demonstrated via the preparation of  $[(dmpe)(dmbpy)UCl_4]$  (**3.4**) (dmbpy = 4,4'-dimethyl-2,2'-bipyridine). Herein, we describe the preparation, characterization, and structures of the mono- and tetranuclear octacoordinate U(IV) complexes **3.1–3.4**.

### **3.2 Division of Labor Section**

All experimental work and characterization was performed by Brian S. Newell with help from Trevor C. Schwaab. This has been accepted to *Inorg. Chem.* after being revised based on comments from three external reviewers.

### 3.3 Experimental Section

**3.3.1 Preparation of Compounds.** All manipulations were carried out either inside a dinitrogen- filled glove box (MBRAUN Labmaster 130) or via standard Schlenk techniques on a dinitrogen manifold. Pentane was distilled over sodium metal, degassed by three freeze-pump-thaw cycles, and stored under an atmosphere of dinitrogen. All other solvents were reagent grade, passed through alumina, degassed and stored under dinitrogen. The compounds  $\text{UCl}_4$ ,<sup>20</sup>  $[(\text{dmpe})_2\text{UCl}_4]$  (**3.1**) and  $[(\text{dmpe})_2\text{UMe}_4]$  (**3.2**) (dmpe = 1,2-bis(dimethylphosphino)ethane) were prepared according to the literature.<sup>18</sup> Methylithium was titrated prior to use with accurately weighed amounts of menthol and 2,2'-bipyridyl. All other reagents were obtained from commercial vendors and used without further purification.

*Caution! Depleted uranium (primary isotope  $^{238}\text{U}$ ) is a weak  $\alpha$  emitter (4.197 MeV) with a half-life of  $4.47 \times 10^9$  years; manipulations and reactions should be carried out in monitored fume hoods or in an inert atmosphere glove box in a radiation laboratory equipped with  $\alpha$ - and  $\beta$ -particle counting equipment.*

**$[(\text{dmpe})_2\text{UCl}_4]$  (3.1).** Liquid dmpe (2.012 g, 13.40 mmol) was added to a stirring slurry of  $\text{UCl}_4$  (3.310 g, 8.714 mmol) in 175 mL of dichloromethane, and the resulting green mixture was stirred overnight at ambient temperature. The mixture was filtered, and the volume of the blue-green filtrate was reduced to ca. 5 mL under reduced pressure, then the filtrate was maintained at  $-35^\circ\text{C}$  for 8 h to afford a blue-green crystalline solid. The solid was collected by filtration and dried in vacuo to yield a blue-green crystalline powder (5.028 g, 85 % based on  $\text{UCl}_4$ ). Single crystals suitable for X-ray analysis were grown from a concentrated dichloromethane solution maintained at  $-35^\circ\text{C}$  for 8 h.

Absorption spectrum ( $\text{CH}_2\text{Cl}_2$ )  $\lambda_{\text{max}}$  ( $\epsilon_{\text{M}}$ ): 458 (61), 509 (44), 529 (43), 591 (36), 632 (16), 654 (19), 668 (47), 686 (208), 699 (173), 852 (8), 920 (18), 934 (19), 960 nm (10  $\text{L}\cdot\text{mol}^{-1}\cdot\text{cm}^{-1}$ ). Absorption spectrum ( $(\text{CH}_3)_2\text{SO}$ )  $\lambda_{\text{max}}$  ( $\epsilon_{\text{M}}$ ): 442 (22), 495 (38), 560 (32), 650 (73), 678 (99), 913 nm (17  $\text{L}\cdot\text{mol}^{-1}\cdot\text{cm}^{-1}$ ).  $^1\text{H}$  NMR (293 K, toluene- $d_8$ ):  $\delta$  2.19 (s, 24 H,  $\text{PCH}_3$ ),  $-20.56$  ppm (s, 8 H,  $\text{PCH}_2$ ); the spectrum matches that reported by Andersen and coworkers,<sup>18</sup> which is not the same as free dmpe.  $^1\text{H}$  NMR (293 K,  $\text{CD}_2\text{Cl}_2$ ):  $\delta$  2.36 (24 H,  $\text{PCH}_3$ ),  $-19.4$  ppm (8 H,  $\text{PCH}_2$ ).  $\{^1\text{H}\}^{31}\text{P}$  NMR (293 K,  $\text{CD}_2\text{Cl}_2$ ):  $\delta$   $-48.01$  ppm. The  $^1\text{H}$  spectrum obtained in  $\text{CD}_2\text{Cl}_2$  does not match that obtained for free dmpe. The  $\{^1\text{H}\}^{31}\text{P}$  NMR spectrum appears to be dominated by the free dmpe signal (Figure A2.15).  $^1\text{H}$  NMR (293 K,  $(\text{CD}_3)_2\text{SO}$ ):  $\delta$  1.36 (t ( $j_{12} = 5$  Hz) and ( $j_{23} = 5$  Hz), 4 H,  $\text{PCH}_2$ ), 0.96 ppm (s, 12 H,  $\text{PCH}_3$ ).  $\{^1\text{H}\}^{31}\text{P}$  NMR (293 K,  $(\text{CD}_3)_2\text{SO}$ ):  $\delta$   $-48.69$  ppm. Note: the spectra collected in DMSO match those obtained for free dmpe. IR (mineral oil): 631 (w), 646 (w), 705 (m), 722 (m), 771 (w), 815 (w), 830 (w), 867 (m), 934 (m), 994 (w), 1086 (w), 1132 (w), 1156 (w), 1168 (w), 1277 (m), 1291 (m), 1377 (s), 1422 (m), 1461 (s), 2671 (w), 2724 (w), 2840 (s), 2924 (s)  $\text{cm}^{-1}$ . Magnetic susceptibility (SQUID, 300 K):  $\mu_{\text{eff}} = 3.40 \mu_{\text{B}}$ . Anal. Calcd. for  $\text{C}_{12}\text{H}_{32}\text{P}_4\text{UCl}_4$ : C, 21.19; H, 4.74. Found: C, 21.27; H, 4.70.

**[(dmpe)<sub>2</sub>UMe<sub>4</sub>] (3.2).** Methyl lithium (6.0 mL, 9.8 mmol) was added drop-wise to a stirring solution of **3.1** (1.498 g, 2.203 mmol) in 80 mL of diethyl ether held at  $-20^\circ\text{C}$ . The resulting yellow-brown mixture was stirred for 30 min at  $-20^\circ\text{C}$ . All volatiles were removed in vacuo to afford a yellow residue. The crude product was extracted into pentane ( $3 \times 10$  mL) and filtered, and the volume of the filtrate was reduced to ca. 5 mL under reduced pressure. After standing for 8 h at  $-35^\circ\text{C}$ , a yellow crystalline solid formed. The product was collected by filtration and dried in vacuo to yield a dark yellow

powder (0.815 g, 62 % based on **3.1**). Single crystals suitable for X-ray analysis were grown from a concentrated pentane solution maintained at  $-35\text{ }^{\circ}\text{C}$  for 8 h.  $^1\text{H}$  NMR (213 K, toluene- $d_8$ ):  $\delta$  11.27 (s, 12 H,  $\text{UCH}_3$ ),  $-1.53$  (s, 24 H,  $\text{PCH}_3$ ),  $-43.93$  ppm (s, 8 H,  $\text{PCH}_2$ ). The spectrum changes significantly upon warming to room temperature; see Figure A2.16 in the Appendix 2. IR (mineral oil): 629 (w), 641 (w), 695 (m), 723 (m), 770 (w), 826 (w), 862 (m), 889 (w), 939 (m), 966 (w), 997 (w), 1031 (w), 1084 (w), 1134 (w), 1155 (w), 1168 (w), 1278 (m), 1294 (m), 1377 (s), 1422 (m), 1468 (s), 2671 (w), 2725 (w), 2832 (s), 2946 (s)  $\text{cm}^{-1}$ . Magnetic susceptibility (SQUID, 300 K):  $\mu_{\text{eff}} = 3.23\ \mu_{\text{B}}$ . Anal. Calcd. for  $\text{C}_{16}\text{H}_{44}\text{P}_4\text{U}$ : C, 32.11; H, 7.41. Found: C, 31.34; H, 7.37.

**$[(\text{dmpe})_4\text{U}_4\text{Cl}_{16}] \cdot 2\text{CH}_2\text{Cl}_2$  (**3.3**·**2CH<sub>2</sub>Cl<sub>2</sub>**)**. Liquid dmpe (0.9980 g, 6.647 mmol) was added to a stirring slurry of  $\text{UCl}_4$  (2.000 g, 5.265 mmol) in 100 mL of dichloromethane, and the resulting green mixture was stirred overnight at ambient temperature. The mixture was filtered, the green filtrate was collected, and the volume was reduced to a volume of ca. 5 mL under reduced pressure. After standing 8 h at  $-35\text{ }^{\circ}\text{C}$ , a green crystalline solid formed. The solid was collected by filtration and dried in vacuo to afford a green powder (2.360 g, 85 % based on  $\text{UCl}_4$ ). Single crystals suitable for X-ray analysis were grown from a concentrated dichloromethane solution maintained at  $-35\text{ }^{\circ}\text{C}$  for 8 h. Absorption spectrum ( $(\text{CH}_3)_2\text{SO}$ )  $\lambda_{\text{max}}$  ( $\epsilon_{\text{M}}$ ): 442 (11), 469 (8), 496 (21), 560 (17), 650 (41), 678 (57), 906 nm ( $8\ \text{L} \cdot \text{mol}^{-1} \cdot \text{cm}^{-1}$ ).  $^1\text{H}$  NMR (293 K,  $\text{CD}_2\text{Cl}_2$ ):  $\delta$  2.35 (48 H,  $\text{PCH}_3$ ),  $-19.45$  ppm (16 H,  $\text{PCH}_2$ ).  $\{^1\text{H}\}^{31}\text{P}$  NMR (293 K,  $\text{CD}_2\text{Cl}_2$ ):  $\delta$   $-9.402$  (d,  $j = 56.7$  Hz),  $-12.122$  (d,  $j = 56.7$  Hz),  $-14.834$  (d,  $j = 56.7$  Hz),  $-46.877$  ppm (d,  $j = 54.3$  Hz). The  $^1\text{H}$  spectra obtained in  $\text{CD}_2\text{Cl}_2$  contain a very small amount of free dmpe (Figure A2.19). The  $\{^1\text{H}\}^{31}\text{P}$  NMR spectrum appears to be dominated by the free dmpe signal

(Figure A2.20).  $^1\text{H}$  NMR (293 K,  $(\text{CD}_3)_2\text{SO}$ ):  $\delta$  1.35 (br, 4 H,  $\text{PCH}_2$ ), 0.95 ppm (br, 12 H,  $\text{PCH}_3$ ).  $\{^1\text{H}\}^{31}\text{P}$  NMR (293 K,  $(\text{CD}_3)_2\text{SO}$ ):  $\delta$   $-48.69$  ppm. Note: the spectra collected in DMSO match those obtained for free dmpe. IR (mineral oil): 2924 (s), 2840 (s), 2724 (w), 2671 (w), 1462 (s), 1418 (m), 1377 (s), 1296 (m), 1278 (m), 1167 (w), 1155 (w), 1134 (w), 1086 (w), 995 (w), 947 (m), 932 (m), 895 (m), 867 (m), 833 (w), 805 (w), 772 (w), 737 (m), 724 (m), 706 (m)  $\text{cm}^{-1}$ . Magnetic susceptibility (SQUID, 300 K):  $\mu_{\text{eff}} = 5.39 \mu_{\text{B}}$ . Anal. Calcd. for  $\text{C}_{26}\text{H}_{68}\text{P}_8\text{U}_4\text{Cl}_{20}$ : C, 13.64; H, 2.99. Found: C, 12.83; H, 2.98. Although single crystals have approximately 7.75  $\text{CH}_2\text{Cl}_2$  solvate molecules per **3.3**, elemental analysis of the bulk product best matches the formula **3.3** $\cdot 2\text{CH}_2\text{Cl}_2$ . Even so, elemental analysis reveals a deficiency in the observed percent of carbon; however, a small amount of dark gray material remains after combustion, consistent with the production of refractory uranium carbides. Further details are provided in the Supporting Information.

Of the solvents tried (hexanes, pentane, dimethylsulfoxide, dichloromethane, acetonitrile, benzene, toluene, diethyl ether, and tetrahydrofuran) **3.3** is only readily soluble in dimethylsulfoxide and slightly soluble in dichloromethane.

**[(dmpe)(dmbpy)UCl<sub>4</sub>] (3.4)**. Solid **3.3** $\cdot 2\text{CH}_2\text{Cl}_2$  (0.292 g, 0.128 mmol) was combined with 4,4'-dimethyl-2,2'-bipyridine (0.095 g, 0.52 mmol) and 15 mL of dichloromethane. The resulting light green mixture was stirred at ambient temperature for 8 h. The mixture was filtered, the filtrate was collected, dried in vacuo, and recrystallized from acetonitrile to afford a light green solid (0.300 g recovered, 82% based on **3.3** $\cdot 2\text{CH}_2\text{Cl}_2$ ). Single crystals suitable for X-ray analysis were grown from a concentrated acetonitrile solution maintained at  $-35$  °C for 8 h. Absorption spectrum ( $\text{CH}_3\text{CN}$ )  $\lambda_{\text{max}}$

( $\epsilon_M$ ): 457 (52), 489 (20), 508 (38), 522 (28), 590 (24), 630 (16), 680 (105), 685 (122), 698 (92), 847 (10), 920 (14), 946 (14), 959 (12), 1075 nm (27 L·mol<sup>-1</sup>·cm<sup>-1</sup>). <sup>1</sup>H NMR (293 K, CD<sub>3</sub>CN):  $\delta$  8.52 (d ( $j = 5$  Hz), 2 H, Ar), 8.26 (s, 2 H, Ar), 7.28 (d ( $j = 5$  Hz), 2 H, Ar), 2.46 (s, 6 H, Ar-CH<sub>3</sub>), 2.08 (br, 4 H, PCH<sub>2</sub>), 1.38 (br, 12 H, PCH<sub>3</sub>). IR (mineral oil): 3735 (w), 2944 (s), 2840 (s), 2724 (w), 2670 (w), 1613 (w), 1596 (w), 1560 (w), 1550 (w), 1460 (s), 1377 (s), 1297 (m), 1278 (m), 1168 (w), 1155 (w), 1134 (w), 1103(w), 1086 (w), 1040 (w), 1009 (w), 991 (w), 947 (m), 932 (m), 894 (w), 867 (m), 820 (w), 770 (w), 722 (m), 670 (w), 647 (w), 633 (w) cm<sup>-1</sup>. Magnetic susceptibility (SQUID, 300 K):  $\mu_{\text{eff}} = 2.73 \mu_B$ . Anal. Calcd. for C<sub>18</sub>H<sub>28</sub>N<sub>2</sub>P<sub>2</sub>UCl<sub>4</sub>: C, 30.27; H, 3.95; N, 3.92. Found: C, 30.10; H, 3.80; N, 3.90.

Of the solvents tried (hexanes, pentane, dimethylsulfoxide, dichloromethane, acetonitrile, benzene, toluene, diethyl ether, and tetrahydrofuran) **3.4** is only readily soluble in acetonitrile.

**3.3.2 X-ray Structure Determinations.** Structures were determined for the compounds listed in Table 3.1. Single crystals were coated with Paratone-N oil in the glove box and mounted under a cold stream of dinitrogen gas. Single crystal X-ray diffraction data were acquired on a Bruker Kappa APEX II CCD diffractometer with Mo K $\alpha$  radiation ( $\lambda = 0.71073 \text{ \AA}$ ) and a graphite monochromator. Initial lattice parameters were obtained from a least-squares analysis of more than 100 reflections; these parameters were later refined against all data. None of the crystals showed significant decay during data collection. Data were integrated and corrected for Lorentz and polarization effects using Bruker APEX2 software, and semiempirical absorption corrections were applied using SCALE with the aid of numerical face indexing.<sup>21</sup> Space

group assignments were based on systematic absences, *E* statistics, and successful refinement of the structures. Structures were solved by the Patterson method and were refined with the aid of successive Fourier difference maps against all data using the SHELXTL 6.14 software package.<sup>22</sup> Thermal parameters for all non-hydrogen atoms were refined anisotropically. All hydrogen atoms were assigned to ideal positions and refined using a riding model with an isotropic thermal parameter 1.2 times that of the attached carbon atom (1.5 times for methyl hydrogens). Selected bond distances and angles for crystals of compounds **3.1**, **3.2**, and **3.4** are collected in Table 3.2 while those for compound **3.3**·2CH<sub>2</sub>Cl<sub>2</sub> are collected in Table 3.3. All other metric parameters can be found in the cif files included with the Appendix 2. In the structure of **3.3**·2CH<sub>2</sub>Cl<sub>2</sub>, there are several disordered components. The dmpe and one of the chloride (Cl<sub>2</sub>) ligands bound to U1 are disordered over two sites, with a site occupancy ratio refining to 52:48. The dmpe and chloride ligands bound to U2 are also disordered over two sites, with a site occupancy ratio refining to 51:49. For **3.3**·2CH<sub>2</sub>Cl<sub>2</sub>, thermal parameters for all chemically equivalent disordered atoms were refined anisotropically and restrained to have the same  $U_{ij}$  parameters. A dichloromethane solvate molecule (two per U<sub>4</sub> cluster) was found in Fourier difference maps to be disordered over two sites; the site occupancy ratio refined to 54:46. After numerous attempts to model the remaining disorder failed to improve agreement factors, SQUEEZE<sup>23</sup> was used to remove the remaining disordered components. According to the SQUEEZE output, approximately 5.75 dichloromethane solvent molecules are present per U<sub>4</sub> cluster in the void space and were removed. The chemical data presented for **3.3**·2CH<sub>2</sub>Cl<sub>2</sub> in Tables 3.1 and 3.3 do not include the components removed by SQUEEZE.

**Table 3.1.** Crystallographic data for compounds [(dmpe)<sub>2</sub>UCl<sub>4</sub>] (**3.1**), [(dmpe)<sub>2</sub>UMe<sub>4</sub>] (**3.2**), [(dmpe)<sub>4</sub>U<sub>4</sub>Cl<sub>16</sub>]·2CH<sub>2</sub>Cl<sub>2</sub> (**3.3**·2CH<sub>2</sub>Cl<sub>2</sub>), and [(dmpe)(dmbpy)UCl<sub>4</sub>] (**3.4**).

	<b>3.1</b>	<b>3.2</b>	<b>3.3</b> ·2CH <sub>2</sub> Cl <sub>2</sub>	<b>3.4</b>
formula	C <sub>12</sub> H <sub>32</sub> P <sub>4</sub> UCl <sub>4</sub>	C <sub>16</sub> H <sub>44</sub> P <sub>4</sub> U	C <sub>26</sub> H <sub>68</sub> P <sub>8</sub> U <sub>4</sub> Cl <sub>20</sub>	C <sub>18</sub> H <sub>28</sub> N <sub>2</sub> P <sub>2</sub> UCl <sub>4</sub>
formula wt	680.09	598.42	2289.69	714.19
color, habit	blue-green cube	yellow block	green rod	light green rod
<i>T</i> , K	120(2)	120(2)	120(2)	120(2)
space group	<i>P</i> 2 <sub>1</sub> 2 <sub>1</sub> 2 <sub>1</sub>	<i>P</i> 4 <sub>3</sub> 2 <sub>1</sub> 2	<i>I</i> 4 <sub>1</sub> / <i>a</i>	<i>P</i> 2 <sub>1</sub> 2 <sub>1</sub> 2 <sub>1</sub>
<i>Z</i>	12	4	8	4
<i>a</i> , Å	12.6594(5)	12.2692(9)	37.3334(7)	9.2997(2)
<i>b</i> , Å	14.0045(6)	12.2692(9)	37.3334(7)	14.4254(4)
<i>c</i> , Å	41.7425(19)	17.0398(14)	12.9469(3)	18.5866(5)
<i>V</i> , Å <sup>3</sup>	7400.5(5)	2565.1(3)	18045.2(6)	2493.43(11)
<i>d</i> <sub>calc</sub> , g/cm <sup>3</sup>	1.831	1.550	1.686	1.903
GOF	1.02	1.30	1.09	1.03
<i>R</i> <sub>1</sub> ( <i>wR</i> <sub>2</sub> ) <sup><i>b</i></sup> , %	3.09(5.51)	3.18(8.41)	5.92(19.06)	2.43(4.47)

<sup>*a*</sup> Obtained with graphite-monochromated Mo Kα ( $\lambda = 0.71073$  Å) radiation.

<sup>*b*</sup>  $R_1 = \sum ||F_o| - |F_c|| / \sum |F_o|$ ,  $wR_2 = \{ \sum [w(F_o^2 - F_c^2)^2] / \sum [w(F_o^2)^2] \}^{1/2}$  for  $F_o > 4\sigma(F_o)$ .

**3.3.3 Magnetic Susceptibility Measurements.** Magnetic susceptibility measurements were collected using a Quantum Design MPMS XL SQUID magnetometer. Powdered microcrystalline samples were loaded into gelatin capsules in the glove box, inserted into a straw and transported to the SQUID magnetometer under dinitrogen. DC magnetic susceptibility data were collected at temperatures ranging from 2 to 300 K at an applied field of 0.1 T. Susceptibility data reproducibility were confirmed by conducting spot checks on samples made in separate batches. Magnetization measurements were collected at temperatures ranging from 2 to 35 K at applied fields of 1, 2, 3, 4, and 5 T. AC magnetic susceptibility data were collected at temperatures ranging from 1.8 to 4 K at an applied AC field of 4 Oe with switching frequencies of 200 and 1488 Hz with and without an applied DC field (see Appendix 2). Contributions to the magnetization from the gelatin capsule and the straw were measured independently and

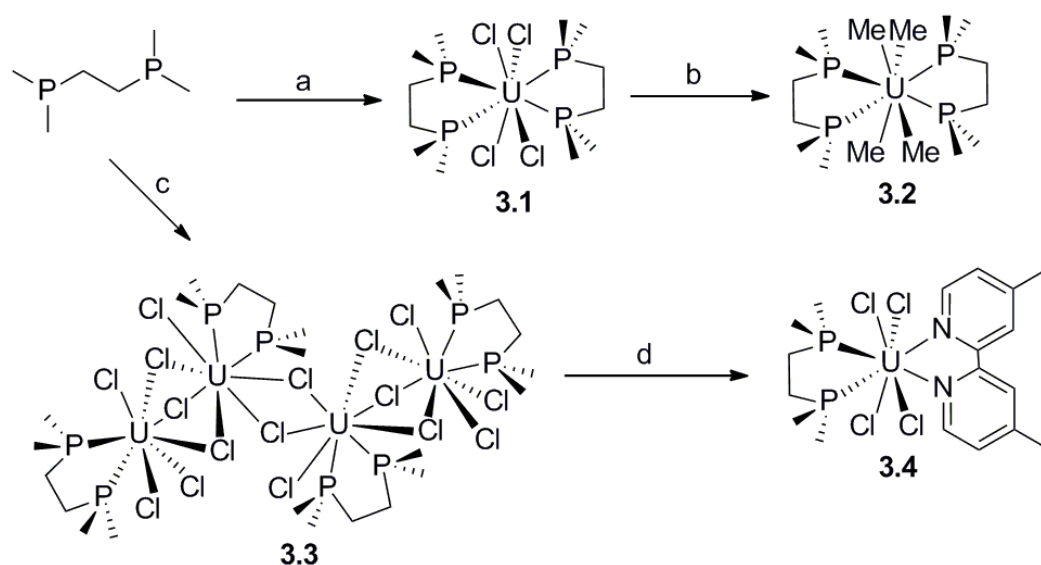
subtracted from the total measured signal. Data were corrected for diamagnetic contributions using Pascal's constants.<sup>24</sup>

**3.3.4 Other Physical Measurements.** Electronic absorption spectra were obtained in solution in an air-free glass cell of path length 1 cm on an Agilent 8453 spectrophotometer. <sup>1</sup>H NMR spectra were recorded using a Varian INOVA 500 MHz instrument, and the spectra were referenced internally using residual protio solvent resonances relative to tetramethylsilane ( $\delta = 0$  ppm). Infrared spectra were collected on a Thermo Nicolet 380 FTIR spectrometer as mineral oil mulls pressed between sodium chloride plates. Elemental analyses were performed by the Micro-Mass facility at the University of California, Berkeley.

### 3.4 Results and Discussion

**3.4.1 Syntheses and Characterizations of [(dmpe)<sub>2</sub>UX<sub>4</sub>] (X = Cl, Me).** Andersen and coworkers originally reported the synthesis of [(dmpe)<sub>2</sub>UCl<sub>4</sub>] (**3.1**); they also showed that substitution of **3.1** with methyllithium or phenol affords the tetramethyl (**3.2**) or tetraphenoxide complexes, respectively.<sup>18</sup> Since complexes **3.1** and **3.2** represent potential precursors for uranium acetylide species that may have interesting magnetic properties,<sup>17,19</sup> we have reproduced the syntheses to isolate **3.1** and **3.2** for use as building blocks in further studies (Scheme 3.1). These complexes can be handled under inert atmosphere in the solid state, although the methyl complex appears to be less thermally stable. For both **3.1** and **3.2**, we report infrared spectra and magnetic susceptibilities. Solution colors of the chloride complex **1** in degassed solvents do not change over time, and the compound can be recrystallized from tetrahydrofuran, diethyl ether and dichloromethane. It is interesting to note that the electronic absorption spectrum of **3.1** is

quite different in dichloromethane compared to dimethyl sulfoxide (Figures A2.5-A2.6). The dichloromethane solution has a blue-green color, very similar to the solid, however the color of the dimethyl sulfoxide solution is pale green. From  $^1\text{H}$  and  $^{31}\text{P}$  NMR experiments (Figures A2.12-A2.15), we surmise that the complex maintains structural integrity in the less polar solvent, but is labile in the more strongly coordinating dimethyl sulfoxide solvent: free dmpe is observed in DMSO, but not in dichloromethane. In contrast, the methyl complex **3.2** turns black in solution when warmed from  $-60\text{ }^\circ\text{C}$  to ambient temperatures: changes in the  $^1\text{H}$  NMR spectrum indicates decomposition to as-yet unidentified products (Figure A2.16).



**Scheme 3.1.** Syntheses of chelating phosphine complexes of U(IV): a = 0.5 eq.  $\text{UCl}_4$  in  $\text{CH}_2\text{Cl}_2$  at  $23\text{ }^\circ\text{C}$ ; b = 4 eq.  $\text{MeLi}$  in  $\text{Et}_2\text{O}$  at  $-20\text{ }^\circ\text{C}$ ; c =  $\text{UCl}_4$  in  $\text{CH}_2\text{Cl}_2$  at  $23\text{ }^\circ\text{C}$ ; d = dmbpy in  $\text{CH}_2\text{Cl}_2$  at  $23\text{ }^\circ\text{C}$ .

As part of the characterization protocol, molecular structures were obtained via single-crystal X-ray analysis (Figure 3.1). Compound **3.1** crystallizes in the orthorhombic space group  $P2_12_12_1$  (no. 19) with  $Z = 12$ . There are three crystallographically independent complex molecules in each unit cell owing to slight variations in the dmpe backbones. The structure of one of the chemically equivalent complexes in **3.1** is shown in Figure 3.1 and selected bond lengths and angles are given in Table 3.2. Single crystal X-ray analysis of **3.1** reveals the uranium ion is ligated by four phosphorus atoms and four chloride ligands. The phosphine ligands are rotated by approximately  $90^\circ$  with respect to each other.

Compound **3.2** crystallizes in the tetragonal space group  $P4_32_12$  (no. 96) with  $Z = 4$ ; there is one independent complex molecule in each unit cell. The structure of **3.2** is shown in Figure 3.1 and selected bond lengths and angles are given in Table 3.2. Similar to the chloride complex, **3.2** contains a uranium ion ligated by four phosphorus atoms and four carbon atoms. The phosphine ligands are rotated by approximately  $90^\circ$  with respect to each other.

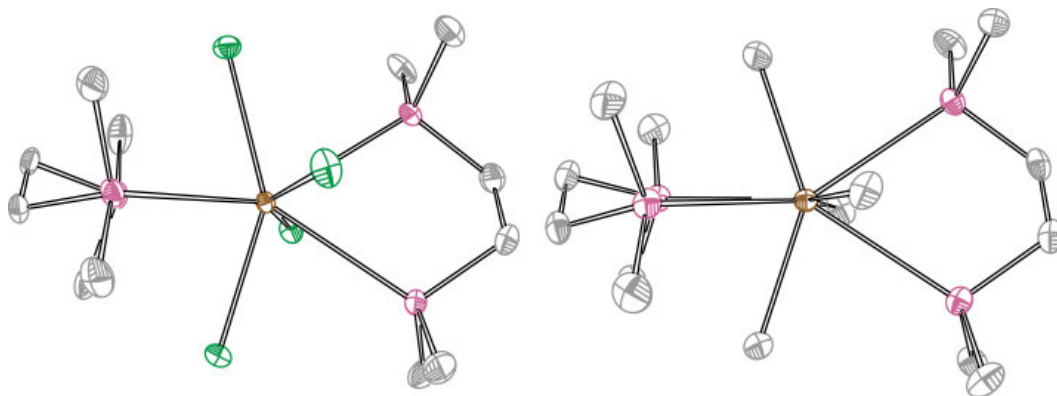


**Figure 3.1.** Molecular structures of the U(IV) phosphine complexes in compounds **3.1** (left) and **3.2** (right), rendered with 40% ellipsoids. Brown, purple, green, and gray ellipsoids represent U, P, Cl and C atoms, respectively. Hydrogen atoms are omitted for clarity.

**3.4.2 A New Tetranuclear U(IV) Species as “(dmpe)UX<sub>4</sub>” Synthone.** It has been reported that blue-green **3.1** can be prepared by addition of three equivalents of dmpe per UCl<sub>4</sub>.<sup>18</sup> However, when the reaction is carried out with a deficiency of chelating ligand (1.2:1 dmpe:UCl<sub>4</sub>), the green tetranuclear species [(dmpe)<sub>4</sub>U<sub>4</sub>Cl<sub>16</sub>]·2CH<sub>2</sub>Cl<sub>2</sub> (**3.3**·2CH<sub>2</sub>Cl<sub>2</sub>) is obtained as the only isolable product (Figure 3.2). Probing the effects of altering reactant stoichiometry via electronic absorption spectroscopy, we find that a 2:1 dmpe:UCl<sub>4</sub> ratio exclusively affords the originally targeted mononuclear compound **3.1**. At larger scales, we find that **3.1** is isolated from 2:1 dmpe:UCl<sub>4</sub> combinations in greater than 75% isolated yield. We note that the electronic absorption spectra of **3.1** and **3.3** are virtually identical in DMSO (Figures A2.6-A2.7); these spectra combined with NMR data indicate that the dmpe ligands dissociate from uranium when **3.3** is dissolved in DMSO. The electronic absorption spectra are also very similar in CH<sub>2</sub>Cl<sub>2</sub> (Figures A2.5 and A2.8). More importantly, the <sup>1</sup>H NMR spectra for **3.3** and **3.1** are also similar, and the main signals are *not* free dmpe (Figures A2.14 and A2.19). The main signal in the {<sup>1</sup>H}<sup>31</sup>P NMR spectra for **3.1** and **3.3** are consistent with free dmpe; the phosphorus atoms bound to the uranium center may be too broadened to be visible. Interestingly, an additional resonance with complex splitting is observed for **3.3** in the {<sup>1</sup>H}<sup>31</sup>P NMR spectrum (Figure A2.20), perhaps indicative of an additional phosphorus environment as expected for the tetranuclear complex (*vide infra*) compared to **3.1**. The spectral data show that **3.1** and **3.3** may form similar compounds when dissolved, regardless of solvent; however, the differential solubilities of the mono- and tetranuclear complexes (**3.3** is much less soluble in dichloromethane than **3.1**) may give rise to distinct reactivities, as described below.

Compound  $3.3 \cdot 2\text{CH}_2\text{Cl}_2$  crystallizes in the tetragonal space group  $I4_1/a$  (no. 88) with  $Z = 8$ ; there is one independent complex molecule in each unit cell. The structure of  $3.3 \cdot 2\text{CH}_2\text{Cl}_2$  is shown in Figure 3.2 and selected bond lengths and angles are given in Table 3.3. Single crystal X-ray analysis of  $3.3 \cdot 2\text{CH}_2\text{Cl}_2$  reveals that each U(IV) is ligated by two phosphorus atoms and by six chloride ligands. There are two different uranium environments in compound  $3.3 \cdot 2\text{CH}_2\text{Cl}_2$ . The terminal uranium atoms have three bridging chloride ligands while the internal uranium atoms are bridged by five chlorides, three to the external uranium atoms and two to the symmetry equivalent internal uranium. Important average bond distances in  $3.3 \cdot 2\text{CH}_2\text{Cl}_2$  are U–Cl (bridge) = 2.776(5) Å, U–Cl (terminal) = 2.604(6) Å, and U–P = 2.976(8) Å. The U $\cdots$ U separation is 4.0668(7) Å. These values are comparable to other literature reports of uranium complexes featuring bridging and terminal chloride atoms.<sup>25-27</sup>

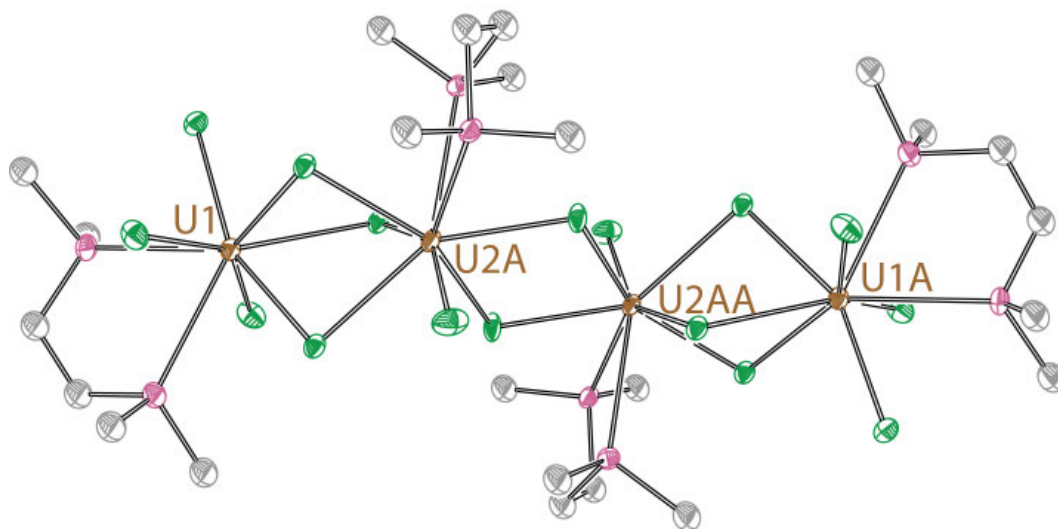


**Figure 3.2.** Crystal structure of the U(IV) phosphine complex in  $3.3 \cdot 2\text{CH}_2\text{Cl}_2$ , rendered with 40% ellipsoids. Brown, purple, green, and gray ellipsoids represent U, P, Cl and C atoms, respectively. Hydrogen atoms, solvent molecules, and disordered components in  $3.3 \cdot 2\text{CH}_2\text{Cl}_2$  are omitted for clarity. The complex sits on a crystallographic two-fold axis.

We have found that **3.3**·2CH<sub>2</sub>Cl<sub>2</sub> can perform as a “(dmpe)UCl<sub>4</sub>” species, allowing for the production of mixed-chelating ligand U(IV) complexes. Combining (green) **3.3**·2CH<sub>2</sub>Cl<sub>2</sub> with approximately four equivalents of 4,4'-dimethylbipyridine in dichloromethane affords a light green solid. Structural and elemental analyses demonstrate this to be a mixed-chelating ligand U(IV) complex with the formula [(dmpe)(dmbpy)UCl<sub>4</sub>] (**3.4**). The combination of the bis(dmpe) complex **3.1** with one equivalent of dmbpy in dichloromethane gives an electronic absorption spectrum with similar features as found in **3.4**, but molar absorptivities do not match exactly, even if mixtures of **3.1** and **3.4** are assumed (Figure A2.26). We can conclude that the reactivity of **3.1** and **3.3** toward ligand substitution with dmbpy are similar, but mixed-ligand complexes are more cleanly (and economically) isolated by using the tetranuclear complex **3.3**. We note that NMR studies undertaken in the coordinating solvent acetonitrile show that dmbpy appears to dissociate from **3.4** but dmpe remains bound (Figure A2.21). Going forward, we anticipate that this synthetic control may be expanded and exploited to confer steric and electronic tunability to U-dmpe complexes; exploratory synthetic studies are underway.

Compound **3.4** crystallizes in the orthorhombic space group  $P2_12_12_1$  (no. 19) with  $Z = 4$ ; there is one crystallographically-independent complex molecule in each unit cell. The structure of **3.4** is shown in Figure 3.3 and selected bond lengths and angles are given in Table 3.2. Single crystal X-ray analysis of **3.4** shows the uranium ion is bound by two phosphorus atoms, two nitrogen atoms, and four chlorides. The phosphine and bipyridine ligands are rotated by approximately 90° with respect to each other.

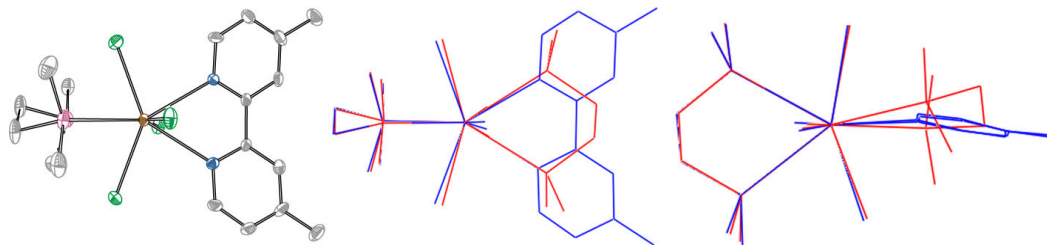


**Figure 3.3.** Left: crystal structure of the U(IV) phosphine complex in **3.4**, rendered with 40% ellipsoids. Brown, purple, green, blue, and gray ellipsoids represent U, P, Cl, N and C atoms, respectively. Hydrogen atoms are omitted for clarity. Middle and right: overlay of representative U(IV) complexes in compounds **3.1** (red) and **3.4** (blue); two different orientations are shown for clarity.

**3.4.3 Structural Comparisons.** Structures were determined via X-ray analysis for the compounds listed in Table 3.1. The structure of representative uranium complexes are shown in Figures 3.1-3.3 and selected bond lengths and angles are given in Tables 3.2-3.3. For all four structures, the U–Cl and U–P distances are comparable to other reported uranium(IV) phosphine compounds with eight coordinate environments;<sup>4,28-33</sup> the U–P distances are all shorter than those reported for the tetraphenoxide complex [(dmpe)<sub>2</sub>U(OPh)<sub>4</sub>].<sup>18</sup> For the structure of **3.2**, the average U–C distance (2.5134(7) Å) is longer than that reported for other U(IV) compounds, although the structures that contain such U–C bonds are of mainly four-, five-, and six-coordinate uranium centers.<sup>29,34,35</sup>

**Table 3.2.** Selected bond distances (Å) and angles (°) for the crystallographically-determined structures [(dmpe)<sub>2</sub>UCl<sub>4</sub>] (**3.1**), [(dmpe)<sub>2</sub>UMe<sub>4</sub>] (**3.2**), [(dmpe)(dmbpy)UCl<sub>4</sub>] (**3.4**) and [(dmpe)<sub>2</sub>U(OPh)<sub>4</sub>].

	<b>3.1</b>	<b>3.2</b>	<b>3.4</b>	[(dmpe) <sub>2</sub> U(OPh) <sub>4</sub> ] <sup>18</sup>
U–P	2.9939(14)	3.0031(19)	3.0074(20)	3.104(6)
U–N			2.642(6)	
U–X <sup>a</sup>	2.6480(13)	2.5134(7)	2.6457(18)	2.17(1)
X <sub>cis</sub> –U–X <sub>cis</sub>	89.89(5)	94.0(3)	95.33(7)	94.6(4)
X <sub>cis</sub> –U–X <sub>trans</sub>	148.54(4)	143.5(4)	151.74(6)	147.2(1)
P <sub>cis</sub> –U–Y <sub>cis</sub> <sup>b</sup>	66.23(4)	66.77(7)	63.98(11)	64.7(6)
P <sub>cis</sub> –U–Y <sub>trans</sub> <sup>b</sup>	128.95(5)	129.23(5)	135.97(13)	135.5(2.2)

<sup>a</sup> X = Cl, Me, or OPh. <sup>b</sup> Y = P or N

**Table 3.3.** Selected bond distances (Å) and angles (°) for the structure of [(dmpe)<sub>4</sub>U<sub>4</sub>Cl<sub>16</sub>]·2CH<sub>2</sub>Cl<sub>2</sub> (**3.3**·2CH<sub>2</sub>Cl<sub>2</sub>).

<b>3.3</b> ·2CH <sub>2</sub> Cl <sub>2</sub>	
U–P	2.976(8)
U–Cl (bridge)	2.776(5)
U–Cl (terminal)	2.604(6)
U–U	4.0668(7)
Cl <sub>cis</sub> –U <sub>terminal</sub> –Cl <sub>cis</sub>	90.95(19)
Cl <sub>cis</sub> –U <sub>terminal</sub> –Cl <sub>trans</sub>	146.09(12)
P–U <sub>terminal</sub> –P	66.22(15)
Cl <sub>cis</sub> –U <sub>bridging</sub> –Cl <sub>cis</sub>	93.8(3)
Cl <sub>cis</sub> –U <sub>bridging</sub> –Cl <sub>trans</sub>	142.48(7)
P–U <sub>bridging</sub> –P	67.4(4)

To compare the U(IV) coordination polyhedra, the SHAPE protocol described by Raymond has been implemented.<sup>36</sup> This program compares all of the dihedral angles in the first coordination sphere of the uranium ion (one for each pair of adjacent triangular planes) to ideal values for selected polyhedra. The shape measure, *S*, is used to evaluate the degree of distortion from an ideal geometry. *S* is the minimal variance of dihedral angles along all edges and the lowest output value represents the most closely related polyhedron.<sup>36</sup> The results of these calculations for compounds **3.1**–**3.4** are presented in Table 3.4. For all U(IV) centers in this study, the local coordination geometries deviate significantly from ideal polyhedra, but resemble most closely trigonal dodecahedra (*D*<sub>2d</sub>). Interestingly, the U(IV) ions in the bis(dmpe) chloride compound **3.1** are significantly more distorted than the other complexes. No solvate molecules are present in the structure of **3.1**, and therefore no obvious hydrogen bonding pathways account for the distortions.

**Table 3.4.** SHAPE analyses for compounds **3.1**–**3.4**. The smallest number indicates the most closely related polyhedron shape.<sup>36</sup>

	<b>3.1</b> <sup>a</sup>	<b>3.2</b>	<b>3.3</b> ·2CH <sub>2</sub> Cl <sub>2</sub>	<b>3.4</b>
<i>S</i> ( <i>D</i> <sub>2d</sub> )	25.96 (24.77, 25.10, 27.96)	13.36	13.16	14.31
<i>S</i> ( <i>C</i> <sub>2v</sub> )	26.36 (25.46, 25.25, 28.36)	14.94	14.11	17.07
<i>S</i> ( <i>D</i> <sub>4d</sub> )	29.49 (28.60, 28.95, 30.92)	17.48	17.19	19.30

<sup>a</sup> Values for **3.1** are averaged from the three crystallographically independent complexes; numbers in parentheses correspond to individual complexes.

The structures of **3.1** and **3.4** were compared to probe distortions caused by the introduction of the 4,4'-dimethylbipyridine ligand into the coordination sphere of the U(IV) ion. The results of this overlay are presented in Figure 3.3. It can be seen that the chloride ligands in **3.4** are slightly distorted toward dmpe relative to the orientation in **3.1**, perhaps due to steric crowding by the larger dmbpy ligand. This is best seen by comparing the Cl–U–Cl and X–U–X (X = P or N) angles (Table 3.2), where all increase upon replacing dmpe with dmbpy. The effect is strongest for the chlorides in the same plane as dmbpy. Also, a slight curvature of the dmbpy rings is noted, as well as a tilting “down” of the entire dmbpy ligand relative to the plane that bisects the U(dmpe) moiety. Distortions for both **3.1** and **3.4** may be due to packing forces; a more detailed investigation of the contributions of weak intermolecular interactions to uranium-ligand binding is in progress.<sup>37</sup>

**3.4.4 Magnetic Properties.** Due to the nature of crystal field splitting being of approximately the same magnitude as spin-orbit coupling, both of which are greater than *kT*, the magnetic behaviors of U(IV) compounds are quite complicated.<sup>38,39</sup> Russell-Saunders coupling breaks down and is not sufficiently replaced by a *jj* coupling model.<sup>39</sup> The magnetic moment of the actinides often reflects a mixing, especially at lower

temperatures, of the large spin-orbit coupling and ligand field effects into the free ion term. As a result, the term “spin-only” often holds little meaning.<sup>40</sup>

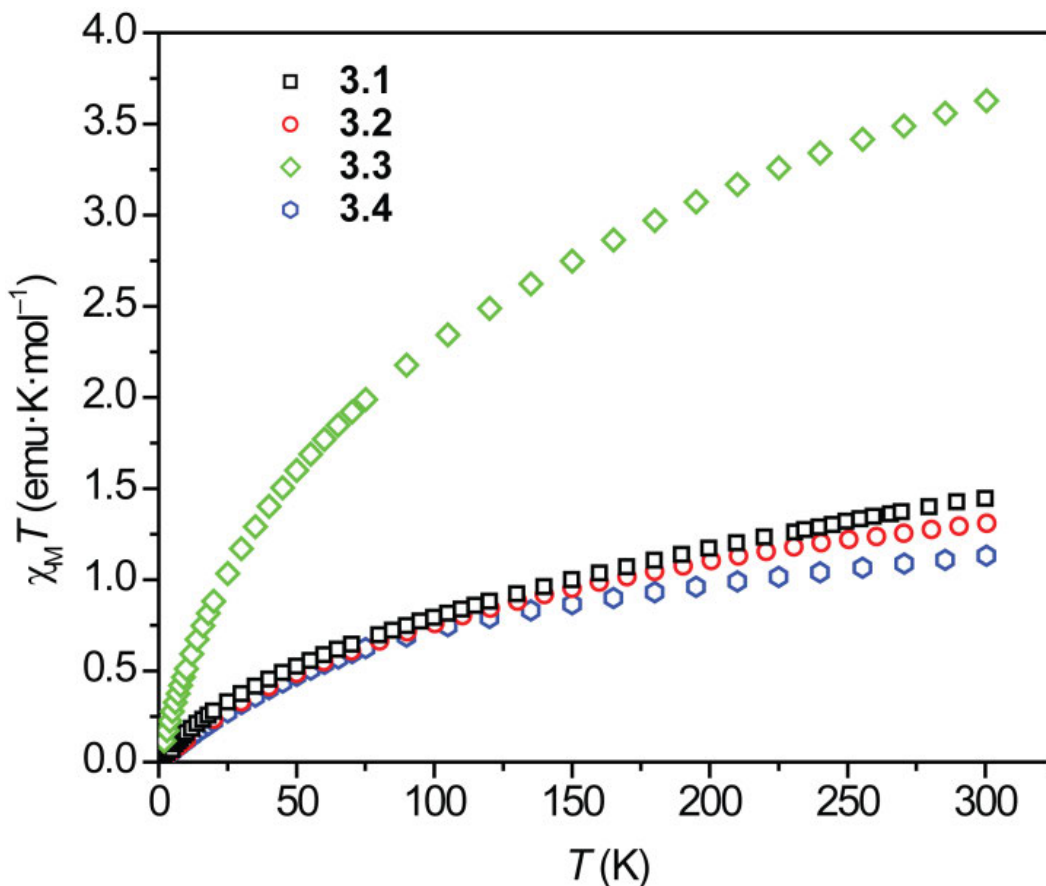


**Figure 3.4.** Temperature dependence of the magnetic susceptibility for compounds **3.1**–**3.4**, obtained at a measuring field of 1000 Oe. A plot showing the temperature dependence of  $\mu_{\text{eff}}$  values for compounds **3.1**–**3.4** appear in Appendix 2 (Figure A2.30).

With this in mind, variable temperature magnetic susceptibility data were collected for compounds **3.1**–**3.4** and are presented in Figure 3.4. At 300 K the measured susceptibilities are 1.45 and 1.31  $\text{emu}\cdot\text{K}\cdot\text{mol}^{-1}$  for compounds **3.1** and **3.2**, respectively. These values are somewhat larger than the predicted value of 1.00  $\text{emu}\cdot\text{K}\cdot\text{mol}^{-1}$  for one  $S = 1$  ion with  $g = 2.00$ . In contrast, the measured susceptibility for compound **4** at 300 K is 1.13  $\text{emu}\cdot\text{K}\cdot\text{mol}^{-1}$ , which is closer to the predicted value. The  $\chi_{\text{M}}T$  values for the

mononuclear complexes decrease in a nearly linear fashion to 0.75 (**3.1**), 0.71 (**3.2**), and 0.69 (**3.4**)  $\text{emu}\cdot\text{K}\cdot\text{mol}^{-1}$ , respectively, at 90 K. This drop in the measured magnetic susceptibility is most likely due to depopulation of the Stark sublevels. The susceptibilities for compounds **3.1**, **3.2**, and **3.4** all trend toward zero at low temperatures with values of 0.04, 0.03, and 0.02  $\text{emu}\cdot\text{K}\cdot\text{mol}^{-1}$ , respectively, at 2 K. The magnetic behavior of compounds **3.1**, **3.2**, and **3.4** can be interpreted as ground state diamagnetic  $f^2$  species, which are paramagnetic at room temperature due to spin-orbit coupling, temperature-independent paramagnetism (TIP), and thermal population of paramagnetic excited states. This behavior is similar to that observed for other U(IV) compounds in octacoordinate ligand fields,<sup>41-44</sup> with perhaps some contributions from U(IV) single-ion anisotropy.<sup>45,46</sup> Here, it appears that ligand distortions—replacement of Cl with Me or dmpe with dmbpy—make only slight changes to the observed magnetic properties.

Very few examples of magnetic investigations on polynuclear bridging uranium(IV) compounds have been reported.<sup>42,47-49</sup> The room temperature magnetic susceptibility of the tetranuclear compound **3.3**·2CH<sub>2</sub>Cl<sub>2</sub> (Figure 3.4) is 3.63  $\text{emu}\cdot\text{K}\cdot\text{mol}^{-1}$ , slightly below the predicted value of 4.00  $\text{emu}\cdot\text{K}\cdot\text{mol}^{-1}$  for four uncoupled  $S = 1$  ions with  $g = 2.00$ . The susceptibility decreases gradually to 2.18  $\text{emu}\cdot\text{K}\cdot\text{mol}^{-1}$  at 90 K, and is followed by a sharper drop to 0.12  $\text{emu}\cdot\text{K}\cdot\text{mol}^{-1}$  at 2 K. Similar to the mononuclear complexes, the magnetic behavior of compound **3.3**·2CH<sub>2</sub>Cl<sub>2</sub> can be interpreted as a ground state diamagnetic  $f^2$  species, which is paramagnetic at room temperature, although magnetic coupling *may* be operative, as discussed below.

Comparing **3.1** and **3.3**·2CH<sub>2</sub>Cl<sub>2</sub>, multiplying  $\chi_{\text{M}}T$  values for **3.1** by four gives qualitatively the same temperature-dependent magnetic behavior as **3.3**·2CH<sub>2</sub>Cl<sub>2</sub>,

although at 300 K this value is larger than that of the tetranuclear compound (4.51 versus 3.63 emu·K·mol<sup>-1</sup>).<sup>50</sup> This difference may be due to reduction in complex symmetry and/or covalency in U-ligand bonding, which could remove orbital degeneracy.<sup>39,45,46,51</sup> Although the magnetism in both compounds is dominated by single-ion effects, we cannot entirely rule out the possibility of magnetic exchange between U(IV) ions in **3.3**·2CH<sub>2</sub>Cl<sub>2</sub> based on susceptibility data alone. The variable temperature magnetic properties for UCl<sub>4</sub> have been interpreted as showing Curie-Weiss behavior ( $\theta = -28.8$  K and  $C = 1.726$ ) and having a nonmagnetic ground state and a low-lying paramagnetic first excited state (at 110 cm<sup>-1</sup>);<sup>52</sup> the negative Weiss constant is consistent with antiferromagnetic coupling of paramagnetic centers, but spin-orbit coupling could account for most of the downturn in susceptibility-temperature product. Ephritikhine and coworkers reported the synthesis and magnetic characterization of the dinuclear U(IV) complex [L<sup>1</sup>U<sub>2</sub>( $\mu$ -Cl)<sub>2</sub>Cl<sub>2</sub>] (H<sub>4</sub>L<sup>1</sup> = [N, N':N', N'-bis(2,2'-dihydroxy-3,3'-dimethylidene-5,5'-di-*tert*-butylbiphenyl)benzene-1,2-diamine]);<sup>42</sup> the  $\chi_M T$  value of 3.00 emu·K·mol<sup>-1</sup> at 300 K is larger than expected for two free 5f<sup>2</sup> ions, but its decrease with temperature to a value of 0 emu·K·mol<sup>-1</sup> at 2 K is argued to include a contribution from antiferromagnetic coupling. The decrease in  $\chi_M T$  in that compound is more rapid than observed with our tetranuclear complex **3.3**.

The magnetization plots of compounds **3.1** and **3.3**·2CH<sub>2</sub>Cl<sub>2</sub> (Figure A2.27) both exhibit non-superposition of isofield data, a hallmark of magnetic anisotropy. The data for **3.3**·2CH<sub>2</sub>Cl<sub>2</sub> plotted on a per uranium basis match very closely to the data for mononuclear **3.1**. We provisionally take this as evidence *against* antiferromagnetic exchange coupling occurring between U(IV) ions in **3.3**. At the minimum, it would

appear that single ion effects obscure any exchange interactions in the tetranuclear complex.

To ascertain if the tetranuclear **3.3**·2CH<sub>2</sub>Cl<sub>2</sub> displays characteristics of a single-molecule magnet, ac susceptibility measurements were obtained with and without a perpendicularly-applied 0.1 T DC field. No frequency dependence of the AC susceptibility was observed (Figure A2.28).

### 3.5 Summary and Outlook

In the course of structurally characterizing complexes **3.1** and **3.2** for uranium magnetochemical studies, we have isolated the tetranuclear compound [(dmpe)<sub>4</sub>U<sub>4</sub>Cl<sub>16</sub>]·2CH<sub>2</sub>Cl<sub>2</sub> (**3.3**·2CH<sub>2</sub>Cl<sub>2</sub>), and find that it acts as a “(dmpe)UCl<sub>4</sub>” synthon for the preparation of mixed chelating-ligand U(IV) complexes, as evidenced by the synthesis of [(dmpe)(dmbpy)UCl<sub>4</sub>] (**3.4**). All of the compounds presented here display magnetism indicative of non-magnetic ground states, consistent with those described elsewhere in the literature.<sup>35,38,48,51,53-62</sup> If there is magnetic coupling between U(IV) ions in the tetranuclear complex **3.3**, it is obscured by U(IV) single-ion behavior. Nevertheless, the capability to make heteroleptic complexes offers opportunities for exploring steric and electronic tuning of the uranium ion, with implications for utilizing actinide elements in the generation of new SMMs, and for further probing actinide-ligand bonding.

**3.6 Acknowledgments.** This research was supported by Colorado State University and the ACS Petroleum Research Fund (44691-G3). We thank Ms. Susie Miller and Prof. Oren Anderson for advice on crystal structure refinements and Dr. Christopher Rithner

for assistance with NMR data collection. We thank NSF-REU (CHE-1004924) for partial support of TCS.

### 3.7 References:

- (1) Marvaud, V.; Herrera, J. M.; Barilero, T.; Tuyeras, F.; Garde, R.; Sculler, A.; Decroix, C.; Cantuel, M.; Desplanches, C., *Mon. Chem.* **2003**, *134*, 149.
- (2) Toshiba Introduces Industry's Highest Areal Density 2.5-inch 750GB Hard Disk Drives. [http://www.toshiba.co.jp/about/press/2010\\_03/pr2501.htm](http://www.toshiba.co.jp/about/press/2010_03/pr2501.htm) (accessed June 30, 2011).
- (3) Pedersen, K. S.; Schau-Magnussen, M.; Bendix, J.; Weihe, H.; Palii, A. V.; Klokishner, S. I.; Ostrovsky, S.; Reu, O. S.; Mutka, H.; Tregenna-Piggott, P. L. W., *Chem. Eur. J.* **2010**, *16*, 13458.
- (4) Rinehart, J. D.; Harris, T. D.; Kozimor, S. A.; Bartlett, B. M.; Long, J. R., *Inorg. Chem.* **2009**, *48*, 3382.
- (5) Lin, P. H.; Burchell, T. J.; Ungur, L.; Chibotaru, L. F.; Wernsdorfer, W.; Murugesu, M., *Angew. Chem. Int. Ed.* **2009**, *48*, 9489.
- (6) Gatteschi, D.; Sessoli, R.; Cornia, A., *Chem. Commun.* **2000**, 725.
- (7) Schelter, E. J.; Veauthier, J. M.; Thompson, J. D.; Scott, B. L.; John, K. D.; Morris, D. E.; Kiplinger, J. L., *J. Am. Chem. Soc.* **2006**, *128*, 2198.
- (8) Schelter, E. J.; Wu, R. L.; Scott, B. L.; Thompson, J. D.; Morris, D. E.; Kiplinger, J. L., *Angew. Chem. Int. Ed.* **2008**, *47*, 2993.
- (9) Schmid, G.; Noth, H., *Z. Naturforsch., B* **1965**, *B 20*, 1008.
- (10) Rinehart, J. D.; Kozimor, S. A.; Long, J. R., *Angew. Chem. Int. Ed.* **2010**, *49*, 2560.
- (11) Muller, A.; Peters, F.; Pope, M. T.; Gatteschi, D., *Chem. Rev.* **1998**, *98*, 239.
- (12) Wang, M.; Yuan, D. Q.; Ma, C. B.; Yuan, M. J.; Hu, M. Q.; Li, N.; Chen, H.; Chen, C. N.; Liu, Q. T., *Dalton Trans.* **2010**, *39*, 7276.
- (13) Li, P. X.; Mao, J. G., *Cryst. Growth Des.* **2008**, *8*, 3385.

- (14) Chandrasekhar, V.; Pandian, B. M.; Boomishankar, R.; Steiner, A.; Viftal, J. J.; Hourri, A.; Clerac, R., *Inorg. Chem.* **2008**, *47*, 4918.
- (15) Mereacre, V. M.; Ako, A. M.; Clerac, R.; Wernsdorfer, W.; Filoti, G.; Bartolome, J.; Anson, C. E.; Powell, A. K., *J. Am. Chem. Soc.* **2007**, *129*, 9248.
- (16) Ako, A. M.; Hewitt, I. J.; Mereacre, V.; Clerac, R.; Wernsdorfer, W.; Anson, C. E.; Powell, A. K., *Angew. Chem. Int. Ed.* **2006**, *45*, 4926.
- (17) Newell, B. S.; Rappe, A. K.; Shores, M. P., *Inorg. Chem.* **2010**, *49*, 1595.
- (18) Edwards, P. G.; Andersen, R. A.; Zalkin, A., *J. Am. Chem. Soc.* **1981**, *103*, 7792.
- (19) Boaretto, R.; Roussel, P.; Alcock, N. W.; Kingsley, A. J.; Munslow, I. J.; Sanders, C. J.; Scott, P., *J. Organomet. Chem.* **1999**, *591*, 174.
- (20) Hermann, J. A.; Suttle, J. F., *Inorg. Synth.* **1957**, *5*, 143.
- (21) Sheldrick, G. *SADABS*, Bruker AXS: Madison, WI, 1997.
- (22) Sheldrick, G. *SHELXTL*, 6.14; Bruker AXS: Madison, WI, 2004.
- (23) Spek, A. L., *J. Appl. Crystallogr.* **2003**, *36*, 7.
- (24) AlDamen, M. A.; Clemente-Juan, J. M.; Coronado, E.; Marti-Gastaldo, C.; Gaita-Arino, A., *J. Am. Chem. Soc.* **2008**, *130*, 8874.
- (25) Moisan, L.; Le Borgne, T.; Thuery, P.; Ephritikhine, M., *Acta Cryst. Sect. C Cryst. Struct. Commun.* **2002**, *58*, m98.
- (26) Old, J.; Danopoulos, A. A.; Winston, S., *New J. Chem.* **2003**, *27*, 672.
- (27) Campbell, G. C.; Cotton, F. A.; Haw, J. F.; Schwotzer, W., *Organometallics* **1986**, *5*, 274.
- (28) Edwards, P. G.; Parry, J. S.; Read, P. W., *Organometallics* **1995**, *14*, 3649.

- (29) Edwards, P. G.; Andersen, R. A.; Zalkin, A., *Organometallics* **1984**, *3*, 293.
- (30) Brennan, J.; Shinomoto, R.; Zalkin, A.; Edelstein, N., *Inorg. Chem.* **1984**, *23*, 4143.
- (31) Spencer, L. P.; Gdula, R. L.; Hayton, T. W.; Scott, B. L.; Boncella, J. M., *Chem. Commun.* **2008**, 4986.
- (32) Toffoli, P.; Khodadad, P.; Rodier, N., *Acta Cryst. Sect. C Cryst. Struct. Commun.* **1987**, *43*, 1704.
- (33) Coles, S. J.; Danopoulos, A. A.; Edwards, P. G.; Hursthouse, M. B.; Read, P. W., *J. Chem. Soc., Dalton Trans.* **1995**, 3401.
- (34) Boaretto, R.; Roussel, P.; J. Kingsley, A.; J. Munslow, I.; J. Sanders, C.; W. Alcock, N.; Scott, P., *Chem. Commun.* **1999**, 1701.
- (35) Schelter, E. J.; Veauthier, J. M.; Graves, C. R.; John, K. D.; Scott, B. L.; Thompson, J. D.; Pool-Davis-Tournear, J. A.; Morris, D. E.; Kiplinger, J. L., *Chem. Eur. J.* **2008**, *14*, 7782.
- (36) Xu, J. D.; Radkov, E.; Ziegler, M.; Raymond, K. N., *Inorg. Chem.* **2000**, *39*, 4156.
- (37) Rinehart, J. D.; Long, J. R., *J. Am. Chem. Soc.* **2009**, *131*, 12558.
- (38) Edelstein, N. M.; Lander, G. H.; Morss, L. R.; Fuger, J., *The Chemistry of the Actinide and Transactinide Elements*. 2006; Vol. 4, Ch. 20, p 2225.
- (39) Siddall, T. H., *Theory and Applications of Molecular Paramagnetism*. Boudreaux, E. A.; Mulay, L. N., Eds. John Wiley & Sons: New York, 1976.
- (40) Stewart, J. L.; Andersen, R. A., *New J. Chem.* **1995**, *19*, 587.
- (41) Lai, Y. L.; Chiang, R. K.; Lii, K. H.; Wang, S. L., *Chem. Mat.* **2008**, *20*, 523.

- (42) Salmon, L.; Thuery, P.; Riviere, E.; Miyamoto, S.; Yamato, T.; Ephritikhine, M., *New J. Chem.* **2006**, *30*, 1220.
- (43) Nocton, G.; Burdet, F.; Pecaut, J.; Mazzanti, M., *Angew. Chem. Int. Ed.* **2007**, *46*, 7574.
- (44) Nocton, G.; Pecaut, J.; Mazzanti, M., *Angew. Chem. Int. Ed.* **2008**, *47*, 3040.
- (45) Jantunen, K. C.; Batchelor, R. J.; Leznoff, D. B., *Organometallics* **2004**, *23*, 2186.
- (46) Jantunen, K. C.; Haftbaradaran, F.; Katz, M. J.; Batchelor, R. J.; Schatte, G.; Leznoff, D. B., *Dalton Trans.* **2005**, 3083.
- (47) Calderazzo, F.; Dellamico, G.; Pasquali, M.; Perego, G., *Inorg. Chem.* **1978**, *17*, 474.
- (48) Spirlet, M. R.; Rebizant, J.; Apostolidis, C.; Dornberger, E.; Kanellakopulos, B.; Powietzka, B., *Poly* **1996**, *15*, 1503.
- (49) Castro-Rodriguez, I.; Olsen, K.; Gantzel, P.; Meyer, K., *Chem. Commun.* **2002**, 2764.
- (50) For consistency, we have reported all magnetic data assuming the formula **3.3**·2CH<sub>2</sub>Cl<sub>2</sub>. If bulk samples of **3.3** were to contain variable amounts of dichloromethane solvate,  $\chi_{MT}$  values may show better or worse agreement with what is observed for **1** (Figure A2.29).
- (51) Kanellakopulos, B.; Marks, T. J.; Fischer, R. D., *Organometallics of the f-Elements*. In *NATO Advanced Study Institutes Series*, Marks, T. J.; Fischer, R. D., Eds. D. Reidel: Dordrecht, 1978.
- (52) Gamp, E.; Edelstein, N.; Malek, C. K.; Hubert, S.; Genet, M., *J. Chem. Phys.* **1983**, *79*, 2023.
- (53) Almond, P. M.; Deakin, L.; Porter, M. J.; Mar, A.; Albrecht-Schmitt, T. E., *Chem. Mat.* **2000**, *12*, 3208.

- (54) Roussel, P.; Boaretto, R.; Kingsley, A. J.; Alcock, N. W.; Scott, P., *J. Chem. Soc., Dalton Trans.* **2002**, 1423.
- (55) Boudreaux, E.; Mulay, L. N., *Theory and Application of Molecular Paramagnetism*. John Wiley & Sons: New York, 1976; p 510.
- (56) Graves, C. R.; Vaughn, A. E.; Schelter, E. J.; Scott, B. L.; Thompson, J. D.; Morris, D. E.; Kiplinger, J. L., *Inorg. Chem.* **2008**, *47*, 11879.
- (57) Kreindlin, A. Z.; Dolgushin, F. M.; Yanovsky, A. I.; Kerzina, Z. A.; Petrovskii, P. V.; Rybinskaya, M. I., *J. Organomet. Chem.* **2000**, *616*, 106.
- (58) Kiplinger, J. L.; Pool, J. A.; Schelter, E. J.; Thompson, J. D.; Scott, B. L.; Morris, D. E., *Angew. Chem. Int. Ed.* **2006**, *45*, 2036.
- (59) Schelter, E. J.; Morris, D. E.; Scott, B. L.; Thompson, J. D.; Kiplinger, J. L., *Inorg. Chem.* **2007**, *46*, 5528.
- (60) Suski, W.; Baran, A.; Folcik, L.; Wochowski, K.; Mydlarz, T., *J. Alloy* **1992**, *181*, 249.
- (61) Karbowiak, M.; Drozdzyński, J., *J. Alloy* **1998**, *271*, 863.
- (62) Salmon, L.; Thuery, P.; Riviere, E.; Girerd, J. J.; Ephritikhine, M., *Chem. Commun.* **2003**, 762.

**Chapter 4. Preparation and Attempt at the Magnetic Characterization of Eight- and Nine Coordinate Uranium(IV) Arylacetylide Complexes Based on 1,2-Bis(dimethylphosphino)ethane**

**4.1 Introduction**

In Chapter 2, weak magnetic communication between pentacoordinate U(IV) centers was observed. Upon implantation of a subtraction scheme we were able to model ferromagnetic interactions for these compounds. We believe that the small magnitude of these exchange interactions was due to the hardness of the triamidoamine ligand set used.

Complexes that are based on a softer phosphine scaffold seem ripe for exploration due to both the ability for easily accessible cubic ligand field environments and the potential to display a paramagnetic ground state, at least in theory (Figure 4.1). However, this hypothesis was tested, to a certain extent, in Chapter 3 where we saw that the magnetism for the cubic U(IV) compounds [(dmpe)<sub>2</sub>UCl<sub>4</sub>] (**3.1**), [(dmpe)<sub>2</sub>UMe<sub>4</sub>] (**3.2**), and [(dmpe)<sub>4</sub>U<sub>4</sub>Cl<sub>16</sub>]·2CH<sub>2</sub>Cl<sub>2</sub> (**3.3**) displayed magnetism indicative of non-magnetic ground states. If magnetic coupling was present between U(IV) ions in the tetranuclear complex **3.3**, it is obscured by the single-ion behavior.

We hypothesized that preparing complexes that contain U(IV) in a cubic ligand field environment, using acetylide ligands, might allow for the isolation of compounds exhibiting enhanced magnetic coupling. In that vein, we report the synthesis and characterization of [(dmpe)<sub>2</sub>U(CCPh)<sub>4</sub>] (**4.1**) (CCPh = phenylacetylide) and [(dmpe)<sub>2</sub>U(CCPh)<sub>5</sub>(Li·Et<sub>2</sub>O)] (**4.2**).

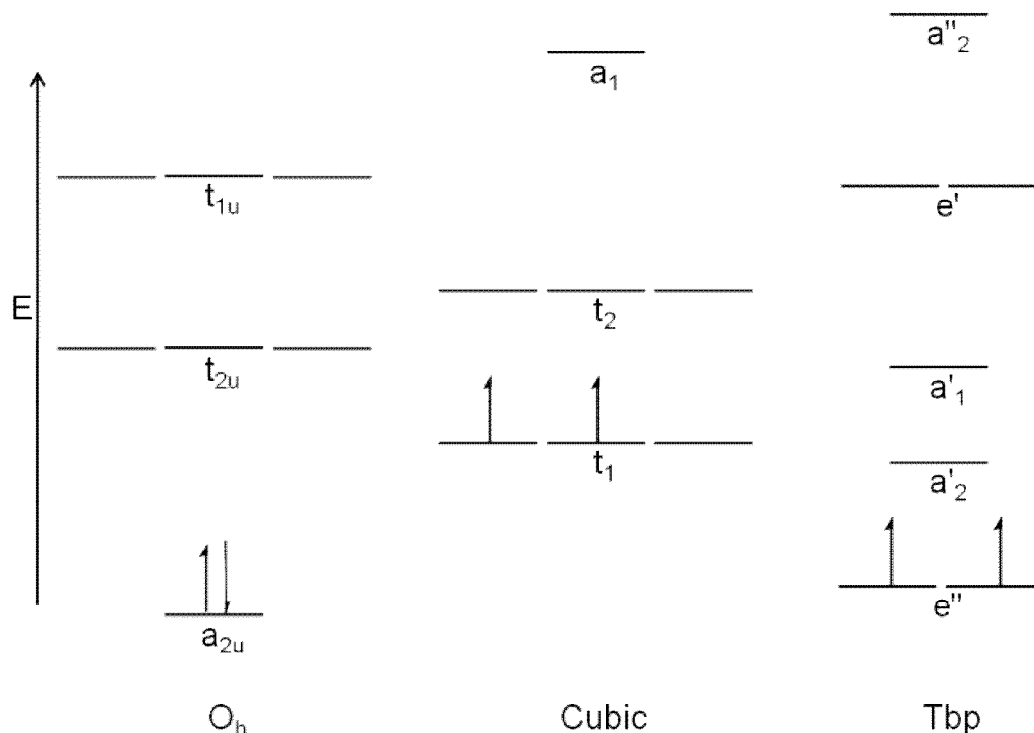


**Figure 4.1.** Energy diagram representing the crystal field splittings of an  $f^2$  configuration in octahedral (left), cubic (middle), and trigonal bipyramidal (right) ligand fields. This diagram neglects spin-orbit coupling and was adapted from reference 1.

## 4.2 Division of Labor Section

All experimental work and characterization was performed by Brian S. Newell.

## 4.3 Experimental Section

**4.3.1 Preparation of Compounds.** All manipulations were carried out in an inert dinitrogen atmosphere; either in a glove box (MBRAUN Labmaster 130) or via standard Schlenk techniques. Pentane was distilled over sodium metal, degassed by three freeze-pump-thaw cycles, and stored under an atmosphere of dinitrogen. All other solvents were reagent grade, passed through alumina, degassed and stored under dinitrogen. The compounds  $[(dmpe)_2UCl_4]$  and  $[(dmpe)_2UMe_4]$  were prepared according to the methods outlined in Chapter 3.<sup>2</sup> All other reagents were obtained from commercial vendors and used without further purification.

**Caution!** Depleted uranium (primary isotope  $^{238}\text{U}$ ) is a weak  $\alpha$  emitter (4.197 MeV) with a half-life of  $4.47 \times 10^9$  years; manipulations and reactions should be carried out in monitored fume hoods or in an inert atmosphere glove box in a radiation laboratory equipped with  $\alpha$ - and  $\beta$ -particle counting equipment.

**[(dmpe) $_2$ U(CCPh) $_4$ ] (4.1).** Phenylacetylene (145  $\mu\text{L}$ , 1.32 mmol) was added dropwise to a stirred solution of [(dmpe) $_2$ U $\text{Me}_4$ ] (175 mg, 0.292 mmol) in 15 mL of pentane at  $-40$   $^\circ\text{C}$ , and the resulting dark purple solution was stirred for 30 min. All volatiles were removed in vacuo to afford a purple solid (225 mg, 82% yield based on [(dmpe) $_2$ U $\text{Me}_4$ ]). Single crystals suitable for X-ray analysis were grown from a concentrated pentane solution maintained at  $-40$   $^\circ\text{C}$  for 8 h. Absorption spectrum ( $\text{Et}_2\text{O}$ )  $\lambda_{\text{max}}$  ( $\epsilon_{\text{M}}$ ): 721 nm ( $138 \text{ L} \cdot \text{mol}^{-1} \cdot \text{cm}^{-1}$ ).  $^1\text{H}$  NMR (293 K,  $\text{C}_6\text{D}_6$ ):  $\delta$  15.87 (s, 8 H, Ar- $H$ ), 11.98 (s, 4 H, Ar- $H$ ), 9.19 (s, 8 H, Ar- $H$ ), 1.85 (s, 24 H,  $\text{PCH}_3$ ),  $-28.13$  ppm (s, 8 H,  $\text{PCH}_2$ ). IR (mineral oil): 643 (w), 691 (m), 723 (m), 754 (w), 773 (w), 830 (w), 864 (m), 890 (m), 929 (m), 944 (m), 996 (w), 1023 (w), 1067 (w), 1085 (w), 1155 (w), 1170 (w), 1194 (w), 1275 (m), 1292 (m), 1304 (m), 1377 (s), 1461 (s), 1591 (m), 2047 (m), 2671 (w), 2724 (w), 2840 (s), 2924 (s)  $\text{cm}^{-1}$ . Anal. Calcd. for  $\text{C}_{44}\text{H}_{52}\text{P}_4\text{U}$ : C, 56.05; H, 5.56;. Found: C, 53.55; H, 5.81. The results of elemental analysis and the magnetic susceptibility data have, thus far, not been reproducible. Some discussion into the lack of reproducibility is offered in section 4.3.3.

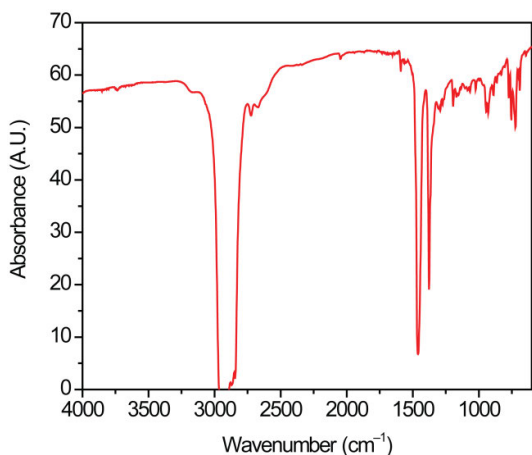


**Figure 4.2.** Full IR spectrum of **4.1** taken as a mineral oil mull. The peaks at  $\sim 3000$ ,  $1460$ , and  $1377\text{ cm}^{-1}$  are due to mineral oil. A minimum of 32 transients were recorded.

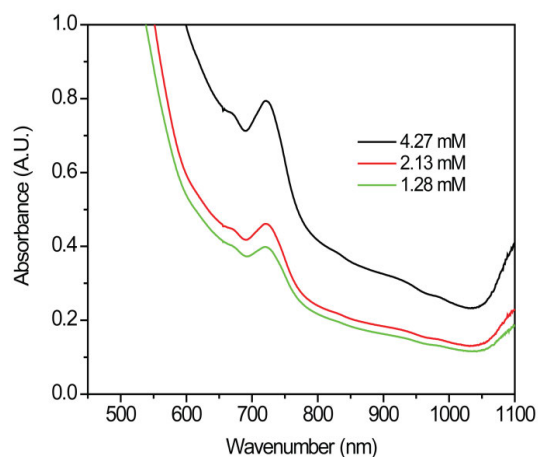


**Figure 4.3.** Electronic absorption spectrum of **4.1**, collected in  $\text{Et}_2\text{O}$  solution.

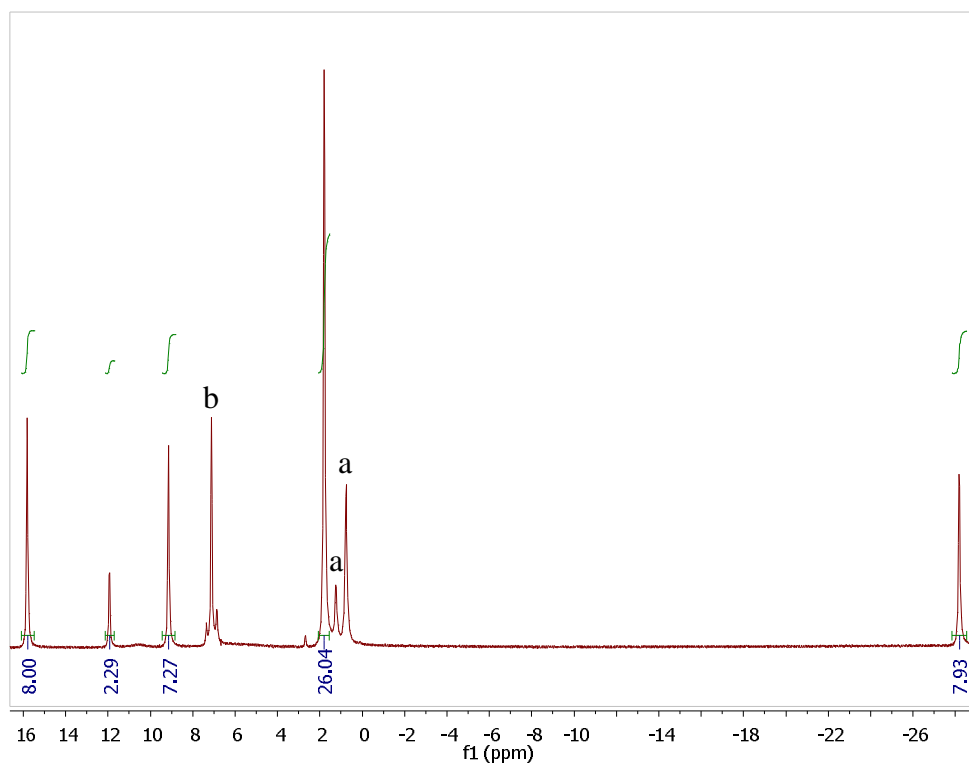


**Figure 4.4.**  $^1\text{H}$  NMR spectrum of  $[(\text{dmpe})_2\text{U}(\text{CCPh})_4]$  (**4.1**) obtained in  $\text{C}_6\text{D}_6$  at ambient temperature with a 500 MHz spectrometer. The labeled peaks (a) and (b) represent pentane and residual solvent peaks for  $\text{C}_6\text{D}_6$ , respectively.

**[(dmpe)<sub>2</sub>U(CPh)<sub>5</sub>(Li·Et<sub>2</sub>O)] (4.2).** A glass vial was charged with [(dmpe)<sub>2</sub>UCl<sub>4</sub>] (280 mg, 0.412 mmol) and LiCPh (230 mg, 2.13 mmol) and cooled to −40 °C for 1 hr. Cold Et<sub>2</sub>O (15 mL, −40 °C) was added subsequently, and the resulting wine-red mixture was stirred for 30 min. The solution was filtered, concentrated to ca. 3 mL under reduced pressure, and then cooled to −40 °C. After 8 h, a red-brown microcrystalline precipitate was observed. The product was collected by filtration and dried in vacuo to afford a red-brown crystalline solid (0.380 g, 82% yield based on [(dmpe)<sub>2</sub>UCl<sub>4</sub>]). Single crystals suitable for X-ray analysis were grown from a concentrated Et<sub>2</sub>O solution maintained at −40 °C for 8 h. Absorption spectrum (Et<sub>2</sub>O) λ<sub>max</sub> (ε<sub>M</sub>): 486 (233), 534 (217), 559 (245), 668 (83), 739 (359), 907 (53), 954 (83), 1007 nm (43 L·mol<sup>−1</sup>·cm<sup>−1</sup>). IR (mineral oil): 642 (w), 691 (m), 727 (m), 755 (w), 772 (w), 831 (w), 865 (m), 890 (m), 929 (m), 943 (m), 975 (m), 997 (w), 1024 (w), 1066 (w), 1091 (w), 1153 (w), 1173 (w), 1194 (w), 1270 (m), 1286 (m), 1304 (m), 1377 (s), 1461 (s), 1566 (m), 1591 (m), 2042 (m), 2671 (w), 2724 (w), 2840 (s), 2924 (s) cm<sup>−1</sup>. Anal. Calcd. for C<sub>56</sub>H<sub>67</sub>P<sub>4</sub>UOLi: C, 59.79; H, 6.00;. Found: C, 59.90; H, 6.20.

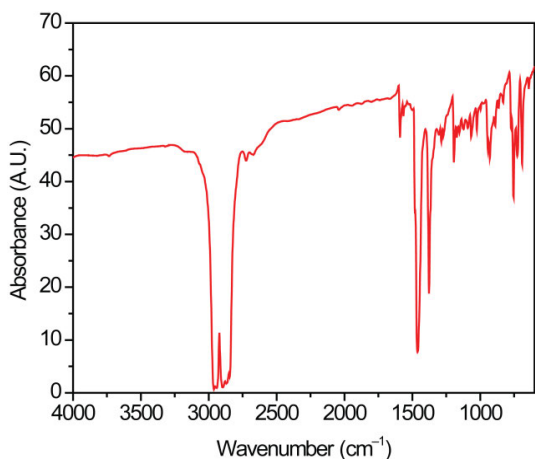


**Figure 4.5.** Full IR spectrum of **4.2** taken as a mineral oil mull. The peaks at  $\sim 3000$ ,  $1460$ , and  $1377\text{ cm}^{-1}$  are due to mineral oil. A minimum of 32 transients were recorded.

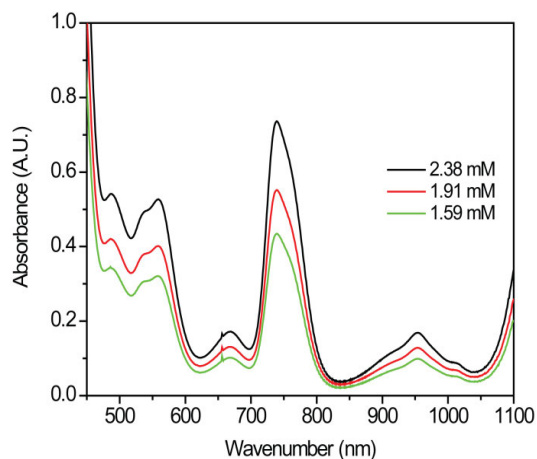


**Figure 4.6.** Electronic absorption spectrum of **4.2**, collected in  $\text{Et}_2\text{O}$  solution.

**4.3.2 X-ray Structure Determinations.** X-ray crystal structures were determined for the compounds listed in Table 4.1. Single crystals were coated with Paratone-N oil in the glove box and mounted under a cold stream of dinitrogen gas. Single crystal X-ray diffraction data were acquired on a Bruker Kappa APEX II CCD diffractometer with  $\text{Mo K}_\alpha$  radiation ( $\lambda = 0.71073\text{ \AA}$ ) and a graphite monochromator. Initial lattice parameters were obtained from a least-squares analysis of more than 100 reflections; these parameters were later refined against all data. Data sets were collected targeting a four-fold redundancy. None of the crystals showed significant decay during data collection. Data were integrated and corrected for Lorentz and polarization effects using Bruker APEX2 software, and semiempirical absorption corrections were applied using SCALE with the aid of numerical face indexing.<sup>3</sup> Space group assignments were based on systematic absences,  $E$  statistics, and successful refinement of the structures. Structures were solved by the Patterson method and were refined with the aid of successive Fourier difference maps against all data using the SHELXTL 6.14 software package.<sup>4</sup> Thermal

parameters for all atoms with  $Z \geq 3$  were refined anisotropically. All hydrogen atoms were assigned to ideal positions and refined using a riding model with an isotropic thermal parameter 1.2 times that of the attached carbon atom (1.5 times for methyl hydrogens). Selected bond distances and angles for crystals of compounds **4.1** and **4.2** are presented in Table 4.2. Full details for **4.1** and **4.2** are given in the form of cif files at the end of the chapter. In the structure of **4.2**, there are several disordered components including: the dmpe ligands, two phenylacetylide ligands, and the coordinated Et<sub>2</sub>O solvent, which are disordered over two sites. The dmpe ligands bound to the uranium center have a site occupancy ratio refining to 80:20. The two disordered phenylacetylide ligands involve C14–C20 and C31–C36 with site occupancy ratios refining to 46:54 and 49:51, respectively. For the coordinated Et<sub>2</sub>O solvent, C53–C56 are disordered with a site occupancy ratio refining to 45:55. For **4.2**, thermal parameters for all chemically equivalent disordered atoms were refined anisotropically. Full structures of **4.1** and **4.2** are depicted in Figures 4.7 and 4.8, respectively.

**Table 4.1.** Crystallographic data for compounds [(dmpe)<sub>2</sub>U(CCPPh)<sub>4</sub>] (**4.1**) and [(dmpe)<sub>2</sub>U(CCPPh)<sub>5</sub>(Li·Et<sub>2</sub>O)] (**4.2**).

	<b>4.1</b>	<b>4.2</b>
formula	C <sub>44</sub> H <sub>52</sub> P <sub>4</sub> U	C <sub>56</sub> H <sub>57</sub> LiOP <sub>4</sub> U
formula wt	942.77	1124.95
color, habit	purple block	red-brown block
<i>T</i> , K	120(2)	120(2)
space group	<i>P</i> 2 <sub>1</sub> / <i>c</i>	<i>P</i> 4 <sub>3</sub> 2 <sub>1</sub> 2
<i>Z</i>	4	2
<i>a</i> , Å	21.7865(6)	11.5046(3)
<i>b</i> , Å	13.5803(4)	13.8617(3)
<i>c</i> , Å	14.8702(4)	20.6359(5)
<i>α</i> , deg	90	70.407(1)
<i>β</i> , deg	99.865(2)	86.074(1)
<i>γ</i> , deg	90	69.160(1)
<i>V</i> , Å <sup>3</sup>	4334.6(2)	2892.67(12)
<i>d</i> <sub>calc.</sub> , g/cm <sup>3</sup>	1.445	1.292
GOF	1.04	1.12
<i>R</i> <sub>1</sub> ( <i>wR</i> <sub>2</sub> ) <sup>b</sup> , %	3.21(5.68)	4.17(11.36)

<sup>a</sup> Obtained with graphite-monochromated Mo Kα ( $\lambda = 0.71073$  Å) radiation.

<sup>b</sup>  $R_1 = \sum ||F_o| - |F_c|| / \sum |F_o|$ ,  $wR_2 = \{ \sum [w(F_o^2 - F_c^2)^2] / \sum [w(F_o^2)^2] \}^{1/2}$  for  $F_o > 4\sigma(F_o)$ .

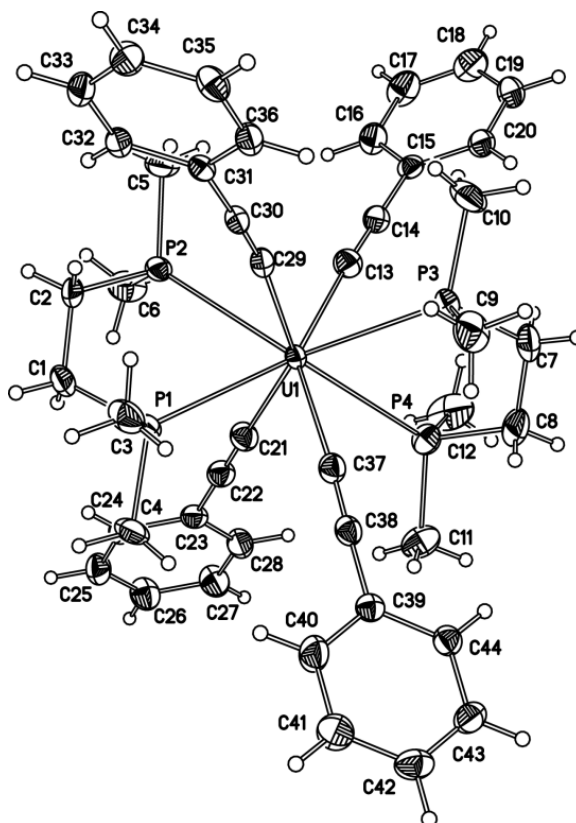


**Figure 4.7.** The U-containing complex in the crystal structure of **4.1**, rendered with 40% ellipsoids.

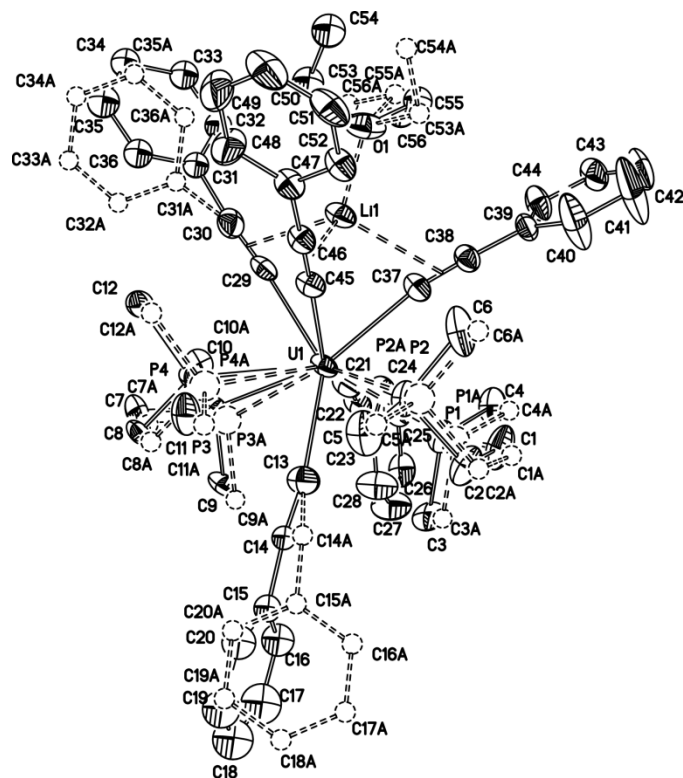


**Figure 4.8.** The U-containing complex in the crystal structure of **4.2**, rendered with 40% ellipsoids. Hydrogen atoms have been omitted for clarity. There are several groups disordered over two positions; the disordered parts appear as dashed circles in the figure.

**4.3.3 Magnetic Susceptibility Measurements.** Magnetic susceptibility measurements were collected using a Quantum Design MPMS XL SQUID magnetometer. Powdered microcrystalline samples were loaded into quartz tubes in the glove box, encased in Eicosane, sealed, inserted into a straw and transported to the SQUID magnetometer. DC magnetic susceptibility data were collected at temperatures ranging from 2 to 300 K at an applied field of 0.1 T. Magnetization measurements were collected at temperatures ranging from 2 to 35 K at applied fields of 1, 2, 3, 4, and 5 T. AC magnetic susceptibility data were collected at temperatures ranging from 1.8 to 10 K at an applied AC field of 4 Oe with switching frequencies of 200 and 1000 Hz and with an applied 0.1 T DC field. Contributions to the magnetization from the quartz tube and

the straw were measured independently and subtracted from the total measured signal. Data were corrected for diamagnetic contributions using Pascal's constants.<sup>5</sup>

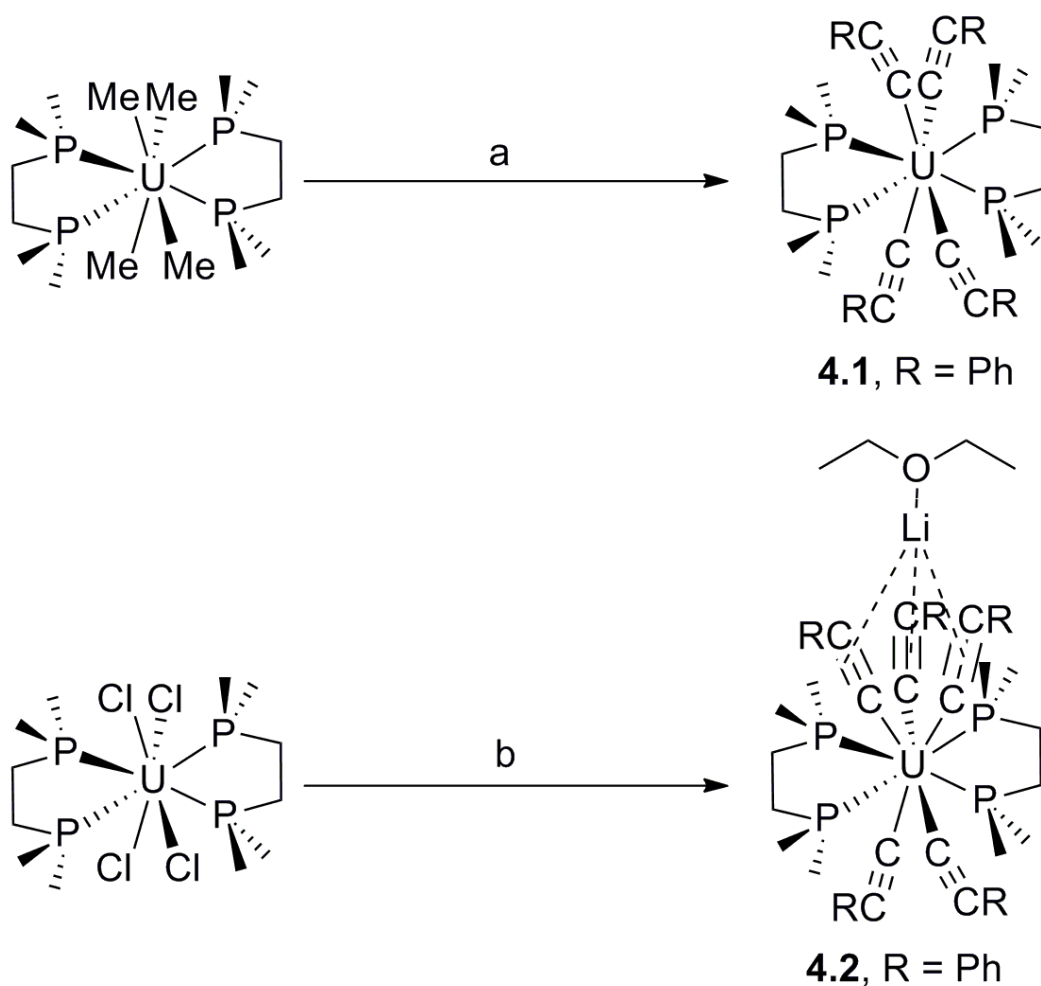
**4.3.4 Other Physical Measurements.** Electronic absorption spectra were obtained in Et<sub>2</sub>O solutions in an airfree glass cell of path length 1 cm on an Agilent 8453 spectrophotometer. <sup>1</sup>H NMR spectra were recorded using a Varian INOVA 500 MHz instrument, and the spectra were referenced internally using residual protio solvent resonances relative to tetramethylsilane ( $\delta = 0$  ppm). Infrared spectra were collected on a Thermo Nicolet 380 FTIR spectrometer as mineral oil mulls pressed between sodium chloride plates. Elemental analyses were performed by the Micro-Mass facility at the University of California, Berkeley.

## 4.4 Results and Discussion

### 4.4.1 Syntheses and Characterization of Eight- and Nine-Coordinate [(dmpe)<sub>2</sub>U]-Acetylide Complexes.

We hypothesized that [(dmpe)<sub>2</sub>UX<sub>4</sub>] (X = Cl or Me) compounds could serve as interesting starting materials that could be used to target assemblies with larger more interesting topologies. Similar to our work, and following Scott's precedent,<sup>6,7</sup> these complexes appear suitable for substitution with acetylide-type ligands. By utilizing phenylacetylide ligands, we have isolated two U(IV) phosphine compounds with eight- and nine-coordinate U(IV) centers supported by softer phosphine ligands. It is easy to envisage the use of the acetylide ligands to synthesize a compound where four or five metal centers could bridge each of the phenylacetylide ligands. This opens the possibility to the synthesis of compounds that may exhibit interesting magnetic properties through a larger motif. Utilizing the tetramethyl derivative originally reported by Andersen and

coworkers,<sup>2</sup> we were able to isolate the purple eight-coordinate  $[(\text{dmpe})_2\text{U}(\text{CCPh})_4]$  (**4.1**) (Scheme 4.1). Initial reaction of  $[(\text{dmpe})_2\text{UCl}_4]$  with four equivalents of lithium phenylacetylide led to the formation of red-brown nine-coordinate  $[(\text{dmpe})_2\text{U}(\text{CCPh})_5(\text{Li}\cdot\text{Et}_2\text{O})]$  (**4.2**) as the only isolable product. By optimizing the stoichiometry and reaction conditions, the isolated yield of **4.2** is greatly improved (Scheme 4.1).



**Scheme 4.1.** Syntheses of chelating phosphine complexes of U(IV): a = 4 eq. HCCPh in pentane at  $-40\text{ }^\circ\text{C}$ ; b = 5 eq. LiCCPh in  $\text{Et}_2\text{O}$  at  $-40\text{ }^\circ\text{C}$ .

**4.4.2 Structural Comparisons.** The crystal structure of **4.1** is depicted in Figure 4.9. The average U–P bond distance in **4.1** is  $2.9773(6)\text{ \AA}$  and the average U–C bond distance

is 2.472(2) Å, both of which compare well to other published U(IV) compounds with arylacetylide and/or phosphine ligands namely,  $(\text{Me}_2\text{Pz})_4\text{U}(\mu\text{-dmpe})$ ,  $(\text{C}_5\text{Me}_5)_2\text{U}(\text{NPh}_2)(\text{CCPh})$ ,  $\text{U}(\text{CH}_2\text{C}_6\text{H}_5)_3\text{Me}(\text{Me}_2\text{PCH}_2\text{CH}_2\text{PMe}_2)$ ,  $(\text{C}_5\text{H}_5)_2\text{U}(\text{N}^i\text{Bu})_2(\text{dmpe})$ , and  $\text{U}\{\text{P}(\text{CH}_2\text{CH}_2\text{PMe}_2)_2\}_4$ .<sup>7-12</sup> As seen with the complexes in Chapter 3, the phosphine ligands are rotated by approximately 90° relative to each other. Selected bond distances and angles are presented in Table 4.2.

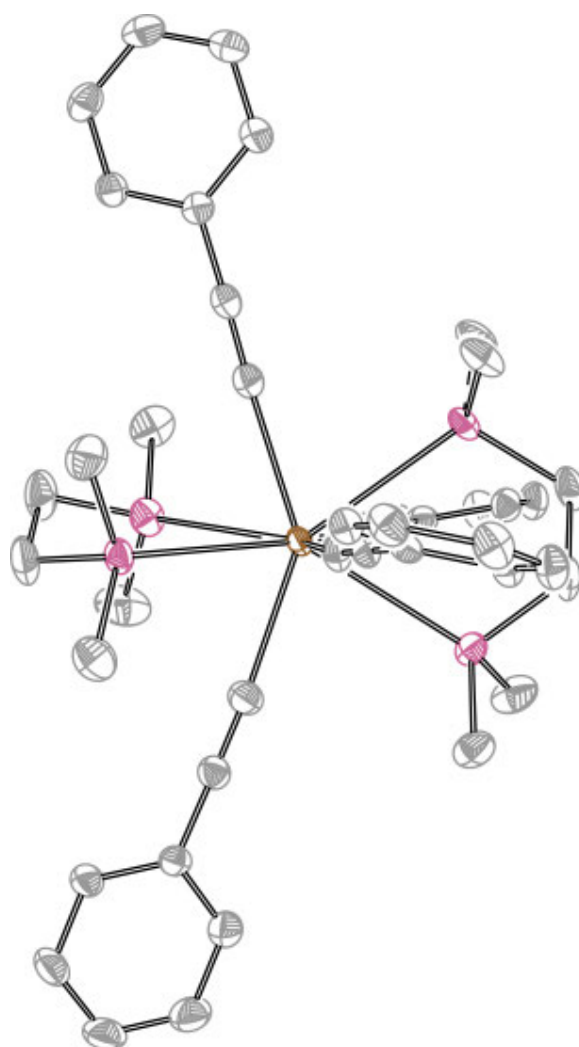


**Figure 4.9.** Crystal structure of the U(IV) arylacetylide complex in compound **4.1** rendered with 40% ellipsoids. Brown, purple, and gray ellipsoids represent U, P, and C atoms, respectively. Hydrogen atoms are omitted for clarity.

The crystal structure of **4.2** is depicted in Figure 4.10. The average U–P bond distance in **4.2** is 3.0105(6) Å and the average U–C bond distance is 2.5296(4) Å. The phosphine ligands are essentially related by a mirror plane in the molecule. Both the U–P and U–C bond lengths are shorter in **4.1** than **4.2**, which is most likely a result of steric crowding around the uranium center in **4.2**. The difference in coordination and ligand field strengths around the uranium center **4.2** might lead to an effect on the magnetic properties.

**Table 4.2.** Selected bond distances (Å) and angles (°) for crystallographically-determined structures [(dmpe)<sub>2</sub>U(CCPPh)<sub>4</sub>] (**4.1**) and [(dmpe)<sub>2</sub>U(CCPPh)<sub>5</sub>(Li·Et<sub>2</sub>O)] (**4.2**).

	<b>4.1</b>	<b>4.2</b>
U–P	2.9773(6)	3.0105(6)
U–CC	2.472(2)	2.5296(4)
CC <sub>cis</sub> –U–CC <sub>cis</sub>	95.52(8)	82.23(14)
CC <sub>cis</sub> –U–CC <sub>trans</sub>	143.89(8)	142.90(16)
P <sub>cis</sub> –U–P <sub>cis</sub>	67.39(18)	65.67(14)
P <sub>cis</sub> –U–P <sub>trans</sub>	133.917(18)	143.285(15)

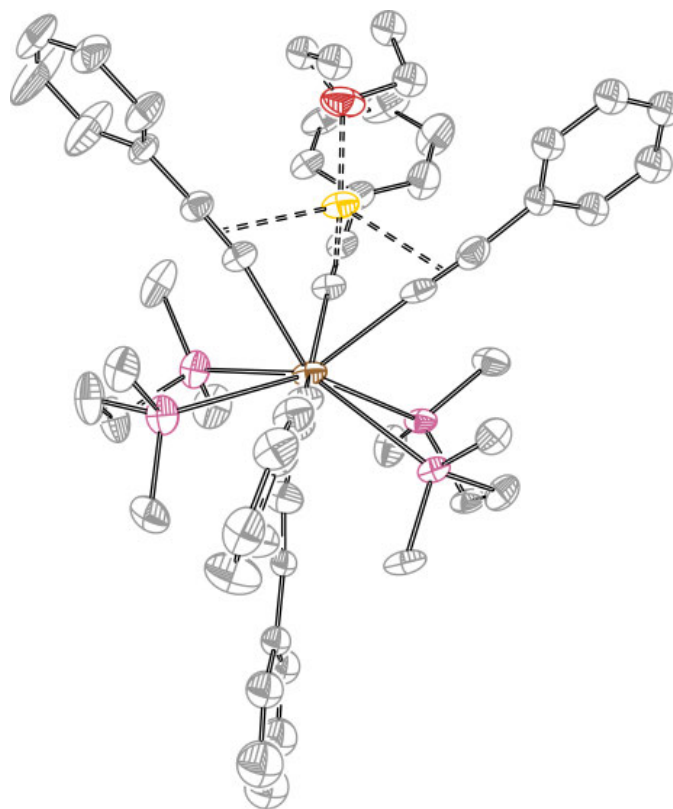


**Figure 4.10.** Crystal structure of the U(IV) arylacetylide complex in compound **4.2** rendered with 40% ellipsoids. Brown, purple, yellow, red, and gray ellipsoids represent U, P, Li, O, and C atoms, respectively. Hydrogen atoms are omitted for clarity.

**4.4.3 Magnetic Properties.** The temperature dependencies of the magnetic susceptibilities (2-300 K),  $\chi_M T$ , for the U(IV) arylacetylide complexes **4.1** and **4.2** are shown in Figure 4.11.<sup>13</sup> The temperature dependence of the inverse susceptibility for compounds 4.1 and 4.2 are shown in Figure 4.12. Reproducibility of the magnetic data has been poor and suggests that these compounds are not thermally and/or chemically stable. Several different techniques have been tried to acquire reproducible data (Figures 4.13-4.14), including quartz tubes sealed by flame, Apiezon M vacuum grease, or Eicosane, as well as the polycarbonate gel capsules. When flame sealing quartz tubes it was noted that the quartz transferred the heat to the sample and on several instances, even after cooling the sample in liquid nitrogen, caused the decomposition of the material as

noted by a color change to dark brown/black. Apiezon M grease and Eicosane were also used in an attempt to ‘plug’ the quartz tube and prevent exposure of the sample to oxygen but again, no reproducibility was achieved via these methods. Upon addition of **4.2** to a polycarbonate gel capsule the compound immediately starts to turn black and is completely decomposed in a matter of minutes. With this in mind the two runs that appeared most similar between compounds **4.1** (notebook reference: 534-bsn\_chiquartz\_eicosane2) and **4.2** (notebook reference: 537-bsn\_chiquartz\_eicosane1) were used in the following discussion.

The room temperature  $\chi_M T$  values for **4.1** and **4.2** (1.45 and 1.22  $\text{emu}\cdot\text{K}\cdot\text{mol}^{-1}$ , respectively) are consistent with the presence of paramagnetic state(s) at room temperature (Figure 4.11). Upon decreasing the temperature, higher energy Stark sublevels begin to depopulate, resulting in a subsequent decrease in the magnitude of the total angular momentum vector. This phenomenon leads to a variation in the thermal population of the many states that are energetically comparable to the ground state.<sup>9</sup> The physical manifestation of this decrease in the angular momentum is evident by the decrease in the observed magnetic susceptibility. As can be seen in a plot of  $\chi_M T$  versus  $T$  for **4.1**, a gradual decrease to 0.65  $\text{emu}\cdot\text{K}\cdot\text{mol}^{-1}$  at 90 K occurs, followed by a slight decrease to 0.50  $\text{emu}\cdot\text{K}\cdot\text{mol}^{-1}$  at 25 K. Below 25 K there is a sharp drop off in the magnetic susceptibility to 0.09  $\text{emu}\cdot\text{K}\cdot\text{mol}^{-1}$  at 2 K. In contrast,  $\chi_M T$  for compound **4.2** displays a gradual decrease to 0.72  $\text{emu}\cdot\text{K}\cdot\text{mol}^{-1}$  as the temperature is reduced to 120 K. The measured susceptibility is essentially constant at a value of 0.69  $\text{emu}\cdot\text{K}\cdot\text{mol}^{-1}$  down to 25 K. As the temperature is decreased further there is a sharp drop in the susceptibility to a value of 0.17  $\text{emu}\cdot\text{K}\cdot\text{mol}^{-1}$  at 2 K. A poorly isolated singlet ground state is not

atypical for complexes with  $5f^2$  valence configurations;<sup>14-17</sup> further, it is well-known that a cubic ligand field can result in a diamagnetic ground state for a  $5f^2$  electronic configuration.<sup>2</sup> Although both species display magnetic properties which appear to be consistent with a non-magnetic ground state,<sup>16,18,19</sup> there seems to be less influence from TIP on **4.2** than observed for **4.1** (vide infra). It is possible that the downturn at low temperature is due to intermolecular antiferromagnetic coupling but upon examination of the structures there are no apparent close contacts that would allow for intermolecular communication. The closest intermolecular contact is 4.243 Å between U1 and H43A.

Overall, the foregoing results imply that coordination geometry differences impart an effect on the magnetic properties of these [(dmpe)<sub>2</sub>U]-containing complexes. Comparing the magnetic properties with compounds reported in Chapter 2, which show a more classical response of the temperature dependence of the magnetic susceptibility, these compounds display very different magnetic behavior and warrant further study.

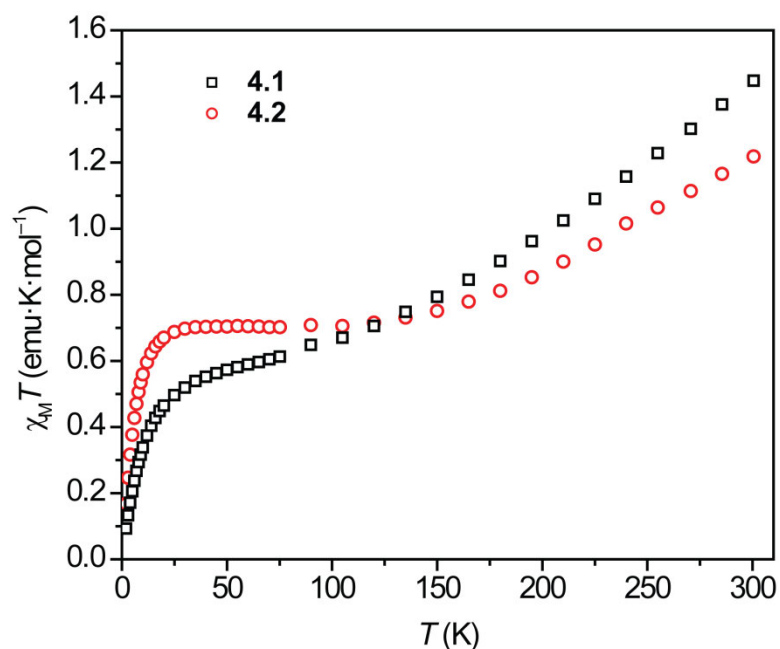


**Figure 4.11.** Temperature dependence of the magnetic susceptibility for  $[(\text{dmpe})_2\text{U}(\text{CCPh})_4]$  (**4.1**, notebook reference: 534-bsn\_chiquartz\_icosane2) and  $[(\text{dmpe})_2\text{U}(\text{CCPh})_5(\text{Li}\cdot\text{Et}_2\text{O})]$  (**4.2**, notebook reference: 537-bsn\_chiquartz\_icosane1), obtained at a measuring field of 1000 G.

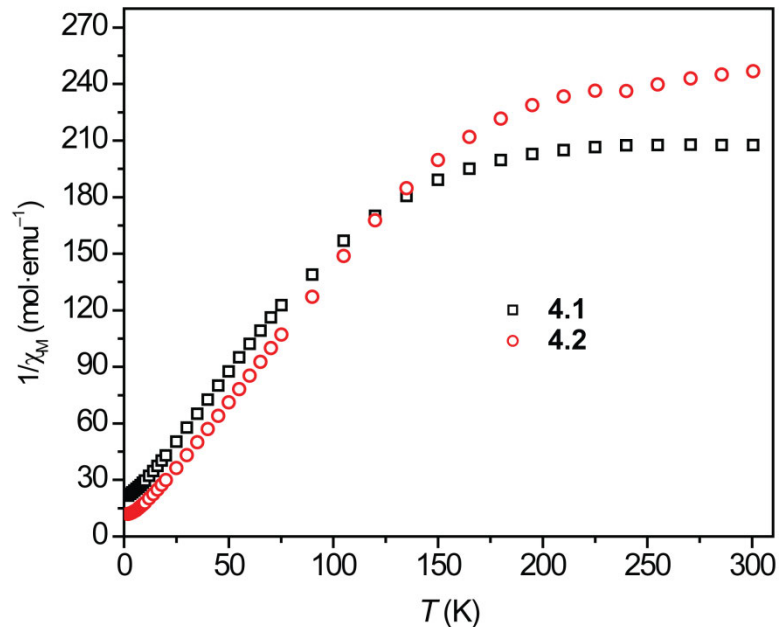


**Figure 4.12.** Temperature dependence of the inverse susceptibility for compounds **4.1** (notebook reference: 534-bsn\_chiquartz\_icosane2) and **4.2** (notebook reference: 537-bsn\_chiquartz\_icosane1) obtained at a measuring field of 1000 G. Crystals of **4.1** and **4.2** were finely ground and encased in hot Eicosane prior to measurement.

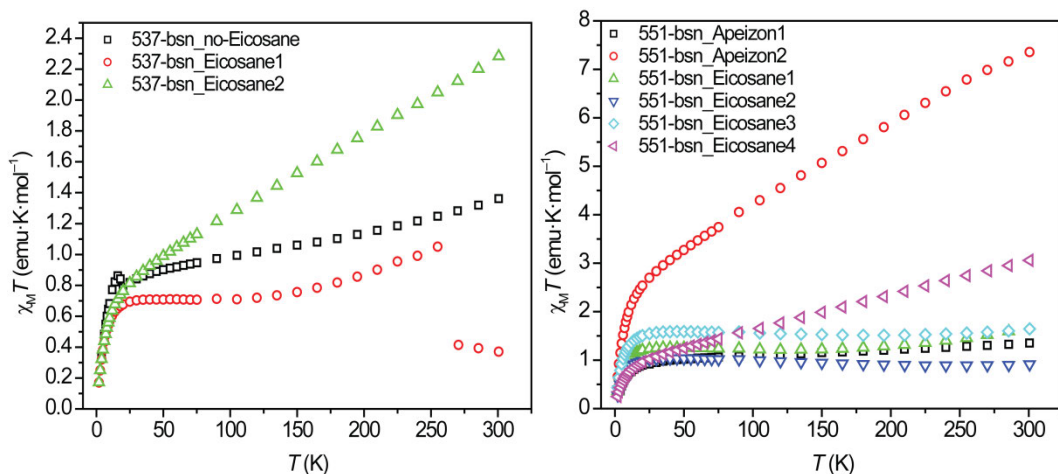


**Figure 4.13.** Several attempts at collecting reproducible data for the temperature dependence of the magnetic susceptibility for compound **4.2** obtained at a measuring field of 1000 G. The plot on the left represents several attempts from the batch 537-bsn. The plot on the right represents several attempts from the batch 551-bsn.

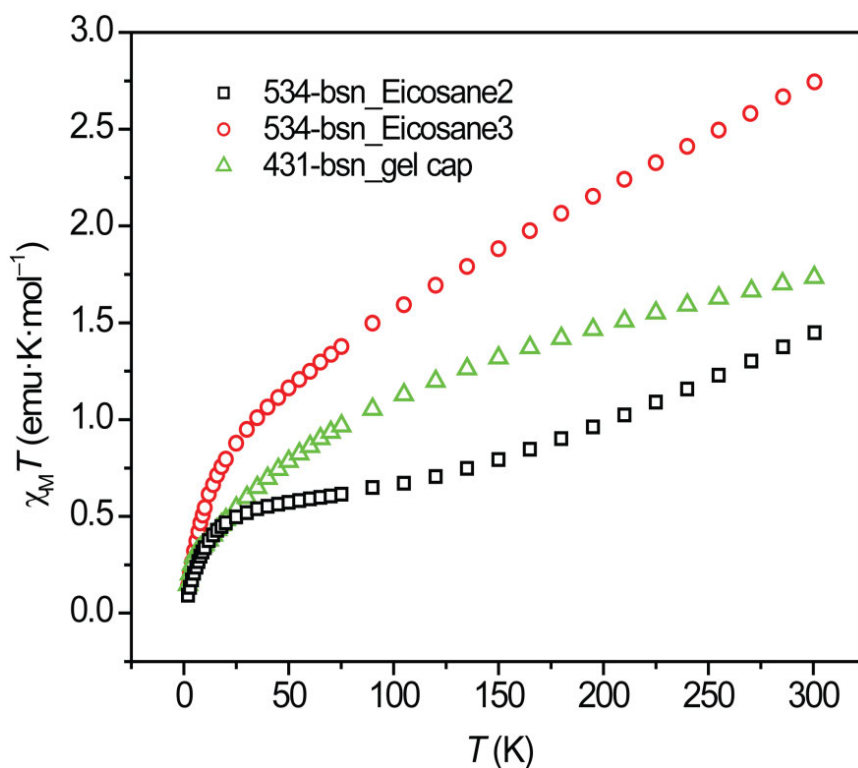


**Figure 4.14.** Several attempts at collecting reproducible data for the temperature dependence of the magnetic susceptibility for compound **4.1** obtained at a measuring field of 1000 G.

To ascertain if the nine-coordinate **4.2** displays characteristics of a single-molecule magnet, measurements were obtained with and without a perpendicularly-applied 0.1 T DC field. No frequency dependence of the AC susceptibility was observed (Figure 4.15).

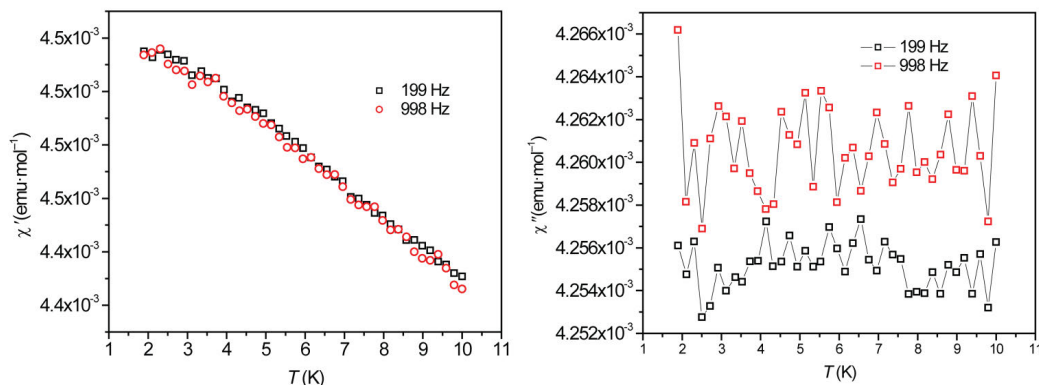


**Figure 4.15.** Temperature dependence of the in-phase ( $\chi'$ , left) and out-of-phase ( $\chi''$ , right) components of the AC susceptibility for **4.2** (notebook reference: 537-bsn\_chi Quartz\_icosane1). The sample was encased in Eicosane, and data were collected at various frequencies under a 0.1 T applied DC field with an oscillating 4 Oe AC field.

#### 4.5 Summary and Outlook

We have prepared eight- and nine-coordinate U(IV) acetylide complexes supported by anionic ethynylbenzene and phosphine ligands, and have used multiple techniques to characterize them. Despite the fact that the compounds presented in this study give non-magnetic ground states at low temperature, which are consistent with those described elsewhere in the literature,<sup>20-23</sup> they seem to display interesting magnetic behavior (although not reproducible) and therefore deserve more attention. Efforts to further study the reactivity of these compounds are underway in our laboratory.

**4.6 Acknowledgments.** This research was supported by Colorado State University. We thank the ACS Petroleum Research Fund (44691-G3) for support of the IR and UV-visible instrumentation. We thank Ms. Susie Miller and Prof. Oren Anderson for advice

on crystal structure refinements and Dr. Christopher Rithner for assistance with NMR data collection.

#### 4.7 Crystallographic Information Formatted (cif) files for crystals 4.1 and 4.2

```

data_msn219 (4.1)                _symmetry_space_group_name_H-M
                                   P2(1)/c
_audit_creation_method           'Bruker
  SHELXTL'
_chemical_name_systematic        loop_
                                   _symmetry_equiv_pos_as_xyz
                                   'x, y, z'
                                   '-x, y+1/2, -z+1/2'
                                   '-x, -y, -z'
                                   'x, -y-1/2, z-1/2'
_chemical_name_common            ?
_chemical_melting_point          ?
_chemical_formula_moiety         'C44
  H52 P4 U'
_chemical_formula_sum             'C44 H52 P4 U'
_chemical_formula_weight         942.77
loop_
  _atom_type_symbol              _cell_length_a                21.7865(6)
  _atom_type_description         _cell_length_b                13.5803(4)
  _atom_type_scatter_dispersion_real _cell_length_c                14.8702(4)
  _atom_type_scatter_dispersion_imag _cell_angle_alpha             90.00
  _atom_type_scatter_source      _cell_angle_beta              99.865(2)
  'C' 'C' 0.0033 0.0016         _cell_angle_gamma            90.00
  'International Tables Vol C Tables _cell_volume                  4334.6(2)
  4.2.6.8 and 6.1.1.4'         _cell_formula_units_Z         4
  'H' 'H' 0.0000 0.0000         _cell_measurement_temperature
  'International Tables Vol C Tables 120(2)
  4.2.6.8 and 6.1.1.4'         _cell_measurement_reflns_used 9804
  'P' 'P' 0.1023 0.0942         _cell_measurement_theta_min   2.35
  'International Tables Vol C Tables _cell_measurement_theta_max   32.44
  4.2.6.8 and 6.1.1.4'         _exptl_crystal_description    block
  'U' 'U' -9.6767 9.6646         _exptl_crystal_colour         purple
  'International Tables Vol C Tables _exptl_crystal_size_max       0.35
  4.2.6.8 and 6.1.1.4'         _exptl_crystal_size_mid       0.21
  _symmetry_cell_setting         _exptl_crystal_size_min       0.09
  Monoclinic                    _exptl_crystal_density_meas   'not
                                   measured'
                                   _exptl_crystal_density_diffrn 1.445
                                   _exptl_crystal_density_method 'not
                                   measured'
                                   _exptl_crystal_F_000          1872
                                   _exptl_absorpt_coefficient_mu  3.920
                                   _exptl_absorpt_correction_type multi-
                                   scan

```

```

_exptl_absorpt_correction_T_min      0.3416
_exptl_absorpt_correction_T_max      0.7292
_exptl_absorpt_process_details        'SADABS, Sheldrick, 1997'

_exptl_special_details
;
?
;

_diffrn_ambient_temperature          120(2)
_diffrn_radiation_wavelength          0.71073
_diffrn_radiation_type                MoK\alpha
_diffrn_radiation_source               'fine-focus sealed tube'
_diffrn_radiation_monochromator        graphite
_diffrn_measurement_device_type        'Bruker APEX-II CCD'
_diffrn_measurement_method             '\f and \w scans'
_diffrn_detector_area_resol_mean      ?
_diffrn_reflns_number                  63424
_diffrn_reflns_av_R_equivalents        0.0377
_diffrn_reflns_av_signal/netI          0.0515
_diffrn_reflns_limit_h_min             -33
_diffrn_reflns_limit_h_max             32
_diffrn_reflns_limit_k_min             -20
_diffrn_reflns_limit_k_max             20
_diffrn_reflns_limit_l_min             -22
_diffrn_reflns_limit_l_max             20
_diffrn_reflns_theta_min               1.90
_diffrn_reflns_theta_max               33.19
_reflns_number_total                   16545
_reflns_number_gt                      11609
_reflns_threshold_expression            >2sigma(I)

_computing_data_collection             'Bruker APEX2'
_computing_cell_refinement             'Bruker SAINT'

_computing_data_reduction              'Bruker SAINT'
_computing_structure_solution          'SHELXS-97 (Sheldrick, 2008)'
_computing_structure_refinement        'SHELXL-97 (Sheldrick, 2008)'
_computing_molecular_graphics          'Bruker SHELXTL'
_computing_publication_material        'Bruker SHELXTL'

_refine_special_details
;
Refinement of F^2 against ALL reflections. The weighted R-factor wR and goodness of fit S are based on F^2, conventional R-factors R are based on F, with F set to zero for negative F^2. The threshold expression of F^2 > 2sigma(F^2) is used only for calculating R-factors(gt) etc. and is not relevant to the choice of reflections for refinement. R-factors based on F^2 are statistically about twice as large as those based on F, and R-factors based on ALL data will be even larger.
;

_refine_ls_structure_factor_coef       Fsqd
_refine_ls_matrix_type                 full
_refine_ls_weighting_scheme            calc
_refine_ls_weighting_details           'calc
w=1/[s^2(Fo^2)+(0.0163P)^2+1.2067P] where P=(Fo^2+2Fc^2)/3'
_atom_sites_solution_primary           direct
_atom_sites_solution_secondary         difmap
_atom_sites_solution_hydrogens         geom
_refine_ls_hydrogen_treatment          constr
_refine_ls_extinction_method           none
_refine_ls_extinction_coef             ?
_refine_ls_number_reflns               16545
_refine_ls_number_parameters           450

```

_refine_ls_number_restraints	0	H3B	H	0.1522	0.2142	0.0821	0.067
_refine_ls_R_factor_all	0.0641						Uiso 1 1 calc R . .
_refine_ls_R_factor_gt	0.0321	H3C	H	0.1211	0.1198	0.0336	0.067
_refine_ls_wR_factor_ref	0.0568						Uiso 1 1 calc R . .
_refine_ls_wR_factor_gt	0.0511	C4	C	0.22766(13)	0.01540(19)	-	
_refine_ls_goodness_of_fit_ref	1.039					0.02897(16)	0.0440(7) Uani 1 1 d . .
_refine_ls_restrained_S_all	1.039						.
_refine_ls_shift/su_max	0.004	H4A	H	0.1928	-0.0286	-0.0328	0.066
_refine_ls_shift/su_mean	0.000						Uiso 1 1 calc R . .
loop_		H4B	H	0.2656	-0.0220	-0.0206	0.066
_atom_site_label							Uiso 1 1 calc R . .
_atom_site_type_symbol		H4C	H	0.2241	0.0530	-0.0843	0.066
_atom_site_fract_x							Uiso 1 1 calc R . .
_atom_site_fract_y		C5	C	0.34324(12)	0.2783(2)		
_atom_site_fract_z						0.32458(17)	0.0427(7) Uani 1 1 d . .
_atom_site_U_iso_or_equiv							.
_atom_site_adp_type		H5A	H	0.3619	0.2484	0.3812	0.064
_atom_site_occupancy							Uiso 1 1 calc R . .
_atom_site_symmetry_multiplicity		H5B	H	0.3032	0.3048	0.3304	0.064
_atom_site_calc_flag							Uiso 1 1 calc R . .
_atom_site_refinement_flags		H5C	H	0.3696	0.3304	0.3097	0.064
_atom_site_disorder_assembly							Uiso 1 1 calc R . .
_atom_site_disorder_group		C6	C	0.41375(11)	0.1626(2)	0.2193(2)	
U1	U					0.0505(8)	Uani 1 1 d . . .
		H6A	H	0.4349	0.2240	0.2156	0.076
							Uiso 1 1 calc R . .
		H6B	H	0.4136	0.1259	0.1640	0.076
							Uiso 1 1 calc R . .
C1	C	H6C	H	0.4348	0.1253	0.2702	0.076
							Uiso 1 1 calc R . .
		C7	C	0.19091(14)	-0.1592(2)		
						0.44257(19)	0.0499(7) Uani 1 1 d . .
							.
H1A	H	H7A	H	0.2288	-0.1590	0.4877	0.060
							Uiso 1 1 calc R . .
H1B	H	H7B	H	0.1568	-0.1784	0.4729	0.060
							Uiso 1 1 calc R . .
C2	C	C8	C	0.19729(15)	-0.2337(2)	0.3687(2)	
						0.0532(8)	Uani 1 1 d . . .
		H8A	H	0.1583	-0.2379	0.3263	0.064
							Uiso 1 1 calc R . .
H2A	H	H8B	H	0.2060	-0.2980	0.3962	0.064
							Uiso 1 1 calc R . .
H2B	H	C9	C	0.09263(12)	-0.0325(2)	0.3571(2)	
						0.0512(8)	Uani 1 1 d . . .
C3	C						
H3A	H						

H9A	H	0.0718	-0.0492	0.4069	0.077				
		Uiso 1 1 calc R . .							
H9B	H	0.0817	-0.0794	0.3086	0.077				
		Uiso 1 1 calc R . .							
H9C	H	0.0802	0.0322	0.3352	0.077				
		Uiso 1 1 calc R . .							
C10	C	0.18488(14)		0.0410(2)					
		0.49813(18) 0.0539(8) Uani 1 1 d . .							
		.							
H10A	H	0.1691	0.1058	0.4823	0.081				
		Uiso 1 1 calc R . .							
H10B	H	0.2281	0.0451	0.5252	0.081				
		Uiso 1 1 calc R . .							
H10C	H	0.1618	0.0120	0.5409	0.081				
		Uiso 1 1 calc R . .							
C11	C	0.25066(12)	-0.2901(2)	0.2148(2)					
		0.0499(7) Uani 1 1 d . . .							
H11A	H	0.2836	-0.2828	0.1799	0.075				
		Uiso 1 1 calc R . .							
H11B	H	0.2112	-0.2803	0.1758	0.075				
		Uiso 1 1 calc R . .							
H11C	H	0.2521	-0.3550	0.2406	0.075				
		Uiso 1 1 calc R . .							
C12	C	0.33083(15)	-0.2421(2)	0.3783(2)					
		0.0705(10) Uani 1 1 d . . .							
H12A	H	0.3268	-0.3109	0.3912	0.106				
		Uiso 1 1 calc R . .							
H12B	H	0.3374	-0.2056	0.4344	0.106				
		Uiso 1 1 calc R . .							
H12C	H	0.3656	-0.2326	0.3474	0.106				
		Uiso 1 1 calc R . .							
C13	C	0.32419(11)		0.01481(18)					
		0.40321(16) 0.0358(6) Uani 1 1 d . .							
		.							
C14	C	0.35603(11)		0.01336(17)					
		0.47876(16) 0.0320(5) Uani 1 1 d . .							
		.							
C15	C	0.39178(10)		0.01324(16)					
		0.56989(15) 0.0288(5) Uani 1 1 d . .							
		.							
C16	C	0.45300(12)		0.0487(2)					
		0.58679(18) 0.0407(6) Uani 1 1 d . .							
		.							
H16	H	0.4716	0.0695	0.5382	0.049	Uiso			
		1 1 calc R . .							
		.							
C17	C	0.48617(13)	0.0533(2)	0.6746(2)					
		0.0522(8) Uani 1 1 d . . .							
H17	H	0.5266	0.0780	0.6847	0.063	Uiso			
		1 1 calc R . .							
C18	C	0.45994(15)	0.0218(2)	0.7466(2)					
		0.0553(9) Uani 1 1 d . . .							
H18	H	0.4822	0.0258	0.8057	0.066	Uiso			
		1 1 calc R . .							
C19	C	0.40027(14)		-0.0161(2)					
		0.73112(18) 0.0461(7) Uani 1 1 d . .							
		.							
H19	H	0.3827	-0.0389	0.7799	0.055	Uiso			
		1 1 calc R . .							
C20	C	0.36651(11)		-0.02046(18)					
		0.64361(16) 0.0343(6) Uani 1 1 d . .							
		.							
H20	H	0.3264	-0.0463	0.6341	0.041	Uiso			
		1 1 calc R . .							
C21	C	0.33073(11)		-0.05881(19)					
		0.17202(17) 0.0347(6) Uani 1 1 d . .							
		.							
C22	C	0.36884(11)		-0.09513(18)					
		0.13227(16) 0.0334(6) Uani 1 1 d . .							
		.							
C23	C	0.41481(10)		-0.13840(18)					
		0.08462(16) 0.0303(5) Uani 1 1 d . .							
		.							
C24	C	0.43416(11)		-0.08891(18)					
		0.01217(16) 0.0345(6) Uani 1 1 d . .							
		.							
H24	H	0.4172	-0.0278	-0.0061	0.041	Uiso			
		1 1 calc R . .							
C25	C	0.47861(12)		-0.1305(2)					
		0.03283(18) 0.0412(6) Uani 1 1 d . .							
		.							
H25	H	0.4914	-0.0969	-0.0809	0.049	Uiso			
		1 1 calc R . .							
C26	C	0.50390(12)		-0.2209(2)					
		0.00685(19) 0.0456(7) Uani 1 1 d . .							
		.							
H26	H	0.5335	-0.2487	-0.0373	0.055	Uiso			
		1 1 calc R . .							
C27	C	0.48500(13)		-0.2700(2)					
		0.06461(19) 0.0462(7) Uani 1 1 d . .							
		.							



\_atom\_site\_aniso\_U\_13  
 \_atom\_site\_aniso\_U\_12  
 U1 0.02684(4) 0.02158(4) 0.01778(4)  
     0.00282(4) 0.00405(3) 0.00056(4)  
 C1 0.0614(17) 0.0375(16) 0.0265(13)  
     0.0037(11) 0.0205(12) 0.0026(13)  
 C2 0.0591(16) 0.0286(14) 0.0342(14)  
     0.0033(11) 0.0254(12) -0.0078(12)  
 C3 0.0562(16) 0.0475(18) 0.0260(13)  
     0.0027(12) -0.0036(12) 0.0140(13)  
 C4 0.0678(18) 0.0406(16) 0.0216(11) -  
     0.0067(11) 0.0017(11) 0.0079(14)  
 C5 0.0451(15) 0.0463(17) 0.0408(15) -  
     0.0187(13) 0.0184(12) -0.0127(12)  
 C6 0.0319(13) 0.068(2) 0.0564(18) -  
     0.0216(16) 0.0202(13) -0.0121(13)  
 C7 0.073(2) 0.0406(18) 0.0407(16)  
     0.0135(13) 0.0241(14) -0.0044(14)  
 C8 0.079(2) 0.0285(16) 0.0559(19)  
     0.0129(14) 0.0218(16) -0.0027(14)  
 C9 0.0362(14) 0.066(2) 0.0548(18) -  
     0.0010(16) 0.0182(13) -0.0061(13)  
 C10 0.0644(19) 0.068(2) 0.0350(15) -  
     0.0146(15) 0.0239(14) -0.0064(16)  
 C11 0.0510(17) 0.0311(16) 0.0673(19) -  
     0.0078(14) 0.0091(14) 0.0080(12)  
 C12 0.084(2) 0.0405(19) 0.072(2)  
     0.0039(16) -0.0289(18) 0.0228(17)  
 C13 0.0396(13) 0.0356(15) 0.0311(12)  
     0.0008(11) 0.0028(10) 0.0004(11)  
 C14 0.0361(12) 0.0292(13) 0.0305(12)  
     0.0013(10) 0.0050(10) 0.0007(10)  
 C15 0.0356(11) 0.0206(12) 0.0284(11) -  
     0.0004(9) 0.0002(9) 0.0012(9)  
 C16 0.0403(14) 0.0401(16) 0.0403(15)  
     0.0052(12) 0.0033(11) -0.0041(12)  
 C17 0.0460(16) 0.0489(19) 0.0540(18)  
     0.0066(15) -0.0133(14) -0.0106(13)  
 C18 0.072(2) 0.0457(18) 0.0372(15)  
     0.0066(14) -0.0209(14) -0.0083(15)  
 C19 0.0682(19) 0.0406(17) 0.0272(13)  
     0.0085(12) 0.0017(13) -0.0021(14)  
 C20 0.0411(13) 0.0303(14) 0.0296(12)  
     0.0027(11) 0.0008(10) -0.0016(11)  
 C21 0.0374(13) 0.0348(15) 0.0332(13)  
     0.0002(11) 0.0101(11) 0.0031(11)  
 C22 0.0350(13) 0.0320(14) 0.0319(13) -  
     0.0011(11) 0.0018(10) -0.0019(10)  
 C23 0.0299(12) 0.0324(14) 0.0281(12) -  
     0.0056(10) 0.0040(10) -0.0033(10)  
 C24 0.0393(13) 0.0285(14) 0.0358(14)  
     0.0023(11) 0.0064(11) 0.0004(10)  
 C25 0.0436(14) 0.0429(17) 0.0405(15)  
     0.0049(13) 0.0170(12) -0.0051(12)  
 C26 0.0480(16) 0.0470(19) 0.0454(17)  
     0.0013(13) 0.0180(13) 0.0109(13)  
 C27 0.0605(18) 0.0381(17) 0.0428(16)  
     0.0027(13) 0.0164(14) 0.0170(14)  
 C28 0.0492(15) 0.0358(16) 0.0347(14)  
     0.0034(11) 0.0133(12) 0.0047(12)  
 C29 0.0369(13) 0.0279(14) 0.0258(12)  
     0.0043(10) 0.0099(10) -0.0010(10)  
 C30 0.0325(12) 0.0294(14) 0.0203(11)  
     0.0021(9) 0.0064(9) -0.0031(10)  
 C31 0.0283(11) 0.0279(13) 0.0177(10) -  
     0.0006(9) 0.0010(8) -0.0006(9)  
 C32 0.0335(12) 0.0281(13) 0.0253(12)  
     0.0025(10) 0.0083(9) 0.0007(10)  
 C33 0.0443(14) 0.0271(15) 0.0345(13)  
     0.0066(10) 0.0111(11) 0.0019(11)  
 C34 0.0436(14) 0.0308(15) 0.0371(14)  
     0.0027(11) 0.0096(11) 0.0116(11)  
 C35 0.0319(12) 0.0444(17) 0.0293(13)  
     0.0019(11) 0.0100(10) 0.0068(11)  
 C36 0.0318(12) 0.0338(14) 0.0259(12)  
     0.0039(10) 0.0048(10) -0.0029(10)  
 C37 0.0358(12) 0.0292(14) 0.0286(12)  
     0.0039(10) 0.0060(10) 0.0019(10)  
 C38 0.0341(12) 0.0282(13) 0.0266(12)  
     0.0035(10) 0.0073(10) 0.0050(10)  
 C39 0.0253(11) 0.0287(13) 0.0285(12) -  
     0.0024(10) 0.0067(9) 0.0017(9)  
 C40 0.0500(16) 0.0439(17) 0.0357(14)  
     0.0111(12) -0.0025(12) -0.0114(13)  
 C41 0.0520(17) 0.055(2) 0.0370(15)  
     0.0060(14) -0.0107(13) -0.0111(14)  
 C42 0.0334(13) 0.0479(18) 0.0434(16) -  
     0.0128(13) 0.0028(12) -0.0070(12)  
 C43 0.0401(14) 0.0304(15) 0.0454(16) -  
     0.0065(12) 0.0140(12) -0.0060(11)  
 C44 0.0337(12) 0.0312(14) 0.0299(12)  
     0.0005(10) 0.0080(10) 0.0010(10)

P1 0.0419(3) 0.0269(3) 0.0168(3)  
 0.0003(2) 0.0035(2) 0.0043(3)  
 P2 0.0315(3) 0.0326(4) 0.0284(3) -  
 0.0071(3) 0.0139(3) -0.0067(3)  
 P3 0.0365(3) 0.0320(4) 0.0251(3)  
 0.0001(3) 0.0130(2) -0.0025(3)  
 P4 0.0447(4) 0.0238(4) 0.0399(4)  
 0.0048(3) 0.0069(3) 0.0089(3)

\_geom\_special\_details

;

All esds (except the esd in the dihedral angle between two l.s. planes) are estimated using the full covariance matrix. The cell esds are taken into account individually in the estimation of esds in distances, angles and torsion angles; correlations between esds in cell parameters are only used when they are defined by crystal symmetry. An approximate (isotropic) treatment of cell esds is used for estimating esds involving l.s. planes.

loop\_

\_geom\_bond\_atom\_site\_label\_1  
 \_geom\_bond\_atom\_site\_label\_2  
 \_geom\_bond\_distance  
 \_geom\_bond\_site\_symmetry\_2  
 \_geom\_bond\_publ\_flag

U1 C21 2.457(2) . ?  
 U1 C13 2.475(2) . ?  
 U1 C29 2.477(2) . ?  
 U1 C37 2.479(2) . ?  
 U1 P3 2.9661(6) . ?  
 U1 P4 2.9781(7) . ?  
 U1 P1 2.9797(6) . ?  
 U1 P2 2.9854(6) . ?  
 C1 C2 1.527(3) . ?  
 C1 P1 1.835(3) . ?  
 C2 P2 1.831(2) . ?  
 C3 P1 1.822(2) . ?  
 C4 P1 1.819(2) . ?  
 C5 P2 1.820(2) . ?  
 C6 P2 1.824(2) . ?

C7 C8 1.517(4) . ?  
 C7 P3 1.833(3) . ?  
 C8 P4 1.845(3) . ?  
 C9 P3 1.820(3) . ?  
 C10 P3 1.821(3) . ?  
 C11 P4 1.820(3) . ?  
 C12 P4 1.813(3) . ?  
 C13 C14 1.215(3) . ?  
 C14 C15 1.443(3) . ?  
 C15 C20 1.386(3) . ?  
 C15 C16 1.400(3) . ?  
 C16 C17 1.381(3) . ?  
 C17 C18 1.366(4) . ?  
 C18 C19 1.380(4) . ?  
 C19 C20 1.382(3) . ?  
 C21 C22 1.204(3) . ?  
 C22 C23 1.447(3) . ?  
 C23 C28 1.392(3) . ?  
 C23 C24 1.395(3) . ?  
 C24 C25 1.388(3) . ?  
 C25 C26 1.374(4) . ?  
 C26 C27 1.376(4) . ?  
 C27 C28 1.378(4) . ?  
 C29 C30 1.219(3) . ?  
 C30 C31 1.438(3) . ?  
 C31 C32 1.397(3) . ?  
 C31 C36 1.403(3) . ?  
 C32 C33 1.377(3) . ?  
 C33 C34 1.375(4) . ?  
 C34 C35 1.378(3) . ?  
 C35 C36 1.378(3) . ?  
 C37 C38 1.221(3) . ?  
 C38 C39 1.445(3) . ?  
 C39 C40 1.388(3) . ?  
 C39 C44 1.391(3) . ?  
 C40 C41 1.386(3) . ?  
 C41 C42 1.372(4) . ?  
 C42 C43 1.375(4) . ?  
 C43 C44 1.383(3) . ?

loop\_

\_geom\_angle\_atom\_site\_label\_1  
 \_geom\_angle\_atom\_site\_label\_2  
 \_geom\_angle\_atom\_site\_label\_3  
 \_geom\_angle  
 \_geom\_angle\_site\_symmetry\_1  
 \_geom\_angle\_site\_symmetry\_3

\_geom\_angle\_publ\_flag  
 C21 U1 C13 93.99(8) .. ?  
 C21 U1 C29 144.57(8) .. ?  
 C13 U1 C29 97.81(8) .. ?  
 C21 U1 C37 96.19(8) .. ?  
 C13 U1 C37 143.16(8) .. ?  
 C29 U1 C37 94.07(8) .. ?  
 C21 U1 P3 141.82(6) .. ?  
 C13 U1 P3 73.26(6) .. ?  
 C29 U1 P3 73.59(5) .. ?  
 C37 U1 P3 76.98(6) .. ?  
 C21 U1 P4 74.63(6) .. ?  
 C13 U1 P4 77.44(6) .. ?  
 C29 U1 P4 140.59(5) .. ?  
 C37 U1 P4 71.40(5) .. ?  
 P3 U1 P4 67.554(19) .. ?  
 C21 U1 P1 73.51(6) .. ?  
 C13 U1 P1 144.59(6) .. ?  
 C29 U1 P1 77.65(5) .. ?  
 C37 U1 P1 72.09(5) .. ?  
 P3 U1 P1 135.602(17) .. ?  
 P4 U1 P1 127.693(18) .. ?  
 C21 U1 P2 78.05(6) .. ?  
 C13 U1 P2 77.90(6) .. ?  
 C29 U1 P2 72.04(5) .. ?  
 C37 U1 P2 138.88(5) .. ?  
 P3 U1 P2 130.921(17) .. ?  
 P4 U1 P2 141.450(18) .. ?  
 P1 U1 P2 67.226(17) .. ?  
 C2 C1 P1 111.19(16) .. ?  
 C1 C2 P2 111.31(17) .. ?  
 C8 C7 P3 111.74(18) .. ?  
 C7 C8 P4 111.4(2) .. ?  
 C14 C13 U1 175.8(2) .. ?  
 C13 C14 C15 177.7(3) .. ?  
 C20 C15 C16 117.8(2) .. ?  
 C20 C15 C14 121.3(2) .. ?  
 C16 C15 C14 120.8(2) .. ?  
 C17 C16 C15 120.9(3) .. ?  
 C18 C17 C16 120.4(3) .. ?  
 C17 C18 C19 119.7(2) .. ?  
 C18 C19 C20 120.5(3) .. ?  
 C19 C20 C15 120.7(2) .. ?  
 C22 C21 U1 179.1(2) .. ?  
 C21 C22 C23 179.8(3) .. ?  
 C28 C23 C24 118.5(2) .. ?

C28 C23 C22 121.0(2) .. ?  
 C24 C23 C22 120.6(2) .. ?  
 C25 C24 C23 120.3(2) .. ?  
 C26 C25 C24 120.5(2) .. ?  
 C25 C26 C27 119.4(3) .. ?  
 C26 C27 C28 120.9(3) .. ?  
 C27 C28 C23 120.4(2) .. ?  
 C30 C29 U1 172.01(19) .. ?  
 C29 C30 C31 177.2(2) .. ?  
 C32 C31 C36 117.8(2) .. ?  
 C32 C31 C30 120.4(2) .. ?  
 C36 C31 C30 121.8(2) .. ?  
 C33 C32 C31 120.8(2) .. ?  
 C34 C33 C32 120.7(2) .. ?  
 C33 C34 C35 119.6(2) .. ?  
 C34 C35 C36 120.5(2) .. ?  
 C35 C36 C31 120.7(2) .. ?  
 C38 C37 U1 173.2(2) .. ?  
 C37 C38 C39 177.6(2) .. ?  
 C40 C39 C44 117.7(2) .. ?  
 C40 C39 C38 121.5(2) .. ?  
 C44 C39 C38 120.8(2) .. ?  
 C41 C40 C39 121.0(2) .. ?  
 C42 C41 C40 120.2(2) .. ?  
 C41 C42 C43 119.9(2) .. ?  
 C42 C43 C44 119.9(2) .. ?  
 C43 C44 C39 121.3(2) .. ?  
 C4 P1 C3 102.78(12) .. ?  
 C4 P1 C1 102.75(12) .. ?  
 C3 P1 C1 102.52(13) .. ?  
 C4 P1 U1 118.00(9) .. ?  
 C3 P1 U1 115.83(9) .. ?  
 C1 P1 U1 112.98(8) .. ?  
 C5 P2 C6 102.79(12) .. ?  
 C5 P2 C2 103.15(12) .. ?  
 C6 P2 C2 101.99(13) .. ?  
 C5 P2 U1 117.58(9) .. ?  
 C6 P2 U1 117.80(10) .. ?  
 C2 P2 U1 111.44(8) .. ?  
 C9 P3 C10 101.86(14) .. ?  
 C9 P3 C7 103.46(14) .. ?  
 C10 P3 C7 102.56(14) .. ?  
 C9 P3 U1 115.30(10) .. ?  
 C10 P3 U1 118.74(10) .. ?  
 C7 P3 U1 112.94(9) .. ?  
 C12 P4 C11 101.61(14) .. ?

C12 P4 C8 104.43(15) . . ?	_diffn_reflns_theta_full	33.19
C11 P4 C8 101.81(14) . . ?	_diffn_measured_fraction_theta_full	
C12 P4 U1 117.74(11) . . ?		0.997
C11 P4 U1 117.93(10) . . ?	_refine_diff_density_max	1.722
C8 P4 U1 111.31(9) . . ?	_refine_diff_density_min	-1.084
	_refine_diff_density_rms	0.109
_diffn_measured_fraction_theta_max		
0.997		
data_msn191 (4.2)	'U' 'U' -9.6767 9.6646	
	'International Tables Vol C Tables	
	4.2.6.8 and 6.1.1.4'	
_audit_creation_method		
SHELXL-97		
_chemical_name_systematic	_symmetry_cell_setting	Triclinic
;	_symmetry_space_group_name_H-M	
?	'P -1'	
;		
_chemical_name_common	?	loop_
_chemical_melting_point	?	_symmetry_equiv_pos_as_xyz
_chemical_formula_moiety	'C56	'x, y, z'
H57 Li O P4 U'		'-x, -y, -z'
_chemical_formula_sum		
'C56 H67 Li O P4 U'	_cell_length_a	11.5046(3)
_chemical_formula_weight	_cell_length_b	13.8617(3)
1124.95	_cell_length_c	20.6359(5)
	_cell_angle_alpha	70.4070(10)
loop_	_cell_angle_beta	86.0740(10)
_atom_type_symbol	_cell_angle_gamma	
_atom_type_description	69.1600(10)	
_atom_type_scatter_dispersion_real	_cell_volume	2892.67(12)
_atom_type_scatter_dispersion_imag	_cell_formula_units_Z	2
_atom_type_scatter_source	_cell_measurement_temperature	
'C' 'C' 0.0033 0.0016	120(2)	
'International Tables Vol C Tables	_cell_measurement_reflns_used	9947
4.2.6.8 and 6.1.1.4'	_cell_measurement_theta_min	2.75
'H' 'H' 0.0000 0.0000	_cell_measurement_theta_max	29.60
'International Tables Vol C Tables		
4.2.6.8 and 6.1.1.4'	_exptl_crystal_description	block
'Li' 'Li' -0.0003 0.0001	_exptl_crystal_colour	purple
'International Tables Vol C Tables	_exptl_crystal_size_max	0.26
4.2.6.8 and 6.1.1.4'	_exptl_crystal_size_mid	0.26
'O' 'O' 0.0106 0.0060	_exptl_crystal_size_min	0.13
'International Tables Vol C Tables	_exptl_crystal_density_meas	'not
4.2.6.8 and 6.1.1.4'	measured'	
'P' 'P' 0.1023 0.0942	_exptl_crystal_density_diffn	1.292
'International Tables Vol C Tables	_exptl_crystal_density_method	'not
4.2.6.8 and 6.1.1.4'	measured'	

```

_exptl_crystal_F_000          1132
_exptl_absorpt_coefficient_mu  2.950
_exptl_absorpt_correction_type
    numerical
_exptl_absorpt_correction_T_min
    0.5098
_exptl_absorpt_correction_T_max
    0.7076
_exptl_absorpt_process_details
    'SCALE (Bruker, 2009)'

_exptl_special_details
;
?
;

_diffrn_ambient_temperature    120(2)
_diffrn_radiation_wavelength
    0.71073
_diffrn_radiation_type          MoK\alpha
_diffrn_radiation_source        'fine-
    focus sealed tube'
_diffrn_radiation_monochromator
    graphite
_diffrn_measurement_device_type
    'Bruker APEX-II CCD'
_diffrn_measurement_method      '\f
    and \w scans'
_diffrn_detector_area_resol_mean ?
_diffrn_reflns_number           64014
_diffrn_reflns_av_R_equivalents
    0.0350
_diffrn_reflns_av_sigmaI/netI   0.0411
_diffrn_reflns_limit_h_min      -12
_diffrn_reflns_limit_h_max      15
_diffrn_reflns_limit_k_min      -17
_diffrn_reflns_limit_k_max      18
_diffrn_reflns_limit_l_min      -27
_diffrn_reflns_limit_l_max      27
_diffrn_reflns_theta_min        1.90
_diffrn_reflns_theta_max        28.28
_reflns_number_total            14168
_reflns_number_gt               11489
_reflns_threshold_expression
    >2sigma(I)

_computing_data_collection      'Bruker
    APEX2 (Bruker, 2009)'
_computing_cell_refinement
    'Bruker APEX2 (Bruker, 2009)'
_computing_data_reduction       'Bruker
    APEX2 (Bruker, 2009)'
_computing_structure_solution
    'SHELXTL (Sheldrick, 2008)'
_computing_structure_refinement
    'SHELXLL (Sheldrick, 2008)'
_computing_molecular_graphics
    'SHELXTL (Sheldrick, 2008)'
_computing_publication_material
    'SHELXTL (Sheldrick, 2008)'

_refine_special_details
;
Refinement of F^2 against ALL
reflections. The weighted R-factor
wR and
goodness of fit S are based on F^2,
conventional R-factors R are based
on F, with F set to zero for negative
F^2. The threshold expression of
F^2 > 2sigma(F^2) is used only for
calculating R-factors(gt) etc. and is
not relevant to the choice of reflections
for refinement. R-factors based
on F^2 are statistically about twice as
large as those based on F, and R-
factors based on ALL data will be even
larger.
;

_refine_ls_structure_factor_coef Fsqd
_refine_ls_matrix_type          full
_refine_ls_weighting_scheme      calc
_refine_ls_weighting_details
    'calc
    w=1/[s^2*(Fo^2)+(0.0620P)^2+1.
    4862P] where P=(Fo^2+2Fc^2)/3'
_atom_sites_solution_primary     direct
_atom_sites_solution_secondary
    difmap
_atom_sites_solution_hydrogens    geom
_refine_ls_hydrogen_treatment    constr

```

_refine_ls_extinction_method	none	H25A	H	1.5300	0.3604	0.8755	0.063
_refine_ls_extinction_coef	?						Uiso 1 1 calc R . .
_refine_ls_number_reflns	14168	C26	C	1.5231(4)	0.3496(4)	0.7803(3)	
_refine_ls_number_parameters	603						0.0577(14) Uani 1 1 d . . .
_refine_ls_number_restraints	38	H26A	H	1.6024	0.2976	0.7831	0.069
_refine_ls_R_factor_all	0.0564						Uiso 1 1 calc R A .
_refine_ls_R_factor_gt	0.0417	C27	C	1.4470(5)	0.3913(6)	0.7221(4)	
_refine_ls_wR_factor_ref	0.1136						0.0725(18) Uani 1 1 d . A .
_refine_ls_wR_factor_gt	0.1078	H27A	H	1.4757	0.3688	0.6845	0.087
_refine_ls_goodness_of_fit_ref	1.118						Uiso 1 1 calc R . .
_refine_ls_restrained_S_all	1.124	C28	C	1.3289(5)	0.4660(5)	0.7181(3)	
_refine_ls_shift/su_max	0.002						0.0688(17) Uani 1 1 d . . .
_refine_ls_shift/su_mean	0.000	H28A	H	1.2788	0.4923	0.6780	0.083
							Uiso 1 1 calc R A .
loop_		C29	C	0.8649(4)	0.8660(4)	0.8048(2)	
_atom_site_label							0.0382(10) Uani 1 1 d . A .
_atom_site_type_symbol		C30	C	0.8642(5)	0.9290(4)	0.8334(3)	
_atom_site_fract_x							0.0522(12) Uani 1 1 d . . .
_atom_site_fract_y		C37	C	0.7916(4)	0.6433(4)	0.8484(2)	
_atom_site_fract_z							0.0409(10) Uani 1 1 d . A .
_atom_site_U_iso_or_equiv		C38	C	0.7798(4)	0.5732(4)	0.9005(2)	
_atom_site_adp_type							0.0411(10) Uani 1 1 d . . .
_atom_site_occupancy		C39	C	0.7707(4)	0.4862(4)	0.9606(2)	
_atom_site_symmetry_multiplicity							0.0418(10) Uani 1 1 d . A .
_atom_site_calc_flag		C40	C	0.6690(8)	0.4536(7)	0.9673(4)	
_atom_site_refinement_flags							0.115(3) Uani 1 1 d . . .
_atom_site_disorder_assembly		H40A	H	0.6057	0.4875	0.9327	0.138
_atom_site_disorder_group							Uiso 1 1 calc R A .
U1	U	C41	C	0.6616(10)	0.3707(9)	1.0255(5)	
							0.147(5) Uani 1 1 d . A .
		H41A	H	0.5912	0.3513	1.0305	0.177
							Uiso 1 1 calc R . .
C13	C	C42	C	0.7553(7)	0.3164(6)	1.0759(4)	
							0.083(2) Uani 1 1 d . . .
C21	C	H42A	H	0.7508	0.2581	1.1136	0.099
							Uiso 1 1 calc R A .
C22	C	C43	C	0.8537(6)	0.3478(4)	1.0706(3)	
							0.0595(14) Uani 1 1 d . A .
C23	C	H43A	H	0.9165	0.3135	1.1055	0.071
							Uiso 1 1 calc R . .
C24	C	C44	C	0.8614(4)	0.4323(4)	1.0125(3)	
							0.0549(13) Uani 1 1 d . . .
H24A	H	H44A	H	0.9310	0.4527	1.0089	0.066
							Uiso 1 1 calc R A .
C25	C	C45	C	0.6192(4)	0.8742(4)	0.7645(2)	
							0.0386(9) Uani 1 1 d . A .

C46 C 0.5252(4) 0.9293(4) 0.7845(2) 0.0377(9) Uani 1 1 d . . .	H2B H 0.6898 0.6063 0.6269 0.069 Uiso 0.80(2) 1 calc PR A 1
C47 C 0.4149(4) 0.9952(4) 0.8079(2) 0.0417(10) Uani 1 1 d . A .	C3 C 0.9864(9) 0.5069(11) 0.6590(4) 0.055(3) Uani 0.80(2) 1 d PD A 1
C48 C 0.4036(6) 1.0950(5) 0.8119(4) 0.081(2) Uani 1 1 d . . .	H3A H 1.0042 0.4317 0.6635 0.083 Uiso 0.80(2) 1 calc PR A 1
H48A H 0.4687 1.1213 0.7996 0.097 Uiso 1 1 calc R A .	H3B H 1.0631 0.5194 0.6596 0.083 Uiso 0.80(2) 1 calc PR A 1
C49 C 0.2941(7) 1.1571(5) 0.8343(5) 0.099(3) Uani 1 1 d . A .	H3C H 0.9394 0.5536 0.6163 0.083 Uiso 0.80(2) 1 calc PR A 1
H49A H 0.2865 1.2256 0.8354 0.119 Uiso 1 1 calc R . .	C4 C 0.9873(9) 0.4211(7) 0.8042(5) 0.056(2) Uani 0.80(2) 1 d PD A 1
C50 C 0.2004(5) 1.1204(5) 0.8541(3) 0.079(2) Uani 1 1 d . . .	H4A H 1.0015 0.3538 0.7959 0.084 Uiso 0.80(2) 1 calc PR A 1
H50A H 0.1293 1.1619 0.8701 0.094 Uiso 1 1 calc R A .	H4B H 0.9424 0.4212 0.8451 0.084 Uiso 0.80(2) 1 calc PR A 1
C51 C 0.2098(4) 1.0221(5) 0.8506(3) 0.0592(15) Uani 1 1 d . A .	H4C H 1.0658 0.4278 0.8100 0.084 Uiso 0.80(2) 1 calc PR A 1
H51A H 0.1441 0.9967 0.8637 0.071 Uiso 1 1 calc R . .	C5 C 0.4974(11) 0.8116(9) 0.6284(6) 0.068(3) Uani 0.80(2) 1 d PD A 1
C52 C 0.3154(4) 0.9595(4) 0.8279(2) 0.0449(11) Uani 1 1 d . . .	H5A H 0.4345 0.7828 0.6248 0.102 Uiso 0.80(2) 1 calc PR A 1
H52A H 0.3202 0.8921 0.8260 0.054 Uiso 1 1 calc R A .	H5B H 0.5388 0.8240 0.5860 0.102 Uiso 0.80(2) 1 calc PR A 1
Li1 Li 0.7205(7) 0.8045(7) 0.8676(4) 0.0449(18) Uani 1 1 d . A .	H5C H 0.4595 0.8794 0.6373 0.102 Uiso 0.80(2) 1 calc PR A 1
O1 O 0.6519(3) 0.8075(4) 0.9539(2) 0.0663(11) Uani 1 1 d D . .	C6 C 0.5096(9) 0.6810(9) 0.7696(5) 0.069(3) Uani 0.80(2) 1 d PD A 1
P1 P 0.8961(5) 0.5369(4) 0.7305(3) 0.0467(10) Uani 0.80(2) 1 d PD A 1	H6A H 0.4440 0.6661 0.7532 0.104 Uiso 0.80(2) 1 calc PR A 1
P2 P 0.6111(5) 0.7131(5) 0.6992(3) 0.0451(10) Uani 0.80(2) 1 d PD A 1	H6B H 0.4743 0.7423 0.7857 0.104 Uiso 0.80(2) 1 calc PR A 1
P3 P 1.0229(4) 0.8637(3) 0.6662(2) 0.0356(8) Uani 0.80(2) 1 d PD A 1	H6C H 0.5576 0.6180 0.8068 0.104 Uiso 0.80(2) 1 calc PR A 1
P4 P 0.7249(5) 1.0026(4) 0.6366(2) 0.0371(9) Uani 0.80(2) 1 d PD A 1	C7 C 0.9595(8) 1.0091(6) 0.6133(4) 0.052(2) Uani 0.80(2) 1 d PD A 1
C1 C 0.7634(8) 0.4967(6) 0.7251(6) 0.067(3) Uani 0.80(2) 1 d PD A 1	H7A H 0.9471 1.0534 0.6426 0.062 Uiso 0.80(2) 1 calc PR A 1
H1A H 0.7909 0.4323 0.7110 0.080 Uiso 0.80(2) 1 calc PR A 1	H7B H 1.0193 1.0260 0.5800 0.062 Uiso 0.80(2) 1 calc PR A 1
H1B H 0.7302 0.4777 0.7702 0.080 Uiso 0.80(2) 1 calc PR A 1	C8 C 0.8365(8) 1.0383(6) 0.5753(3) 0.0423(18) Uani 0.80(2) 1 d PD A 1
C2 C 0.6591(9) 0.5902(6) 0.6728(5) 0.058(3) Uani 0.80(2) 1 d PD A 1	H8A H 0.8495 0.9989 0.5429 0.051 Uiso 0.80(2) 1 calc PR A 1
H2A H 0.5884 0.5679 0.6722 0.069 Uiso 0.80(2) 1 calc PR A 1	H8B H 0.8042 1.1161 0.5496 0.051 Uiso 0.80(2) 1 calc PR A 1

C9 C 1.1198(9) 0.8013(7) 0.6069(4)  
0.055(2) Uani 0.80(2) 1 d PD A 1  
H9A H 1.1784 0.8372 0.5889 0.082  
Uiso 0.80(2) 1 calc PR A 1  
H9B H 1.0681 0.8086 0.5697 0.082  
Uiso 0.80(2) 1 calc PR A 1  
H9C H 1.1641 0.7250 0.6310 0.082  
Uiso 0.80(2) 1 calc PR A 1  
C10 C 1.1402(6) 0.8624(7) 0.7218(5)  
0.0471(18) Uani 0.80(2) 1 d PD A 1  
H10A H 1.1947 0.8963 0.6940 0.071  
Uiso 0.80(2) 1 calc PR A 1  
H10B H 1.1877 0.7881 0.7484 0.071  
Uiso 0.80(2) 1 calc PR A 1  
H10C H 1.1000 0.9020 0.7522 0.071  
Uiso 0.80(2) 1 calc PR A 1  
C11 C 0.5890(8) 1.0471(7) 0.5785(5)  
0.060(2) Uani 0.80(2) 1 d PD A 1  
H11A H 0.5673 1.1235 0.5524 0.091  
Uiso 0.80(2) 1 calc PR A 1  
H11B H 0.5201 1.0356 0.6049 0.091  
Uiso 0.80(2) 1 calc PR A 1  
H11C H 0.6080 1.0056 0.5477 0.091  
Uiso 0.80(2) 1 calc PR A 1  
C12 C 0.6788(13) 1.1112(7) 0.6745(5)  
0.062(3) Uani 0.80(2) 1 d PD A 1  
H12A H 0.6489 1.1810 0.6386 0.093  
Uiso 0.80(2) 1 calc PR A 1  
H12B H 0.7493 1.1063 0.6994 0.093  
Uiso 0.80(2) 1 calc PR A 1  
H12C H 0.6139 1.1034 0.7054 0.093  
Uiso 0.80(2) 1 calc PR A 1  
P1A P 0.8758(17) 0.5224(14) 0.7296(9)  
0.033(3) Uani 0.20(2) 1 d PD A 2  
P2A P 0.5935(16) 0.6981(15) 0.7026(9)  
0.030(3) Uani 0.20(2) 1 d PD A 2  
P3A P 1.0012(14) 0.8489(13) 0.6562(9)  
0.037(3) Uani 0.20(2) 1 d PD A 2  
P4A P 0.7016(16) 0.9886(14)  
0.6313(10) 0.034(3) Uani 0.20(2) 1 d  
PD A 2  
C1A C 0.743(2) 0.486(2) 0.7193(15)  
0.030(7) Uiso 0.20(2) 1 d PD A 2  
H1AA H 0.7712 0.4258 0.7009 0.036  
Uiso 0.20(2) 1 calc PR A 2  
H1AB H 0.7125 0.4594 0.7644 0.036  
Uiso 0.20(2) 1 calc PR A 2  
C2A C 0.634(3) 0.581(2) 0.6715(18)  
0.073(18) Uiso 0.20(2) 1 d PD A 2  
H2AA H 0.5632 0.5583 0.6727 0.088  
Uiso 0.20(2) 1 calc PR A 2  
H2AB H 0.6595 0.6005 0.6245 0.088  
Uiso 0.20(2) 1 calc PR A 2  
C3A C 0.978(4) 0.488(5) 0.662(2)  
0.09(3) Uiso 0.20(2) 1 d PD A 2  
H3AA H 0.9895 0.4147 0.6648 0.134  
Uiso 0.20(2) 1 calc PR A 2  
H3AB H 1.0568 0.4930 0.6691 0.134  
Uiso 0.20(2) 1 calc PR A 2  
H3AC H 0.9401 0.5382 0.6180 0.134  
Uiso 0.20(2) 1 calc PR A 2  
C4A C 0.962(3) 0.403(3) 0.8033(15)  
0.044(10) Uiso 0.20(2) 1 d PD A 2  
H4AA H 0.9695 0.3370 0.7951 0.066  
Uiso 0.20(2) 1 calc PR A 2  
H4AB H 0.9187 0.4058 0.8444 0.066  
Uiso 0.20(2) 1 calc PR A 2  
H4AC H 1.0441 0.4040 0.8089 0.066  
Uiso 0.20(2) 1 calc PR A 2  
C5A C 0.475(3) 0.804(2) 0.6377(14)  
0.027(7) Uiso 0.20(2) 1 d PD A 2  
H5AA H 0.4119 0.7767 0.6320 0.040  
Uiso 0.20(2) 1 calc PR A 2  
H5AB H 0.5124 0.8248 0.5947 0.040  
Uiso 0.20(2) 1 calc PR A 2  
H5AC H 0.4377 0.8669 0.6523 0.040  
Uiso 0.20(2) 1 calc PR A 2  
C6A C 0.503(3) 0.657(2) 0.7769(11)  
0.019(6) Uiso 0.20(2) 1 d PD A 2  
H6AA H 0.4363 0.6411 0.7625 0.029  
Uiso 0.20(2) 1 calc PR A 2  
H6AB H 0.4683 0.7162 0.7953 0.029  
Uiso 0.20(2) 1 calc PR A 2  
H6AC H 0.5558 0.5937 0.8117 0.029  
Uiso 0.20(2) 1 calc PR A 2  
C7A C 0.937(3) 0.9950(19) 0.6029(18)  
0.068(16) Uiso 0.20(2) 1 d PD A 2  
H7AA H 0.9293 1.0395 0.6316 0.082  
Uiso 0.20(2) 1 calc PR A 2  
H7AB H 0.9939 1.0109 0.5677 0.082  
Uiso 0.20(2) 1 calc PR A 2

C8A C 0.810(2) 1.026(3) 0.5687(15)  
0.074(18) Uiso 0.20(2) 1 d PD A 2  
H8AA H 0.8192 0.9884 0.5353 0.089  
Uiso 0.20(2) 1 calc PR A 2  
H8AB H 0.7774 1.1038 0.5443 0.089  
Uiso 0.20(2) 1 calc PR A 2  
C9A C 1.087(3) 0.790(2) 0.5928(15)  
0.047(9) Uiso 0.20(2) 1 d PD A 2  
H9AA H 1.1419 0.8284 0.5710 0.071  
Uiso 0.20(2) 1 calc PR A 2  
H9AB H 1.0298 0.7962 0.5587 0.071  
Uiso 0.20(2) 1 calc PR A 2  
H9AC H 1.1355 0.7141 0.6153 0.071  
Uiso 0.20(2) 1 calc PR A 2  
C10A C 1.123(3) 0.850(3) 0.7066(17)  
0.051(11) Uiso 0.20(2) 1 d PD A 2  
H10D H 1.1765 0.8812 0.6763 0.076  
Uiso 0.20(2) 1 calc PR A 2  
H10E H 1.1698 0.7762 0.7343 0.076  
Uiso 0.20(2) 1 calc PR A 2  
H10F H 1.0859 0.8926 0.7358 0.076  
Uiso 0.20(2) 1 calc PR A 2  
C11A C 0.567(2) 1.025(2) 0.5738(13)  
0.036(7) Uiso 0.20(2) 1 d PD A 2  
H11D H 0.5430 1.1010 0.5461 0.054  
Uiso 0.20(2) 1 calc PR A 2  
H11E H 0.4996 1.0123 0.6006 0.054  
Uiso 0.20(2) 1 calc PR A 2  
H11F H 0.5895 0.9810 0.5444 0.054  
Uiso 0.20(2) 1 calc PR A 2  
C12A C 0.650(2) 1.100(2) 0.6666(16)  
0.026(6) Uiso 0.20(2) 1 d PD A 2  
H12D H 0.6112 1.1684 0.6302 0.039  
Uiso 0.20(2) 1 calc PR A 2  
H12E H 0.7197 1.1031 0.6875 0.039  
Uiso 0.20(2) 1 calc PR A 2  
H12F H 0.5903 1.0884 0.7006 0.039  
Uiso 0.20(2) 1 calc PR A 2  
C14 C 0.8454(9) 0.7883(7) 0.5455(5)  
0.0310(19) Uiso 0.461(6) 1 d P A 3  
C15 C 0.8754(7) 0.7898(6) 0.4740(3)  
0.040(2) Uiso 0.461(6) 1 d PG A 3  
C16 C 0.9936(6) 0.7254(6) 0.4628(4)  
0.061(3) Uiso 0.461(6) 1 d PG A 3  
H16A H 1.0509 0.6802 0.4999 0.073  
Uiso 0.461(6) 1 calc PR A 3  
C17 C 1.0262(7) 0.7284(8) 0.3962(5)  
0.096(5) Uiso 0.461(6) 1 d PG A 3  
H17A H 1.1053 0.6853 0.3887 0.115  
Uiso 0.461(6) 1 calc PR A 3  
C18 C 0.9406(10) 0.7958(9) 0.3409(3)  
0.092(5) Uiso 0.461(6) 1 d PG A 3  
H18A H 0.9624 0.7978 0.2963 0.110  
Uiso 0.461(6) 1 calc PR A 3  
C19 C 0.8224(8) 0.8602(8) 0.3521(4)  
0.074(4) Uiso 0.461(6) 1 d PG A 3  
H19A H 0.7651 0.9053 0.3150 0.089  
Uiso 0.461(6) 1 calc PR A 3  
C20 C 0.7898(6) 0.8572(7) 0.4187(4)  
0.061(4) Uiso 0.461(6) 1 d PG A 3  
H20A H 0.7107 0.9003 0.4262 0.073  
Uiso 0.461(6) 1 calc PR A 3  
C14A C 0.7923(9) 0.7784(7) 0.5496(5)  
0.042(2) Uiso 0.539(6) 1 d P A 4  
C15A C 0.7736(6) 0.7824(5) 0.4795(3)  
0.043(2) Uiso 0.539(6) 1 d PG A 4  
C16A C 0.7609(7) 0.6943(5) 0.4667(3)  
0.074(3) Uiso 0.539(6) 1 d PG A 4  
H16B H 0.7609 0.6328 0.5033 0.089  
Uiso 0.539(6) 1 calc PR A 4  
C17A C 0.7483(8) 0.6980(6) 0.3993(4)  
0.091(4) Uiso 0.539(6) 1 d PG A 4  
H17B H 0.7398 0.6391 0.3908 0.109  
Uiso 0.539(6) 1 calc PR A 4  
C18A C 0.7483(8) 0.7900(7) 0.3447(3)  
0.084(4) Uiso 0.539(6) 1 d PG A 4  
H18B H 0.7399 0.7925 0.2996 0.101  
Uiso 0.539(6) 1 calc PR A 4  
C19A C 0.7610(8) 0.8781(6) 0.3574(3)  
0.065(3) Uiso 0.539(6) 1 d PG A 4  
H19B H 0.7610 0.9397 0.3209 0.078  
Uiso 0.539(6) 1 calc PR A 4  
C20A C 0.7736(7) 0.8744(5) 0.4248(3)  
0.049(3) Uiso 0.539(6) 1 d PG A 4  
H20B H 0.7821 0.9334 0.4334 0.059  
Uiso 0.539(6) 1 calc PR A 4  
C31 C 0.8802(8) 0.9925(7) 0.8784(5)  
0.0386(19) Uiso 0.506(5) 1 d P A 5  
C32 C 0.9419(8) 0.9455(8) 0.9442(5)  
0.044(2) Uiso 0.506(5) 1 d P A 5  
H32A H 0.9800 0.8699 0.9632 0.053  
Uiso 0.506(5) 1 calc PR A 5

C33 C 0.9457(9) 1.0122(9) 0.9806(6)  
 0.050(2) Uiso 0.506(5) 1 d P A 5  
 H33A H 0.9838 0.9815 1.0247 0.061  
 Uiso 0.506(5) 1 calc PR A 5  
 C34 C 0.8916(9) 1.1265(9) 0.9504(5)  
 0.051(2) Uiso 0.506(5) 1 d P A 5  
 H34A H 0.8932 1.1724 0.9742 0.061  
 Uiso 0.506(5) 1 calc PR A 5  
 C35 C 0.8383(11) 1.1676(12) 0.8872(6)  
 0.061(3) Uiso 0.506(5) 1 d P A 5  
 H35A H 0.8044 1.2433 0.8667 0.073  
 Uiso 0.506(5) 1 calc PR A 5  
 C36 C 0.8311(9) 1.1024(8) 0.8507(5)  
 0.047(2) Uiso 0.506(5) 1 d P A 5  
 H36A H 0.7922 1.1346 0.8067 0.057  
 Uiso 0.506(5) 1 calc PR A 5  
 C31A C 0.8398(7) 1.0332(5) 0.8432(4)  
 0.043(2) Uiso 0.494(5) 1 d PG A 6  
 C32A C 0.8980(7) 1.1040(6) 0.8037(3)  
 0.058(3) Uiso 0.494(5) 1 d PG A 6  
 H32B H 0.9415 1.0905 0.7661 0.070  
 Uiso 0.494(5) 1 calc PR A 6  
 C33A C 0.8910(8) 1.1951(6) 0.8202(4)  
 0.069(3) Uiso 0.494(5) 1 d PG A 6  
 H33B H 0.9299 1.2425 0.7938 0.083  
 Uiso 0.494(5) 1 calc PR A 6  
 C34A C 0.8259(8) 1.2154(6) 0.8764(4)  
 0.072(4) Uiso 0.494(5) 1 d PG A 6  
 H34B H 0.8212 1.2763 0.8875 0.087  
 Uiso 0.494(5) 1 calc PR A 6  
 C35A C 0.7678(7) 1.1445(7) 0.9160(4)  
 0.076(4) Uiso 0.494(5) 1 d PG A 6  
 H35B H 0.7243 1.1581 0.9535 0.092  
 Uiso 0.494(5) 1 calc PR A 6  
 C36A C 0.7748(7) 1.0534(6) 0.8994(3)  
 0.052(3) Uiso 0.494(5) 1 d PG A 6  
 H36B H 0.7359 1.0060 0.9258 0.062  
 Uiso 0.494(5) 1 calc PR A 6  
 C53 C 0.6014(10) 0.9229(9) 0.9566(6)  
 0.054(3) Uiso 0.454(7) 1 d PD A 7  
 H53A H 0.5990 0.9747 0.9109 0.065  
 Uiso 0.454(7) 1 calc PR A 7  
 H53B H 0.6557 0.9309 0.9868 0.065  
 Uiso 0.454(7) 1 calc PR A 7  
 C54 C 0.4639(11) 0.9486(10) 0.9843(7)  
 0.058(3) Uiso 0.454(7) 1 d P A 7  
 H54A H 0.4330 1.0216 0.9863 0.087  
 Uiso 0.454(7) 1 calc PR A 7  
 H54B H 0.4665 0.8972 1.0296 0.087  
 Uiso 0.454(7) 1 calc PR A 7  
 H54C H 0.4099 0.9424 0.9537 0.087  
 Uiso 0.454(7) 1 calc PR A 7  
 C55 C 0.6774(10) 0.7197(8) 1.0118(5)  
 0.046(3) Uiso 0.454(7) 1 d PD A 7  
 H55A H 0.6611 0.6600 1.0045 0.055  
 Uiso 0.454(7) 1 calc PR A 7  
 H55B H 0.6298 0.7379 1.0495 0.055  
 Uiso 0.454(7) 1 calc PR A 7  
 C56 C 0.8197(11) 0.6909(10) 1.0256(6)  
 0.051(3) Uiso 0.454(7) 1 d P A 7  
 H56A H 0.8497 0.6281 1.0665 0.077  
 Uiso 0.454(7) 1 calc PR A 7  
 H56B H 0.8330 0.7520 1.0318 0.077  
 Uiso 0.454(7) 1 calc PR A 7  
 H56C H 0.8640 0.6751 0.9871 0.077  
 Uiso 0.454(7) 1 calc PR A 7  
 C53A C 0.5515(9) 0.7636(8) 0.9693(5)  
 0.053(2) Uiso 0.546(7) 1 d P A 8  
 H53C H 0.5830 0.6890 1.0010 0.064  
 Uiso 0.546(7) 1 calc PR A 8  
 H53D H 0.5196 0.7627 0.9273 0.064  
 Uiso 0.546(7) 1 calc PR A 8  
 C54A C 0.4481(11) 0.8334(10)  
 1.0010(6) 0.073(3) Uiso 0.546(7) 1 d  
 P A 8  
 H54D H 0.3826 0.8037 1.0115 0.109  
 Uiso 0.546(7) 1 calc PR A 8  
 H54E H 0.4159 0.9068 0.9691 0.109  
 Uiso 0.546(7) 1 calc PR A 8  
 H54F H 0.4800 0.8340 1.0426 0.109  
 Uiso 0.546(7) 1 calc PR A 8  
 C55A C 0.7444(11) 0.7320(9) 1.0237(6)  
 0.060(3) Uiso 0.546(7) 1 d P A 8  
 H55C H 0.7017 0.7433 1.0642 0.072  
 Uiso 0.546(7) 1 calc PR A 8  
 H55D H 0.7698 0.6551 1.0288 0.072  
 Uiso 0.546(7) 1 calc PR A 8  
 C56A C 0.8538(12) 0.7654(11)  
 1.0158(7) 0.078(3) Uiso 0.546(7) 1 d  
 P A 8  
 H56D H 0.9095 0.7233 1.0560 0.117  
 Uiso 0.546(7) 1 calc PR A 8

H56E H 0.8275 0.8418 1.0104 0.117	C41 0.153(8) 0.165(9) 0.111(7) 0.058(7)
Uiso 0.546(7) 1 calc PR A 8	-0.035(6) -0.132(8)
H56F H 0.8958 0.7531 0.9760 0.117	C42 0.105(5) 0.060(4) 0.068(4) 0.013(3)
Uiso 0.546(7) 1 calc PR A 8	0.016(4) -0.045(4)
loop_	C43 0.068(3) 0.033(3) 0.051(3) 0.004(2)
_atom_site_aniso_label	0.005(3) -0.005(2)
_atom_site_aniso_U_11	C44 0.040(2) 0.038(3) 0.062(3) 0.006(2)
_atom_site_aniso_U_22	0.007(2) -0.007(2)
_atom_site_aniso_U_33	C45 0.032(2) 0.039(2) 0.032(2) -
_atom_site_aniso_U_23	0.0064(19) 0.0019(16) -0.0019(18)
_atom_site_aniso_U_13	C46 0.030(2) 0.035(2) 0.035(2) -
_atom_site_aniso_U_12	0.0034(19) -0.0001(17) -0.0043(17)
U1 0.03035(8) 0.03089(10) 0.02298(9) -	C47 0.0265(19) 0.039(3) 0.044(3) -
0.00006(6) 0.00320(5) 0.00405(6)	0.007(2) 0.0067(17) -0.0009(18)
C13 0.062(3) 0.035(3) 0.038(3) -	C48 0.074(4) 0.063(4) 0.125(6) -
0.006(2) -0.006(2) 0.009(2)	0.056(4) 0.067(4) -0.032(3)
C21 0.039(2) 0.043(3) 0.034(2) -	C49 0.106(6) 0.046(4) 0.140(7) -
0.005(2) 0.0073(18) -0.003(2)	0.042(4) 0.077(5) -0.022(4)
C22 0.035(2) 0.040(3) 0.035(2) -	C50 0.051(3) 0.058(4) 0.075(4) 0.000(3)
0.004(2) 0.0032(18) -0.0001(19)	0.033(3) 0.014(3)
C23 0.032(2) 0.030(2) 0.042(2) -	C51 0.031(2) 0.071(4) 0.048(3) 0.001(3)
0.0005(19) 0.0027(18) -0.0008(17)	0.009(2) -0.008(2)
C24 0.042(2) 0.036(3) 0.042(3) -	C52 0.034(2) 0.044(3) 0.042(3) -
0.002(2) 0.002(2) -0.002(2)	0.002(2) 0.0026(18) -0.009(2)
C25 0.040(2) 0.044(3) 0.052(3) -	Li1 0.040(4) 0.052(5) 0.034(4) -0.011(4)
0.001(2) -0.004(2) -0.002(2)	0.010(3) -0.011(4)
C26 0.032(2) 0.039(3) 0.083(4) -	O1 0.055(2) 0.102(3) 0.056(2) -0.043(2)
0.011(3) 0.001(2) 0.001(2)	0.0227(18) -0.031(2)
C27 0.040(3) 0.087(5) 0.076(4) -	P1 0.0368(15) 0.0286(16) 0.0590(17) -
0.042(4) 0.003(3) 0.009(3)	0.0083(13) -0.0100(11) 0.0029(11)
C28 0.037(3) 0.088(4) 0.058(3) -	P2 0.0319(15) 0.0298(16) 0.0599(18) -
0.029(3) -0.011(2) 0.013(3)	0.0054(13) -0.0097(11) -0.0018(12)
C29 0.034(2) 0.037(2) 0.025(2)	P3 0.0331(14) 0.0386(13) 0.0283(11) -
0.0008(18) 0.0075(16) -0.0024(18)	0.0058(8) 0.0060(9) -0.0107(9)
C30 0.048(3) 0.047(3) 0.061(3) -	P4 0.0444(17) 0.0274(13) 0.0226(11) -
0.017(3) 0.024(2) -0.020(2)	0.0006(9) 0.0013(11) -0.0003(11)
C37 0.033(2) 0.036(2) 0.038(2) -	C1 0.051(4) 0.031(4) 0.107(8) -0.015(4)
0.004(2) 0.0060(18) -0.0043(18)	-0.024(4) -0.005(3)
C38 0.039(2) 0.034(2) 0.040(2) -	C2 0.044(4) 0.033(4) 0.086(7) -0.019(4)
0.006(2) 0.0069(18) -0.0075(19)	-0.022(4) 0.002(3)
C39 0.048(2) 0.032(2) 0.040(2) -	C3 0.052(5) 0.036(4) 0.059(6) -0.021(3)
0.005(2) 0.014(2) -0.016(2)	-0.004(3) 0.012(3)
C40 0.133(7) 0.137(7) 0.076(5) 0.034(5)	C4 0.047(4) 0.025(4) 0.070(5) 0.001(3) -
-0.030(5) -0.108(6)	0.013(3) 0.005(3)
	C5 0.051(6) 0.053(5) 0.071(6) 0.005(4) -
	0.029(5) -0.002(4)

C6 0.040(4) 0.052(6) 0.089(7) 0.016(5) - 0.012(4) -0.020(4)	_geom_bond_publ_flag
C7 0.055(4) 0.038(4) 0.046(4) 0.006(3) 0.001(3) -0.016(4)	U1 C21 2.503(4) . ?
C8 0.053(4) 0.032(3) 0.024(3) 0.003(2) 0.007(3) -0.006(3)	U1 C13 2.505(5) . ?
C9 0.056(4) 0.067(5) 0.032(4) -0.011(3) 0.019(3) -0.021(4)	U1 C45 2.535(4) . ?
C10 0.032(3) 0.052(4) 0.052(4) - 0.012(4) -0.001(3) -0.014(3)	U1 C37 2.549(4) . ?
C11 0.055(4) 0.038(4) 0.068(5) 0.005(4) -0.017(4) -0.010(4)	U1 C29 2.556(5) . ?
C12 0.101(8) 0.030(4) 0.034(4) - 0.005(3) 0.010(5) -0.006(4)	U1 P3A 2.794(15) . ?
P1A 0.037(6) 0.020(4) 0.031(5) - 0.004(3) 0.006(4) -0.003(4)	U1 P1 2.960(6) . ?
P2A 0.032(5) 0.028(5) 0.027(4) 0.001(3) -0.003(3) -0.015(3)	U1 P2 2.973(7) . ?
P3A 0.032(4) 0.042(5) 0.036(5) - 0.004(3) -0.003(3) -0.019(3)	U1 P4A 2.983(17) . ?
P4A 0.038(5) 0.036(5) 0.023(4) - 0.004(3) 0.002(3) -0.012(4)	U1 P4 3.053(4) . ?
	U1 P3 3.056(5) . ?
	U1 Li1 3.151(8) . ?
_geom_special_details	C13 C14A 1.231(10) . ?
;	C13 C14 1.247(10) . ?
All esds (except the esd in the dihedral angle between two l.s. planes)	C21 C22 1.215(6) . ?
are estimated using the full covariance matrix. The cell esds are taken	C22 C23 1.443(6) . ?
into account individually in the estimation of esds in distances, angles	C23 C28 1.388(7) . ?
and torsion angles; correlations between esds in cell parameters are only	C23 C24 1.392(7) . ?
used when they are defined by crystal symmetry. An approximate (isotropic)	C24 C25 1.376(6) . ?
treatment of cell esds is used for estimating esds involving l.s. planes.	C25 C26 1.400(8) . ?
;	C26 C27 1.364(8) . ?
	C27 C28 1.372(7) . ?
	C29 C30 1.204(7) . ?
loop_	C29 Li1 2.267(9) . ?
_geom_bond_atom_site_label_1	C30 C31A 1.452(7) . ?
_geom_bond_atom_site_label_2	C30 C31 1.536(10) . ?
_geom_bond_distance	C30 Li1 2.694(9) . ?
_geom_bond_site_symmetry_2	C37 C38 1.222(6) . ?
	C37 Li1 2.252(10) . ?
	C38 C39 1.440(6) . ?
	C39 C44 1.362(7) . ?
	C39 C40 1.380(8) . ?
	C40 C41 1.379(10) . ?
	C41 C42 1.365(11) . ?
	C42 C43 1.335(9) . ?
	C43 C44 1.392(7) . ?
	C45 C46 1.220(6) . ?
	C45 Li1 2.232(9) . ?
	C46 C47 1.437(6) . ?
	C46 Li1 2.599(9) . ?
	C47 C48 1.371(7) . ?
	C47 C52 1.389(6) . ?
	C48 C49 1.399(8) . ?
	C49 C50 1.335(9) . ?
	C50 C51 1.353(9) . ?

C51 C52 1.375(7) . ?  
Li1 O1 1.906(8) . ?  
O1 C55 1.347(10) . ?  
O1 C53A 1.458(10) . ?  
O1 C53 1.514(10) . ?  
O1 C55A 1.645(12) . ?  
P1 C1 1.823(9) . ?  
P1 C3 1.824(7) . ?  
P1 C4 1.836(6) . ?  
P2 C5 1.834(7) . ?  
P2 C6 1.838(8) . ?  
P2 C2 1.848(8) . ?  
P3 C10 1.821(9) . ?  
P3 C9 1.823(7) . ?  
P3 C7 1.836(6) . ?  
P4 C8 1.818(7) . ?  
P4 C12 1.821(7) . ?  
P4 C11 1.827(8) . ?  
C1 C2 1.554(9) . ?  
C7 C8 1.521(12) . ?  
P1A C1A 1.816(18) . ?  
P1A C3A 1.829(18) . ?  
P1A C4A 1.841(17) . ?  
P2A C5A 1.823(16) . ?  
P2A C6A 1.839(16) . ?  
P2A C2A 1.844(17) . ?  
P3A C10A 1.802(18) . ?  
P3A C9A 1.824(17) . ?  
P3A C7A 1.847(17) . ?  
P4A C8A 1.811(18) . ?  
P4A C12A 1.823(16) . ?  
P4A C11A 1.827(17) . ?  
C1A C2A 1.548(18) . ?  
C7A C8A 1.52(2) . ?  
C14 C15 1.486(11) . ?  
C15 C16 1.3900 . ?  
C15 C20 1.3900 . ?  
C16 C17 1.3900 . ?  
C17 C18 1.3900 . ?  
C18 C19 1.3900 . ?  
C19 C20 1.3900 . ?  
C14A C15A 1.457(10) . ?  
C15A C16A 1.3900 . ?  
C15A C20A 1.3900 . ?  
C16A C17A 1.3900 . ?  
C17A C18A 1.3900 . ?

C18A C19A 1.3900 . ?  
C19A C20A 1.3900 . ?  
C31 C36 1.347(13) . ?  
C31 C32 1.408(13) . ?  
C32 C33 1.385(13) . ?  
C33 C34 1.405(15) . ?  
C34 C35 1.329(16) . ?  
C35 C36 1.382(16) . ?  
C31A C32A 1.3900 . ?  
C31A C36A 1.3900 . ?  
C32A C33A 1.3900 . ?  
C33A C34A 1.3900 . ?  
C34A C35A 1.3900 . ?  
C35A C36A 1.3900 . ?  
C53 C54 1.603(16) . ?  
C55 C56 1.563(15) . ?  
C53A C54A 1.509(14) . ?  
C55A C56A 1.470(16) . ?

loop\_

\_geom\_angle\_atom\_site\_label\_1  
\_geom\_angle\_atom\_site\_label\_2  
\_geom\_angle\_atom\_site\_label\_3  
\_geom\_angle  
\_geom\_angle\_site\_symmetry\_1  
\_geom\_angle\_site\_symmetry\_3  
\_geom\_angle\_publ\_flag  
C21 U1 C13 98.76(16) . . ?  
C21 U1 C45 149.46(14) . . ?  
C13 U1 C45 111.77(15) . . ?  
C21 U1 C37 83.35(14) . . ?  
C13 U1 C37 139.18(17) . . ?  
C45 U1 C37 74.22(14) . . ?  
C21 U1 C29 85.38(15) . . ?  
C13 U1 C29 140.05(16) . . ?  
C45 U1 C29 70.95(13) . . ?  
C37 U1 C29 80.73(14) . . ?  
C21 U1 P3A 64.6(3) . . ?  
C13 U1 P3A 68.1(4) . . ?  
C45 U1 P3A 125.8(3) . . ?  
C37 U1 P3A 142.8(4) . . ?  
C29 U1 P3A 78.4(4) . . ?  
C21 U1 P1 63.31(16) . . ?  
C13 U1 P1 74.02(17) . . ?  
C45 U1 P1 125.02(16) . . ?  
C37 U1 P1 70.74(16) . . ?

C29 U1 P1 139.19(15) .. ?  
P3A U1 P1 107.5(3) .. ?  
C21 U1 P2 130.02(15) .. ?  
C13 U1 P2 69.63(18) .. ?  
C45 U1 P2 65.40(14) .. ?  
C37 U1 P2 77.95(15) .. ?  
C29 U1 P2 135.09(14) .. ?  
P3A U1 P2 137.1(4) .. ?  
P1 U1 P2 66.80(16) .. ?  
C21 U1 P4A 133.5(4) .. ?  
C13 U1 P4A 64.5(4) .. ?  
C45 U1 P4A 64.3(4) .. ?  
C37 U1 P4A 138.4(4) .. ?  
C29 U1 P4A 83.9(4) .. ?  
P3A U1 P4A 69.0(4) .. ?  
P1 U1 P4A 136.5(4) .. ?  
P2 U1 P4A 86.6(3) .. ?  
C21 U1 P4 127.77(16) .. ?  
C13 U1 P4 68.89(15) .. ?  
C45 U1 P4 66.45(14) .. ?  
C37 U1 P4 139.34(13) .. ?  
C29 U1 P4 77.24(15) .. ?  
P3A U1 P4 63.8(3) .. ?  
P1 U1 P4 142.43(17) .. ?  
P2 U1 P4 94.28(13) .. ?  
P4A U1 P4 7.9(3) .. ?  
C21 U1 P3 63.25(13) .. ?  
C13 U1 P3 75.59(17) .. ?  
C45 U1 P3 122.72(13) .. ?  
C37 U1 P3 137.11(14) .. ?  
C29 U1 P3 71.02(13) .. ?  
P3A U1 P3 7.6(4) .. ?  
P1 U1 P3 111.82(12) .. ?  
P2 U1 P3 144.14(13) .. ?  
P4A U1 P3 70.5(3) .. ?  
P4 U1 P3 64.53(12) .. ?  
C21 U1 Li1 104.88(18) .. ?  
C13 U1 Li1 156.32(19) .. ?  
C45 U1 Li1 44.62(17) .. ?  
C37 U1 Li1 45.01(19) .. ?  
C29 U1 Li1 45.33(18) .. ?  
P3A U1 Li1 123.8(5) .. ?  
P1 U1 Li1 115.7(2) .. ?  
P2 U1 Li1 93.66(18) .. ?  
P4A U1 Li1 99.0(4) .. ?  
P4 U1 Li1 96.87(18) .. ?

P3 U1 Li1 116.35(18) .. ?  
C14A C13 C14 31.2(5) .. ?  
C14A C13 U1 165.9(6) .. ?  
C14 C13 U1 162.9(6) .. ?  
C22 C21 U1 169.3(4) .. ?  
C21 C22 C23 177.0(5) .. ?  
C28 C23 C24 117.4(4) .. ?  
C28 C23 C22 120.4(4) .. ?  
C24 C23 C22 122.3(4) .. ?  
C25 C24 C23 121.0(5) .. ?  
C24 C25 C26 120.5(5) .. ?  
C27 C26 C25 118.4(5) .. ?  
C26 C27 C28 121.2(6) .. ?  
C27 C28 C23 121.5(5) .. ?  
C30 C29 Li1 97.1(4) .. ?  
C30 C29 U1 168.3(4) .. ?  
Li1 C29 U1 81.4(3) .. ?  
C29 C30 C31A 158.4(6) .. ?  
C29 C30 C31 170.3(6) .. ?  
C31A C30 C31 31.0(4) .. ?  
C29 C30 Li1 56.6(3) .. ?  
C31A C30 Li1 127.4(4) .. ?  
C31 C30 Li1 122.5(4) .. ?  
C38 C37 Li1 108.0(4) .. ?  
C38 C37 U1 170.2(4) .. ?  
Li1 C37 U1 81.8(2) .. ?  
C37 C38 C39 177.0(5) .. ?  
C44 C39 C40 117.4(5) .. ?  
C44 C39 C38 121.9(4) .. ?  
C40 C39 C38 120.6(5) .. ?  
C41 C40 C39 119.8(7) .. ?  
C42 C41 C40 121.5(7) .. ?  
C43 C42 C41 119.4(6) .. ?  
C42 C43 C44 119.5(6) .. ?  
C39 C44 C43 122.3(5) .. ?  
C46 C45 Li1 93.0(4) .. ?  
C46 C45 U1 174.3(4) .. ?  
Li1 C45 U1 82.5(2) .. ?  
C45 C46 C47 179.4(5) .. ?  
C45 C46 Li1 59.0(3) .. ?  
C47 C46 Li1 121.0(3) .. ?  
C48 C47 C52 117.3(4) .. ?  
C48 C47 C46 121.8(4) .. ?  
C52 C47 C46 120.8(4) .. ?  
C47 C48 C49 120.0(5) .. ?  
C50 C49 C48 121.5(6) .. ?

C49 C50 C51 119.4(5) .. ?  
C50 C51 C52 120.7(5) .. ?  
C51 C52 C47 121.1(5) .. ?  
O1 Li1 C45 127.6(4) .. ?  
O1 Li1 C37 118.2(4) .. ?  
C45 Li1 C37 86.3(3) .. ?  
O1 Li1 C29 134.7(5) .. ?  
C45 Li1 C29 82.1(3) .. ?  
C37 Li1 C29 94.1(3) .. ?  
O1 Li1 C46 100.4(3) .. ?  
C45 Li1 C46 27.94(17) .. ?  
C37 Li1 C46 107.0(3) .. ?  
C29 Li1 C46 99.1(3) .. ?  
O1 Li1 C30 109.2(4) .. ?  
C45 Li1 C30 95.2(3) .. ?  
C37 Li1 C30 117.7(3) .. ?  
C29 Li1 C30 26.33(18) .. ?  
C46 Li1 C30 101.3(3) .. ?  
O1 Li1 U1 170.8(4) .. ?  
C45 Li1 U1 52.91(19) .. ?  
C37 Li1 U1 53.21(19) .. ?  
C29 Li1 U1 53.32(19) .. ?  
C46 Li1 U1 80.8(2) .. ?  
C30 Li1 U1 79.2(2) .. ?  
C55 O1 C53A 67.4(6) .. ?  
C55 O1 C53 121.4(7) .. ?  
C53A O1 C53 107.8(6) .. ?  
C55 O1 C55A 33.6(5) .. ?  
C53A O1 C55A 100.4(6) .. ?  
C53 O1 C55A 106.2(6) .. ?  
C55 O1 Li1 124.4(6) .. ?  
C53A O1 Li1 113.0(5) .. ?  
C53 O1 Li1 111.3(6) .. ?  
C55A O1 Li1 117.2(5) .. ?  
C1 P1 C3 102.7(6) .. ?  
C1 P1 C4 100.4(5) .. ?  
C3 P1 C4 101.2(4) .. ?  
C1 P1 U1 114.1(3) .. ?  
C3 P1 U1 115.6(5) .. ?  
C4 P1 U1 120.3(4) .. ?  
C5 P2 C6 101.9(5) .. ?  
C5 P2 C2 100.4(5) .. ?  
C6 P2 C2 102.0(5) .. ?  
C5 P2 U1 119.8(5) .. ?  
C6 P2 U1 117.4(4) .. ?  
C2 P2 U1 112.6(4) .. ?  
C10 P3 C9 101.4(4) .. ?  
C10 P3 C7 101.7(4) .. ?  
C9 P3 C7 102.6(4) .. ?  
C10 P3 U1 119.5(3) .. ?  
C9 P3 U1 114.6(3) .. ?  
C7 P3 U1 114.6(3) .. ?  
C8 P4 C12 102.7(5) .. ?  
C8 P4 C11 100.5(4) .. ?  
C12 P4 C11 100.7(5) .. ?  
C8 P4 U1 112.2(3) .. ?  
C12 P4 U1 119.4(4) .. ?  
C11 P4 U1 118.6(3) .. ?  
C2 C1 P1 111.5(7) .. ?  
C1 C2 P2 108.7(6) .. ?  
C8 C7 P3 112.2(6) .. ?  
C7 C8 P4 109.8(4) .. ?  
C1A P1A C3A 104.0(18) .. ?  
C1A P1A C4A 100.3(12) .. ?  
C3A P1A C4A 97.8(16) .. ?  
C1A P1A U1 118.8(10) .. ?  
C3A P1A U1 113(2) .. ?  
C4A P1A U1 119.7(13) .. ?  
C5A P2A C6A 103.2(13) .. ?  
C5A P2A C2A 102.2(13) .. ?  
C6A P2A C2A 101.3(14) .. ?  
C5A P2A U1 115.4(13) .. ?  
C6A P2A U1 116.9(11) .. ?  
C2A P2A U1 115.6(12) .. ?  
C10A P3A C9A 102.9(14) .. ?  
C10A P3A C7A 100.5(13) .. ?  
C9A P3A C7A 100.5(14) .. ?  
C10A P3A U1 116.2(14) .. ?  
C9A P3A U1 119.1(11) .. ?  
C7A P3A U1 114.8(11) .. ?  
C8A P4A C12A 103.1(14) .. ?  
C8A P4A C11A 100.1(13) .. ?  
C12A P4A C11A 101.0(12) .. ?  
C8A P4A U1 109.6(12) .. ?  
C12A P4A U1 116.8(13) .. ?  
C11A P4A U1 123.4(11) .. ?  
C2A C1A P1A 114.3(18) .. ?  
C1A C2A P2A 107.9(17) .. ?  
C8A C7A P3A 112.4(19) .. ?  
C7A C8A P4A 111.5(19) .. ?  
C13 C14 C15 174.1(9) .. ?  
C16 C15 C20 120.0 .. ?

C16 C15 C14 118.6(6) .. ?  
 C20 C15 C14 121.3(6) .. ?  
 C17 C16 C15 120.0 .. ?  
 C16 C17 C18 120.0 .. ?  
 C19 C18 C17 120.0 .. ?  
 C18 C19 C20 120.0 .. ?  
 C19 C20 C15 120.0 .. ?  
 C13 C14A C15A 173.3(9) .. ?  
 C16A C15A C20A 120.0 .. ?  
 C16A C15A C14A 121.0(5) .. ?  
 C20A C15A C14A 119.0(5) .. ?  
 C17A C16A C15A 120.0 .. ?  
 C16A C17A C18A 120.0 .. ?  
 C19A C18A C17A 120.0 .. ?  
 C18A C19A C20A 120.0 .. ?  
 C19A C20A C15A 120.0 .. ?  
 C36 C31 C32 118.9(8) .. ?  
 C36 C31 C30 115.5(8) .. ?  
 C32 C31 C30 125.6(8) .. ?  
 C33 C32 C31 119.8(9) .. ?  
 C32 C33 C34 119.6(10) .. ?  
 C35 C34 C33 118.6(11) .. ?  
 C34 C35 C36 122.6(12) .. ?  
 C31 C36 C35 120.4(10) .. ?  
 C32A C31A C36A 120.0 .. ?  
 C32A C31A C30 119.9(4) .. ?  
 C36A C31A C30 119.3(5) .. ?  
 C31A C32A C33A 120.0 .. ?  
 C32A C33A C34A 120.0 .. ?  
 C35A C34A C33A 120.0 .. ?  
 C34A C35A C36A 120.0 .. ?  
 C35A C36A C31A 120.0 .. ?  
 O1 C53 C54 110.0(8) .. ?  
 O1 C55 C56 101.5(8) .. ?  
 O1 C53A C54A 109.8(8) .. ?  
 C56A C55A O1 107.4(9) .. ?

\_diffn\_measured\_fraction\_theta\_max  
 0.986  
 \_diffn\_reflns\_theta\_full 28.28  
 \_diffn\_measured\_fraction\_theta\_full  
 0.986  
 \_refine\_diff\_density\_max 1.534  
 \_refine\_diff\_density\_min -2.375  
 \_refine\_diff\_density\_rms 0.162

## 4.8 References

- (1) Figgis, B. N., *Ligand field theory and its applications*. Wiley-VCH: New York, 2000.
- (2) Edwards, P. G.; Andersen, R. A.; Zalkin, A., *J. Am. Chem. Soc.* **1981**, *103*, 7792.
- (3) Sheldrick, G. M. *SADABS*, Bruker AXS: Madison, WI.
- (4) Sheldrick, G. M. *SHELXTL*, Bruker AXS: Madison, WI, 2004.
- (5) AlDamen, M. A.; Clemente-Juan, J. M.; Coronado, E.; Marti-Gastaldo, C.; Gaita-Arino, A., *J. Am. Chem. Soc.* **2008**, *130*, 8874.
- (6) Boaretto, R.; Roussel, P.; Alcock, N. W.; Kingsley, A. J.; Munslow, I. J.; Sanders, C. J.; Scott, P., *J. Organomet. Chem.* **1999**, *591*, 174.
- (7) Newell, B. S.; Rappe, A. K.; Shores, M. P., *Inorg. Chem.* **2010**, *49*, 1595.
- (8) Graves, C. R.; Scott, B. L.; Morris, D. E.; Kiplinger, J. L., *Organometallics* **2008**, *27*, 3335.
- (9) Rinehart, J. D.; Harris, T. D.; Kozimor, S. A.; Bartlett, B. M.; Long, J. R., *Inorg. Chem.* **2009**, *48*, 3382.
- (10) Edwards, P. G.; Andersen, R. A.; Zalkin, A., *Organometallics* **1984**, *3*, 293.
- (11) Edwards, P. G.; Parry, J. S.; Read, P. W., *Organometallics* **1995**, *14*, 3649.
- (12) Spencer, L. P.; Gdula, R. L.; Hayton, T. W.; Scott, B. L.; Boncella, J. M., *Chem. Commun.* **2008**, 4986.
- (13) Numerous attempts to obtain reproducible magnetic susceptibility data on **4.2** was unsuccessful (Figure 4.13). As a result of several failed attempts to obtain publishable elemental analysis data on **4.1**, only a few attempts were made at obtaining reproducible magnetic susceptibility data (Figure 4.14).

- (14) Siddall, T. H., *Theory and Applications of Molecular Paramagnetism*. Boudreaux, E. A.; Mulay, L. N., Eds. John Wiley & Sons: New York, 1976.
- (15) Edelstein, N. M.; Lander, G. H.; Morss, L. R.; Fuger, J., *The Chemistry of the Actinide and Transactinide Elements*. 2006; p 2225.
- (16) Almond, P. M.; Deakin, L.; Porter, M. J.; Mar, A.; Albrecht-Schmitt, T. E., *Chem. Mat.* **2000**, *12*, 3208.
- (17) Kanellakopoulos, B.; Marks, T. J.; Fischer, R. D., *Organometallics of the f-Elements*. In *NATO Advanced Study Institutes Series*, Marks, T. J.; Fischer, R. D., Eds. D. Reidel: Dordrecht, 1978.
- (18) Kiplinger, J. L.; Pool, J. A.; Schelter, E. J.; Thompson, J. D.; Scott, B. L.; Morris, D. E., *Angew. Chem. Int. Ed.* **2006**, *45*, 2036.
- (19) Schelter, E. J.; Morris, D. E.; Scott, B. L.; Thompson, J. D.; Kiplinger, J. L., *Inorg. Chem.* **2007**, *46*, 5528.
- (20) Lai, Y. L.; Chiang, R. K.; Lii, K. H.; Wang, S. L., *Chem. Mat.* **2008**, *20*, 523.
- (21) Salmon, L.; Thuery, P.; Riviere, E.; Miyamoto, S.; Yamato, T.; Ephritikhine, M., *New J. Chem.* **2006**, *30*, 1220.
- (22) Nocton, G.; Burdet, F.; Pecaut, J.; Mazzanti, M., *Angew. Chem. Int. Ed.* **2007**, *46*, 7574.
- (23) Nocton, G.; Pecaut, J.; Mazzanti, M., *Angew. Chem. Int. Ed.* **2008**, *47*, 3040.

**Chapter 5. Evidence for Interesting U-Cl...HC Interactions in the Mixed  
Chelating Ligand Complex [(dmpe)(dmbpy)UCl<sub>4</sub>]**

**5.1 Introduction**

Halogen bonds are considered non-covalent interactions that are similar to hydrogen bonds except that a polarized halogen replaces the hydrogen in the Lewis acid/base pair. A comparison of the geometries of these interactions is presented in Figure 5.1. It is interesting to note the similarities between these types of interactions.<sup>1,2</sup> Hydrogen bond donors (D) consist of electronegative atoms able to polarize D–H bonds, while the halogen bond donors (X = F, Cl, Br, or I) are themselves polarized along the C–X bond. The geometries that define a good interaction are similar between the two.

In the 1950s chemists originally characterized these interactions as charge-transfer bonds. In the 1980s the name was changed to halogen bonds to highlight their similarity to hydrogen bonds.<sup>3,4</sup> Recently, halogen bonds have received more attention with regards to molecular and structure-based drug design.<sup>5</sup> In addition to their role in bonding, halogens play an important chemical role due to their great ability as leaving groups in substitution reactions.<sup>1,2,4</sup> With the advancement of biomolecules, particularly nucleic acids, in the design of nanomechanical devices, understanding and optimizing these interactions are becoming increasingly important.<sup>6</sup> As such, there has been a resurgence of researchers interested in these so-called halogen-bonding interactions.

Upon examination of the crystal structure of [(dmpe)(dmbpy)UCl<sub>4</sub>] (**3.4**), we noticed there was a bending of the dmbpy ligand due to an apparent interaction with a chloride on a neighboring complex. This led us to take a closer look at the structure of **3.1** where we noted interesting U–Cl···H–C interactions. Through several computation methods, we were able to determine that the intermolecular M–Cl···H–C distance dependence on approach angles suggest that Cl is acting more like chlorine and less like chloride. This provides a route to study U–L bonding. Here we present a representative set of X-ray structural results that have been extracted from the Cambridge Crystallographic Data Centre (CCDC) to determine the types of M–Cl···H–C interactions and compare with those of the mixed chelating-ligand U(IV) complex, [(dmpe)(dmbpy)UCl<sub>4</sub>] (**3.4**), presented in Chapter 3.

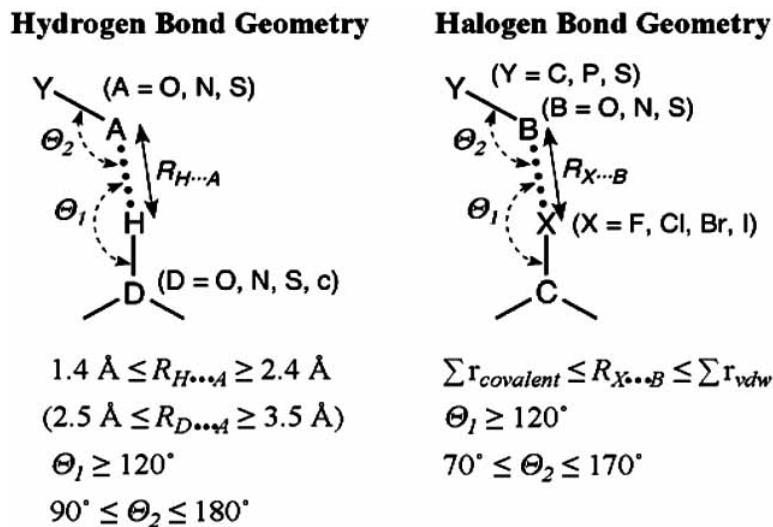


**Figure 5.1.** Comparison of hydrogen bond and halogen bond geometries. Figure taken from reference 7.



## 5.4 Results and Discussion

The structures of **3.1** and **3.4** were originally compared to probe distortions caused by the introduction of the 4,4'-dimethylbipyridine ligand into the coordination sphere of the U(IV) ion. The results of this overlay are presented in Figure 5.3. It can be seen that the chloride ligands in **3.4** are slightly displaced toward dmpe relative to the orientation in **3.1**, perhaps due to steric crowding by the larger dmbpy ligand. This is best seen by comparing the Cl–U–Cl and X–U–X (X = P or N) angles (Table 5.1), where all increase upon replacing dmpe with dmbpy. The effect is strongest for the chlorides in the same plane as dmbpy. Also, a slight curvature of the dmbpy rings is noted, as well as a tilting “down” of the entire dmbpy ligand relative to the plane that bisects the U(dmpe) moiety. This distortion is an apparent result of these halogen bonding interactions which are depicted in plots for **3.1** and **3.4** in Figures 5.4 and 5.5, respectively. The distances and angles of all the halogen-bonding interactions observed for **3.1** and **3.4** are listed in Tables 5.2 and 5.3, respectively. Here it can be seen that approach from 100° affords longer halogen-bonding interactions versus approach from 150°.

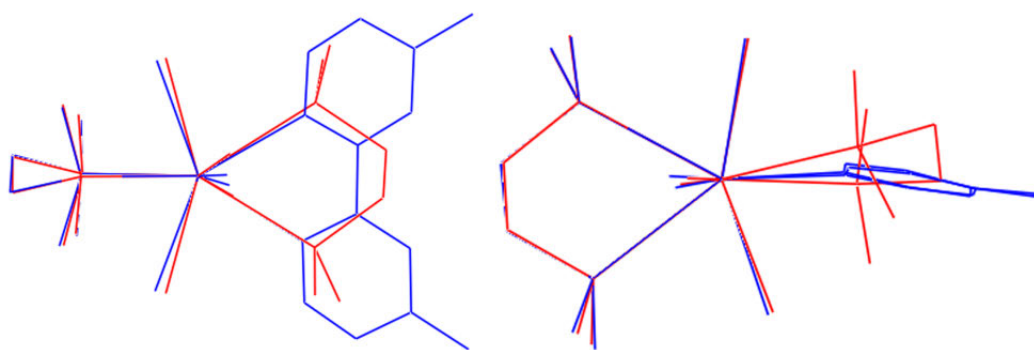


**Figure 5.3.** Overlay of representative U(IV) complexes in compounds **3.1** (red) and **3.4** (blue); two different orientations are show for clarity.

**Table 5.1.** Selected bond distances (Å) and angles (°) for the crystallographically-determined structures [(dmpe)<sub>2</sub>UCl<sub>4</sub>] (**3.1**) and [(dmpe)(dmbpy)UCl<sub>4</sub>] (**3.4**). This data is originally presented in Chapter 3.

	<b>3.1</b> <sup>a</sup>	<b>3.4</b>
U–P	2.9939(14)	3.0074(20)
U–N		2.642(6)
U–Cl	2.6480(13)	2.6457(18)
Cl <sub>cis</sub> –U–Cl <sub>cis</sub>	89.89(5)	95.33(7)
Cl <sub>cis</sub> –U–Cl <sub>trans</sub>	148.54(4)	151.74(6)
P <sub>cis</sub> –U–Y <sub>cis</sub> <sup>b</sup>	66.23(4)	63.98(11)
P <sub>cis</sub> –U–Y <sub>trans</sub> <sup>b</sup>	128.95(5)	135.97(13)

<sup>a</sup> averages from complex containing U1, <sup>b</sup> Y = P or N

**Table 5.2.** Selected bond distances (Å) and angles (°) for the halogen bonds in the crystallographically-determined structure [(dmpe)<sub>2</sub>UCl<sub>4</sub>] (**3.1**).

<b>Atom1</b>	<b>Atom2</b>	<b>Distance (Å)</b>	<b>U–Cl–H Angle (°)</b>
Cl2A	H10A	2.861	164.12

**Table 5.3.** Selected bond distances (Å) and angles (°) for the halogen bonds in the crystallographically-determined structure [(dmpe)(dmbpy)UCl<sub>4</sub>] (**3.4**).

<b>Atom1</b>	<b>Atom2</b>	<b>Distance (Å)</b>	<b>U–Cl–H Angle (°)</b>
Cl2	H8	2.861	108.18
Cl3	H18C	2.833	100.12
Cl4	H4A	2.801	107.98
Cl2	H5C	2.696	154.00
Cl1	H15	2.677	150.17

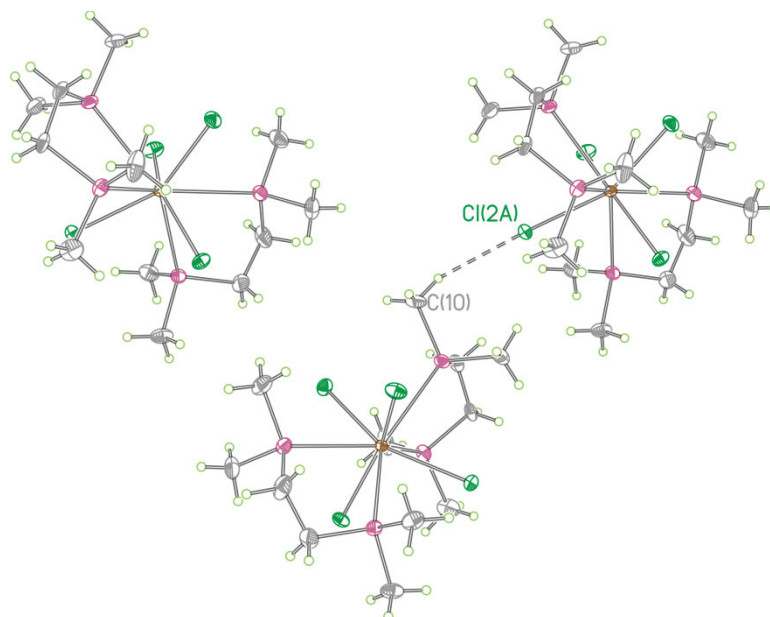


**Figure 5.4.** Plot of the U(IV) phosphine complex in **3.1**, rendered with 20% ellipsoids showing the parallel U–Cl···H–C interactions. Brown, purple, green, and gray ellipsoids represent U, P, Cl, and C atoms, respectively. Several Cl···HC interactions are shown.

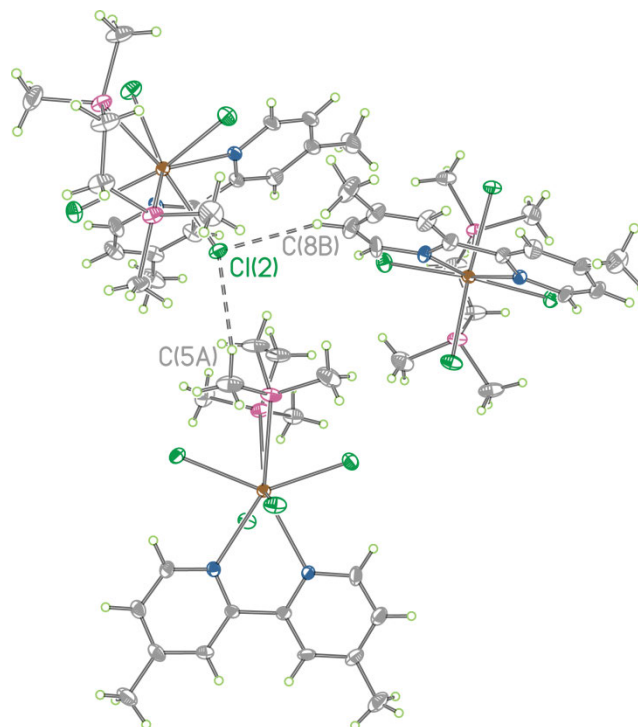


**Figure 5.5.** Plot of the U(IV) phosphine complex in **3.4**, rendered with 40% ellipsoids showing both parallel and perpendicular U–Cl···H–C interactions. Brown, purple, green, blue, and gray ellipsoids represent U, P, Cl, N, and C atoms, respectively.

To ascertain what degree of distortion could be found in X-ray crystal structures reported in the literature, a search using the CCDC was performed. The search criteria involved any M–Cl···HX (X = C, N, or O) interactions between 2–3 Å in the range of 60–180°. The results of these searches are shown in Figure 5.7. Here, it can be seen that both M–Cl···HN and M–Cl···HO interactions are similar to each other but different than the M–Cl···HC interactions. It was determined that the data for M–Cl···HC interactions follows a  $\cos^2$  function as demonstrated in Figure 5.6. The shape profile of an atomic  $p$  orbital follows cosine while the density probability follows a  $\cos^2$  function. This is an intriguing result because it suggests that the angular dependence of the M–Cl···HC distance is modeled by the probability density function of an atomic  $p$  orbital. This suggests that the Cl ligand is acting more like a chlorine and less like a chloride with regards to bonding in these complexes. A representation of this is presented in Figure 5.6 where the sigma hole that is formed by the approaching H–C group is represented with a black arrow. If the Cl was acting more like a chloride than the electron density about the Cl would be such that this sigma hole would not exist. This analysis method has provided an interesting way to study U–L bonding interactions. Others have used spectroscopic techniques including X-ray photoelectron spectroscopy (XPS), polarized X-ray spectroscopy, and time dependent DFT or thermodynamic properties to study U–L bonding interactions.<sup>8-20</sup> It seems that this technique may be an interesting addition as a way to investigate the covalency of U–L bonding interactions.

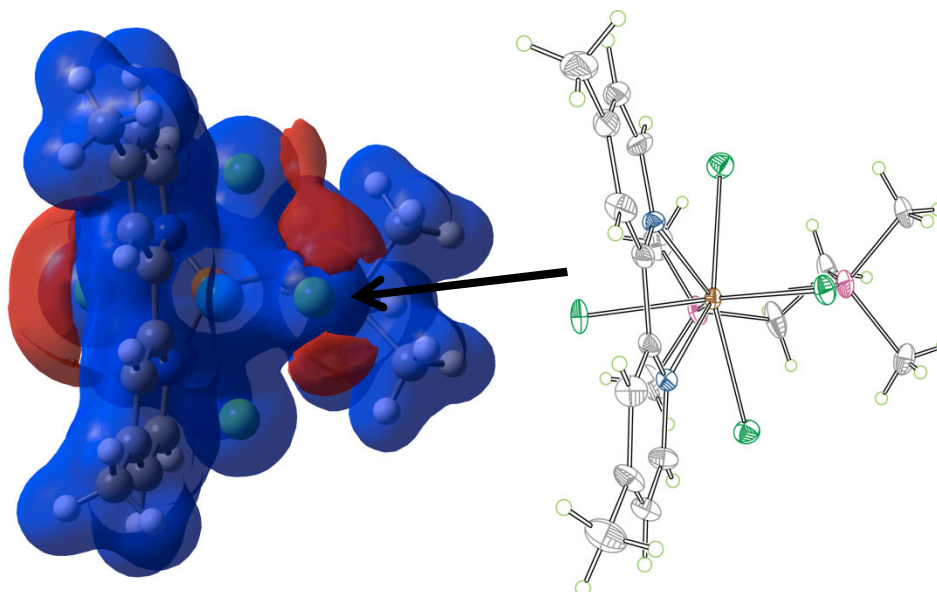


**Figure 5.6.** (Left) Illustration of **3.4** showing a sigma hole (designated with a black arrow) that is formed by the approach of the H–C group. (Right). Plot of the U(IV) phosphine complex in **3.4**, rendered with 40% ellipsoids. Brown, purple, green, blue, and gray ellipsoids represent U, P, Cl, N, and C atoms.

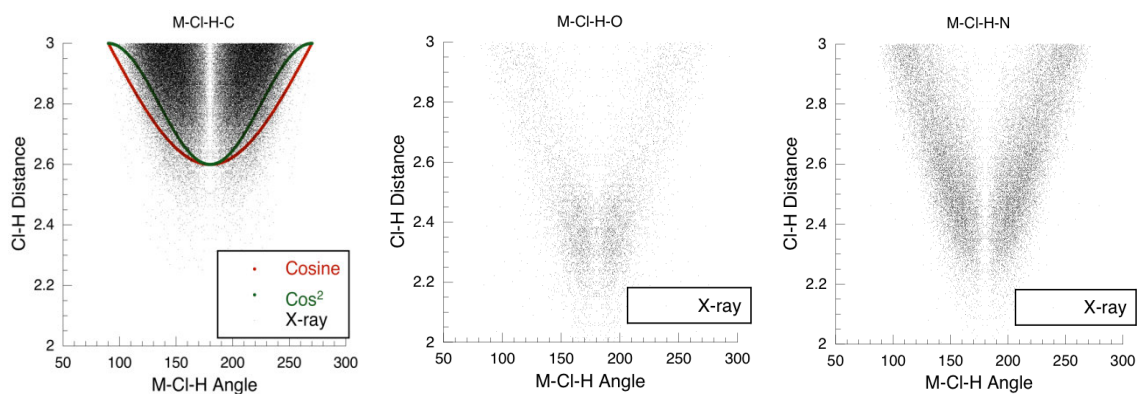


**Figure 5.7.** Results of search through the CCDC showing the M–Cl···HC (49087 structures represented), M–Cl···HO (4585 structures represented) and M–Cl···HN (14291 structures represented) angles versus the M–Cl···HX (X = C, N, or O) distances.

It is interesting to think about how the energetics of these interactions change as a function of M–Cl···HC distance. To model this system, two different approaches were used to look at the interaction energy as a C–H bond in methane approached a chlorine



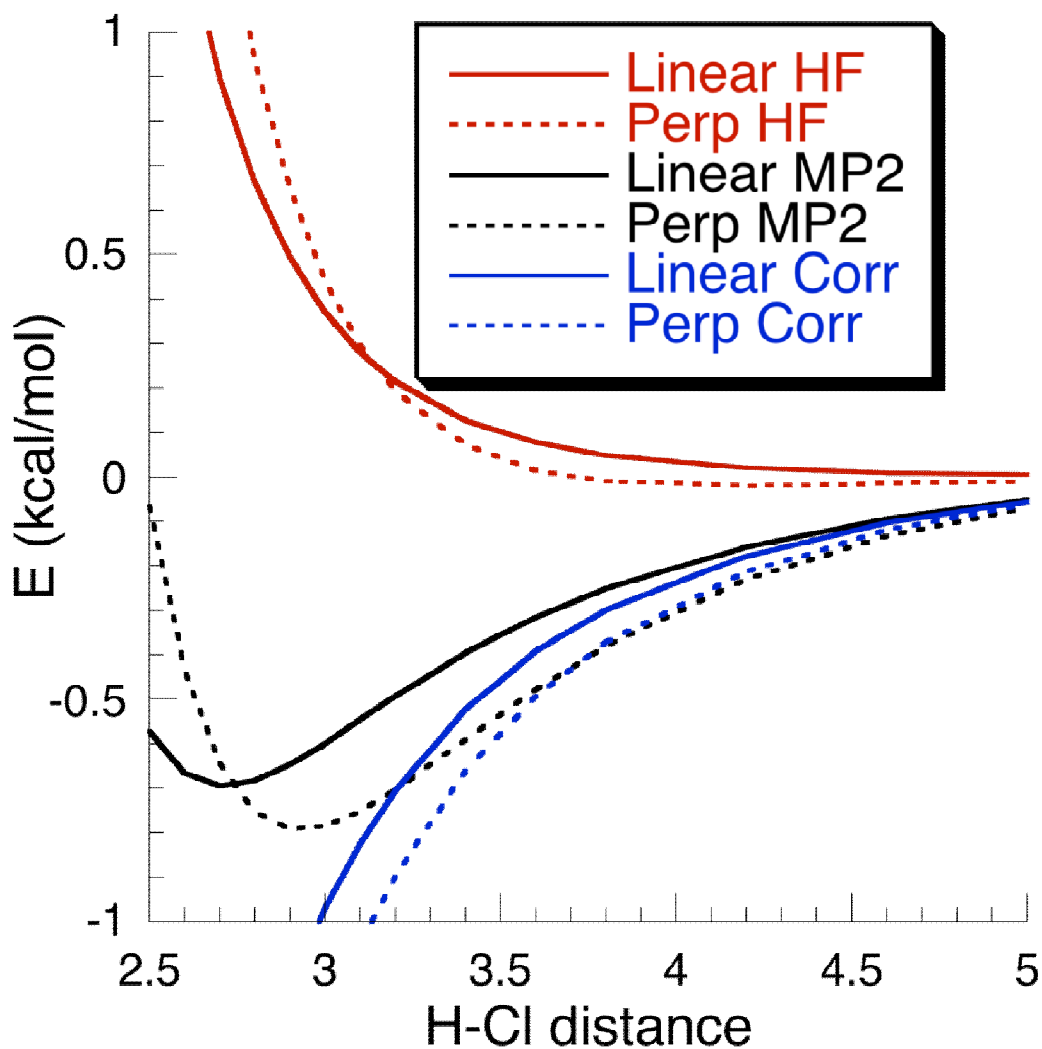


**Figure 5.9.** Results of calculations showing the interaction energy of  $\text{Cl}_2 + \text{CH}_4$  as a co-linear approach of a C–H bond to  $\text{Cl}_2$  and perpendicular approach of a C–H bond to  $\text{Cl}_2$  ( $90^\circ$  Cl–Cl–H angle). The black curves are the binding energy curves, the co-linear approach is shorter than the perpendicular approach (in agreement with the crystal structure of 3.4).

### 5.5 Summary and Outlook

Upon comparison with X-ray crystal structures in the literature, it was found that the distance of  $\text{M–Cl}\cdots\text{H–C}$  interactions versus the Cl–H–C angle follows a  $\cos^2$  dependence. Upon comparison with other chloride interactions, namely  $\text{M–Cl}\cdots\text{H–O}$  and  $\text{M–Cl}\cdots\text{H–N}$ , it is clear that the  $\text{M–Cl}\cdots\text{H–C}$  interactions are unique. The angular dependence of the Cl $\cdots$ H distance suggests that the Cl is acting more like a chlorine and less like a chloride

with regards to bonding in this complex. This seems like an interesting route for the study of U–L bonding interactions and might serve as a way to probe the convalency of uranium-containing, or even more broadly, metal-containing assemblies.

**5.6 Acknowledgments.** This research was supported by Colorado State University.

## 5.7 References

- (1) McDonald, I. K.; Thornton, J. M., *J. Mol. Biol.* **1994**, *238*, 777.
- (2) Auffinger, P.; Hays, F. A.; Westhof, E.; Ho, P. S., *Proc. Natl. Acad. Sci. U. S. A.* **2004**, *101*, 16789.
- (3) Metrangolo, P.; Resnati, G., *Chem. Eur. J.* **2001**, *7*, 2511.
- (4) Metrangolo, P.; Neukirch, H.; Pilati, T.; Resnati, G., *Accounts Chem. Res.* **2005**, *38*, 386.
- (5) Voth, A. R.; Hays, F. A.; Ho, P. S., *Proc. Natl. Acad. Sci. U. S. A.* **2007**, *104*, 6188.
- (6) Seeman, N. C., *Trends Biochem.Sci.* **2005**, *30*, 119.
- (7) Voth, A. R.; Ho, P. S., *Curr. Top. Med. Chem.* **2007**, *7*, 1336.
- (8) Rao, L. F., *Progress in Chemistry* **2011**, *23*, 1295.
- (9) Streitwi, A.; Dempf, D.; Lamar, G. N.; Karraker, D. G.; Edelstein, J., *J. Am. Chem. Soc.* **1971**, *93*, 7343.
- (10) Brennan, J. G.; Green, J. C.; Redfern, C. M., *J. Am. Chem. Soc.* **1989**, *111*, 2373.
- (11) Gulino, A.; Ciliberto, E.; Dibella, S.; Fragala, I.; Seyam, A. M.; Marks, T. J., *Organometallics* **1992**, *11*, 3248.
- (12) Dibella, S.; Gulino, A.; Lanza, G.; Fragala, I. L.; Marks, T. J., *J. Phys. Chem.* **1993**, *97*, 11673.
- (13) Denning, R. G.; Green, J. C.; Hutchings, T. E.; Dallera, C.; Tagliaferri, A.; Giarda, K.; Brookes, N. B.; Braicovich, L., *J. Chem. Phys.* **2002**, *117*, 8008.
- (14) Graves, C. R.; Vaughn, A. E.; Schelter, E. J.; Scott, B. L.; Thompson, J. D.; Morris, D. E.; Kiplinger, J. L., *Inorg. Chem.* **2008**, *47*, 11879.

- (15) Graves, C. R.; Yang, P.; Kozimor, S. A.; Vaughn, A. E.; Clark, D. L.; Conradson, S. D.; Schelter, E. J.; Scott, B. L.; Thompson, J. D.; Hay, P. J.; Morris, D. E.; Kiplinger, J. L., *J. Am. Chem. Soc.* **2008**, *130*, 5272.
- (16) Gaunt, A. J.; Reilly, S. D.; Enriquez, A. E.; Scott, B. L.; Ibers, J. A.; Sekar, P.; Ingram, K. I. M.; Kaltsoyannis, N.; Neu, M. P., *Inorg. Chem.* **2008**, *47*, 29.
- (17) Carlson, C. N.; Palmer, P. D.; Clark, D. L.; Conradson, S. D.; John, K. D.; Schwarz, D. E.; Wilkerson, M. P., *Abstr. Pap. Am. Chem. Soc.* **2006**, 232,
- (18) Petit, L.; Borel, A.; Daul, C.; Maldivi, P.; Adamo, C., *Inorg. Chem.* **2006**, *45*, 7382.
- (19) Schindler, M.; Hawthorne, F. C.; Freund, M. S.; Burns, P. C., *Geochim. Cosmochim. Acta* **2009**, *73*, 2471.
- (20) Kozimor, S. A.; Yang, P.; Batista, E. R.; Boland, K. S.; Burns, C. J.; Clark, D. L.; Conradson, S. D.; Martin, R. L.; Wilkerson, M. P.; Wolfsberg, L. E., *J. Am. Chem. Soc.* **2009**, *131*, 12125.
- (21) Moller, C.; Plesset, M. S., *Phys. Rev.* **1934**, *46*, 0618.
- (22) Schrodinger, E., *Ann. Phys. Berlin* **1926**, *80*, 437.

## Chapter 6. Synthesis and Characterization of a Linear *5f-3d* Arylacetylide-Bridged U<sup>IV</sup>-Fe<sup>II</sup> Complex

### 6.1 Introduction

Understanding the nature of bonding and magnetism in multinuclear *5f-3d* assemblies is a driving force to be able to better understand molecular magnetism of heavy atom systems.<sup>1-8</sup> The promise of stronger exchange coupling between spin centers as a result of the more diffuse *5f* orbitals along with the notion that the larger single-ion anisotropy might act to modulate the magnetic effects of the transition metal creates a desire to study these assemblies in more detail.<sup>3,8-14</sup> In addition, while the magnetic properties of multinuclear *5f-3d* complexes are of interest on a fundamental level, they can also potentially be exploited in producing SMMs.<sup>3,8,13</sup>

There are only a few reported cases of actinide-containing molecules for which the presence of magnetic exchange coupling has been established.<sup>3,8-14</sup> This is due in part to the difficulties in determining ligand field parameters and the complications arising from relativistic effects as well as *d* and *f* electron correlations,<sup>15,16</sup> but also the deficiency of approaches for generating multinuclear *5f-3d* assemblies.<sup>17-22</sup> Therefore, advancement in this area is dependent upon achieving greater synthetic control over paramagnetic uranium ligand field and spin-orbit parameters, so as to optimize exchange coupling between uranium and transition-metal species, and ultimately to control molecular magnetic anisotropy.

Herein, we present a new strategy for synthesizing arylacetylide-bridged *5f-3d* clusters, and provide structural and magnetic characterization for a linear U(IV)–C≡C–Ph–C≡C–Fe(II) species. As seen in Chapter 2, only a minimal amount of coupling was observed through the ethynylbenzene bridging ligands but others have seen that ethynylbenzene ligands have the ability to mediate strong exchange coupling between paramagnetic metal species, namely Fe(III), while enforcing a rigid geometry.<sup>23-25</sup> As a result, we would like to study other compounds containing these ligands as potential bridging options.

## 6.2 Division of Labor Section

All experimental work and characterization for compounds **6.1** and **6.2** was performed by Wesley A. Hoffert with help from Brian S. Newell. All experimental work and characterization for compound **6.3** was performed by Brian S. Newell with help from Trevor C. Schwaab.

## 6.3 Experimental Section

**6.3.1 Preparation of Compounds.** All manipulations were carried out either inside a dinitrogen-filled glove box (MBRAUN Labmaster 130) or via standard Schlenk techniques on a N<sub>2</sub> manifold. Pentane was distilled over sodium metal, degassed (freeze-pump-thawed 3 × 20 min) and stored under an atmosphere of dinitrogen. All other solvents were reagent grade, passed through alumina, degassed and stored under dinitrogen. The compounds 1-ethynyl-4-(triisopropylsilylethynyl)benzene (*i*-Pr<sub>3</sub>SiDEBH),<sup>26</sup> [(dmpe)<sub>2</sub>FeCl<sub>2</sub>],<sup>27</sup> and [(*bit*-NN'<sub>3</sub>)U] (where *bit*-NN'<sub>3</sub> = [N(CH<sub>2</sub>CH<sub>2</sub>NSi<sup>*i*</sup>BuMe<sub>2</sub>)<sub>2</sub>(CH<sub>2</sub>CH<sub>2</sub>Si<sup>*i*</sup>BuMeCH<sub>2</sub>)])<sup>28</sup> were prepared according to the

literature. All other reagents were obtained from commercial vendors and used without further purification.

**Caution!** Depleted uranium (primary isotope  $^{238}\text{U}$ ) is a weak  $\alpha$  emitter (4.197 MeV) with a half-life of  $4.47 \times 10^9$  years; manipulations and reactions should be carried out in monitored fume hoods or in an inert atmosphere glove box in a radiation laboratory equipped with  $\alpha$ - and  $\beta$ -counting equipment.

**[(dmpe)<sub>2</sub>FeCl(*i*Pr<sub>3</sub>SiDEB)] (6.1).** Triethylamine (1 mL, 7 mmol) was added to solution of [(dmpe)<sub>2</sub>FeCl<sub>2</sub>] (0.390 g, 0.915 mmol) and <sup>i</sup>Pr<sub>3</sub>SiDEBH (0.280 g, 0.915 mmol) in methanol (10 mL). The solution immediately turned orange. After 10 minutes, an orange solid precipitated which was isolated by filtration, washed with methanol (2 × 5 mL) then dried under vacuum for 1 h at 293 K to afford 0.400 g of product (0.574 mmol, 63%). IR (ATR):  $\nu_{\text{C}=\text{CSi}}$  2148 cm<sup>-1</sup>,  $\nu_{\text{C}=\text{CFe}}$  2035 cm<sup>-1</sup>. <sup>1</sup>H NMR (293 K, C<sub>6</sub>D<sub>6</sub>):  $\delta$  7.44 (d, 2H, Ar-H), 6.94 (d, 2H, Ar-H), 1.55 (m, 8H, PCH<sub>2</sub>), 1.34 (s, 12H, PCH<sub>3</sub>), 1.27 (s, 12H, PCH<sub>3</sub>), 1.21 ppm (s, 21H, SiC<sub>3</sub>H<sub>7</sub>). Anal. Calcd. for C<sub>31</sub>H<sub>57</sub>P<sub>4</sub>Si<sub>4</sub>Fe: C, 55.32; H, 8.54. Found: C, 55.20; H, 8.59 (notebook reference WH9-145a, Wesley Hoffert).

**[(dmpe)<sub>2</sub>FeCl(*p*-DEBH)] (6.2).** Slightly wet (ca. 5% H<sub>2</sub>O) tetrabutylammonium fluoride (0.51 mL of a 1M THF solution, 0.48 mmol) was added to solution of **1** (0.355 g, 0.509 mmol) in THF (5 mL). After stirring for 3 h at room temperature, the solution was evaporated, and the orange residue was treated with methanol (5 mL). The mixture was placed in a -40 °C freezer for 1 h. The orange solid was isolated by filtration, washed with cold (-40 °C) methanol (2 × 5 mL), then dried under vacuum for 1 h at 293 K to afford 0.202 g of product (0.391 mmol, 76%). IR (ATR):  $\nu_{\text{C}=\text{C}}$  2040, 2021, 2011 cm<sup>-1</sup>. <sup>1</sup>H NMR (293 K, C<sub>6</sub>D<sub>6</sub>):  $\delta$  7.40 (d, 2H, Ar-H), 6.92 (d, 2H, Ar-H), 2.83 (s, 1H, CCH), 1.55

(m, 8H,  $PCH_2$ ), 1.34 (s, 12H,  $PCH_3$ ), 1.27 ppm (s, 12H,  $PCH_3$ ).  $^{13}C$  NMR (293 K,  $CD_2Cl_2$ ):  $\delta$  131.89 (s, 2C,  $C_{Ar-H}$ ), 130.97 (s, 1C, Fe-CC-Ar), 129.65 ( $C_{Ar-H}$ ), 120.23 (s, 1C,  $C_{Ar-C_2H}$ ), 114.85 (s, 1C,  $C_{Ar-C_2Fe}$ ), 84.85 (s, 1C, CCH), 76.92 (s, 1C, CCH), 30.30 (p, 4C,  $PCH_2$ ), 15.59 (m, 4C,  $PCH_3$ ), 13.28 ppm (m, 4C,  $PCH_3$ ). The resonance for the carbon atom ligated to  $Fe^{II}$  was not observed. Absorption spectrum (toluene):  $\lambda_{max}$  ( $\epsilon_M$ ): 405 nm ( $47340 L \cdot mol^{-1} \cdot cm^{-1}$ ). Anal. Calcd. for  $C_{22}H_{37}P_4FeCl$ : C, 51.14; H, 7.22. Found: C, 51.12; H, 6.99 (notebook reference WH9-145b, Wesley Hoffert).

**[(NN')<sub>3</sub>U(*p*-DEB)FeCl(dmpe)<sub>2</sub>] (6.3).** [(*bit*-NN')<sub>3</sub>U] (82 mg, 0.11 mmol) in pentane (2 mL) was added to a stirred slurry of **6.2** (58 mg, 0.11 mmol) in pentane (10 mL). Dichloromethane (2 mL) was added to form an orange solution, which was allowed to stir for 1 h before all volatiles were removed in vacuo to afford a red-brown powder (62% yield based on **6.2**). Single crystals suitable for X-ray analysis were grown from a concentrated pentane solution maintained at  $-35$  °C for 8 h. Absorption spectrum (toluene)  $\lambda_{max}$  ( $\epsilon_M$ ): 467 (691), 404 (855), 282 nm ( $1023 L \cdot mol^{-1} \cdot cm^{-1}$ ).  $^1H$  NMR (293 K,  $C_6D_6$ ):  $\delta$  7.41 (br, 2H, Ar-*H*), 7.34 (br, 2H, Ar-*H*), 7.02 (br, 2H, Ar-*H*), 6.94 (br, 2H, Ar-*H*), 2.83 (br, 6H,  $CH_2$ ), 2.38 (br, 6H,  $CH_2$ ), 1.62 (br, 4H,  $PCH_2$ ), 1.53 (br, 4H,  $PCH_2$ ), 1.36 (br, 12H,  $PCH_3$ ), 1.29 (br, 12H,  $PCH_3$ ) 1.00 (s, 27H, *t*Bu), 0.11 ppm (s 18H,  $CH_2Si$ ). IR (mineral oil):  $\nu_{C\equiv C}$  2046 and 2026  $cm^{-1}$ . Magnetic susceptibility (SQUID, 300 K):  $\mu_{eff} = 2.80 \mu_B$ . Anal. Calcd. for  $C_{46}H_{93}N_4Si_3P_4FeUCl$ : C, 44.57; H, 7.56; N, 4.52. Found: C, 40.88; H, 7.54, N, 4.54. Although single crystals were sent for elemental analysis, the results reveal a deficiency in the observed percent of carbon. However, a small amount of dark gray material remains after combustion, consistent with the production of refractory uranium carbides. Calculations for the determination of elemental analysis results on

compound **6.3** are provided below. Initial values of U and C were chosen based on calculated values of 10 mg sample of **6.3**. Assuming all of the uranium reacted to form UC, the amount of carbon should be 43.47% (this is above the value of 40.88% obtained from EA). Next, the value found from EA was used to determine the amount of UC that may have been formed and this may account for the material seen after combustion.

Using calculated values for **6.3**:

$$\frac{1.920 \text{ mg U}}{10 \text{ mg sample}} \times \frac{1 \text{ mmol U}}{238.03 \text{ mg U}} = 0.00081 \text{ mmol U}$$

$$\frac{4.457 \text{ mg C}}{10 \text{ mg sample}} \times \frac{1 \text{ mmol C}}{12.01 \text{ mg C}} = 0.037 \text{ mmol C}$$

If all U reacts to form UC:

$$0.037 \text{ mmol} - 0.00081 \text{ mmol} = 0.036 \text{ mmol C left}$$

$$0.036 \text{ mmol C} \times \frac{12.01 \text{ mg C}}{1 \text{ mmol C}} \times 100 = 43.47\%$$

Using values obtained from EA:

$$\frac{4.088 \text{ mg C}}{10 \text{ mg sample}} \times \frac{1 \text{ mmol C}}{12.01 \text{ mg C}} = 0.034 \text{ mmol C}$$

$$0.037 \text{ mmol} - 0.034 \text{ mmol} = 0.003 \text{ mmol C reacted to form UC:}$$

$$0.003 \text{ mmol C} \times \frac{1 \text{ mmol UC}}{1 \text{ mmol C}} \times \frac{250.04 \text{ mg UC}}{1 \text{ mmol UC}} = 0.75 \text{ mg UC}$$

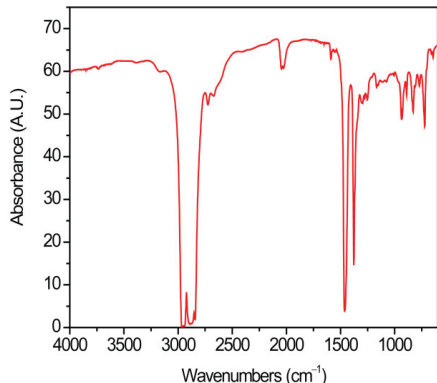


**Figure 6.1.** Full IR spectrum of **6.3** taken as a mineral oil mull. The peaks at  $\sim 3000$ , 1460, and  $1377 \text{ cm}^{-1}$  are due to mineral oil. A minimum of 32 transients were recorded.

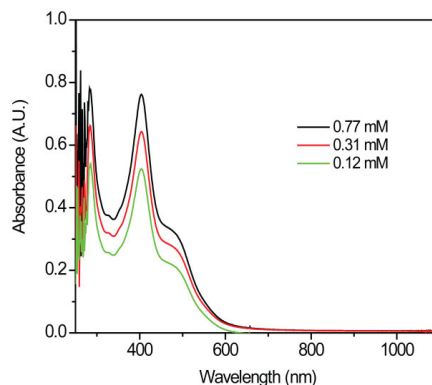


**Figure 6.2.** Electronic absorption spectrum of **6.3**, collected in toluene solution.

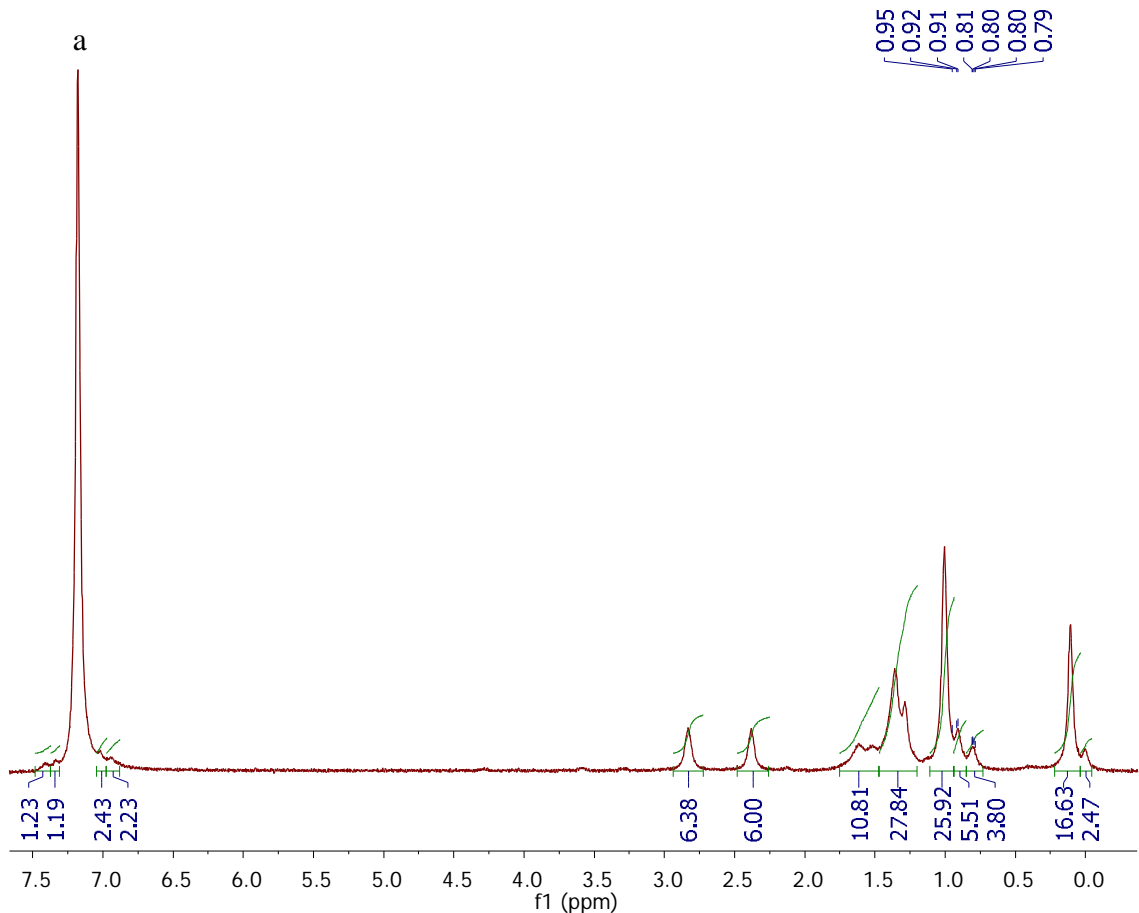


**Figure 6.3.**  $^1\text{H}$  NMR spectrum of  $[(\text{NN}')_3\text{U}(p\text{-DEB})\text{FeCl}(\text{dmpe})_2]$  (**6.3**) obtained in  $\text{C}_6\text{D}_6$  at ambient temperature with a 500 MHz spectrometer. The labeled peak (a) represents residual solvent peaks for  $\text{C}_6\text{D}_6$ , respectively.

**6.3.2 X-ray Structure Determination.** A single crystal structure was determined for compound **6.3**; data are presented in Table 6.1. Single crystals were coated with Paratone-N oil in the glove box and mounted under a cold stream of dinitrogen gas. Single crystal X-ray diffraction data were acquired on a Bruker Kappa APEX II CCD diffractometer with Mo  $K_\alpha$  radiation ( $\lambda = 0.71073 \text{ \AA}$ ) and a graphite monochromator. Initial lattice parameters were obtained from a least-squares analysis of more than 100 reflections; these parameters were later refined against all data. None of the crystals showed significant decay during data collection. Data were integrated and corrected for

Lorentz and polarization effects using Bruker APEX2 software, and semiempirical absorption corrections were applied using SCALE with the aid of numerical face indexing.<sup>29</sup> Space group assignment was based on systematic absences, *E* statistics, and successful refinement of the structure. The structure was solved by the Patterson method and was refined with the aid of successive Fourier difference maps against all data using the SHELXTL 6.14 software package.<sup>30</sup> Thermal parameters for all non-hydrogen atoms were refined anisotropically. All hydrogen atoms were assigned to ideal positions and refined using a riding model with an isotropic thermal parameter 1.2 times that of the attached carbon atom (1.5 times for methyl hydrogens). Selected crystallographic parameters are presented in Table 6.1. Selected bond distances and angles for crystals of compound **6.3** are collected in Table 6.2.

**Table 6.1.** Crystallographic data for compound [(NN')<sub>3</sub>U(*p*-DEB)FeCl(dmpe)<sub>2</sub>] (**6.3**).

	[(NN') <sub>3</sub> U( <i>p</i> -DEB)FeCl(dmpe) <sub>2</sub> ] ( <b>6.3</b> )
formula	C <sub>46</sub> H <sub>93</sub> N <sub>4</sub> Si <sub>3</sub> P <sub>4</sub> FeUCl
formula wt	1239.72
color, habit	orange block
<i>T</i> , K	120(2)
space group	<i>P</i> 21/ <i>c</i>
<i>Z</i>	4
<i>a</i> , Å	16.5308(7)
<i>b</i> , Å	23.7632(10)
<i>c</i> , Å	16.4106(7)
<i>α</i> , deg	90
<i>β</i> , deg	101.130(2)
<i>γ</i> , deg	90
<i>V</i> , Å <sup>3</sup>	6325.2(5)
<i>d</i> <sub>calc</sub> , g/cm <sup>3</sup>	1.30
GOF	1.06
<i>R</i> <sub>1</sub> ( <i>wR</i> <sub>2</sub> ) <sup>b</sup> , %	5.05(13.2)

<sup>a</sup> Obtained with graphite-monochromated Mo K $\alpha$  ( $\lambda = 0.71073$  Å) radiation.

<sup>b</sup>  $R_1 = \sum ||F_o| - |F_c|| / \sum |F_o|$ ,  $wR_2 = \{ \sum [w(F_o^2 - F_c^2)^2] / \sum [w(F_o^2)^2] \}^{1/2}$  for  $F_o > 4\sigma(F_o)$ .

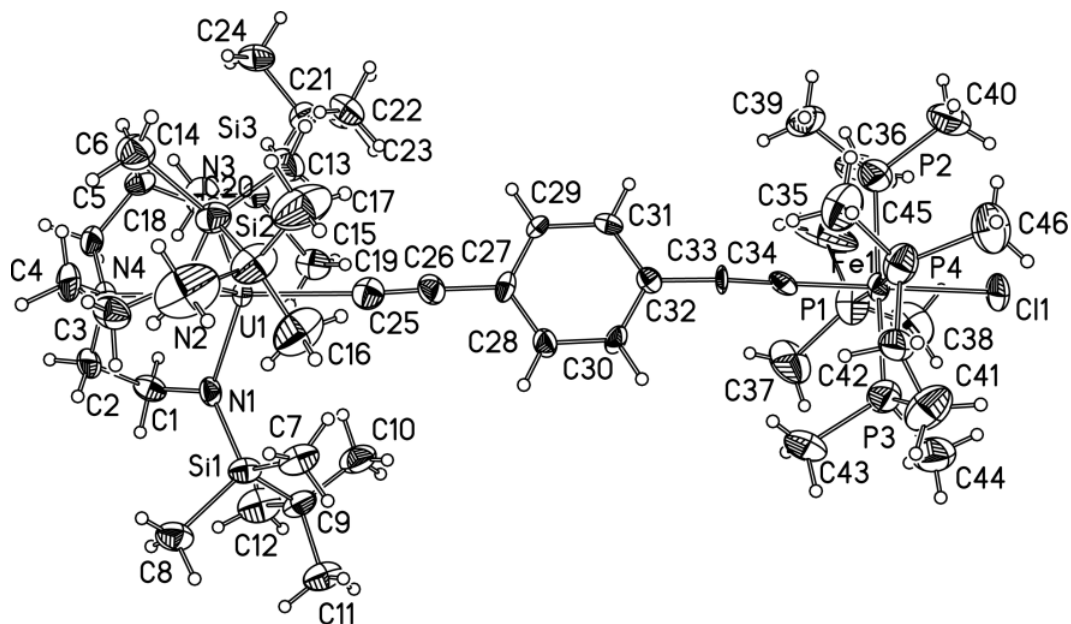


**Figure 6.4.** All the atoms in the crystal structure of **6.3**, rendered with 40% ellipsoids.

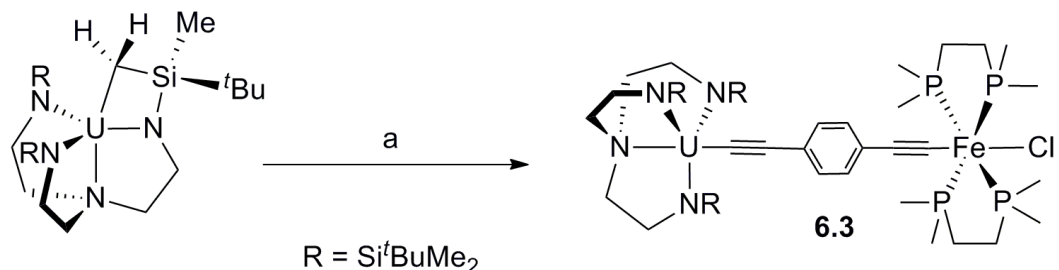
**6.3.3 Magnetic Susceptibility Measurements.** Magnetic susceptibility measurements were collected using a Quantum Design MPMS XL SQUID magnetometer. DC magnetic susceptibility data were collected at temperatures ranging from 2 to 300 K at an applied field of 0.1 T. A powdered microcrystalline sample of **6.3** (14.53 mg, 0.01172 mmol) was loaded into a gelatin capsule in the glove box, inserted into a straw and transported to the SQUID magnetometer under dinitrogen. Contributions to the magnetic susceptibility from the gelatin capsule and the straw were measured independently and subtracted from the total measured signal. Data were corrected for diamagnetic contributions using Pascal's constants.

**6.3.4 Other Physical Measurements.** UV-visible absorption spectra were obtained in dimethyl sulfoxide (toluene for **6.3**) solutions in an airtight glass cell of path length 1 cm on an Agilent 8453 spectrometer.  $^1\text{H}$  NMR spectra were recorded using a Varian INOVA 500 MHz instrument, and the spectra were referenced internally using residual protio solvent resonances relative to tetramethylsilane ( $\delta = 0$  ppm). Infrared spectra were

collected on a Thermo Nicolet 380 FTIR spectrometer as mineral oil mulls pressed between sodium chloride plates. Electrochemical measurements were conducted with a CH Instruments 1232A potentiostat/galvanostat, and the data were processed with CHI software (version 7.20). All experiments were performed in a glove box using a 20 mL glass scintillation vial as the cell. The electrodes consisted of platinum wire microelectrode (0.250 cm diameter), platinum wire mesh counter, and Ag/Ag<sup>+</sup> reference electrodes. Solution concentrations employed during CV studies were typically 3 mM for the uranium complex and 0.1 M for the [Bu<sub>4</sub>N][BAr<sup>F</sup><sub>4</sub>] electrolyte. Elemental analyses for compounds **6.1** and **6.2** were performed by Robertson Microlit Laboratories in Madison, NJ. The elemental analysis for **6.3** was performed by the microanalytical laboratory at the University of California, Berkeley.

## 6.4 Results and Discussion

**6.4.1 Syntheses and Characterizations of [(NN'<sub>3</sub>)U(*p*-DEB)FeCl(dmpe)<sub>2</sub>].** Several monomeric synthons avail themselves for the preparation of 5*f*-bridge-3*d* species.<sup>3,31</sup> Utilizing the procedure published by Scott<sup>28</sup> in the synthesis of **6.3**, we find that mixing [(*bit*-NN'<sub>3</sub>)U] with the appropriate Fe-acetylene leads to a arylacetylide-bridged 5*f*-3*d* dinuclear complex in which the U(IV) center is pentacoordinate and the Fe(II) center is hexacoordinate (Scheme 6.1). In this manner, we have prepared the dinuclear U(IV)-Fe(II) ethynylbenzene bridged complex [(NN'<sub>3</sub>)U(*p*-DEB)FeCl(dmpe)<sub>2</sub>] (**6.3**) in good yield, although acceptable results have not been obtained via elemental analysis. A diffraction quality single crystal was obtained from a concentrated pentane solution for the dinuclear compound **6.3** and the structure is depicted in Figure 6.5.



**Scheme 6.1.** Synthesis of chelating 5*f*-3*d* complex of U(IV)–Fe(II): a = [(dmpe)<sub>2</sub>Fe(*p*-DEBH)Cl] in pentane/dichloromethane (5:1).

We have characterized the ethynylbenzene-bridged species (**6.3**) and the corresponding precursors **6.1** and **6.2** by multiple spectroscopic techniques including infrared spectroscopy and UV-visible absorption spectroscopy (Figures 6.1–6.2). The fingerprint region of the IR is nearly identical to those reported for most of the structurally characterized compounds containing the [(NN'<sub>3</sub>)U] fragment.<sup>28,32-34</sup> The absorption spectrum of **6.3** (Figure 6.2) contains only three features at 467, 404, and 282 nm. While spectral features which would normally mark the presence of a U(IV) ion in solution are absent the presence of Fe(II) is confirmed via comparison with the absorption spectrum of **6.2** obtained by Wesley Hoffert (notebook reference: WH9-145). In addition, X-ray crystallography and infrared spectroscopy confirm the presence of the reported product.

**6.4.2 X-ray Crystallography.** Compound **6.3** crystallizes in monoclinic space group *P*2<sub>1</sub>/*c* (no. 14) with *Z*=4 (Table 6.1); there is one independent complex molecule in each unit cell. The structure of **6.3** is shown in Figure 6.5 and selected bond lengths and angles are given in Table 6.2. Single crystal X-ray analysis of **6.3** reveals that the U(IV) is ligated by three amido nitrogens, one amine nitrogen, and one phenylacetylide carbon atoms in  $\eta^1$  fashion. The triamidoamine ligand adopts a typical trigonal pyramidal geometry around the uranium center in **6.3**. Although not imposed crystallographically,

the ligand is essentially three-fold symmetric about the U center, as measured by the dihedral angles  $N_{ax}-U-N_{eq}-Si$  ( $135-141^\circ$ ) which compares well to other structures containing the  $[(NN'_3)U]$  fragment where dihedral angles of  $131-137^\circ$  are typically observed.<sup>28</sup> The Fe(II) center in **6.3** is ligated by four phosphorous atoms, a chloride atom, and one phenylacetylide carbon atoms in  $\eta^1$  fashion. The phosphorous atoms occupy a square plane around the iron center. The average Fe–P distance in **6.3** is 2.212(5) Å and the Fe–Cl distance is 2.375(3) both of which compare well to other literature values for iron phosphine complexes.<sup>23,24,35</sup> The ligands form a slightly distorted octahedral first coordination sphere about the iron metal center, as evidenced by the  $\Sigma$  parameter (28.67), which is the sum of the deviations from  $90^\circ$  of the twelve *cis* angles ( $\varphi$ ) in the coordination sphere ( $\Sigma = \sum_{i=1}^{12} |90 - \varphi_i|$ ).<sup>36</sup> The N–U(IV)–C–C–Ph–C–C–Fe(II)–Cl backbone is essentially linear with N–U–C, U–C–C, C–C–Ph, Ph–C–C, and C–C–Fe, C–Fe–Cl angles of 177.8(3), 175.3(9), 178.4(12), 176.8(12), 179.3(11), and  $178.6(4)^\circ$ , respectively. To our knowledge, this represents the longest linear chain of elements joining *5f* and *3d* elements.

**Table 6.2.** Selected bond distances (Å) and angles (°) for crystallographically determined structures (**6.3**) of the *5f-3d* complex.

	[(NN' <sub>3</sub> )U( <i>p</i> -DEB)FeCl(dmpe) <sub>2</sub> ] ( <b>6.3</b> )
U–C	2.444(11)
U–N <sub>ax</sub> (amino)	2.696(8)
	2.215(8)
U–N <sub>eq</sub> (amido)	2.220(8)
	2.227(8)
Fe–C	1.863(11)
	2.157(4)
Fe–P	2.186(4)
	2.239(4)
	2.267(4)
Fe–Cl	2.375(3)
C25≡C26	1.229(15)
C33≡C34	1.220(15)
U–C–C	175.3(9)
Fe–C–C	179.3(11)
N <sub>ax</sub> –U–C	177.8(3)
	69.4(3)
N <sub>ax</sub> –U–N <sub>eq</sub>	69.5(3)
	69.5(3)
	107.7(3)
N <sub>eq</sub> –U–N <sub>eq</sub>	108.7(3)
	108.8(3)

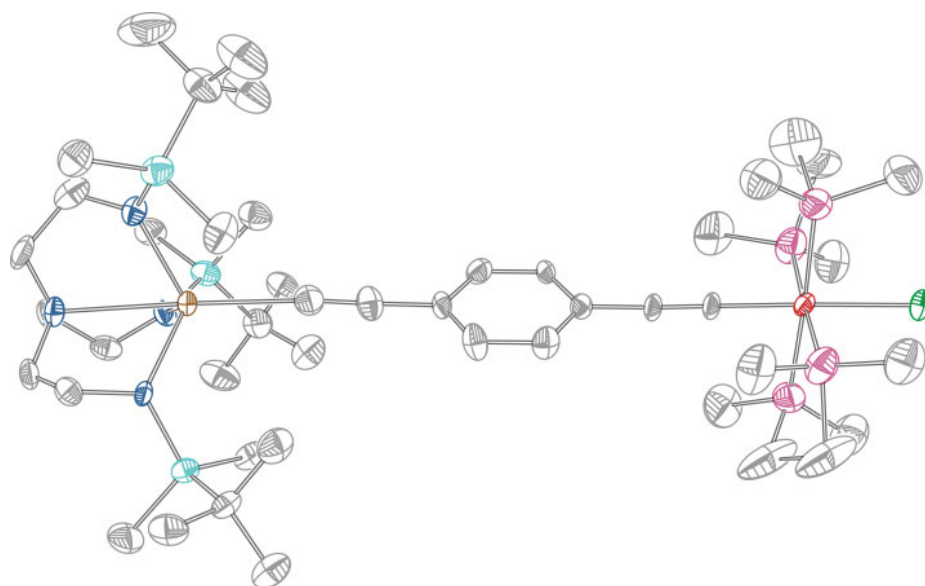


**Figure 6.5.** Crystal structure of the *5f-3d* arylacetylide bridged complex (**6.3**) rendered with 40% ellipsoids. Brown, red, purple, green, light blue, dark blue and gray ellipsoids represent U, Fe, P, Cl, Si, N and C atoms, respectively. Hydrogen atoms are omitted for clarity.

**6.4.3 Magnetic Properties.** Due to the nature of crystal field splittings being of approximately the same magnitude as spin-orbit coupling, both of which are greater than  $kT$ , the magnetic behavior of the actinides is quite complicated.<sup>37,38</sup> In addition, very few examples of magnetic investigations on polynuclear bridging uranium(IV) compounds have been reported.<sup>39-41</sup> With this in mind, variable temperature magnetic susceptibility data were collected for compound **6.3** and are presented in Figure 6.6. At 300 K the measured susceptibility was determined to be  $0.98 \text{ emu}\cdot\text{K}\cdot\text{mol}^{-1}$  for compound **6.3**. This value is close to the predicted value of  $1.00 \text{ emu}\cdot\text{K}\cdot\text{mol}^{-1}$  for one  $S = 1$  ion with  $g = 2.00$ . As the temperature is lowered,  $\chi_M T$  drops off in a nearly linear fashion down to 3 K where the susceptibility trend toward  $0 \text{ emu}\cdot\text{K}\cdot\text{mol}^{-1}$  with a value of  $0.05 \text{ emu}\cdot\text{K}\cdot\text{mol}^{-1}$ . This drop in the measured magnetic susceptibility could most likely be attributed to depopulation of the Stark sublevels. This behavior is solely attributable to the single-ion anisotropy of the uranium ion<sup>42,43</sup> and as such, the magnetic behavior of compound **6.3** can be interpreted as ground state diamagnetic  $f^2$  species, which is paramagnetic at room temperature due to spin-orbit coupling, temperature-independent paramagnetism (TIP), and thermal population of paramagnetic excited states. This behavior compares well with other  $5f$ - $3d$  compounds in the literature.<sup>3,8-14</sup>

In comparison with the pentacoordinate **2.3**, the dinuclear **6.3** is essentially the same as the mononuclear complex except that a heavy atom has been affixed in the *para* position of the diethynylbenzene ligand. Considering the monomer, as the temperature is reduced to 160 K,  $\chi_M T$  reveals a gradual decrease to  $0.99 \text{ emu}\cdot\text{K}\cdot\text{mol}^{-1}$ , followed by a sharper decrease to  $0.03 \text{ emu}\cdot\text{K}\cdot\text{mol}^{-1}$  at 2 K. The pentacoordinate species, **2.3**, seems to show less influence from TIP than observed for **6.3** (vide infra). Overall, the foregoing

results imply that the addition of a transition metal, in this case  $\text{Fe}^{\text{II}}$ , seems to have an effect on the magnetic properties in this  $5f$ - $3d$  bridged complex. It is important to note that bulk amounts of **6.3** analyzed by elemental analysis do not meet the expected amounts of CHN.

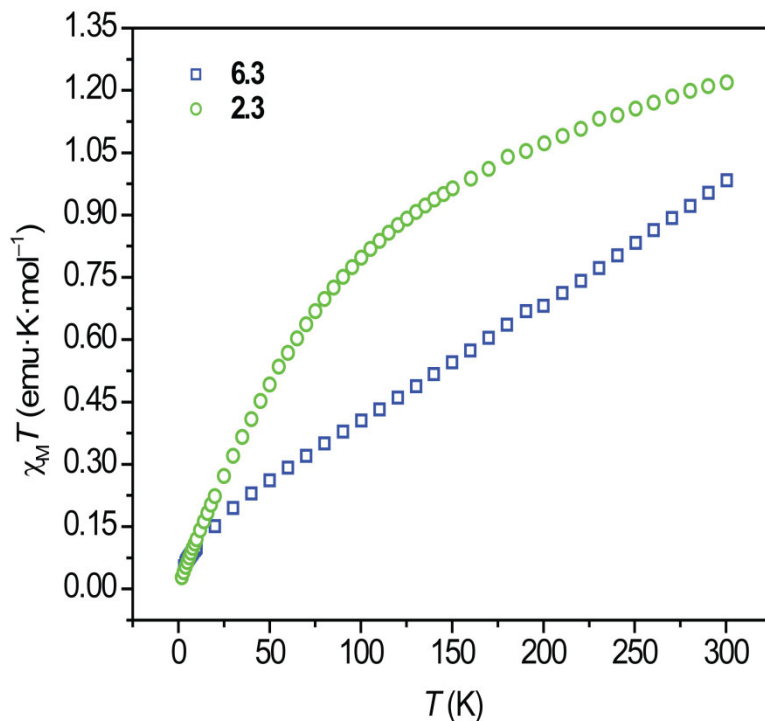


**Figure 6.6.** Temperature dependence of the magnetic susceptibility for compound **6.3**, obtained at a measuring field of 1000 G from 2-300 K. For comparison the temperature dependence of the magnetic susceptibility for compound **2.3** is also plotted.

**6.4.4 Oxidation of the dinuclear  $5f$ - $3d$  arylacetylide complex.** Efforts to produce unambiguously paramagnetic M-containing assemblies, either by oxidations or reductions of **6.3** that may lead to any combination containing a U(V), U(III), Fe(II), or Fe(III) species yield mixed results. Cyclic voltammetry experiments performed on the dinuclear arylacetylide complex **6.3** in *o*-difluorobenzene show a wave centered at about 0.452 V versus a pseudo Ag wire reference at several scan rates (Figure 6.7, left). This

process is assignable to an oxidation of one of the metal centers in the neutral compound and is supported by an agitation experiment where the voltammogram is collected while stirring the sample (Figure 6.7, right). While the cyclic voltammogram suggests a redox couple, a voltammogram was not collected with added ferrocene so the potential of this couple is not well defined. Based upon a cyclic voltammogram for **6.2** obtained by Wesley Hoffert (notebook reference WH9-145b) this redox couple could be a formal oxidation of Fe(II) to Fe(III). In addition, initial attempts to isolate an oxidized complex by chemical oxidation with copper(I) afforded only black solids that show no acetylide resonances in the infrared spectroscopy.

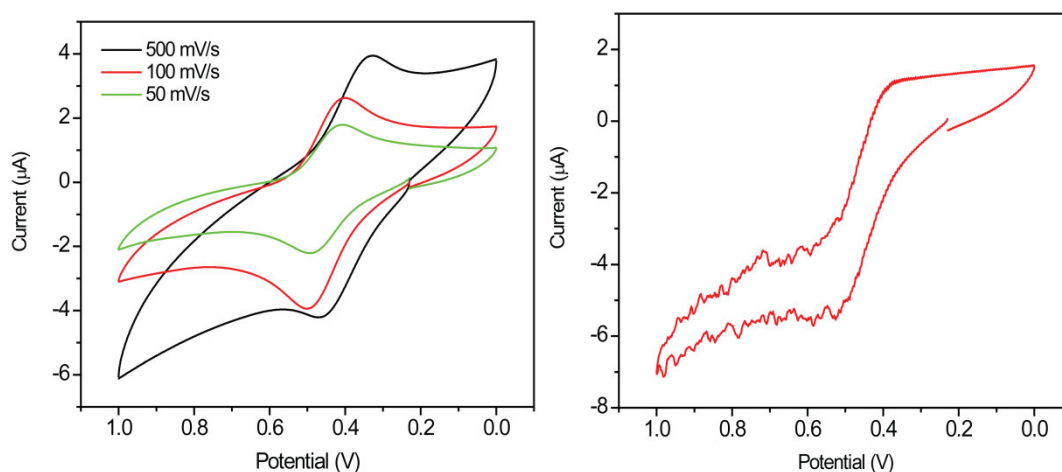


**Figure 6.7.** Electrochemical behavior for compound **6.3** in static solution (left) and while stirring (right) recorded in 0.1 M solution of  $[\text{Bu}_4\text{N}][\text{BAR}^{\text{F}}_4]$  in *o*-difluorobenzene at ambient temperature with a 0.250 mm diameter platinum wire microelectrode.

## 6.5 Summary and Outlook

In conclusion, we have prepared a *5f-3d* bimetallic complex bridged by *para*-diethynylbenzene and have used multiple techniques to characterize it spectroscopically and magnetically. Despite the fact that the compound in this study gives a non-magnetic ground state at low temperature, consistent with those described elsewhere in the

literature,<sup>10,34,38,40,44-53</sup> we are currently exploring efforts to synthesize a complex with one or more of the metal centers in a lower or higher oxidation state to determine the effects on the magnetic properties. This could be promising for future work utilizing 5f-3d compounds in the generation of new SMMs that possess large anisotropy.

**6.6 Acknowledgments.** This research was supported by Colorado State University and the ACS Petroleum Research Fund (44691-G3). We thank Ms. Susie Miller and Prof. Oren Anderson for advice on crystal structure refinements and Dr. Christopher Rithner for assistance with NMR data collection.

### 6.7 Crystallographic Information Formatted (cif) files for crystal 6.3

```

data_msn220 (6.3)          'International Tables Vol C Tables
                           4.2.6.8 and 6.1.1.4'
_audit_creation_method    'N' 'N' 0.0061 0.0033
  SHELXL-97                'International Tables Vol C Tables
                           4.2.6.8 and 6.1.1.4'
_chemical_name_systematic 'Si' 'Si' 0.0817 0.0704
;                           'International Tables Vol C Tables
?                           4.2.6.8 and 6.1.1.4'
;                           'P' 'P' 0.1023 0.0942
_chemical_name_common      ?
_chemical_melting_point    ?
_chemical_formula_moiety    ?
_chemical_formula_sum      'C46 H93 Cl Fe N4 P4 Si3 U'
_chemical_formula_weight    1239.72
                           'Fe' 'Fe' 0.3463 0.8444
                           'International Tables Vol C Tables
                           4.2.6.8 and 6.1.1.4'
loop_                       'U' 'U' -9.6767 9.6646
  _atom_type_symbol        'International Tables Vol C Tables
  _atom_type_description    4.2.6.8 and 6.1.1.4'
  _atom_type_scatter_real   _symmetry_cell_setting      ?
  _atom_type_scatter_imag   _symmetry_space_group_name_H-M
  _atom_type_scatter_source 'C' 'C' 0.0033 0.0016
                           'International Tables Vol C Tables
                           4.2.6.8 and 6.1.1.4'
  'H' 'H' 0.0000 0.0000    loop_

```

_symmetry_equiv_pos_as_xyz		_diffrn_measurement_method	?
'x, y, z'		_diffrn_detector_area_resol_mean	?
'-x, y+1/2, -z+1/2'		_diffrn_reflns_number	66120
'-x, -y, -z'		_diffrn_reflns_av_R_equivalents	
'x, -y-1/2, z-1/2'		0.0888	
_cell_length_a	16.5308(7)	_diffrn_reflns_av_signal/netI	0.0539
_cell_length_b	23.7632(10)	_diffrn_reflns_limit_h_min	-16
_cell_length_c	16.4106(7)	_diffrn_reflns_limit_h_max	16
_cell_angle_alpha	90.00	_diffrn_reflns_limit_k_min	-23
_cell_angle_beta	101.130(2)	_diffrn_reflns_limit_k_max	23
_cell_angle_gamma	90.00	_diffrn_reflns_limit_l_min	-16
_cell_volume	6325.2(5)	_diffrn_reflns_limit_l_max	16
_cell_formula_units_Z	4	_diffrn_reflns_theta_min	1.82
_cell_measurement_temperature		_diffrn_reflns_theta_max	20.60
296(2)		_reflns_number_total	6410
_cell_measurement_reflns_used	?	_reflns_number_gt	4941
_cell_measurement_theta_min	?	_reflns_threshold_expression	
_cell_measurement_theta_max	?	>2sigma(I)	
_exptl_crystal_description	?	_computing_data_collection	?
_exptl_crystal_colour	?	_computing_cell_refinement	?
_exptl_crystal_size_max	?	_computing_data_reduction	?
_exptl_crystal_size_mid	?	_computing_structure_solution	
_exptl_crystal_size_min	?	'SHELXS-97 (Sheldrick, 2008)'	
_exptl_crystal_density_meas	?	_computing_structure_refinement	
_exptl_crystal_density_diffn	1.302	'SHELXL-97 (Sheldrick, 2008)'	
_exptl_crystal_density_method	'not measured'	_computing_molecular_graphics	?
_exptl_crystal_F_000	2536	_computing_publication_material	?
_exptl_absorpt_coefficient_mu	3.017		
_exptl_absorpt_correction_type	?	_refine_special_details	
_exptl_absorpt_correction_T_min	?	;	
_exptl_absorpt_correction_T_max	?	Refinement of F <sup>2</sup> against ALL	
_exptl_absorpt_process_details	?	reflections. The weighted R-factor	
		wR and	
_exptl_special_details		goodness of fit S are based on F <sup>2</sup> ,	
;		conventional R-factors R are based	
_diffrn_ambient_temperature	296(2)	on F, with F set to zero for negative	
_diffrn_radiation_wavelength		F <sup>2</sup> . The threshold expression of	
0.71073		F <sup>2</sup> > 2sigma(F <sup>2</sup> ) is used only for	
_diffrn_radiation_type	MoK $\alpha$	calculating R-factors(gt) etc. and is	
_diffrn_radiation_source	'fine-focus sealed tube'	not relevant to the choice of reflections	
_diffrn_radiation_monochromator	graphite	for refinement. R-factors based	
_diffrn_measurement_device_type	?	on F <sup>2</sup> are statistically about twice as	
		large as those based on F, and R-	
		factors based on ALL data will be even	
		larger.	

```

;
_refine_ls_structure_factor_coef Fsqd
_refine_ls_matrix_type full
_refine_ls_weighting_scheme calc
_refine_ls_weighting_details
'calc
  w=1/[\s^2^(Fo^2^)+(0.0744P)^2^+2
  2.7818P] where
  P=(Fo^2^+2Fc^2^)/3'
_atom_sites_solution_primary direct
_atom_sites_solution_secondary difmap
_atom_sites_solution_hydrogens geom
_refine_ls_hydrogen_treatment mixed
_refine_ls_extinction_method none
_refine_ls_extinction_coef ?
_refine_ls_number_reflns 6410
_refine_ls_number_parameters 564
_refine_ls_number_restraints 14
_refine_ls_R_factor_all 0.0711
_refine_ls_R_factor_gt 0.0505
_refine_ls_wR_factor_ref 0.1323
_refine_ls_wR_factor_gt 0.1236
_refine_ls_goodness_of_fit_ref 1.056
_refine_ls_restrained_S_all 1.059
_refine_ls_shift/su_max 0.002
_refine_ls_shift/su_mean 0.000

loop_
_atom_site_label
_atom_site_type_symbol
_atom_site_fract_x
_atom_site_fract_y
_atom_site_fract_z
_atom_site_U_iso_or_equiv
_atom_site_adp_type
_atom_site_occupancy
_atom_site_symmetry_multiplicity
_atom_site_calc_flag
_atom_site_refinement_flags
_atom_site_disorder_assembly
_atom_site_disorder_group
U1 U 0.52941(2) 0.849880(16)
  0.75552(2) 0.02749(18) Uani 1 1 d . .
. .
N1 N 0.5519(5) 0.7645(4) 0.8096(5)
  0.035(2) Uani 1 1 d . . .
N2 N 0.6490(5) 0.8865(4) 0.7397(6)
  0.037(2) Uani 1 1 d . . .
N3 N 0.4790(5) 0.9043(3) 0.8450(5)
  0.029(2) Uani 1 1 d . . .
N4 N 0.6354(5) 0.8550(4) 0.9016(5)
  0.035(2) Uani 1 1 d . . .
C1 C 0.5738(7) 0.7610(5) 0.9013(7)
  0.044(3) Uani 1 1 d . . .
H1A H 0.5843 0.7222 0.9184 0.052
  Uiso 1 1 calc R . .
H1B H 0.5287 0.7750 0.9256 0.052
  Uiso 1 1 calc R . .
C2 C 0.6509(7) 0.7965(5) 0.9308(7)
  0.043(3) Uani 1 1 d . . .
H2A H 0.6652 0.7958 0.9909 0.052
  Uiso 1 1 calc R . .
H2B H 0.6968 0.7810 0.9091 0.052
  Uiso 1 1 calc R . .
C3 C 0.7225(7) 0.8691(5) 0.7993(8)
  0.055(4) Uani 1 1 d . . .
H3A H 0.7705 0.8888 0.7882 0.066
  Uiso 1 1 calc R . .
H3B H 0.7314 0.8290 0.7941 0.066
  Uiso 1 1 calc R . .
C4 C 0.7101(7) 0.8824(6) 0.8862(8)
  0.054(4) Uani 1 1 d . . .
H4A H 0.7573 0.8694 0.9264 0.065
  Uiso 1 1 calc R . .
H4B H 0.7055 0.9228 0.8926 0.065
  Uiso 1 1 calc R . .
C5 C 0.5404(7) 0.9324(4) 0.9119(7)
  0.038(3) Uani 1 1 d . . .
H5A H 0.5120 0.9525 0.9494 0.046
  Uiso 1 1 calc R . .
H5B H 0.5730 0.9592 0.8875 0.046
  Uiso 1 1 calc R . .
C6 C 0.5954(7) 0.8879(5) 0.9585(7)
  0.044(3) Uani 1 1 d . . .
H6A H 0.6372 0.9055 1.0003 0.052
  Uiso 1 1 calc R . .
H6B H 0.5631 0.8630 0.9865 0.052
  Uiso 1 1 calc R . .
Si1 Si 0.5620(2) 0.70549(13) 0.7512(2)
  0.0428(9) Uani 1 1 d . . .

```



H19B	H	0.2826	0.8265	0.8032	0.077				
		Uiso 1 1 calc R . .							
H19C	H	0.3722	0.8021	0.8156	0.077				
		Uiso 1 1 calc R . .							
C20	C	0.3697(8)	0.8854(6)	0.9658(8)					
		0.068(4) Uani 1 1 d . . .							
H20A	H	0.4045	0.8545	0.9878	0.101				
		Uiso 1 1 calc R . .							
H20B	H	0.3135	0.8769	0.9686	0.101				
		Uiso 1 1 calc R . .							
H20C	H	0.3868	0.9187	0.9977	0.101				
		Uiso 1 1 calc R . .							
C21	C	0.3119(6)	0.9591(5)	0.8132(7)					
		0.039(3) Uani 1 1 d . . .							
C22	C	0.3220(7)	0.9728(5)	0.7246(8)					
		0.057(4) Uani 1 1 d . . .							
H22A	H	0.2901	1.0056	0.7053	0.085				
		Uiso 1 1 calc R . .							
H22B	H	0.3031	0.9416	0.6889	0.085				
		Uiso 1 1 calc R . .							
H22C	H	0.3791	0.9798	0.7241	0.085				
		Uiso 1 1 calc R . .							
C23	C	0.2208(7)	0.9468(5)	0.8129(9)					
		0.061(4) Uani 1 1 d . . .							
H23A	H	0.1878	0.9781	0.7892	0.092				
		Uiso 1 1 calc R . .							
H23B	H	0.2132	0.9408	0.8688	0.092				
		Uiso 1 1 calc R . .							
H23C	H	0.2043	0.9137	0.7804	0.092				
		Uiso 1 1 calc R . .							
C24	C	0.3356(8)	1.0103(5)	0.8692(8)					
		0.056(4) Uani 1 1 d . . .							
H24A	H	0.3919	1.0203	0.8694	0.085				
		Uiso 1 1 calc R . .							
H24B	H	0.3293	1.0014	0.9247	0.085				
		Uiso 1 1 calc R . .							
H24C	H	0.3004	1.0414	0.8486	0.085				
		Uiso 1 1 calc R . .							
C25	C	0.4289(8)	0.8439(5)	0.6249(8)					
		0.048(3) Uani 1 1 d . . .							
C26	C	0.3730(8)	0.8425(5)	0.5630(8)					
		0.043(3) Uani 1 1 d . . .							
C27	C	0.3105(7)	0.8399(5)	0.4880(6)					
		0.031(3) Uani 1 1 d . . .							
C28	C	0.3098(7)	0.7983(5)	0.4308(7)					
		0.038(3) Uani 1 1 d . . .							
H28	H	0.3497	0.7702	0.4407	0.045	Uiso			
		1 1 calc R . .							
C29	C	0.2492(7)	0.8807(5)	0.4736(7)					
		0.043(3) Uani 1 1 d . . .							
H29	H	0.2478	0.9091	0.5123	0.051	Uiso			
		1 1 calc R . .							
C30	C	0.2514(6)	0.7968(5)	0.3585(7)					
		0.036(3) Uani 1 1 d . . .							
H30	H	0.2537	0.7684	0.3201	0.043	Uiso			
		1 1 calc R . .							
C31	C	0.1895(7)	0.8788(5)	0.4006(7)					
		0.042(3) Uani 1 1 d . . .							
H31	H	0.1488	0.9063	0.3912	0.050	Uiso			
		1 1 calc R . .							
C32	C	0.1894(6)	0.8366(4)	0.3416(7)					
		0.030(3) Uani 1 1 d . . .							
C33	C	0.1284(7)	0.8326(4)	0.2674(7)					
		0.030(3) Uani 1 1 d . . .							
C34	C	0.0794(7)	0.8263(5)	0.2033(8)					
		0.038(3) Uani 1 1 d . . .							
Fe1	Fe	0.00086(9)		0.81752(7)					
		0.10479(9) 0.0343(4) Uani 1 1 d . . .							
C35	C	-0.1072(9)	0.8316(7)	0.2395(16)					
		0.149(9) Uani 1 1 d U . .							
H35A	H	-0.1495	0.8171	0.2674	0.179	Uiso			
		1 1 calc R . .							
H35B	H	-0.0607	0.8430	0.2817	0.179	Uiso			
		1 1 calc R . .							
C36	C	-0.1409(11)	0.8829(7)	0.1879(14)					
		0.121(7) Uani 1 1 d U . .							
H36A	H	-0.1514	0.9138	0.2230	0.145	Uiso			
		1 1 calc R . .							
H36B	H	-0.1912	0.8739	0.1490	0.145	Uiso			
		1 1 calc R . .							
C37	C	-0.0348(10)	0.7269(6)	0.2585(10)					
		0.098(6) Uani 1 1 d . . .							
H37A	H	0.0139	0.7414	0.2938	0.146	Uiso			
		1 1 calc R . .							
H37B	H	-0.0210	0.6937	0.2308	0.146	Uiso			
		1 1 calc R . .							
H37C	H	-0.0750	0.7176	0.2915	0.146	Uiso			
		1 1 calc R . .							
C38	C	-0.1732(9)	0.7449(7)	0.1385(11)					
		0.098(6) Uani 1 1 d . . .							
H38A	H	-0.1944	0.7268	0.1822	0.147	Uiso			
		1 1 calc R . .							

H38B H -0.1637 0.7174 0.0986 0.147 Uiso 1 1 calc R . .	H44C H -0.0240 0.6618 0.0773 0.135 Uiso 1 1 calc R . .
H38C H -0.2124 0.7722 0.1118 0.147 Uiso 1 1 calc R . .	C45 C 0.1545(8) 0.9155(6) 0.0769(9) 0.077(4) Uani 1 1 d . . .
C39 C 0.0048(9) 0.9504(6) 0.2020(10) 0.088(5) Uani 1 1 d . . .	H45A H 0.1809 0.9048 0.1321 0.116 Uiso 1 1 calc R . .
H39A H 0.0512 0.9626 0.1792 0.132 Uiso 1 1 calc R . .	H45B H 0.1240 0.9496 0.0792 0.116 Uiso 1 1 calc R . .
H39B H 0.0240 0.9332 0.2552 0.132 Uiso 1 1 calc R . .	H45C H 0.1956 0.9214 0.0436 0.116 Uiso 1 1 calc R . .
H39C H -0.0292 0.9822 0.2084 0.132 Uiso 1 1 calc R . .	C46 C 0.0416(9) 0.8913(7) -0.0689(9) 0.085(5) Uani 1 1 d . . .
C40 C -0.1074(9) 0.9448(6) 0.0503(10) 0.086(5) Uani 1 1 d . . .	H46A H 0.0848 0.9065 -0.0940 0.128 Uiso 1 1 calc R . .
H40A H -0.1411 0.9714 0.0727 0.130 Uiso 1 1 calc R . .	H46B H 0.0039 0.9207 -0.0617 0.128 Uiso 1 1 calc R . .
H40B H -0.1416 0.9223 0.0088 0.130 Uiso 1 1 calc R . .	H46C H 0.0128 0.8626 -0.1041 0.128 Uiso 1 1 calc R . .
H40C H -0.0675 0.9647 0.0258 0.130 Uiso 1 1 calc R . .	Cl1 Cl -0.09996(17) 0.80572(13) - 0.01833(18) 0.0493(8) Uani 1 1 d . . . .
C41 C 0.1110(10) 0.7530(7) -0.0133(10) 0.094(5) Uani 1 1 d U . .	P1 P -0.0771(2) 0.77985(18) 0.1816(2) 0.0687(12) Uani 1 1 d . . .
H41A H 0.1545 0.7259 -0.0150 0.112 Uiso 1 1 calc R . .	P2 P -0.0547(2) 0.89977(16) 0.1327(3) 0.0640(11) Uani 1 1 d . . .
H41B H 0.0735 0.7541 -0.0666 0.112 Uiso 1 1 calc R . .	P3 P 0.0572(2) 0.73968(16) 0.0730(3) 0.0690(12) Uani 1 1 d . . .
C42 C 0.1433(14) 0.8088(7) 0.0135(13) 0.161(10) Uani 1 1 d U . .	P4 P 0.0863(2) 0.86105(16) 0.0321(2) 0.0631(11) Uani 1 1 d . . .
H42A H 0.1731 0.8218 -0.0283 0.193 Uiso 1 1 calc R . .	loop_ _atom_site_aniso_label _atom_site_aniso_U_11 _atom_site_aniso_U_22 _atom_site_aniso_U_33 _atom_site_aniso_U_23 _atom_site_aniso_U_13 _atom_site_aniso_U_12
H42B H 0.1841 0.8030 0.0639 0.193 Uiso 1 1 calc R . .	U1 0.0263(3) 0.0300(3) 0.0238(3) - 0.0015(2) -0.00121(19) -0.0012(2)
C43 C 0.1353(10) 0.7056(7) 0.1484(11) 0.110(7) Uani 1 1 d . . .	N1 0.036(5) 0.046(6) 0.021(6) 0.002(4) 0.000(4) 0.005(4)
H43A H 0.1103 0.6886 0.1905 0.165 Uiso 1 1 calc R . .	N2 0.031(5) 0.037(6) 0.043(6) 0.005(5) 0.004(5) 0.002(4)
H43B H 0.1753 0.7329 0.1734 0.165 Uiso 1 1 calc R . .	N3 0.025(5) 0.030(5) 0.029(5) -0.012(4) 0.000(4) -0.001(4)
H43C H 0.1619 0.6771 0.1215 0.165 Uiso 1 1 calc R . .	
C44 C -0.0038(10) 0.6800(6) 0.0330(10) 0.090(5) Uani 1 1 d . . .	
H44A H 0.0294 0.6541 0.0088 0.135 Uiso 1 1 calc R . .	
H44B H -0.0495 0.6922 -0.0086 0.135 Uiso 1 1 calc R . .	

N4	0.030(5)	0.038(6)	0.034(6)	-0.004(5)	C20	0.067(9)	0.078(10)	0.062(10)	
	-0.005(5)	0.003(5)				0.008(8)	0.022(8)	-0.008(8)	
C1	0.040(7)	0.041(8)	0.054(9)	0.006(6)	C21	0.029(7)	0.042(8)	0.048(8)	-
	0.019(7)	0.011(6)				0.005(6)	0.011(6)	-0.008(6)	
C2	0.055(8)	0.049(8)	0.021(7)	0.004(6)	C22	0.049(8)	0.053(9)	0.068(10)	
	-0.006(6)	0.012(7)				0.015(7)	0.009(7)	0.016(7)	
C3	0.038(8)	0.051(9)	0.079(11)	0.004(7)	C23	0.042(8)	0.047(8)	0.096(11)	-
	0.017(8)	0.005(6)				0.004(8)	0.016(8)	0.001(6)	
C4	0.025(7)	0.068(9)	0.063(10)	-	C24	0.057(8)	0.044(8)	0.073(10)	-
	0.006(7)	-0.008(7)	-0.011(6)			0.005(7)	0.025(8)	0.014(7)	
C5	0.049(7)	0.033(7)	0.037(7)	-0.004(6)	C25	0.050(8)	0.044(8)	0.050(9)	0.003(7)
	0.016(6)	-0.002(6)				0.012(8)	-0.008(7)		
C6	0.043(7)	0.051(8)	0.032(7)	-0.012(6)	C26	0.049(8)	0.038(8)	0.038(8)	0.011(6)
	-0.005(6)	0.005(6)				0.000(8)	-0.003(6)		
Si1	0.052(2)	0.035(2)	0.046(2)	-	C27	0.034(7)	0.037(8)	0.021(7)	-
	0.0031(16)	0.0190(18)	0.0038(16)			0.001(6)	0.001(6)	-0.016(6)	
C7	0.075(10)	0.047(8)	0.065(9)	-	C28	0.029(7)	0.049(8)	0.033(8)	-
	0.015(7)	0.028(8)	-0.004(7)			0.004(7)	0.000(6)	0.011(6)	
C8	0.065(9)	0.051(8)	0.058(9)	-0.001(7)	C29	0.062(8)	0.025(7)	0.032(8)	-
	0.023(7)	0.017(7)				0.011(6)	-0.012(7)	0.004(7)	
C9	0.055(8)	0.042(8)	0.060(9)	-0.020(7)	C30	0.032(7)	0.050(8)	0.025(7)	-
	0.017(7)	-0.004(7)				0.019(6)	0.004(6)	0.009(6)	
C10	0.062(9)	0.040(8)	0.089(11)	-	C31	0.047(8)	0.029(7)	0.047(9)	-
	0.020(8)	0.013(8)	-0.009(7)			0.001(6)	0.002(7)	0.017(6)	
C11	0.086(10)	0.043(8)	0.058(9)	-	C32	0.026(6)	0.035(7)	0.031(7)	0.004(6)
	0.009(7)	0.029(8)	-0.001(7)			0.008(6)	0.004(6)		
C12	0.094(11)	0.057(10)	0.076(11)		C33	0.022(6)	0.046(8)	0.016(7)	-
	0.004(8)	0.045(9)	-0.010(8)			0.006(5)	-0.011(6)	0.006(5)	
Si2	0.046(2)	0.037(2)	0.058(2)	-	C34	0.024(6)	0.037(7)	0.050(9)	0.002(6)
	0.0010(18)	0.0147(19)	-0.0073(17)			0.002(7)	0.018(5)		
C13	0.054(8)	0.040(8)	0.069(9)	0.018(7)	Fe1	0.0202(8)	0.0497(11)	0.0309(10)	-
	0.000(7)	-0.003(6)				0.0070(8)	-0.0003(7)	0.0070(7)	
C14	0.059(9)	0.049(9)	0.075(10)		C35	0.034(9)	0.075(12)	0.35(3)	
	0.003(7)	0.011(8)	-0.005(7)			0.076(14)	0.051(13)	0.023(8)	
C15	0.095(11)	0.047(9)	0.054(9)		C36	0.091(12)	0.091(12)	0.20(2)	
	0.007(7)	0.037(8)	-0.028(8)			0.039(12)	0.081(13)	0.045(10)	
C16	0.130(15)	0.082(12)	0.057(10)	-	C37	0.116(14)	0.081(12)	0.094(13)	
	0.008(9)	0.043(10)	-0.027(10)			0.050(10)	0.014(11)	-0.008(10)	
C17	0.20(2)	0.061(11)	0.076(12)	-	C38	0.070(11)	0.094(13)	0.125(15)	
	0.001(9)	0.052(13)	-0.028(12)			0.032(11)	0.007(10)	-0.020(9)	
C18	0.100(14)	0.118(15)	0.149(18)	-	C39	0.079(11)	0.067(10)	0.106(13)	-
	0.035(13)	0.083(14)	-0.022(11)			0.043(10)	-0.013(10)	0.032(9)	
Si3	0.0323(17)	0.035(2)	0.041(2)		C40	0.089(11)	0.056(10)	0.109(13)	
	0.0001(15)	0.0116(16)	-0.0017(15)			0.010(9)	0.007(10)	0.027(9)	
C19	0.029(7)	0.048(8)	0.081(10)		C41	0.091(12)	0.107(11)	0.092(12)	-
	0.004(7)	0.022(7)	-0.006(6)			0.038(10)	0.041(10)	-0.008(9)	

C42	0.21(2)	0.057(10)	0.150(17)	-	U1 N2	2.221(9)	. ?
	0.041(11)	-0.123(16)	0.053(11)		U1 N3	2.235(8)	. ?
C43	0.109(14)	0.081(12)	0.122(15)	-	U1 C25	2.450(14)	. ?
	0.015(11)	-0.020(12)	0.061(11)		U1 N4	2.685(8)	. ?
C44	0.095(12)	0.057(10)	0.114(14)	-	N1 C1	1.480(14)	. ?
	0.011(10)	0.009(11)	0.000(9)		N1 Si1	1.725(9)	. ?
C45	0.068(10)	0.089(11)	0.076(11)	-	N2 C3	1.464(14)	. ?
	0.010(9)	0.020(9)	-0.028(8)		N2 Si2	1.729(9)	. ?
C46	0.084(11)	0.111(14)	0.062(10)		N3 C5	1.501(13)	. ?
	0.015(9)	0.018(9)	-0.002(10)		N3 Si3	1.716(8)	. ?
C11	0.0318(17)	0.072(2)	0.0386(18)	-	N4 C4	1.461(14)	. ?
	0.0014(16)	-0.0077(15)	-0.0022(15)		N4 C6	1.468(13)	. ?
P1	0.054(2)	0.094(3)	0.059(3)	0.006(2)	N4 C2	1.477(13)	. ?
	0.015(2)	-0.019(2)			C1 C2	1.526(15)	. ?
P2	0.055(2)	0.057(2)	0.074(3)	-0.004(2)	C3 C4	1.513(17)	. ?
	-0.001(2)	0.0094(19)			C5 C6	1.505(15)	. ?
P3	0.059(2)	0.068(3)	0.073(3)	-0.020(2)	Si1 C7	1.827(13)	. ?
	-0.005(2)	0.017(2)			Si1 C8	1.890(12)	. ?
P4	0.051(2)	0.080(3)	0.059(2)	-0.012(2)	Si1 C9	1.910(12)	. ?
	0.011(2)	-0.007(2)			C9 C10	1.501(17)	. ?
					C9 C12	1.539(17)	. ?
					C9 C11	1.543(16)	. ?
					Si2 C14	1.867(12)	. ?
					Si2 C13	1.882(12)	. ?
					Si2 C15	1.908(14)	. ?
					C15 C16	1.487(18)	. ?
					C15 C17	1.496(19)	. ?
					C15 C18	1.54(2)	. ?
					Si3 C19	1.856(12)	. ?
					Si3 C21	1.872(11)	. ?
					Si3 C20	1.873(13)	. ?
					C21 C24	1.529(15)	. ?
					C21 C22	1.530(16)	. ?
					C21 C23	1.534(15)	. ?
					C25 C26	1.234(16)	. ?
					C26 C27	1.448(17)	. ?
					C27 C28	1.363(14)	. ?
					C27 C29	1.389(15)	. ?
					C28 C30	1.378(14)	. ?
					C29 C31	1.398(15)	. ?
					C30 C32	1.381(14)	. ?
					C31 C32	1.394(15)	. ?
					C32 C33	1.426(16)	. ?
					C33 C34	1.207(14)	. ?
					C34 Fe1	1.880(13)	. ?
					Fe1 P1	2.163(4)	. ?

\_geom\_special\_details  
 ;  
 All esds (except the esd in the dihedral angle between two l.s. planes) are estimated using the full covariance matrix. The cell esds are taken into account individually in the estimation of esds in distances, angles and torsion angles; correlations between esds in cell parameters are only used when they are defined by crystal symmetry. An approximate (isotropic) treatment of cell esds is used for estimating esds involving l.s. planes.  
 ;  
 loop\_  
 \_geom\_bond\_atom\_site\_label\_1  
 \_geom\_bond\_atom\_site\_label\_2  
 \_geom\_bond\_distance  
 \_geom\_bond\_site\_symmetry\_2  
 \_geom\_bond\_publ\_flag  
 U1 N1 2.217(8) . ?

Fe1 P3 2.179(4) . ?	C4 N4 C2 112.1(9) . . ?
Fe1 P2 2.244(4) . ?	C6 N4 C2 111.5(9) . . ?
Fe1 P4 2.266(4) . ?	C4 N4 U1 107.1(7) . . ?
Fe1 C11 2.375(3) . ?	C6 N4 U1 107.2(6) . . ?
C35 C36 1.53(2) . ?	C2 N4 U1 106.8(6) . . ?
C35 P1 1.69(2) . ?	N1 C1 C2 108.5(9) . . ?
C36 P2 1.873(16) . ?	N4 C2 C1 109.6(9) . . ?
C37 P1 1.824(14) . ?	N2 C3 C4 108.9(10) . . ?
C38 P1 1.811(15) . ?	N4 C4 C3 110.0(9) . . ?
C39 P2 1.810(13) . ?	N3 C5 C6 108.4(8) . . ?
C40 P2 1.811(14) . ?	N4 C6 C5 110.6(9) . . ?
C41 C42 1.47(2) . ?	N1 Si1 C7 106.2(5) . . ?
C41 P3 1.840(16) . ?	N1 Si1 C8 110.8(5) . . ?
C42 P4 1.623(18) . ?	C7 Si1 C8 108.2(6) . . ?
C43 P3 1.799(14) . ?	N1 Si1 C9 113.8(5) . . ?
C44 P3 1.789(14) . ?	C7 Si1 C9 108.6(6) . . ?
C45 P4 1.780(13) . ?	C8 Si1 C9 109.0(6) . . ?
C46 P4 1.826(14) . ?	C10 C9 C12 108.2(11) . . ?
loop_	C10 C9 C11 110.5(10) . . ?
_geom_angle_atom_site_label_1	C12 C9 C11 108.5(10) . . ?
_geom_angle_atom_site_label_2	C10 C9 Si1 110.3(9) . . ?
_geom_angle_atom_site_label_3	C12 C9 Si1 109.7(9) . . ?
_geom_angle	C11 C9 Si1 109.5(9) . . ?
_geom_angle_site_symmetry_1	N2 Si2 C14 110.7(5) . . ?
_geom_angle_site_symmetry_3	N2 Si2 C13 105.9(5) . . ?
_geom_angle_publ_flag	C14 Si2 C13 108.7(6) . . ?
N1 U1 N2 108.8(3) . . ?	N2 Si2 C15 112.5(5) . . ?
N1 U1 N3 108.8(3) . . ?	C14 Si2 C15 109.9(6) . . ?
N2 U1 N3 107.6(3) . . ?	C13 Si2 C15 108.9(6) . . ?
N1 U1 C25 109.3(3) . . ?	C16 C15 C17 111.3(12) . . ?
N2 U1 C25 112.9(4) . . ?	C16 C15 C18 107.2(13) . . ?
N3 U1 C25 109.4(3) . . ?	C17 C15 C18 107.5(13) . . ?
N1 U1 N4 69.8(3) . . ?	C16 C15 Si2 110.9(9) . . ?
N2 U1 N4 69.2(3) . . ?	C17 C15 Si2 110.7(11) . . ?
N3 U1 N4 69.5(3) . . ?	C18 C15 Si2 109.2(10) . . ?
C25 U1 N4 177.9(3) . . ?	N3 Si3 C19 106.4(5) . . ?
C1 N1 Si1 119.3(7) . . ?	N3 Si3 C21 113.8(5) . . ?
C1 N1 U1 116.5(6) . . ?	C19 Si3 C21 108.8(5) . . ?
Si1 N1 U1 123.2(4) . . ?	N3 Si3 C20 111.2(5) . . ?
C3 N2 Si2 120.6(7) . . ?	C19 Si3 C20 107.1(6) . . ?
C3 N2 U1 116.9(7) . . ?	C21 Si3 C20 109.2(6) . . ?
Si2 N2 U1 121.0(4) . . ?	C24 C21 C22 109.9(10) . . ?
C5 N3 Si3 120.3(6) . . ?	C24 C21 C23 106.9(9) . . ?
C5 N3 U1 116.9(6) . . ?	C22 C21 C23 108.9(10) . . ?
Si3 N3 U1 120.2(4) . . ?	C24 C21 Si3 109.7(8) . . ?
C4 N4 C6 111.8(9) . . ?	C22 C21 Si3 110.5(8) . . ?

C23 C21 Si3 110.8(8) .. ?  
 C26 C25 U1 174.2(10) .. ?  
 C25 C26 C27 177.1(13) .. ?  
 C28 C27 C29 118.7(10) .. ?  
 C28 C27 C26 121.8(11) .. ?  
 C29 C27 C26 119.5(10) .. ?  
 C27 C28 C30 121.5(10) .. ?  
 C27 C29 C31 119.7(10) .. ?  
 C28 C30 C32 121.7(10) .. ?  
 C32 C31 C29 121.6(10) .. ?  
 C30 C32 C31 116.8(10) .. ?  
 C30 C32 C33 120.1(10) .. ?  
 C31 C32 C33 123.1(10) .. ?  
 C34 C33 C32 175.9(11) .. ?  
 C33 C34 Fe1 178.4(10) .. ?  
 C34 Fe1 P1 86.3(4) .. ?  
 C34 Fe1 P3 92.5(3) .. ?  
 P1 Fe1 P3 96.79(18) .. ?  
 C34 Fe1 P2 88.3(3) .. ?  
 P1 Fe1 P2 85.87(17) .. ?  
 P3 Fe1 P2 177.28(19) .. ?  
 C34 Fe1 P4 90.3(4) .. ?  
 P1 Fe1 P4 175.89(16) .. ?  
 P3 Fe1 P4 85.59(16) .. ?  
 P2 Fe1 P4 91.79(16) .. ?  
 C34 Fe1 Cl1 179.0(4) .. ?  
 P1 Fe1 Cl1 92.75(14) .. ?  
 P3 Fe1 Cl1 87.62(13) .. ?  
 P2 Fe1 Cl1 91.67(13) .. ?  
 P4 Fe1 Cl1 90.69(13) .. ?  
 C36 C35 P1 112.7(17) .. ?  
 C35 C36 P2 102.1(10) .. ?  
 C42 C41 P3 97.3(13) .. ?  
 C41 C42 P4 123.8(17) .. ?  
 C35 P1 C38 102.8(8) .. ?  
 C35 P1 C37 103.3(9) .. ?  
 C38 P1 C37 98.3(7) .. ?  
 C35 P1 Fe1 107.5(6) .. ?  
 C38 P1 Fe1 122.6(6) .. ?  
 C37 P1 Fe1 119.8(6) .. ?  
 C39 P2 C40 101.6(7) .. ?  
 C39 P2 C36 102.2(9) .. ?  
 C40 P2 C36 100.8(8) .. ?  
 C39 P2 Fe1 120.9(5) .. ?  
 C40 P2 Fe1 121.3(5) .. ?  
 C36 P2 Fe1 107.0(5) .. ?

C44 P3 C43 100.1(8) .. ?  
 C44 P3 C41 100.1(8) .. ?  
 C43 P3 C41 102.6(9) .. ?  
 C44 P3 Fe1 121.6(5) .. ?  
 C43 P3 Fe1 120.1(5) .. ?  
 C41 P3 Fe1 109.3(6) .. ?  
 C42 P4 C45 106.8(9) .. ?  
 C42 P4 C46 106.2(9) .. ?  
 C45 P4 C46 101.7(7) .. ?  
 C42 P4 Fe1 101.1(10) .. ?  
 C45 P4 Fe1 121.6(5) .. ?  
 C46 P4 Fe1 118.3(5) .. ?

\_diffn\_measured\_fraction\_theta\_max  
     0.995  
 \_diffn\_reflns\_theta\_full          20.60  
 \_diffn\_measured\_fraction\_theta\_full  
     0.995  
 \_refine\_diff\_density\_max      1.685  
 \_refine\_diff\_density\_min     -0.853  
 \_refine\_diff\_density\_rms      0.125

## 6.8 References

- (1) Brooks, M. S. S.; Eriksson, O.; Johansson, B., *J. Alloy* **1995**, *223*, 204.
- (2) Clark, A. E.; Martin, R. L.; Hay, P. J.; Green, J. C.; Jantunen, K. C.; Kiplinger, J. L., *J. Chem. Phys. A* **2005**, *109*, 5481.
- (3) Kozimor, S. A.; Bartlett, B. M.; Rinehart, J. D.; Long, J. R., *J. Am. Chem. Soc.* **2007**, *129*, 10672.
- (4) Mishra, A.; Tasiopoulos, A. J.; Wernsdorfer, W.; Abboud, K. A.; Christou, G., *Inorg. Chem.* **2007**, *46*, 3105.
- (5) Graves, C. R.; Yang, P.; Kozimor, S. A.; Vaughn, A. E.; Clark, D. L.; Conradson, S. D.; Schelter, E. J.; Scott, B. L.; Thompson, J. D.; Hay, P. J.; Morris, D. E.; Kiplinger, J. L., *J. Am. Chem. Soc.* **2008**, *130*, 5272.
- (6) Soderlind, P., *Phys. Rev. B* **2008**, *77*,
- (7) Notter, F. P.; Bolvin, H., *J. Chem. Phys.* **2009**, *130*,
- (8) Rinehart, J. D.; Harris, T. D.; Kozimor, S. A.; Bartlett, B. M.; Long, J. R., *Inorg. Chem.* **2009**, *48*, 3382.
- (9) Le Borgne, T.; Riviere, E.; Marrot, J.; Thuery, P.; Girerd, J. J.; Ephritikhine, M., *Chem. Eur. J.* **2002**, *8*, 774.
- (10) Salmon, L.; Thuery, P.; Riviere, E.; Girerd, J. J.; Ephritikhine, M., *Chem. Commun.* **2003**, 762.
- (11) Salmon, L.; Thuery, P.; Riviere, E.; Girerd, J. J.; Ephritikhine, M., *Dalton Trans.* **2003**, 2872.
- (12) Salmon, L.; Thuery, P.; Riviere, E.; Ephritikhine, M., *Inorg. Chem.* **2006**, *45*, 83.
- (13) Rinehart, J. D.; Bartlett, B. M.; Kozimor, S. A.; Long, J. R., *Inorg. Chimi. Acta* **2008**, *361*, 3534.

- (14) Newell, B. S.; Rappe, A. K.; Shores, M. P., *Inorg. Chem.* **2010**, *49*, 1595.
- (15) Ishikawa, N.; Sugita, M.; Ishikawa, T.; Koshihara, S.; Kaizu, Y., *J. Phys. Chem. B* **2004**, *108*, 11265.
- (16) Schelter, E. J.; Veauthier, J. M.; Thompson, J. D.; Scott, B. L.; John, K. D.; Morris, D. E.; Kiplinger, J. L., *J. Am. Chem. Soc.* **2006**, *128*, 2198.
- (17) Cramer, R. E.; Higa, K. T.; Pruskin, S. L.; Gilje, J. W., *J. Am. Chem. Soc.* **1983**, *105*, 6749.
- (18) Cendrowskiguillaume, S. M.; Lance, M.; Nierlich, M.; Vigner, J.; Ephritikhine, M., *J. Chem. Soc., Chem. Commun.* **1994**, 1655.
- (19) Odom, A. L.; Arnold, P. L.; Cummins, C. C., *J. Am. Chem. Soc.* **1998**, *120*, 5836.
- (20) Evans, W. J.; Nyce, G. W.; Greci, M. A.; Ziller, J. W., *Inorg. Chem.* **2001**, *40*, 6725.
- (21) Arnold, P. L.; Patel, D.; Blake, A. J.; Wilson, C.; Love, J. B., *J. Am. Chem. Soc.* **2006**, *128*, 9610.
- (22) Monreal, M. J.; Carver, C. T.; Diaconescu, P. L., *Inorg. Chem.* **2007**, *46*, 7226.
- (23) Weyland, T.; Lapinte, C.; Frapper, G.; Calhorda, M. J.; Halet, J. F.; Toupet, L., *Organometallics* **1997**, *16*, 2024.
- (24) Paul, F. d. r.; Bondon, A.; da Costa, G. g.; Malvolti, F.; Sinbandhit, S.; Cador, O.; Costuas, K.; Toupet, L.; Boillot, M.-L., *Inorg. Chem.* **2009**, *48*, 10608.
- (25) Hoffert, W. A. Synthesis and Characterization of Low-Dimensional Paramagnetic Acetylide Complexes. Colorado State University, Fort Collins, 2011.
- (26) Onitsuka, K.; Fujimoto, M.; Kitajima, H.; Ohshiro, N.; Takei, F.; Takahashi, S., *Chem. Eur. J.* **2004**, *10*, 6433.

- (27) Girolami, G. S.; Wilkinson, G.; Galas, A. M. R.; Thorntonpett, M.; Hursthouse, M. B., *J. Chem. Soc., Dalton Trans.* **1985**, 1339.
- (28) Boaretto, R.; Roussel, P.; Alcock, N. W.; Kingsley, A. J.; Munslow, I. J.; Sanders, C. J.; Scott, P., *J. Organomet. Chem.* **1999**, *591*, 174.
- (29) Sheldrick, G. *SADABS*, Bruker AXS: Madison, WI, 1997.
- (30) Sheldrick, G. *SHELXTL*, 6.14; Bruker AXS: Madison, WI, 2004.
- (31) Zhang, L. P.; Tanner, P. A.; Mak, T. C. W., *Eur. J. Inorg. Chem.* **2006**, 1543.
- (32) Roussel, P.; Hitchcock, P. B.; Tinker, N.; Scott, P., *Chem. Commun.* **1996**, 2053.
- (33) Roussel, P.; Hitchcock, P. B.; Tinker, N. D.; Scott, P., *Inorg. Chem.* **1997**, *36*, 5716.
- (34) Roussel, P.; Boaretto, R.; Kingsley, A. J.; Alcock, N. W.; Scott, P., *J. Chem. Soc., Dalton Trans.* **2002**, 1423.
- (35) Field, L. D.; George, A. V.; Hambley, T. W., *Inorg. Chem.* **1990**, *29*, 4565.
- (36) Guionneau, P.; Marchivie, M.; Bravic, G.; Letard, J. F.; Chasseau, D., *J. Mater. Chem.* **2002**, *12*, 2546.
- (37) Siddall, T. H., *Theory and Applications of Molecular Paramagnetism*. Boudreaux, E. A.; Mulay, L. N., Eds. John Wiley & Sons: New York, 1976.
- (38) Edelstein, N. M.; Lander, G. H.; Morss, L. R.; Fuger, J., *The Chemistry of the Actinide and Transactinide Elements*. 2006; p 2225.
- (39) Calderazzo, F.; Dellamico, G.; Pasquali, M.; Perego, G., *Inorg. Chem.* **1978**, *17*, 474.
- (40) Spirlet, M. R.; Rebizant, J.; Apostolidis, C.; Dornberger, E.; Kanellakopulos, B.; Powietzka, B., *Poly* **1996**, *15*, 1503.

- (41) Castro-Rodriguez, I.; Olsen, K.; Gantzel, P.; Meyer, K., *Chem. Commun.* **2002**, 2764.
- (42) Jantunen, K. C.; Batchelor, R. J.; Leznoff, D. B., *Organometallics* **2004**, *23*, 2186.
- (43) Jantunen, K. C.; Haftbaradaran, F.; Katz, M. J.; Batchelor, R. J.; Schatte, G.; Leznoff, D. B., *Dalton Trans.* **2005**, 3083.
- (44) Kanellakopulos, B.; Marks, T. J.; Fischer, R. D., *Organometallics of the f-Elements*. In *NATO Advanced Study Institutes Series*, Marks, T. J.; Fischer, R. D., Eds. D. Reidel: Dordrecht, 1978.
- (45) Suski, W.; Baran, A.; Folcik, L.; Wochowski, K.; Mydlarz, T., *J. Alloy* **1992**, *181*, 249.
- (46) Karbowski, M.; Drozdzyński, J., *J. Alloy* **1998**, *271*, 863.
- (47) Almond, P. M.; Deakin, L.; Porter, M. J.; Mar, A.; Albrecht-Schmitt, T. E., *Chem. Mat.* **2000**, *12*, 3208.
- (48) Kreindlin, A. Z.; Dolgushin, F. M.; Yanovsky, A. I.; Kerzina, Z. A.; Petrovskii, P. V.; Rybinskaya, M. I., *J. Organomet. Chem.* **2000**, *616*, 106.
- (49) Kiplinger, J. L.; Pool, J. A.; Schelter, E. J.; Thompson, J. D.; Scott, B. L.; Morris, D. E., *Angew. Chem. Int. Ed.* **2006**, *45*, 2036.
- (50) Schelter, E. J.; Morris, D. E.; Scott, B. L.; Thompson, J. D.; Kiplinger, J. L., *Inorg. Chem.* **2007**, *46*, 5528.
- (51) Graves, C. R.; Vaughn, A. E.; Schelter, E. J.; Scott, B. L.; Thompson, J. D.; Morris, D. E.; Kiplinger, J. L., *Inorg. Chem.* **2008**, *47*, 11879.
- (52) Schelter, E. J.; Veauthier, J. M.; Graves, C. R.; John, K. D.; Scott, B. L.; Thompson, J. D.; Pool-Davis-Tourneir, J. A.; Morris, D. E.; Kiplinger, J. L., *Chem. Eur. J.* **2008**, *14*, 7782.
- (53) Boudreaux, E.; Mulay, L. N., *Theory and Application of Molecular Paramagnetism*. John Wiley & Sons: New York, 1976; p 510.

## Appendix

### A.1 Supporting Information for Chapter 2

X-ray structural data for compounds **2.1-2.6** are available on the Internet as a crystallographic information file at: <http://pubs.acs.org/doi/suppl/10.1021/ic901986w>

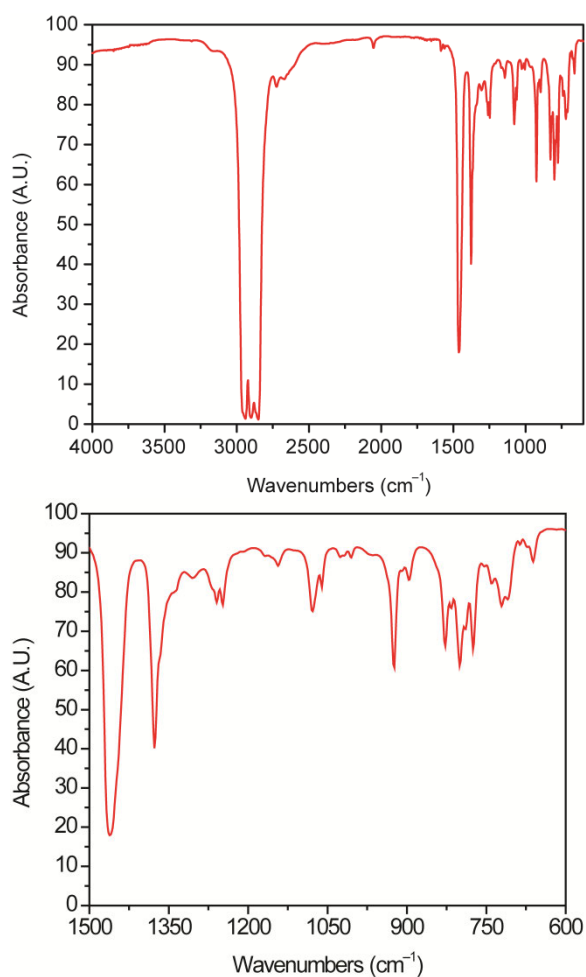


**Figure A1.1.** Full IR spectrum of **2.1** (left) and expanded (right) taken as mineral oil mulls. A minimum of 32 transients were recorded.

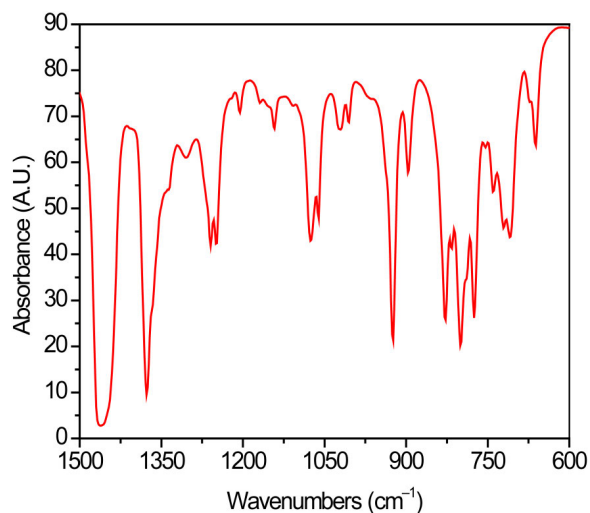


**Figure A1.2.** Expanded IR spectrum of **2.2** taken as a mineral oil mull. A minimum of 32 transients were recorded.

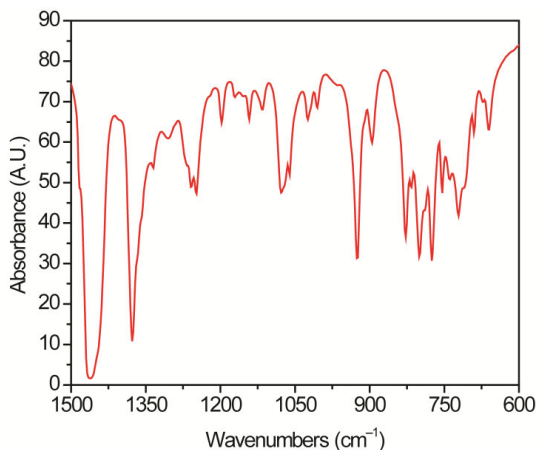


**Figure A1.3.** Expanded IR spectrum of **2.3** taken as a mineral oil mull. A minimum of 32 transients were recorded.

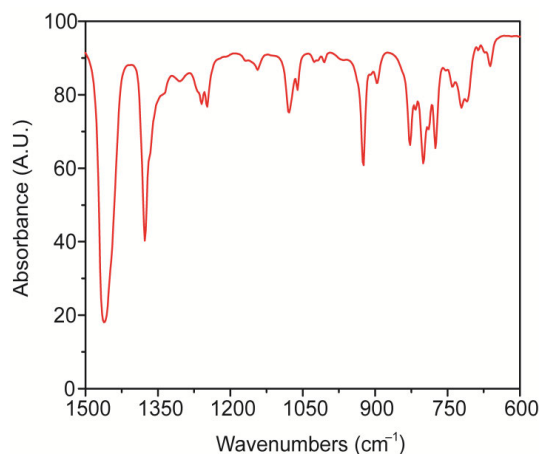


**Figure A1.4.** Expanded IR spectrum of **2.4** taken as a mineral oil mull. A minimum of 32 transients were recorded.

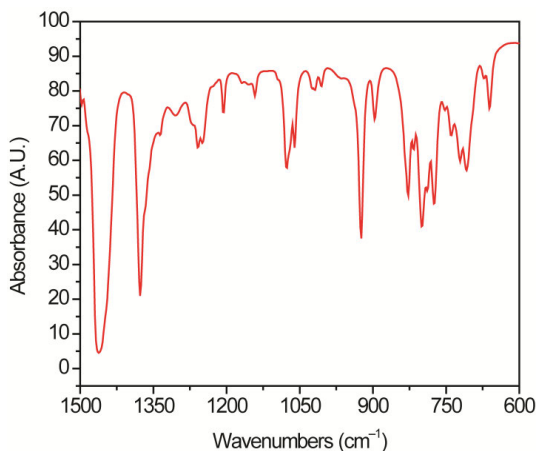


**Figure A1.5.** Expanded IR spectrum of **2.5** taken as a mineral oil mull. A minimum of 32 transients were recorded.

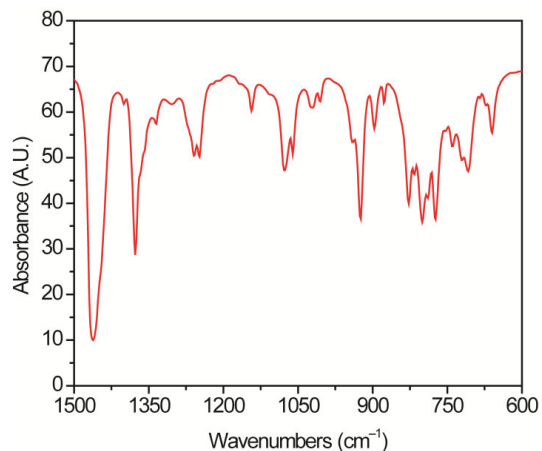


**Figure A1.6.** Expanded IR spectrum of **2.6** taken as a mineral oil mull. A minimum of 32 transients were recorded.

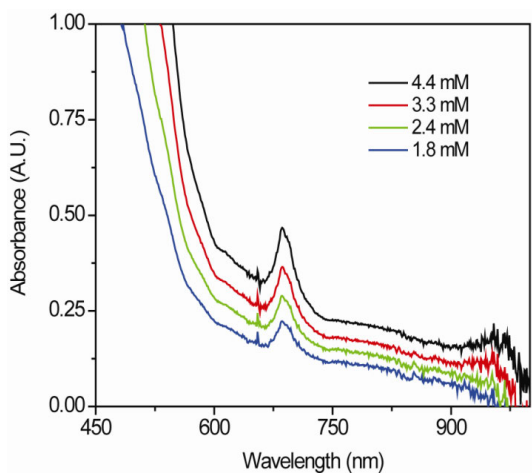


**Figure A1.7.** Quantitative UV-visible spectrum of **2.1** taken in pentane.

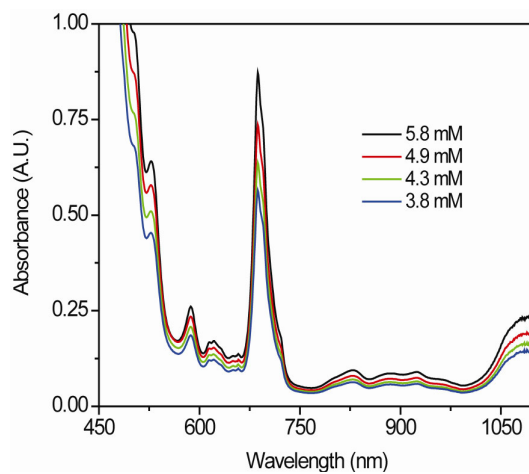


**Figure A1.11.** Quantitative UV-visible spectrum of **2.5** taken in toluene.

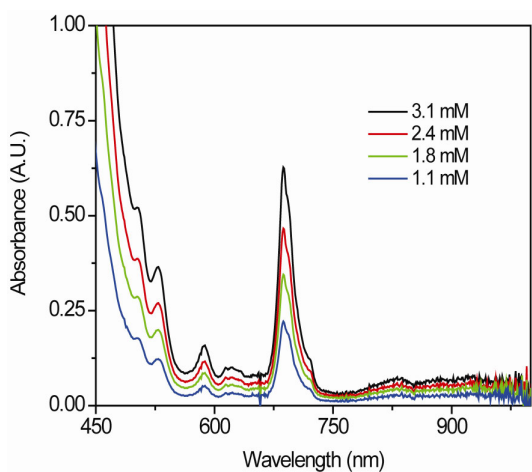


**Figure A1.8.** Quantitative UV-visible spectrum of **2.2** taken in pentane.

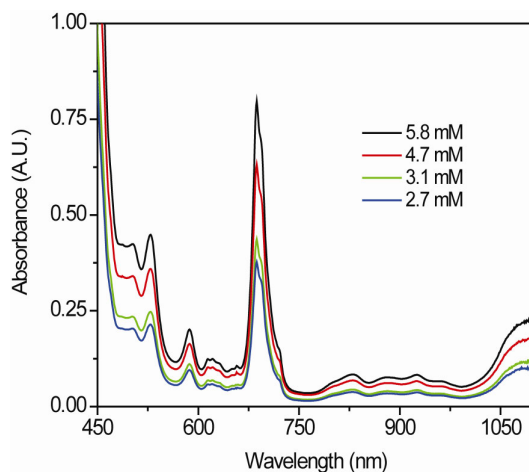


**Figure A1.10.** Quantitative UV-visible spectrum of **2.4** taken in pentane.

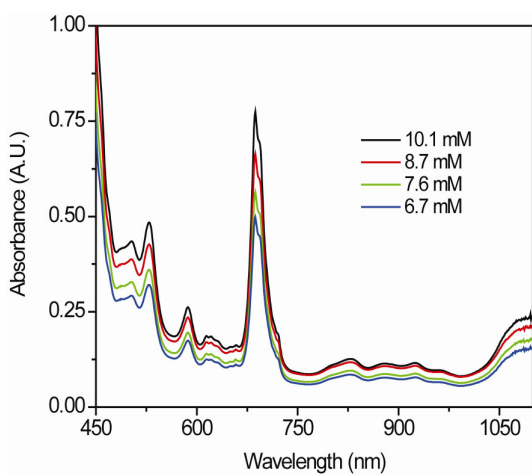


**Figure A1.9.** Quantitative UV-visible spectrum of **2.3** taken in toluene.

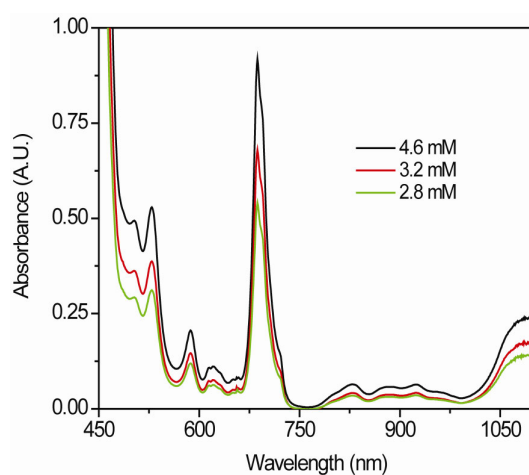


**Figure A1.12.** Quantitative UV-visible spectrum of **2.6** taken in pentane.

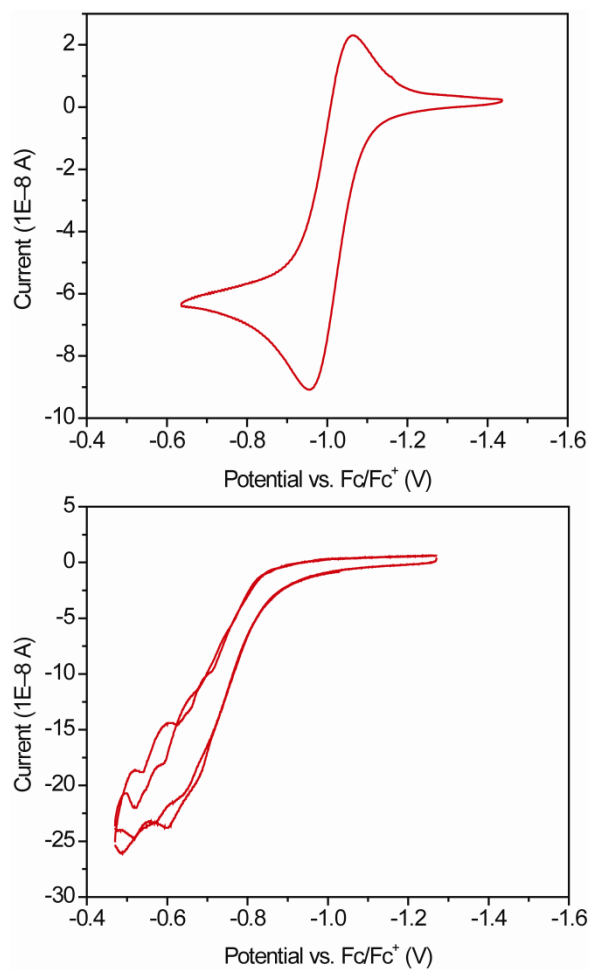


**Figure A1.13.** Electrochemical behavior for **2.3** in static solution (top) and while stirring (bottom) recorded in 0.1 M solution of [TBA][BAR<sup>F</sup><sub>4</sub>] in *o*-difluorobenzene at ambient temperature with a 0.250 mm diameter platinum wire microelectrode. The reference and auxiliary electrodes are described in the main text.

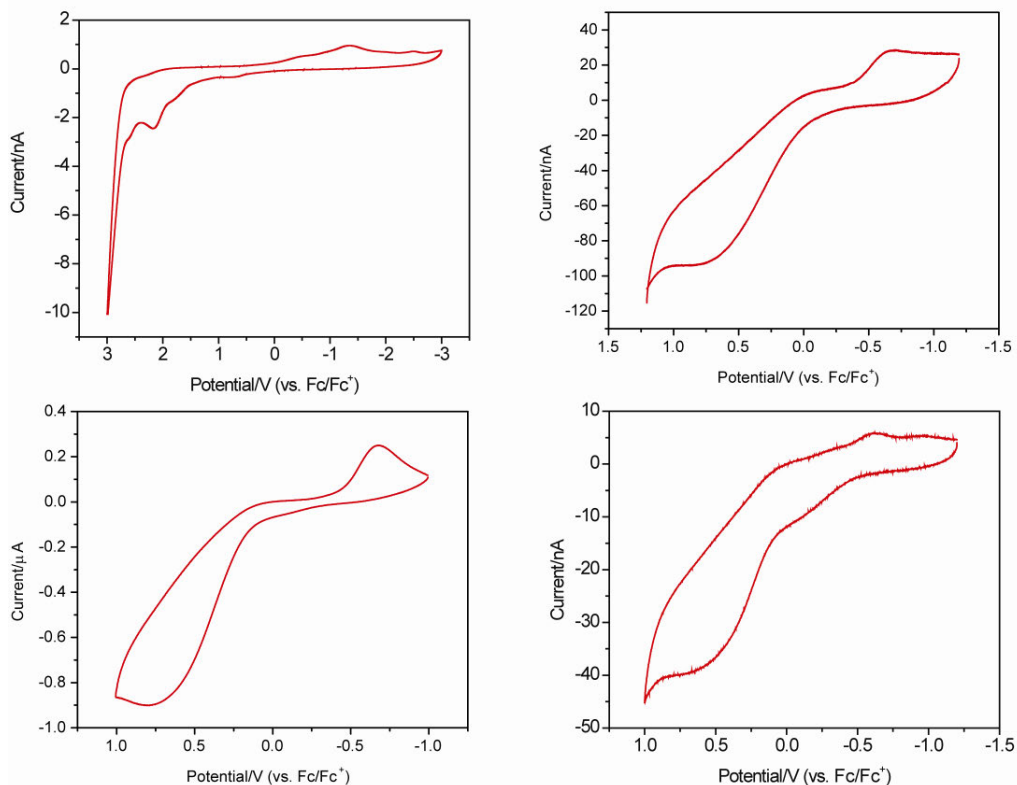


**Figure A1.14.** Electrochemical behavior for **2.2**, **2.4**, **2.5**, and **2.6** in static solution recorded in 0.1 M solution of [TBA][BAR<sub>4</sub><sup>F</sup>] in *o*-difluorobenzene (**2.2** in dichloromethane) at ambient temperature with a 0.250 mm diameter platinum wire microelectrode. The reference and auxiliary electrodes are described in the main text.

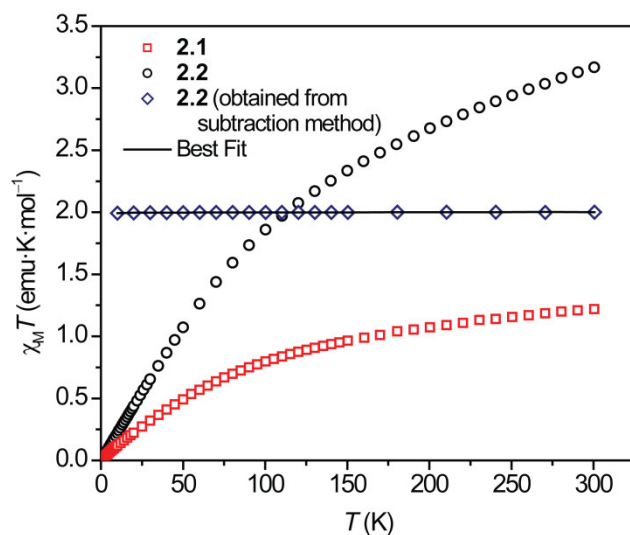


**Figure A1.15.** Temperature dependence of the magnetic susceptibility and fit for compound **2.2** obtained at a measuring field of 1000 G; see text for details of the fitting procedures.

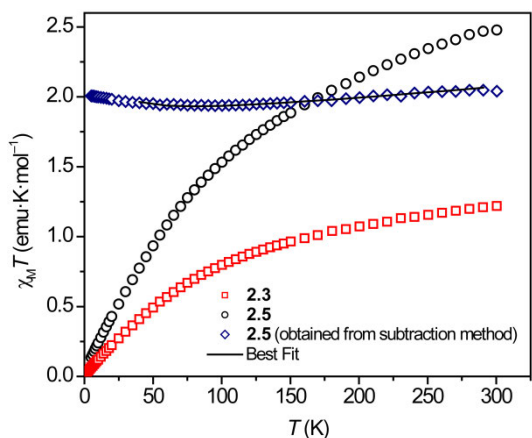


**Figure A1.16.** Temperature dependence of the magnetic susceptibility and fit for compound **2.5** obtained at a measuring field of 1000 G; see text for details of the fitting procedures.

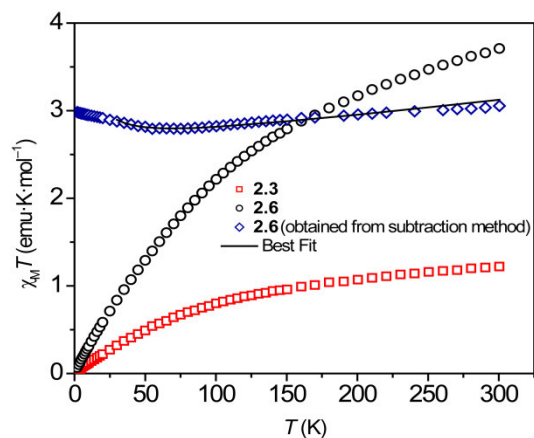


**Figure A1.17.** Temperature dependence of the magnetic susceptibility and fit for compound **2.6** obtained at a measuring field of 1000 G; see text for details of the fitting procedures.

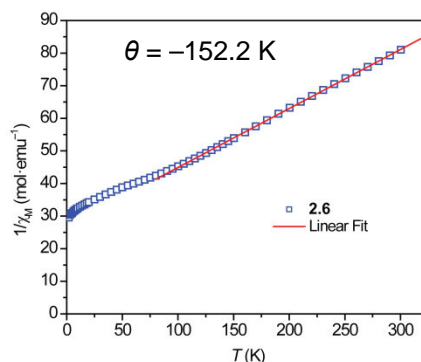
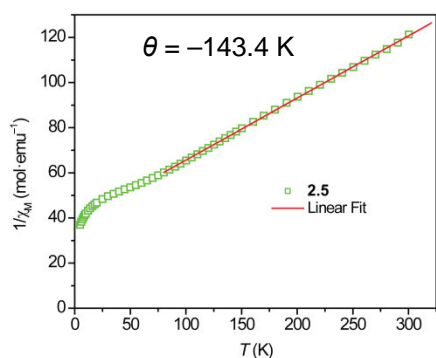
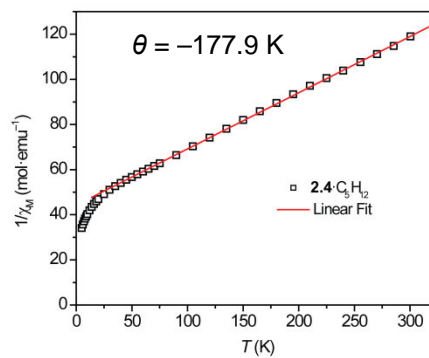
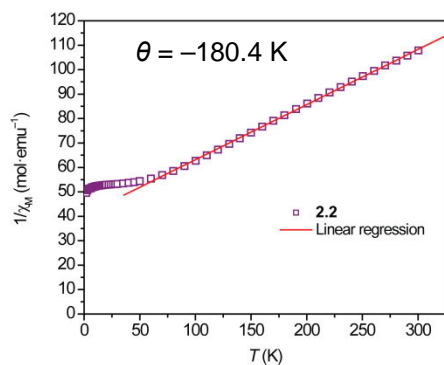


**Figure A1.18.** Temperature dependence of the inverse susceptibility for compounds **2.2** and **2.4–2.6** obtained at a measuring field of 1000 G. Linear regression of the data for **2.2** and **2.4–2.6** (above 50 K) yields  $\theta$  values of  $-180.4$ ,  $-177.9$ ,  $-143.4$ , and  $-152.2$  K with Curie constants ( $C$ )  $5.09$ ,  $4.02$ ,  $3.82$ , and  $5.59$   $\text{cm}^3 \cdot \text{K} \cdot \text{mol}^{-1}$ , for **2.2**, **2.4**, **2.5**, and **2.6**, respectively. For the Curie-Weiss law to be operative it is assumed that the magnetic centers are well isolated and that the ground state is thermally isolated. While we believe the first assumption is valid for these systems (see magnetism discussion) it is not clear that the ground states in these complexes are well isolated.

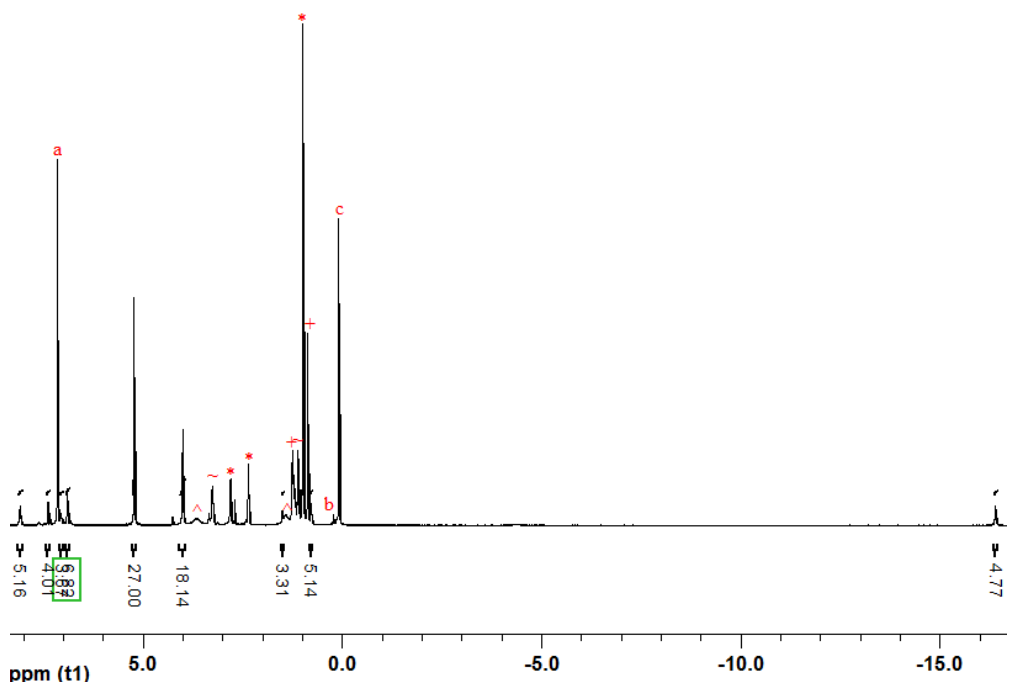


**Figure A1.19.**  $^1\text{H}$  NMR spectrum of  $[(\text{NN}'_3)\text{U}(\text{CCPh})_2(\text{Li}\cdot\text{THF})]$  (**2.1**) obtained in  $\text{C}_6\text{D}_6$  at ambient temperature with a 500 MHz spectrometer. The asterisk (\*) indicates impurities that are present from the synthesis of  $[\text{Li}_3(\text{NN}'_3)(\text{THF})_3]$ , while (a) is  $\text{C}_6\text{D}_6$ , (b) is silicone grease, (c) is TMS, (^) indicates resonances due to THF, (+) pentane, and (~) diethyl ether.

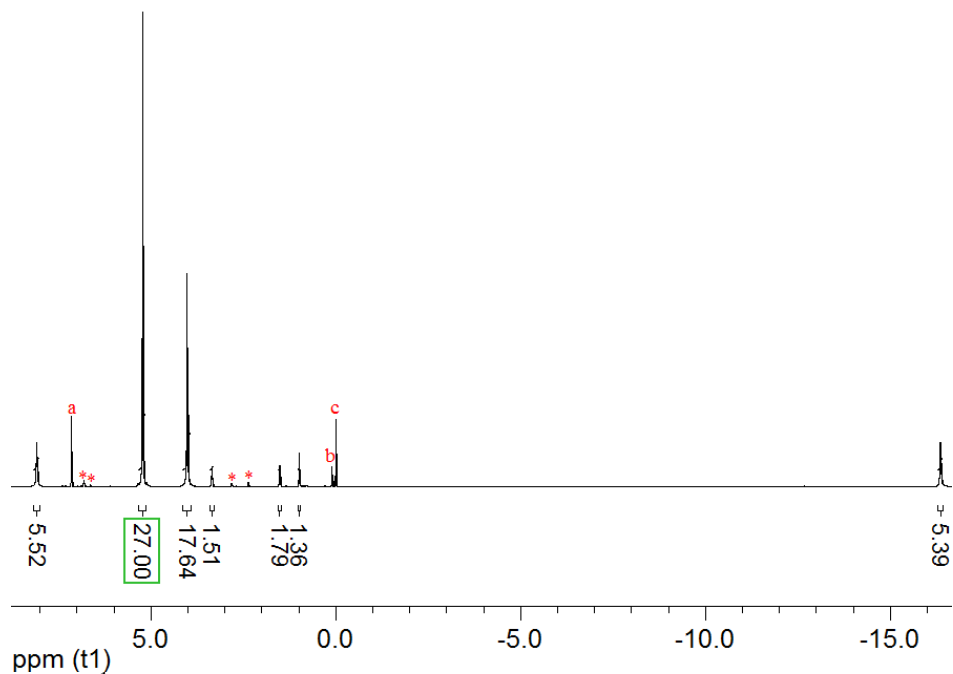


**Figure A1.20.**  $^1\text{H}$  NMR spectrum of  $[(\text{NN}'_3)\text{U}(\text{CCPh})]$  (**2.3**) obtained in  $\text{C}_6\text{D}_6$  at ambient temperature with a 500 MHz spectrometer. The asterisk (\*) indicates impurities that are present from the synthesis of  $[\text{Li}_3(\text{NN}'_3)(\text{THF})_3]$ , while (a) is  $\text{C}_6\text{D}_6$ , (b) is silicone grease, and (c) is TMS.

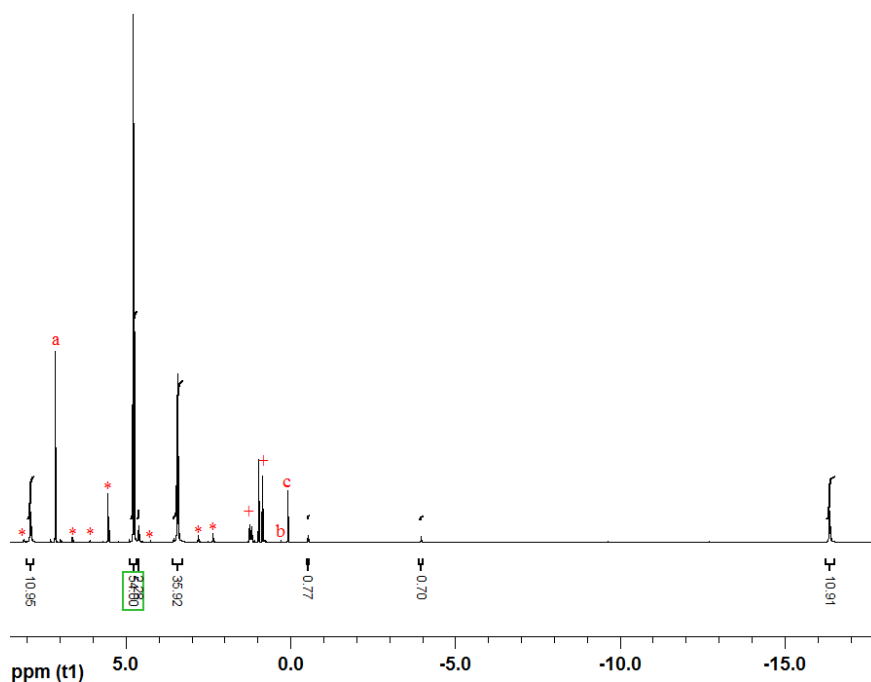


**Figure A1.21.**  $^1\text{H}$  NMR spectrum of  $[(\text{NN}'_3)_2\text{U}_2(m\text{-DEB})]$  (**2.4**) obtained in  $\text{C}_6\text{D}_6$  at ambient temperature with a 500 MHz spectrometer. The asterisk (\*) indicates impurities that are present from the synthesis of  $[\text{Li}_3(\text{NN}'_3)(\text{THF})_3]$ ; (a) is  $\text{C}_6\text{D}_6$ , (b) is silicone grease, (c) is TMS, and (+) indicates resonances due to pentane.

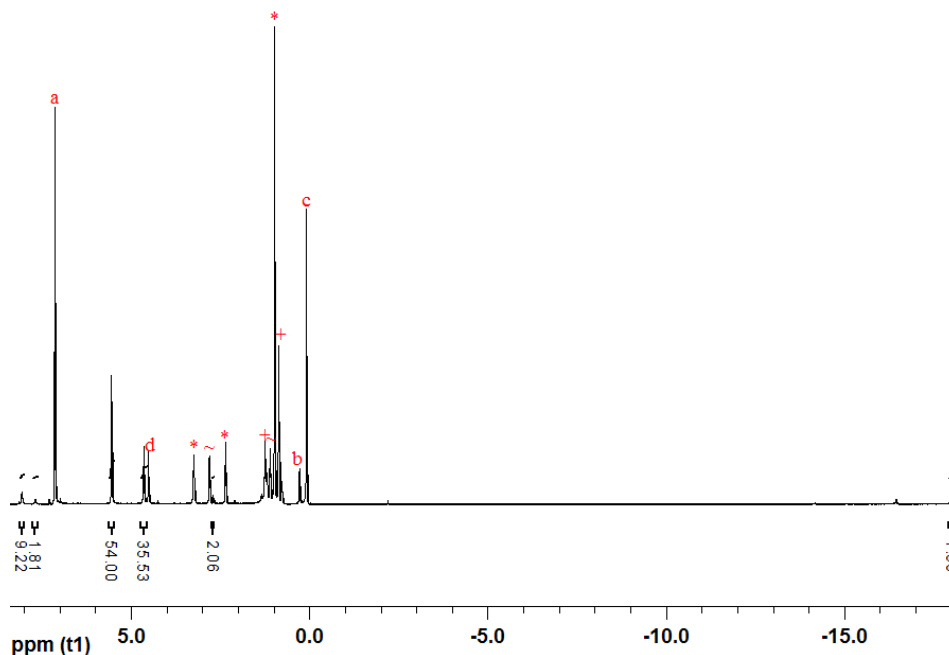


**Figure A1.22.**  $^1\text{H}$  NMR spectrum of  $[(\text{NN}'_3)_2\text{U}_2(p\text{-DEB})]$  (**2.5**) obtained in  $\text{C}_6\text{D}_6$  at ambient temperature with a 500 MHz spectrometer. The asterisk (\*) indicates impurities that are present from the synthesis of  $[\text{Li}_3(\text{NN}'_3)(\text{THF})_3]$ ; (a) is  $\text{C}_6\text{D}_6$ , (b) is silicone grease, (c) is TMS, (+) indicates resonances due to pentane, and (~) diethyl ether.

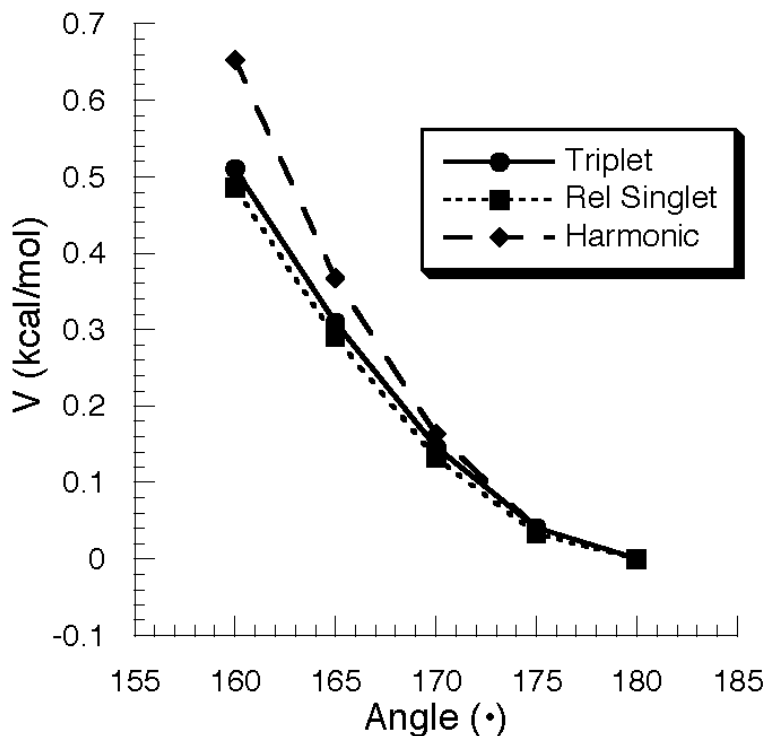


**Figure A1.23.** DFT results for U–CC bending in model complex of **2.3**. Upon bending from linearity, the ground state triplet (Triplet) and lowest excited state singlet (Rel Singlet) energies do not follow that predicted for a harmonic oscillator (Harmonic).

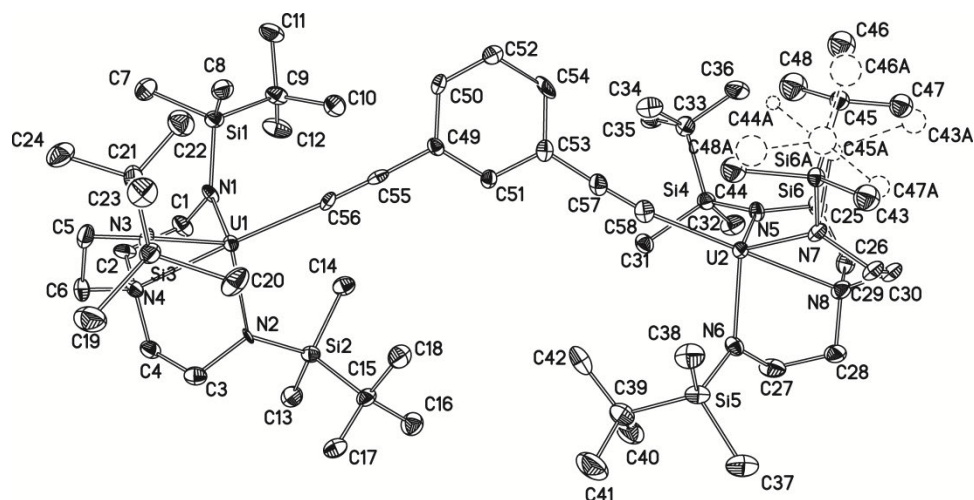


**Figure A1.24.** The U-containing complex in the crystal structure of **2.4**·C<sub>5</sub>H<sub>12</sub> at 100 K rendered with 40% ellipsoids. The hydrogen atoms and solvent molecules have been omitted for clarity. One of the Si'BuMe<sub>2</sub> groups is disordered over two positions and the disordered part appears as dashed circles in the figure.

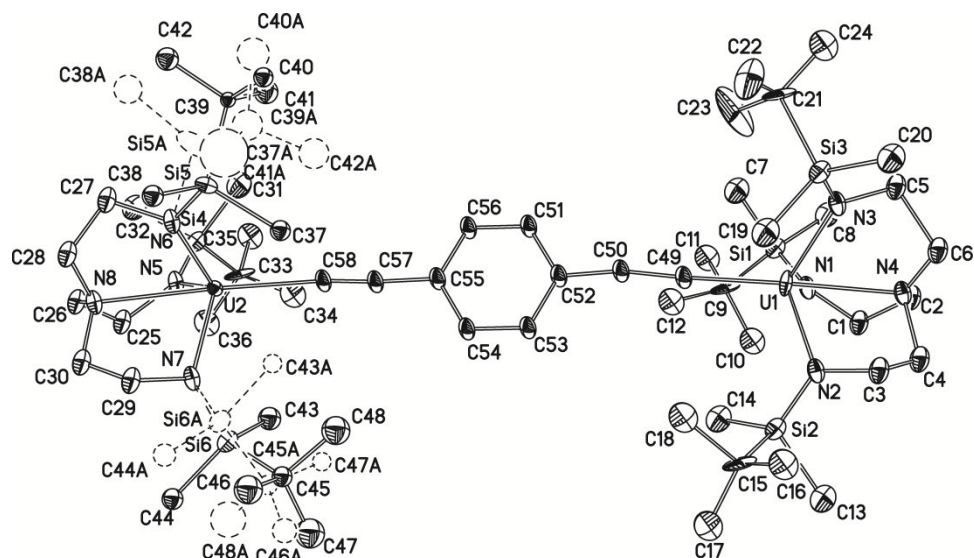


**Figure A1.25.** The U-containing complex in the crystal structure of **2.5**-C<sub>5</sub>H<sub>12</sub> at 100 K rendered with 40% ellipsoids. The hydrogen atoms and solvent molecules have been omitted for clarity. Two of the Si<sup>i</sup>BuMe<sub>2</sub> groups are disordered over two positions and the disordered portions appear as dashed circles in the figure.

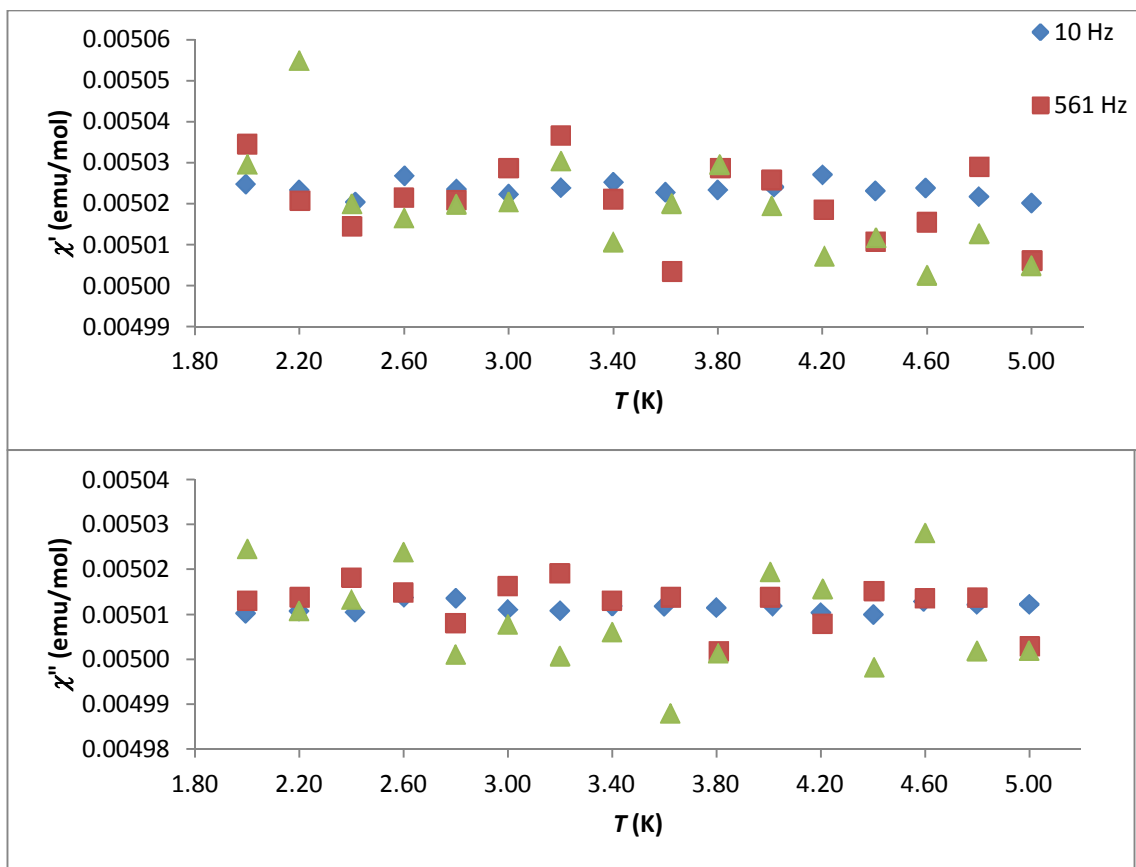


**Figure A1.26.** Temperature dependence of the in-phase ( $\chi'$ , top) and out-of-phase ( $\chi''$ , bottom) components of the AC susceptibility under 1000 Oe applied DC field collected at various AC frequencies for **2.4** encased in Eicosane.

**Table A1.1.** Cartesian coordinates for the calculated complex  $[\text{N}(\text{CH}_2\text{CH}_2\text{NH})_3\text{U}(\text{CCH})]$ , a model for the mononuclear U(IV) complex **2.3**.

atom	Z	x	y	z
1	92	0.692713	-.017371	.005437
2	6	-1.502371	2.436405	-.436252
3	1	-1.846102	2.528885	-1.481686
4	1	-1.679755	3.422159	.023252
5	6	-2.370199	1.417050	.313556
6	1	-2.212648	1.557652	1.386205
7	1	-3.441655	1.581824	.107399
8	6	-1.567744	-.821580	2.303169
9	1	-1.905745	.039561	2.906273
10	1	-1.774816	-1.714107	2.916113
11	6	-2.411116	-.939069	1.027520
12	1	-2.266444	-1.940701	.614481
13	1	-3.484855	-.821699	1.252462
14	6	-1.568788	-1.563543	-1.885308
15	1	-1.946940	-2.506110	-1.451366
16	1	-1.747933	-1.643125	-2.970112
17	6	-2.392432	-.377273	-1.370468
18	1	-2.209727	.476798	-2.028060
19	1	-3.472310	-.601395	-1.405206
20	1	5.447351	.039406	-.022039
21	6	4.378143	.029959	-.018227
22	6	3.149077	.019785	-.014017
23	7	-.107000	2.026655	-.352601
24	7	-.162865	-.714287	1.934426
25	7	-.165671	-1.337529	-1.566375
26	7	-1.974576	.026518	-.007610
27	1	.518568	2.795295	-.601758
28	1	.443117	-.840437	2.748610
29	1	.433634	-1.995801	-2.069465

**Table A1.2.** Cartesian coordinates for the calculated complex **2.4**, a model for the *m*-DEB-bridged dinuclear U(IV) complex **2.4**.

atom	Z	x	y	z
1	92	5.659405	.012521	.040221
2	6	6.798505	-2.236255	-2.114240
3	1	7.428573	-1.791858	-2.905317
4	1	6.434825	-3.191730	-2.526059
5	6	7.653014	-2.570528	-.884500
6	1	7.087247	-3.261615	-.253728
7	1	8.588637	-3.075833	-1.179363
8	6	7.066838	-2.143767	2.140417
9	1	6.806184	-3.191086	1.904964
10	1	7.359049	-2.141840	3.202877
11	6	8.295213	-1.709691	1.330266
12	1	8.702842	-.804675	1.788354
13	1	9.082092	-2.482850	1.356683
14	6	8.831780	.960506	-.163797
15	1	9.329287	1.033262	.819654
16	1	9.416524	1.603706	-.841137
17	6	8.931722	-.473250	-.701814
18	1	8.708411	-.452151	-1.771910
19	1	9.953762	-.871236	-.580698
20	6	2.470498	1.852464	.000538
21	6	3.541902	1.237470	.009407
22	7	5.709239	-1.354056	-1.716922
23	7	5.967439	-1.227323	1.865325
24	7	7.429431	1.351542	-.100492
25	7	7.935843	-1.367698	-.066270
26	1	4.977534	-1.326901	-2.429140
27	1	5.254259	-1.279200	2.595307
28	1	7.331672	2.367007	-.044637
29	6	1.231493	2.563508	-.010342
30	6	.008314	1.869105	-.002250
31	6	1.210734	3.974096	-.029145
32	1	.012752	.784482	.012155
33	6	-1.220149	2.553959	-.012388
34	1	2.151701	4.515395	-.035525
35	6	-1.210806	3.964634	-.031357
36	6	-.002706	4.658789	-.039574
37	1	-2.156019	4.498475	-.039498
38	1	-.007011	5.745774	-.054255
39	92	-5.637659	-.020969	.032996
40	6	-8.084811	-.067504	-2.216082
41	1	-8.015445	-.899738	-2.938965
42	1	-8.700417	.703123	-2.708377
43	6	-8.842164	-.519755	-.960531

**Table A1.2 continued.**

atom	Z	x	y	z
44	1	-9.158972	.372099	-.413229
45	1	-9.749561	-1.087199	-1.229647
46	6	-8.284623	.024684	2.038132
47	1	-9.067210	.736600	1.720815
48	1	-8.449661	-.137682	3.115958
49	6	-8.483914	-1.326046	1.338882
50	1	-7.905117	-2.079057	1.880013
51	1	-9.543593	-1.632531	1.368665
52	6	-6.431168	-3.256872	.067365
53	1	-6.665534	-3.656504	1.070092
54	1	-6.136723	-4.129338	-.539138
55	6	-7.690954	-2.660089	-.572247
56	1	-7.515082	-2.560978	-1.646581
57	1	-8.558945	-3.327535	-.434981
58	6	-2.453791	1.833656	-.003330
59	6	-3.521928	1.213094	.003990
60	7	-6.773784	.432559	-1.826639
61	7	-6.944843	.517356	1.748675
62	7	-5.397558	-2.232639	.112982
63	7	-7.974442	-1.303013	-.051510
64	1	-6.342685	.965794	-2.584238
65	1 -	6.702077	1.302215	2.356985
66	1	-4.489179	-2.639506	.347524

**Table A1.3.** Cartesian coordinates for the calculated complex **2.5**, a model for the *p*-DEB-bridged dinuclear U(IV) complex **2.5**.

atom	Z	x	y	z
1	92	6.532378	-.019749	-.030162
2	6	8.673137	1.341941	2.116421
3	1	9.027916	.646913	2.898087
4	1	8.821209	2.353432	2.528835
5	6	9.556337	1.227406	.866953
6	1	9.386307	2.111168	.246202
7	1	10.625492	1.210863	1.139605
8	6	8.802122	1.177795	-2.137870
9	1	9.123719	2.207860	-1.902462
10	1	9.026440	1.033324	-3.207484
11	6	9.649712	.167352	-1.354611
12	1	9.524304	-.814738	-1.817931
13	1	10.720780	.427952	-1.405620
14	6	8.837956	-2.419848	.130765
15	1	9.240275	-2.729159	-.850294
16	1	9.019216	-3.270645	.808197
17	6	9.631128	-1.225177	.674932
18	1	9.431840	-1.140872	1.746455
19	1	10.716298	-1.379559	.547463
20	6	2.846697	-.019357	-.005320
21	6	4.082873	-.018732	-.007894
22	7	7.287519	1.090113	1.745439
23	7	7.395515	.958460	-1.829952
24	7	7.430547	-2.054590	.055724
25	7	9.196917	.045475	.050238
26	1	6.647815	1.397060	2.480752
27	1	6.792527	1.464436	-2.482185
28	1	6.847275	-2.877769	-.111174
29	6	1.421801	-.019127	-.001958
30	6	.694215	1.191340	-.006301
31	6	.693338	-1.229023	.005031
32	1	1.239400	2.130646	-.011387
33	6	-.693088	1.191787	-.005223
34	1	1.237735	-2.168787	.008838
35	1	-1.237544	2.131514	-.009410
36	6	-1.421615	-.018062	.001672
37	6	-.693975	-1.228463	.007539
38	1	-1.239147	-2.167779	.013283
39	92	-6.532323	-.034081	.004473
40	6	-8.674096	2.497693	-.222930
41	1	-9.026774	2.698326	-1.250239
42	1	-8.824050	3.438451	.331705
43	6	-9.558120	1.433621	.440834

**Table A1.3 continued.**

atom	Z	x	y	z
44	1	-9.390245	1.475187	1.520370
45	1	-10.627044	1.639864	.260253
46	6	-8.811522	-.987599	2.223895
47	1	-9.135650	-.176429	2.899784
48	1	-9.038258	-1.926231	2.755769
49	6	-9.654193	-.975768	.942140
50	1	-9.528159	-1.939461	.441886
51	1	-10.726021	-.857418	1.176420
52	6	-8.828850	-1.361935	-2.011590
53	1	-9.233991	-2.329317	-1.665066
54	1	-9.004292	-1.338647	-3.099835
55	6	-9.623839	-.204060	-1.395439
56	1	-9.418844	.699095	-1.976144
57	1	-10.709115	-.396847	-1.447440
58	6	-2.846565	-.017517	.001631
59	6	-4.082747	-.016749	.000566
60	7	-7.288312	2.050638	-.195319
61	7	-7.403396	-.875577	1.868648
62	7	-7.423254	-1.201288	-1.668042
63	7	-9.196854	.068043	-.003763
64	1	-6.648714	2.822196	-.394619
65	1	-6.803929	-1.084342	2.669959
66	1	-6.836854	-1.831961	-2.219437

### Full Citation for Reference 85:

Frisch, M. J.; Trucks, G. W.; Schlegel, H. B.; Scuseria, G. E.; Robb, M. A.; Cheeseman, J. R.; Montgomery, J., J. A.; Vreven, T.; Kudin, K. N.; Burant, J. C.; Millam, J. M.; Iyengar, S. S.; Tomasi, J.; Barone, V.; Mennucci, B.; Cossi, M.; Scalmani, G.; Rega, N.; Petersson, G. A.; Nakatsuji, H.; Hada, M.; Ehara, M.; Toyota, K.; Fukuda, R.; Hasegawa, J.; Ishida, M.; Nakajima, T.; Honda, Y.; Kitao, O.; Nakai, H.; Klene, M.; Li, X.; Knox, J. E.; Hratchian, H. P.; Cross, J. B.; Bakken, V.; Adamo, C.; Jaramillo, J.; Gomperts, R.; Stratmann, R. E.; Yazyev, O.; Austin, A. J.; Cammi, R.; Pomelli, C.; Ochterski, J. W.; Ayala, P. Y.; Morokuma, G. A.; Voth, G. A.; Salvador, P.; Dannenberg, J. J.; Zakrzewski, V. G.; Dapprich, S.; Daniels, A. D.; Strain, M. C.; Farkas, O.; Malick, D. K.; Rabuck, A. D.; Raghavachari, K.; Foresman, J. B.; Ortiz, J. V.; Cui, Q.; Baboul, A. G.; Clifford, S.; Cioslowski, J.; Stefanov, B. B.; Liu, G.; Liashenko, A.; Piskorz, P.; Komaromi, I.; Martin, R. L.; Fox, D. J.; Keith, T.; Al-Laham, M. A.; Peng, C. Y.; Nanayakkara, A.; Challacombe, M.; Gill, P. M. W.; Johnson, B.; Chen, W.; Wong, M. W.; Gonzalez, C.; Pople, J. A. *Gaussian 03*, Gaussian, Inc.: Wallingford, CT, 2004.

### Discussion of problems with solving the structure of [(NN'<sub>3</sub>)<sub>3</sub>U<sub>3</sub>(TEB)] (2.6, dataset reference number msn270):

Using a Patterson map to solve the position of the uranium atoms works quite well. Structural refinement from there on is quite tedious. Similar to the structures of **2.4** and **2.5** several (NN'<sub>3</sub>) fragments are disordered over several positions. An attempt was made to model the disorder but due to the scattering power of the uranium atoms subsequent refinement via electron density maps is quite difficult. As a result, no publishable solution was obtained but a current version of the cif file is presented here.

```
data_msn170
      _atom_type_scatter_dispers
      _atom_type_scatter_imag
      _atom_type_scatter_source
      'C' 'C' 0.0033 0.0016
      'International Tables Vol C Tables
      4.2.6.8 and 6.1.1.4'
      ;
      'H' 'H' 0.0000 0.0000
      'International Tables Vol C Tables
      4.2.6.8 and 6.1.1.4'
      ;
      _chemical_name_common      ?
      _chemical_melting_point    ?
      _chemical_formula_moiety   ?
      _chemical_formula_sum
      'C84 H174 N12 Si9 U3'
      _chemical_formula_weight
      2319.25
      'Si' 'Si' 0.0817 0.0704
      'International Tables Vol C Tables
      4.2.6.8 and 6.1.1.4'
      'U' 'U' -9.6767 9.6646
      'International Tables Vol C Tables
      4.2.6.8 and 6.1.1.4'
loop_
      _atom_type_symbol
      _atom_type_description
      _atom_type_scatter_dispers
      _atom_type_scatter_real
      _symmetry_cell_setting      ?
```

_symmetry_space_group_name_H-M	?	_diffrn_radiation_wavelength	0.71073
loop_		_diffrn_radiation_type	MoK\alpha
_symmetry_equiv_pos_as_xyz		_diffrn_radiation_source	'fine-focus sealed tube'
'x, y, z'		_diffrn_radiation_monochromator	graphite
'-x+1/2, -y, z+1/2'		_diffrn_measurement_device_type	?
'-x, y+1/2, -z+1/2'		_diffrn_measurement_method	?
'x+1/2, -y+1/2, -z'		_diffrn_detector_area_resol_mean	?
_cell_length_a	18.5219(7)	_diffrn_reflns_number	63662
_cell_length_b	22.2851(8)	_diffrn_reflns_av_R_equivalents	0.0683
_cell_length_c	28.0242(10)	_diffrn_reflns_av_sigmaI/netI	0.0561
_cell_angle_alpha	90.00	_diffrn_reflns_limit_h_min	-18
_cell_angle_beta	90.00	_diffrn_reflns_limit_h_max	16
_cell_angle_gamma	90.00	_diffrn_reflns_limit_k_min	-22
_cell_volume	11567.3(7)	_diffrn_reflns_limit_k_max	22
_cell_formula_units_Z	4	_diffrn_reflns_limit_l_min	-28
_cell_measurement_temperature	296(2)	_diffrn_reflns_limit_l_max	28
_cell_measurement_reflns_used	?	_diffrn_reflns_theta_min	1.97
_cell_measurement_theta_min	?	_diffrn_reflns_theta_max	20.82
_cell_measurement_theta_max	?	_reflns_number_total	12095
_exptl_crystal_description	?	_reflns_number_gt	9870
_exptl_crystal_colour	?	_reflns_threshold_expression	>2sigma(I)
_exptl_crystal_size_max	?	_computing_data_collection	?
_exptl_crystal_size_mid	?	_computing_cell_refinement	?
_exptl_crystal_size_min	?	_computing_data_reduction	?
_exptl_crystal_density_meas	?	_computing_structure_solution	'SHELXS-97 (Sheldrick, 2008)'
_exptl_crystal_density_diffrn	1.332	_computing_structure_refinement	'SHELXL-97 (Sheldrick, 2008)'
_exptl_crystal_density_method	'not measured'	_computing_molecular_graphics	?
_exptl_crystal_F_000	4656	_computing_publication_material	?
_exptl_absorpt_coefficient_mu	4.323	_refine_special_details	;
_exptl_absorpt_correction_type	?		Refinement of F <sup>2</sup> against ALL reflections. The weighted R-factor wR and
_exptl_absorpt_correction_T_min	?		goodness of fit S are based on F <sup>2</sup> , conventional R-factors R are based
_exptl_absorpt_correction_T_max	?		on F, with F set to zero for negative F <sup>2</sup> . The threshold expression of
_exptl_absorpt_process_details	?		
_exptl_special_details			
;			
?			
;			
_diffrn_ambient_temperature	296(2)		

$F^2 > 2\sigma(F^2)$  is used only for calculating R-factors(gt) etc. and is not relevant to the choice of reflections for refinement. R-factors based on  $F^2$  are statistically about twice as large as those based on F, and R-factors based on ALL data will be even larger.

;

```

_refine_ls_structure_factor_coef Fsqd
_refine_ls_matrix_type full
_refine_ls_weighting_scheme calc
_refine_ls_weighting_details
'calc
  w=1/[s^2*(Fo^2)+(0.1000P)^2+0.4780P] where P=(Fo^2+2Fc^2)/3'
_atom_sites_solution_primary direct
_atom_sites_solution_secondary difmap
_atom_sites_solution_hydrogens geom
_refine_ls_hydrogen_treatment mixed
_refine_ls_extinction_method none
_refine_ls_extinction_coef ?
_refine_ls_abs_structure_details
'Flack H D (1983), Acta Cryst. A39,
  876-881'
_refine_ls_abs_structure_Flack 0.48(4)
_refine_ls_number_reflns 12095
_refine_ls_number_parameters 337
_refine_ls_number_restraints 3
_refine_ls_R_factor_all 0.2170
_refine_ls_R_factor_gt 0.1873
_refine_ls_wR_factor_ref 0.4763
_refine_ls_wR_factor_gt 0.4623
_refine_ls_goodness_of_fit_ref 3.465
_refine_ls_restrained_S_all 3.464
_refine_ls_shift/su_max 11.759
_refine_ls_shift/su_mean 0.494

loop_
  _atom_site_label
  _atom_site_type_symbol
  _atom_site_fract_x
  _atom_site_fract_y
  _atom_site_fract_z

```

```

_atom_site_U_iso_or_equiv
_atom_site_adp_type
_atom_site_occupancy
_atom_site_symmetry_multiplicity
_atom_site_calc_flag
_atom_site_refinement_flags
_atom_site_disorder_assembly
_atom_site_disorder_group
U1 U 0.32608(9) 0.65501(8) 0.00312(7)
  0.0384(6) Uiso 1 1 d . . .
U2 U 0.4977(3) 1.06791(17) -
  0.19052(13) 0.0959(16) Uiso 1 1 d .
  B .
U3 U 0.49836(18) 1.07718(11)
  0.18128(9) 0.0751(9) Uiso 1 1 d . . .
N1 N 0.2535(17) 0.6505(16) -
  0.0621(11) 0.021(8) Uiso 1 1 d . . .
N2 N 0.244(2) 0.554(2) 0.0022(19)
  0.071(12) Uiso 1 1 d . A .
N4 N 0.3977(14) 0.5778(12) 0.0072(11)
  0.011(7) Uiso 1 1 d . A .
N5 N 0.471(3) 1.157(3) 0.2508(17)
  0.082(15) Uiso 1 1 d . . .
N6 N 0.561(4) 1.137(4) 0.171(3) 0.15(3)
  Uiso 1 1 d . . .
N7 N 0.379(2) 1.112(2) 0.1742(16)
  0.055(13) Uiso 1 1 d . . .
N8 N 0.508(3) 1.038(2) 0.2548(17)
  0.060(14) Uiso 1 1 d . . .
N9 N 0.4994(7) 1.0430(5) -0.2042(4) -
  0.397(3) Uiso 1 1 d . . .
N10 N 0.464(3) 1.133(2) -0.2631(18)
  0.065(16) Uiso 1 1 d . B .
N12 N 0.385(4) 1.071(3) -0.190(2)
  0.11(2) Uiso 1 1 d . B .
N20 N 0.557(3) 1.140(3) -0.197(2)
  0.092(19) Uiso 1 1 d . . .
N100 N 0.258(7) 0.646(6) 0.092(4)
  0.23(5) Uiso 1 1 d . . .
Si1 Si 0.3140(12) 1.0624(10) -0.1696(8)
  0.090(6) Uiso 1 1 d . . .
Si2 Si 0.548(2) 0.980(2) -0.2810(16)
  0.190(17) Uiso 1 1 d . . .
Si4 Si 0.639(5) 1.182(4) 0.141(3)
  0.35(4) Uiso 1 1 d . . .

```

Si5 Si 0.5805(12) 0.9911(10) 0.2638(8) 0.088(6) Uiso 1 1 d . . .	C17 C 0.397(5) 1.179(4) 0.217(3) 0.14(3) Uiso 1 1 d . . .
Si6 Si 0.3229(17) 1.0732(14) 0.1526(10) 0.130(9) Uiso 1 1 d . . .	C18 C 0.360(3) 1.166(2) 0.1860(18) 0.056(14) Uiso 1 1 d . . .
Si7 Si 0.4896(16) 0.5738(11) 0.0282(8) 0.103(7) Uiso 1 1 d . A 1	C20 C 0.470(3) 1.074(3) 0.291(2) 0.075(19) Uiso 1 1 d . . .
Si7A Si 0.484(2) 0.5767(15) -0.0275(12) 0.160(12) Uiso 1 1 d . A 2	C23 C 0.192(5) 0.622(4) -0.052(3) 0.13(3) Uiso 1 1 d . . .
Si8 Si 0.2729(12) 0.6730(10) -0.1133(8) 0.088(6) Uiso 1 1 d . . .	C24 C 0.205(3) 0.547(2) -0.0393(18) 0.047(14) Uiso 1 1 d . A .
Si10 Si 0.2240(12) 0.7206(11) 0.0928(8) 0.086(6) Uiso 1 1 d . A .	C26 C 0.198(5) 0.566(4) 0.035(3) 0.11(3) Uiso 1 1 d . . .
Si20 Si 0.5893(18) 1.1880(15) - 0.1195(11) 0.136(10) Uiso 1 1 d . B 3	C28 C 0.370(4) 0.520(3) -0.015(2) 0.09(2) Uiso 1 1 d . . .
Si20 Si 0.641(2) 1.149(2) -0.1740(15) 0.192(14) Uiso 1 1 d . B 4	C29 C 0.299(3) 0.501(3) 0.011(2) 0.056(16) Uiso 1 1 d . A .
C1 C 0.4603(15) 0.8540(9) 0.0005(11) 0.038(11) Uiso 1 1 d GD A .	C32 C 0.563(3) 0.584(2) -0.0155(18) 0.050(15) Uiso 1 1 d . . .
C2 C 0.476(2) 0.8804(15) -0.0432(8) 0.09(2) Uiso 1 1 d GD . .	C33 C 0.635(4) 0.566(3) -0.004(3) 0.11(2) Uiso 1 1 d . A .
C3 C 0.503(2) 0.9384(15) -0.0450(9) 0.070(17) Uiso 1 1 d GD . .	C34 C 0.591(6) 0.516(5) -0.069(4) 0.17(4) Uiso 1 1 d . A .
C4 C 0.5155(15) 0.9700(10) -0.0030(12) 0.043(11) Uiso 1 1 d GD . .	C35 C 0.276(10) 0.936(9) 0.113(6) 0.23(8) Uiso 1 1 d . . .
C5 C 0.5001(18) 0.9436(12) 0.0408(9) 0.057(14) Uiso 1 1 d GD . .	C36 C 0.319(3) 1.004(2) 0.1340(15) 0.040(12) Uiso 1 1 d . . .
C6 C 0.4724(16) 0.8856(11) 0.0425(8) 0.009(9) Uiso 1 1 d GD . .	C37 C 0.290(9) 1.072(8) 0.071(6) 0.32(8) Uiso 1 1 d . . .
C7 C 0.519(5) 0.964(4) -0.094(3) 0.13(3) Uiso 1 1 d . B .	C38 C 0.621(7) 0.881(6) 0.286(5) 0.12(5) Uiso 1 1 d . . .
C8 C 0.511(4) 1.005(3) -0.117(3) 0.10(2) Uiso 1 1 d . . .	C39 C 0.487(3) 1.134(2) 0.3022(19) 0.056(16) Uiso 1 1 d . . .
C9 C 0.520(3) 0.972(2) 0.0864(16) 0.030(13) Uiso 1 1 d . . .	C40 C 0.557(4) 0.646(4) -0.031(3) 0.11(3) Uiso 1 1 d . A .
C10 C 0.526(2) 1.0008(19) 0.1193(15) 0.018(11) Uiso 1 1 d . . .	C41 C 0.231(3) 0.769(2) 0.0548(18) 0.049(14) Uiso 1 1 d . . .
C11 C 0.435(2) 0.798(2) -0.0073(19) 0.050(14) Uiso 1 1 d . . .	C42 C 0.134(4) 0.704(3) 0.118(3) 0.09(2) Uiso 1 1 d . . .
C12 C 0.403(2) 0.746(2) 0.005(2) 0.049(13) Uiso 1 1 d . A .	C43 C 0.349(4) 0.671(4) 0.123(3) 0.10(2) Uiso 1 1 d . A .
C15 C 0.374(7) 1.150(7) -0.234(5) 0.15(5) Uiso 1 1 d . B .	C44 C 0.273(7) 0.753(6) 0.159(5) 0.20(6) Uiso 1 1 d . . .
C16 C 0.407(4) 1.116(4) -0.175(3) 0.12(3) Uiso 1 1 d . . .	C46 C 0.374(4) 0.689(4) -0.107(3) 0.10(2) Uiso 1 1 d . A .
	C47 C 0.15(5) 0.74(3) -0.14(4) 0.6(7) Uiso 1 1 d . A .

C48 C 0.298(5) 0.791(4) -0.202(3)  
 0.16(3) Uiso 1 1 d . . .  
 C49 C 0.210(8) 0.636(8) -0.184(6)  
 0.23(7) Uiso 1 1 d . A .  
 C51 C 0.690(4) 1.177(4) 0.093(3)  
 0.10(2) Uiso 1 1 d . . .  
 C52 C 0.674(10) 1.216(8) 0.042(6)  
 0.28(8) Uiso 1 1 d . . .  
 C54 C 0.232(4) 1.075(3) 0.205(2)  
 0.09(2) Uiso 1 1 d . . .  
 C55 C 0.644(4) 0.992(4) 0.222(3)  
 0.11(3) Uiso 1 1 d . . .  
 C57 C 0.633(6) 1.019(5) -0.322(4)  
 0.15(4) Uiso 1 1 d . . .  
 C58 C 0.534(3) 0.927(3) -0.2796(19)  
 0.052(15) Uiso 1 1 d . . .  
 C59 C 0.470(15) 0.828(14) -0.275(10)  
 0.22(16) Uiso 1 1 d . . .  
 C60 C 0.464(2) 1.1056(17) -0.3127(13)  
 0.012(9) Uiso 1 1 d . . .  
 C61 C 0.441(6) 1.049(5) -0.307(4)  
 0.15(4) Uiso 1 1 d . . .  
 C62 C 0.61(3) 1.15(2) -0.255(17) 1.0(4)  
 Uiso 1 1 d . . .  
 C63 C 0.584(8) 1.191(7) -0.215(5)  
 0.22(6) Uiso 1 1 d . B .  
 C64 C 0.354(3) 0.981(2) -0.1799(18)  
 0.046(14) Uiso 1 1 d . . .  
 C100 C 0.526(8) 0.632(7) 0.064(5)  
 0.22(6) Uiso 1 1 d . . .  
 C101 C 0.504(10) 0.486(8) 0.049(6)  
 0.27(8) Uiso 1 1 d . . .  
 C102 C 0.364(4) 0.744(4) 0.143(3)  
 0.15(3) Uiso 1 1 d . A .  
 C103 C 0.164(13) 1.025(10) 0.177(8)  
 0.38(11) Uiso 1 1 d . . .  
 C200 C 0.252(8) 0.609(7) 0.062(6)  
 0.23(6) Uiso 1 1 d . A .  
 C201 C 0.715(16) 1.034(14) -0.161(10)  
 0.81(16) Uiso 1 1 d . B .  
 C202 C 0.519(5) 1.146(4) -0.076(3)  
 0.13(3) Uiso 1 1 d . . .  
 C203 C 0.739(5) 1.193(4) -0.154(3)  
 0.11(3) Uiso 1 1 d . . .  
 C204 C 0.609(6) 1.230(6) -0.105(4)  
 0.19(4) Uiso 1 1 d . . .

C205 C 0.689(6) 1.071(5) -0.130(4)  
 0.14(4) Uiso 1 1 d . . .

\_geom\_special\_details

;  
 All esds (except the esd in the dihedral  
 angle between two l.s. planes)  
 are estimated using the full covariance  
 matrix. The cell esds are taken  
 into account individually in the  
 estimation of esds in distances,  
 angles  
 and torsion angles; correlations between  
 esds in cell parameters are only  
 used when they are defined by crystal  
 symmetry. An approximate  
 (isotropic)  
 treatment of cell esds is used for  
 estimating esds involving l.s. planes.  
 ;

loop\_

\_geom\_bond\_atom\_site\_label\_1  
\_geom\_bond\_atom\_site\_label\_2  
\_geom\_bond\_distance  
\_geom\_bond\_site\_symmetry\_2  
\_geom\_bond\_publ\_flag  
 U1 N4 2.18(3) . ?  
 U1 N1 2.27(3) . ?  
 U1 C12 2.48(5) . ?  
 U1 C200 2.37(15) . ?  
 U1 N2 2.73(5) . ?  
 U1 Si7A 3.51(4) . ?  
 U2 N9 0.676(12) . ?  
 U2 C16 2.04(8) . ?  
 U2 N12 2.09(7) . ?  
 U2 C8 2.51(8) . ?  
 U2 N20 1.96(7) . ?  
 U2 C62 3.3(5) . ?  
 U2 N10 2.57(5) . ?  
 U2 C63 3.25(16) . ?  
 U3 N6 1.78(8) . ?  
 U3 N7 2.35(5) . ?  
 U3 N8 2.25(5) . ?  
 U3 C10 2.49(4) . ?  
 U3 N5 2.68(5) . ?

N1 Si8 1.56(4) . ?	Si10 C42 1.85(8) . ?
N1 C23 1.34(9) . ?	Si10 C200 2.68(17) . ?
N2 C26 1.28(8) . ?	Si10 C44 2.18(14) . ?
N2 C24 1.37(6) . ?	Si20 C204 1.08(12) . ?
N2 C29 1.57(7) . ?	Si20 C203 2.14(10) . ?
N4 C28 1.53(8) . ?	Si20 C205 2.32(11) . ?
N4 Si7 1.80(4) . ?	C1 C11 1.36(5) . ?
N4 Si7A 1.87(4) . ?	C1 C2 1.3900 . ?
N5 C39 1.55(7) . ?	C1 C6 1.3900 . ?
N5 C17 1.74(10) . ?	C2 C3 1.3900 . ?
N6 Si4 1.95(11) . ?	C3 C4 1.3900 . ?
N7 C18 1.31(6) . ?	C3 C7 1.52(9) . ?
N7 Si6 1.48(5) . ?	C4 C5 1.3900 . ?
N8 C20 1.48(8) . ?	C5 C6 1.3900 . ?
N8 Si5 1.72(6) . ?	C5 C9 1.47(5) . ?
N10 C62 2.7(5) . ?	C7 C8 1.13(10) . ?
N10 C60 1.52(6) . ?	C9 C10 1.13(5) . ?
N10 C15 1.91(13) . ?	C11 C12 1.34(7) . ?
N10 C61 2.28(12) . ?	C15 C62 4.4(5) . ?
N12 C16 1.18(9) . ?	C17 C18 1.14(9) . ?
N12 Si1 1.45(6) . ?	C20 C39 1.41(8) . ?
N20 Si20 1.69(7) . ?	C23 C24 1.70(10) . ?
N20 C63 1.33(15) . ?	C24 C26 2.12(9) . ?
N20 Si20 2.49(7) . ?	C28 C29 1.57(8) . ?
N100 C200 1.18(17) . ?	C32 C40 1.45(9) . ?
N100 C43 1.99(14) . ?	C32 C33 1.42(9) . ?
N100 Si10 1.78(13) . ?	C32 C34 2.18(12) . ?
Si1 C64 1.98(6) . ?	C35 C36 1.82(19) . ?
Si2 C58 1.21(6) . ?	C43 C102 1.75(11) . ?
Si2 C57 2.14(12) . ?	C44 C102 1.77(15) . ?
Si4 C51 1.64(10) . ?	C47 C48 3.4(9) . ?
Si5 C55 1.65(8) . ?	C47 C49 2.8(8) . ?
Si5 C38 2.64(14) . ?	C51 C52 1.69(18) . ?
Si6 C36 1.62(5) . ?	C54 C103 1.9(2) . ?
Si6 C37 2.38(17) . ?	C58 C59 2.5(3) . ?
Si6 C54 2.24(8) . ?	C60 C61 1.35(11) . ?
Si7 C100 1.79(16) . ?	C201 C205 1.3(3) . ?
Si7 C32 1.85(6) . ?	
Si7 C101 2.06(17) . ?	loop_
Si7A C32 1.52(6) . ?	_geom_angle_atom_site_label_1
Si7A C40 2.05(9) . ?	_geom_angle_atom_site_label_2
Si7A C34 2.66(12) . ?	_geom_angle_atom_site_label_3
Si8 C49 2.45(16) . ?	_geom_angle
Si8 C46 1.92(8) . ?	_geom_angle_site_symmetry_1
Si8 C47 2.8(9) . ?	_geom_angle_site_symmetry_3
Si10 C41 1.53(6) . ?	_geom_angle_publ_flag

N4 U1 N1 111.6(12) . . ?  
N4 U1 C12 107.4(12) . . ?  
N1 U1 C12 113.3(16) . . ?  
N4 U1 C200 89(4) . . ?  
N1 U1 C200 101(4) . . ?  
C12 U1 C200 132(4) . . ?  
N4 U1 N2 71.7(12) . . ?  
N1 U1 N2 67.9(14) . . ?  
C12 U1 N2 178.7(17) . . ?  
C200 U1 N2 48(4) . . ?  
N4 U1 Si7A 27.4(9) . . ?  
N1 U1 Si7A 105.9(10) . . ?  
C12 U1 Si7A 86.5(12) . . ?  
C200 U1 Si7A 116(4) . . ?  
N2 U1 Si7A 93.0(11) . . ?  
N9 U2 C16 126(3) . . ?  
N9 U2 N12 94(2) . . ?  
C16 U2 N12 33(3) . . ?  
N9 U2 C8 90.2(19) . . ?  
C16 U2 C8 102(3) . . ?  
N12 U2 C8 96(3) . . ?  
N9 U2 N20 127(2) . . ?  
C16 U2 N20 93(3) . . ?  
N12 U2 N20 123(3) . . ?  
C8 U2 N20 119(3) . . ?  
N9 U2 C62 97(9) . . ?  
C16 U2 C62 110(9) . . ?  
N12 U2 C62 128(9) . . ?  
C8 U2 C62 135(9) . . ?  
N20 U2 C62 31(9) . . ?  
N9 U2 N10 91.5(16) . . ?  
C16 U2 N10 71(3) . . ?  
N12 U2 N10 75(2) . . ?  
C8 U2 N10 171(2) . . ?  
N20 U2 N10 66(2) . . ?  
C62 U2 N10 53(9) . . ?  
N9 U2 C63 123(3) . . ?  
C16 U2 C63 90(4) . . ?  
N12 U2 C63 118(3) . . ?  
C8 U2 C63 127(3) . . ?  
N20 U2 C63 8(3) . . ?  
C62 U2 C63 27(9) . . ?  
N10 U2 C63 58(3) . . ?  
N6 U3 N7 111(3) . . ?  
N6 U3 N8 113(3) . . ?  
N7 U3 N8 106.2(18) . . ?

N6 U3 C10 105(3) . . ?  
N7 U3 C10 111.1(15) . . ?  
N8 U3 C10 110.9(16) . . ?  
N6 U3 N5 76(3) . . ?  
N7 U3 N5 70.4(15) . . ?  
N8 U3 N5 66.9(17) . . ?  
C10 U3 N5 177.7(15) . . ?  
Si8 N1 C23 123(4) . . ?  
Si8 N1 U1 126.1(19) . . ?  
C23 N1 U1 110(4) . . ?  
C26 N2 C24 106(5) . . ?  
C26 N2 C29 118(6) . . ?  
C24 N2 C29 114(5) . . ?  
C26 N2 U1 101(5) . . ?  
C24 N2 U1 112(3) . . ?  
C29 N2 U1 104(3) . . ?  
C28 N4 Si7 114(3) . . ?  
C28 N4 Si7A 94(3) . . ?  
Si7 N4 Si7A 50.4(14) . . ?  
C28 N4 U1 116(3) . . ?  
Si7 N4 U1 129.2(16) . . ?  
Si7A N4 U1 120.2(17) . . ?  
C39 N5 C17 139(5) . . ?  
C39 N5 U3 115(4) . . ?  
C17 N5 U3 86(4) . . ?  
Si4 N6 U3 159(6) . . ?  
C18 N7 Si6 116(4) . . ?  
C18 N7 U3 123(4) . . ?  
Si6 N7 U3 120(3) . . ?  
C20 N8 Si5 127(4) . . ?  
C20 N8 U3 113(4) . . ?  
Si5 N8 U3 116(3) . . ?  
C62 N10 C60 98(10) . . ?  
C62 N10 C15 143(10) . . ?  
C60 N10 C15 119(5) . . ?  
C62 N10 C61 110(10) . . ?  
C60 N10 C61 35(3) . . ?  
C15 N10 C61 104(6) . . ?  
C62 N10 U2 77(10) . . ?  
C60 N10 U2 120(3) . . ?  
C15 N10 U2 89(5) . . ?  
C61 N10 U2 90(3) . . ?  
C16 N12 Si1 106(7) . . ?  
C16 N12 U2 71(5) . . ?  
Si1 N12 U2 155(4) . . ?  
Si20 N20 C63 73(7) . . ?

Si20 N20 Si20 53(2) .. ?  
C63 N20 Si20 83(8) .. ?  
Si20 N20 U2 125(4) .. ?  
C63 N20 U2 160(8) .. ?  
Si20 N20 U2 114(3) .. ?  
C200 N100 C43 126(10) .. ?  
C200 N100 Si10 128(10) .. ?  
C43 N100 Si10 92(6) .. ?  
N12 Si1 C64 74(3) .. ?  
C58 Si2 C57 124(5) .. ?  
N6 Si4 C51 138(7) .. ?  
N8 Si5 C55 116(4) .. ?  
N8 Si5 C38 145(4) .. ?  
C55 Si5 C38 89(4) .. ?  
N7 Si6 C36 135(3) .. ?  
N7 Si6 C37 126(5) .. ?  
C36 Si6 C37 71(5) .. ?  
N7 Si6 C54 104(3) .. ?  
C36 Si6 C54 101(3) .. ?  
C37 Si6 C54 116(5) .. ?  
C100 Si7 N4 121(5) .. ?  
C100 Si7 C32 90(5) .. ?  
N4 Si7 C32 118(2) .. ?  
C100 Si7 C101 119(7) .. ?  
N4 Si7 C101 105(5) .. ?  
C32 Si7 C101 102(5) .. ?  
C32 Si7A N4 135(3) .. ?  
C32 Si7A C40 45(3) .. ?  
N4 Si7A C40 126(3) .. ?  
C32 Si7A C34 55(3) .. ?  
N4 Si7A C34 150(3) .. ?  
C40 Si7A C34 82(4) .. ?  
C32 Si7A U1 134(3) .. ?  
N4 Si7A U1 32.4(11) .. ?  
C40 Si7A U1 101(3) .. ?  
C34 Si7A U1 168(3) .. ?  
N1 Si8 C49 122(4) .. ?  
N1 Si8 C46 101(3) .. ?  
C49 Si8 C46 127(4) .. ?  
N1 Si8 C47 105(10) .. ?  
C49 Si8 C47 63(10) .. ?  
C46 Si8 C47 135(10) .. ?  
C41 Si10 C42 119(3) .. ?  
C41 Si10 N100 129(5) .. ?  
C42 Si10 N100 98(5) .. ?  
C41 Si10 C200 115(4) .. ?

C42 Si10 C200 97(4) .. ?  
N100 Si10 C200 20(5) .. ?  
C41 Si10 C44 109(4) .. ?  
C42 Si10 C44 97(4) .. ?  
N100 Si10 C44 100(5) .. ?  
C200 Si10 C44 120(5) .. ?  
C204 Si20 N20 141(7) .. ?  
N20 Si20 C203 159(4) .. ?  
N20 Si20 C205 118(4) .. ?  
C203 Si20 C205 83(4) .. ?  
C11 C1 C2 109(3) .. ?  
C11 C1 C6 131(3) .. ?  
C2 C1 C6 120.0 .. ?  
C1 C2 C3 120.0 .. ?  
C4 C3 C2 120.0 .. ?  
C4 C3 C7 124(4) .. ?  
C2 C3 C7 116(4) .. ?  
C3 C4 C5 120.0 .. ?  
C6 C5 C4 120.0 .. ?  
C6 C5 C9 118(3) .. ?  
C4 C5 C9 122(3) .. ?  
C5 C6 C1 120.0 .. ?  
C8 C7 C3 142(9) .. ?  
C7 C8 U2 158(8) .. ?  
C10 C9 C5 168(5) .. ?  
C9 C10 U3 160(4) .. ?  
C12 C11 C1 154(5) .. ?  
C11 C12 U1 161(4) .. ?  
N10 C15 C62 22(7) .. ?  
N12 C16 U2 76(6) .. ?  
C18 C17 N5 145(8) .. ?  
C17 C18 N7 104(7) .. ?  
C39 C20 N8 124(5) .. ?  
C24 C23 N1 113(6) .. ?  
C23 C24 N2 99(5) .. ?  
C23 C24 C26 90(4) .. ?  
N2 C24 C26 35(3) .. ?  
N2 C26 C24 38(3) .. ?  
C29 C28 N4 108(5) .. ?  
C28 C29 N2 106(5) .. ?  
Si7A C32 C40 87(5) .. ?  
Si7A C32 C33 158(5) .. ?  
C40 C32 C33 114(6) .. ?  
Si7A C32 Si7 54(2) .. ?  
C40 C32 Si7 105(4) .. ?  
C33 C32 Si7 121(5) .. ?

Si7A C32 C34 90(4) . . ?  
 C40 C32 C34 118(5) . . ?  
 C33 C32 C34 75(5) . . ?  
 Si7 C32 C34 123(4) . . ?  
 C32 C34 Si7A 35(2) . . ?  
 C35 C36 Si6 157(7) . . ?  
 C20 C39 N5 94(5) . . ?  
 C32 C40 Si7A 48(3) . . ?  
 C102 C43 N100 122(6) . . ?  
 C102 C44 Si10 98(7) . . ?  
 C48 C47 C49 76(10) . . ?  
 C48 C47 Si8 71(10) . . ?  
 C49 C47 Si8 52(10) . . ?  
 Si8 C49 C47 66(10) . . ?  
 Si4 C51 C52 124(8) . . ?  
 C103 C54 Si6 102(8) . . ?  
 Si2 C58 C59 164(8) . . ?  
 N10 C60 C61 105(5) . . ?  
 C60 C61 N10 40(4) . . ?

N10 C62 C15 15(5) . . ?  
 N10 C62 U2 50(9) . . ?  
 C15 C62 U2 46(7) . . ?  
 N20 C63 U2 12(5) . . ?  
 C43 C102 C44 92(7) . . ?  
 N100 C200 Si10 31(9) . . ?  
 N100 C200 U1 99(10) . . ?  
 Si10 C200 U1 87(5) . . ?  
 C201 C205 Si20 106(10) . . ?

\_diffn\_measured\_fraction\_theta\_max  
 0.998  
 \_diffn\_reflns\_theta\_full 20.82  
 \_diffn\_measured\_fraction\_theta\_full  
 0.998  
 \_refine\_diff\_density\_max 8.446  
 \_refine\_diff\_density\_min -7.304  
 \_refine\_diff\_density\_rms 0.431

## A.2 Supporting Information for Chapter 3

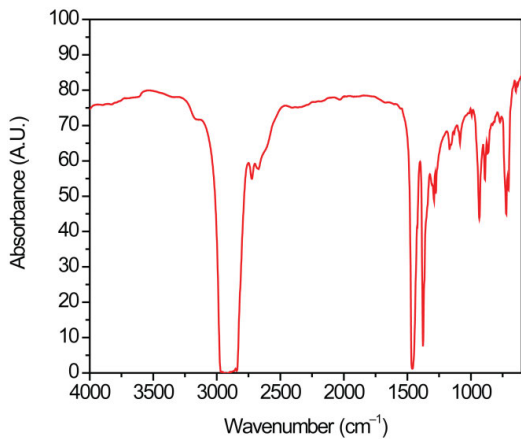


**Figure A2.1.** Full IR spectrum of **3.1** taken as mineral oil mulls. A minimum of 32 transients were recorded.

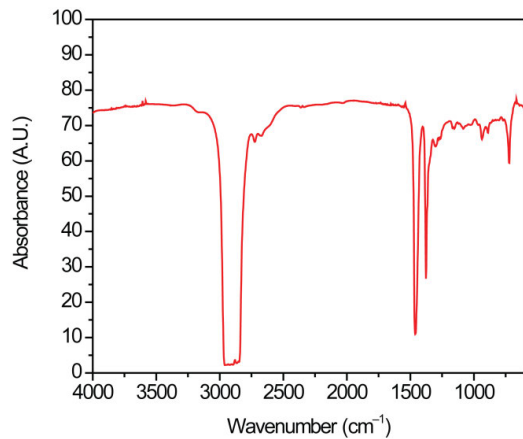


**Figure A2.2.** Full IR spectrum of **3.2** taken as a mineral oil mull. A minimum of 32 transients were recorded.

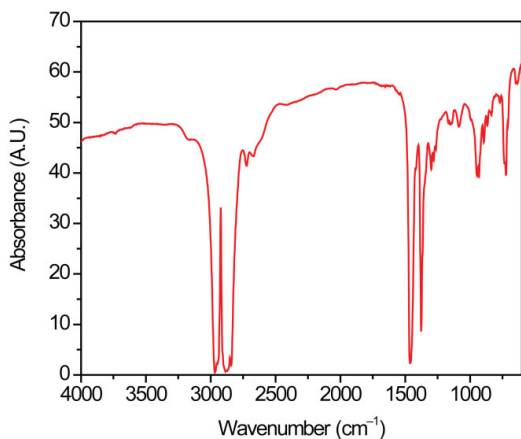


**Figure A2.3.** Full IR spectrum of **3.3** taken as a mineral oil mull. A minimum of 32 transients were recorded.

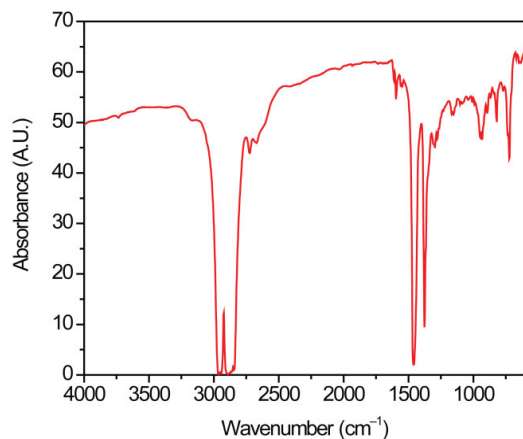


**Figure A2.4.** Full IR spectrum of **3.4** taken as a mineral oil mull. A minimum of 32 transients were recorded.

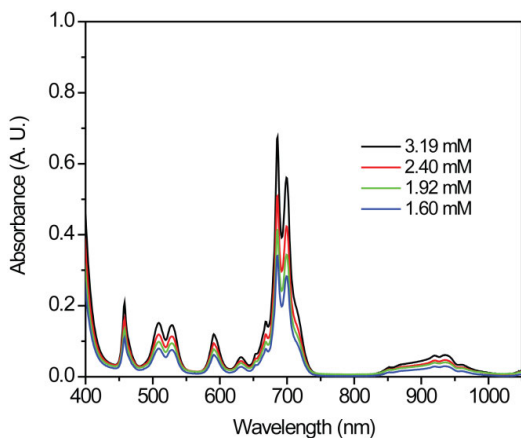


**Figure A2.5.** Electronic absorption spectrum of **3.1** taken in dichloromethane.

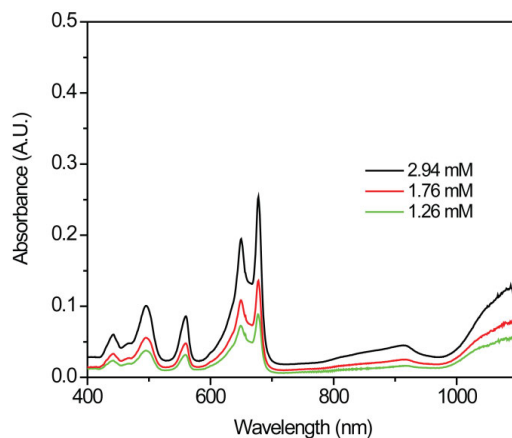


**Figure A2.6.** Electronic absorption spectrum of **3.1** taken in dimethyl sulfoxide.

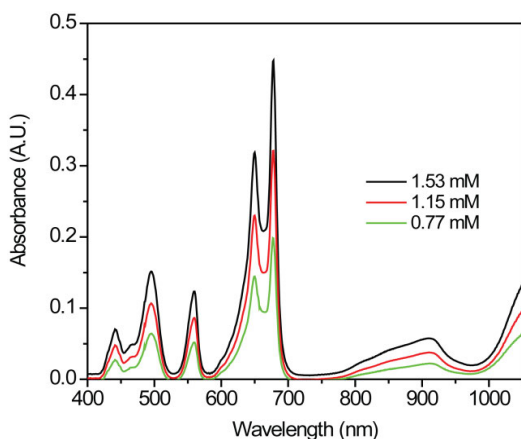


**Figure A2.7.** Electronic absorption spectrum of **3.3** taken in dimethyl sulfoxide.

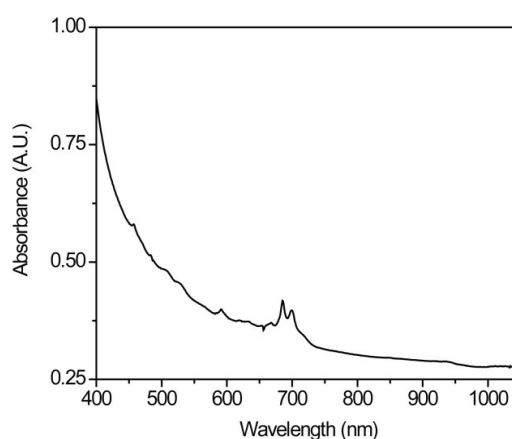


**Figure A2.8.** Electronic absorption spectrum of **3.3** taken in dichloromethane.

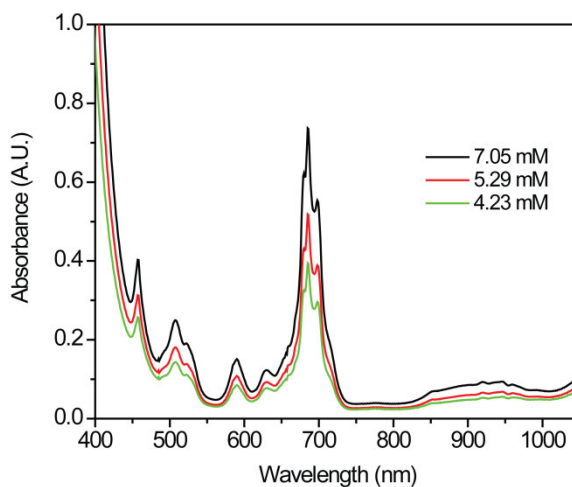


**Figure A2.9.** Electronic absorption spectrum of **3.4** taken in acetonitrile.

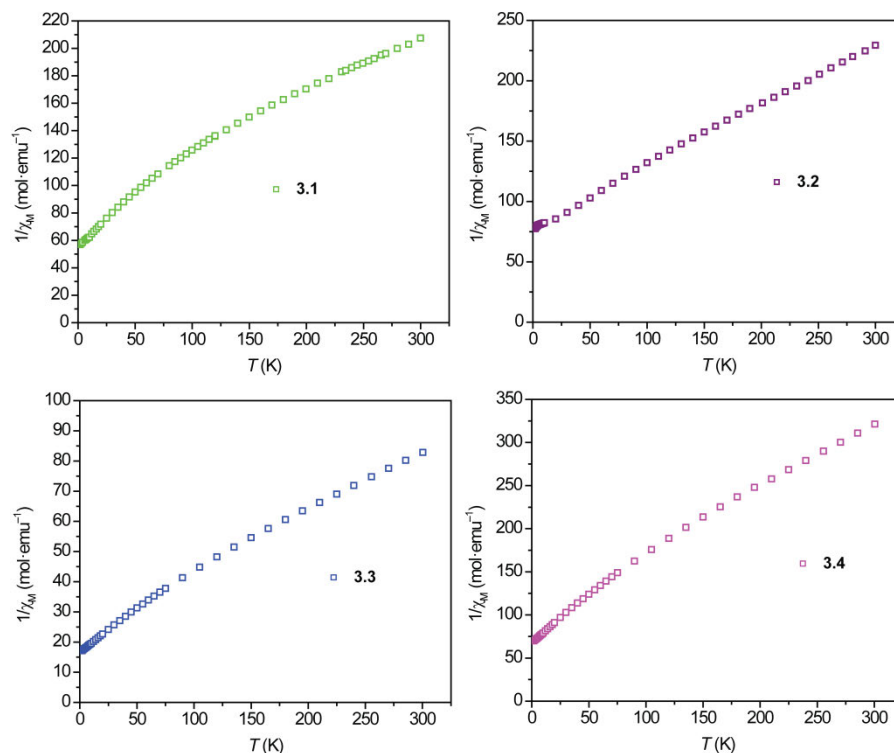


**Figure A2.10.** Temperature dependence of the inverse susceptibility for compounds **3.1**–**3.4** obtained at a measuring field of 1000 G. The linear behavior observed at higher temperatures is consistent with Curie-Weiss behavior but the  $\theta$  values obtained do not correlate to well-isolated paramagnetic ground state.

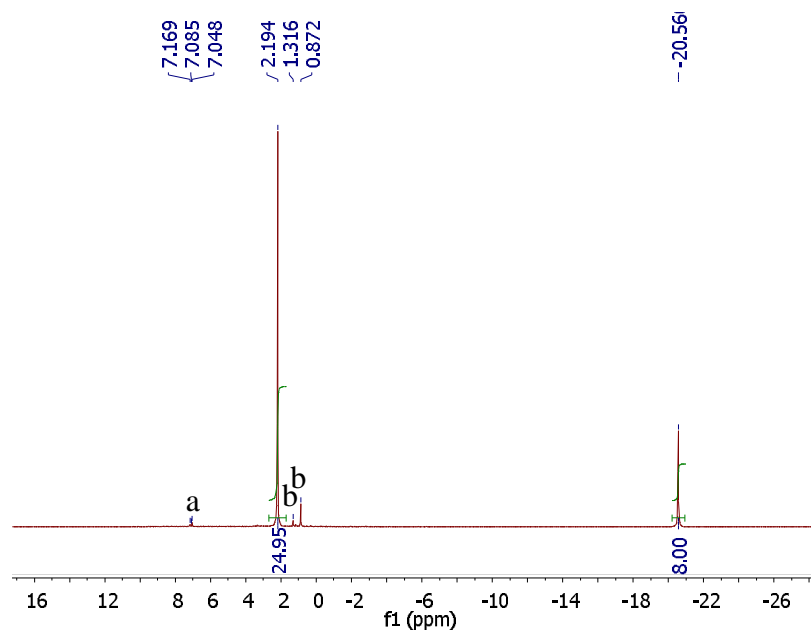


**Figure A2.11.**  $^1\text{H}$  NMR spectrum of **3.1** obtained in toluene- $d_8$  at ambient temperature with a 500 MHz spectrometer. (a) is residual solvent peaks for toluene- $d_8$  and (b) is residual pentane.

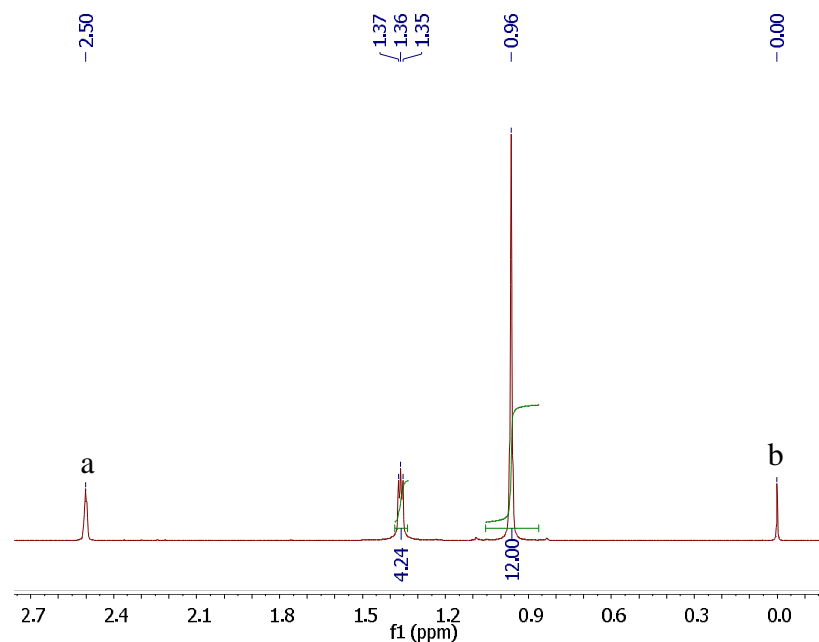


**Figure A2.12.**  $^1\text{H}$  NMR spectrum of **3.1** obtained in  $(\text{CD}_3)_2\text{SO}$  at ambient temperature with a 500 MHz spectrometer; (a) is residual solvent peaks for  $(\text{CD}_3)_2\text{SO}$  and (b) is tetramethylsilane (TMS). This matches the  $^1\text{H}$  NMR spectrum of free dmpe in  $(\text{CD}_3)_2\text{SO}$  (293 K, 500 MHz spectrometer):  $\delta$  0.96 (s, 12 H,  $\text{PCH}_3$ ), 1.36 ppm (t ( $j_{12} = 3.9$  Hz and  $j_{23} = 3.6$  Hz), 4 H,  $\text{PCH}_2$ ).

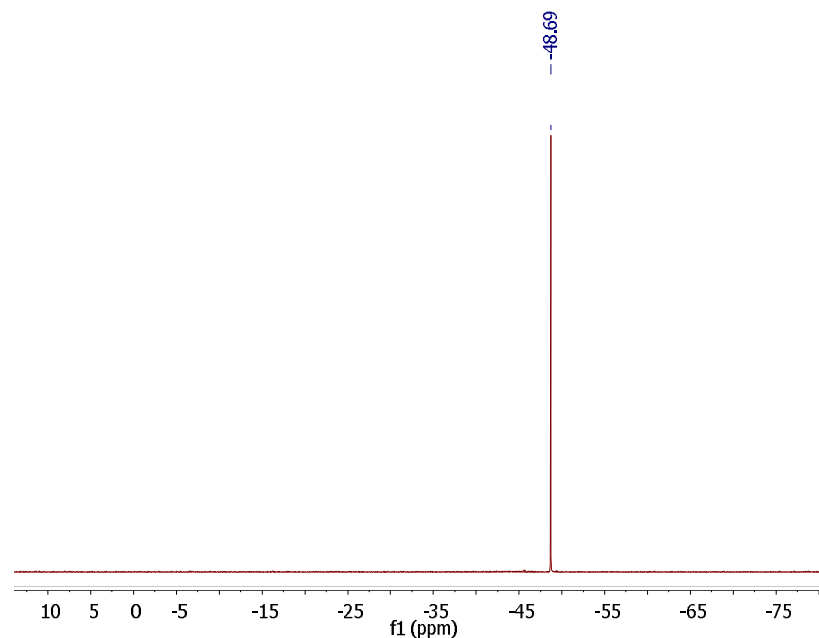


**Figure A2.13.**  $\{^1\text{H}\}^{31}\text{P}$  NMR spectrum of **3.1** obtained in  $(\text{CD}_3)_2\text{SO}$  at ambient temperature with a 500 MHz spectrometer. This matches the  $\{^1\text{H}\}^{31}\text{P}$  NMR spectrum of free dmpe in  $(\text{CD}_3)_2\text{SO}$  (293 K, 500 MHz spectrometer):  $\delta$  -48.651 ppm.

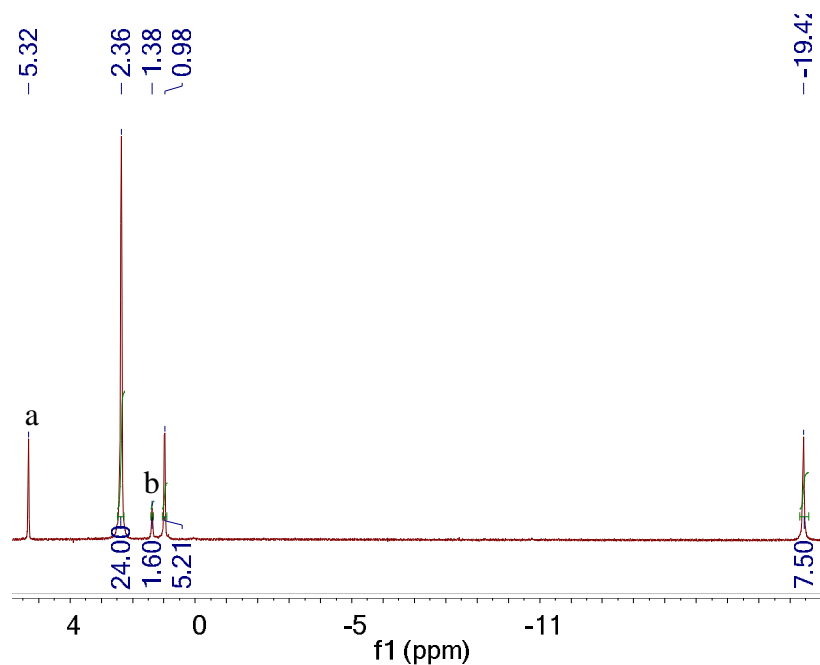


**Figure A2.14.**  $^1\text{H}$  NMR spectrum of **3.1** obtained in  $\text{CD}_2\text{Cl}_2$  at ambient temperature with a 500 MHz spectrometer; (a) is residual solvent peaks for  $\text{CD}_2\text{Cl}_2$  and (b) is free dmpe.

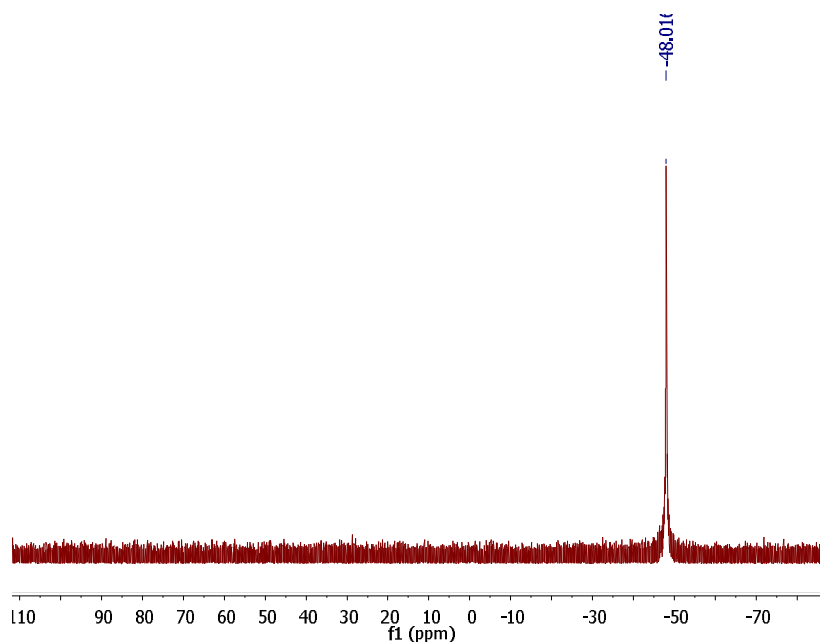


**Figure A2.15.**  $\{^1\text{H}\}^{31}\text{P}$  NMR spectrum of **3.1** obtained in  $\text{CD}_2\text{Cl}_2$  at ambient temperature with a 500 MHz spectrometer. The signal matches that found for free dmpe. Signals for dmpe bound to  $\text{U}(\text{IV})$  may be too broad to be visible.

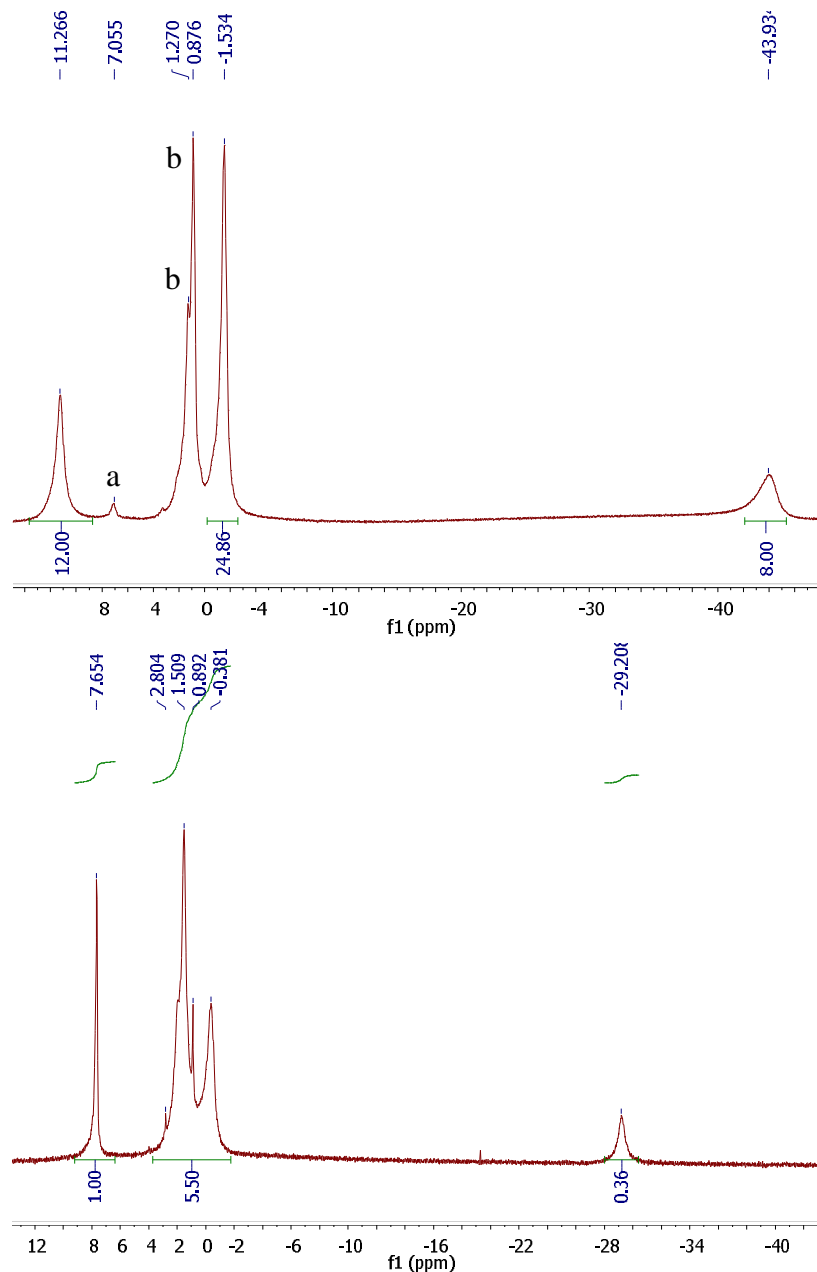


**Figure A2.16.** (Top)  $^1\text{H}$  NMR spectrum of **3.2** obtained in toluene- $d_8$  at  $-80^\circ\text{C}$  with a 500 MHz spectrometer; (a) is residual solvent peaks for toluene- $d_8$  and (b) is residual pentane. (Bottom)  $^1\text{H}$  NMR spectrum of **2** obtained in toluene- $d_8$  at  $25^\circ\text{C}$  with a 500 MHz spectrometer.

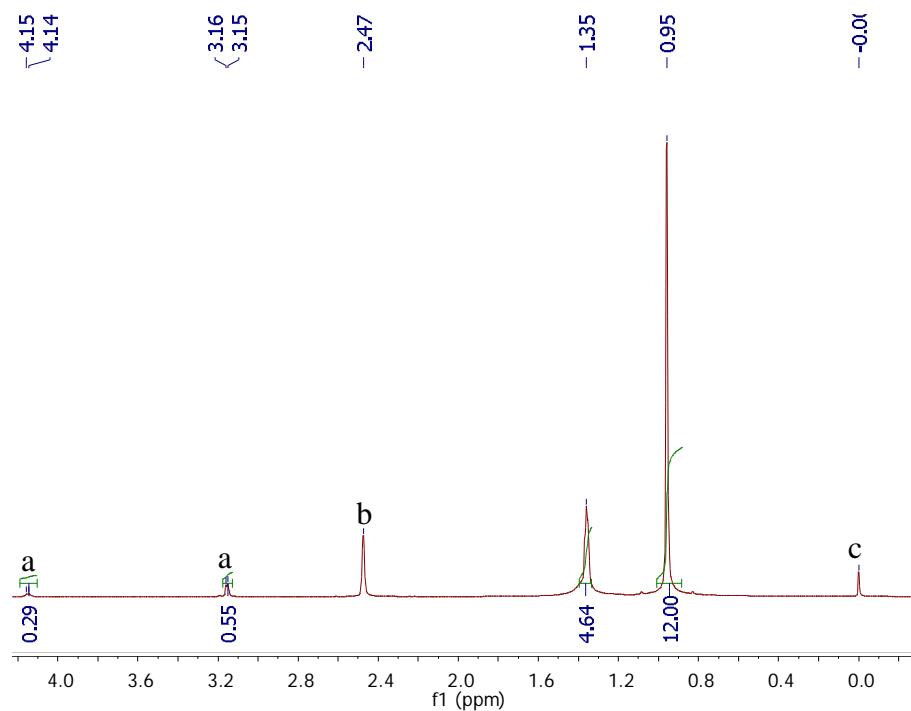


**Figure A2.17.**  $^1\text{H}$  NMR spectrum of **3.3** obtained in  $(\text{CD}_3)_2\text{SO}$  at ambient temperature with a 500 MHz spectrometer. (a) is methanol, (b) is residual solvent peaks for  $(\text{CD}_3)_2\text{SO}$ , and (c) is TMS. This matches the  $^1\text{H}$  NMR spectrum of free dmpe in  $(\text{CD}_3)_2\text{SO}$  (293 K, 500 MHz spectrometer):  $\delta$  0.96 (s, 12 H,  $\text{PCH}_3$ ), 1.36 ppm (t ( $j_{12} = 3.9$  Hz and  $j_{23} = 3.6$  Hz), 4 H,  $\text{PCH}_2$ ).

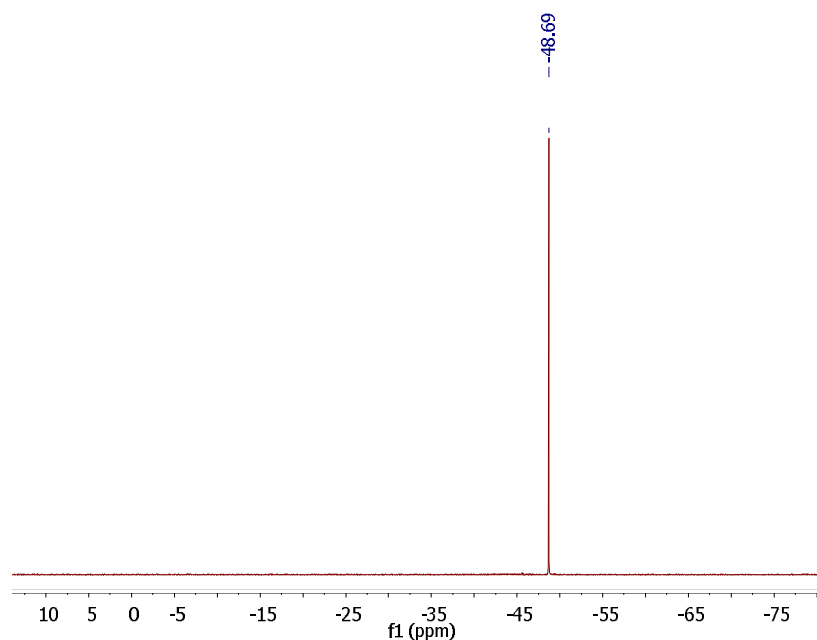


**Figure A2.18.**  $\{^1\text{H}\}^{31}\text{P}$  NMR spectrum of **3.3** obtained in  $(\text{CD}_3)_2\text{SO}$  at ambient temperature with a 500 MHz spectrometer. This matches the  $\{^1\text{H}\}^{31}\text{P}$  NMR spectrum of free dmpe in  $(\text{CD}_3)_2\text{SO}$  (293 K, 500 MHz spectrometer):  $\delta$  -48.651 ppm.

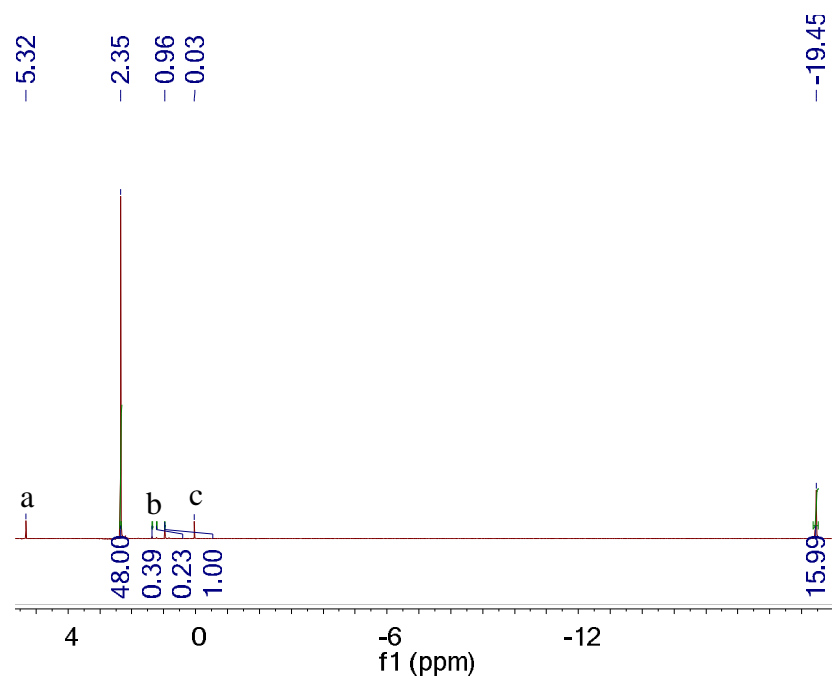


**Figure A2.19.**  $^1\text{H}$  NMR spectrum of **3.3** obtained in  $\text{CD}_2\text{Cl}_2$  at ambient temperature with a 500 MHz spectrometer; (a) is residual solvent peaks for  $\text{CD}_2\text{Cl}_2$ , (b) is free dmpe, and (c) is tetramethylsilane (TMS).

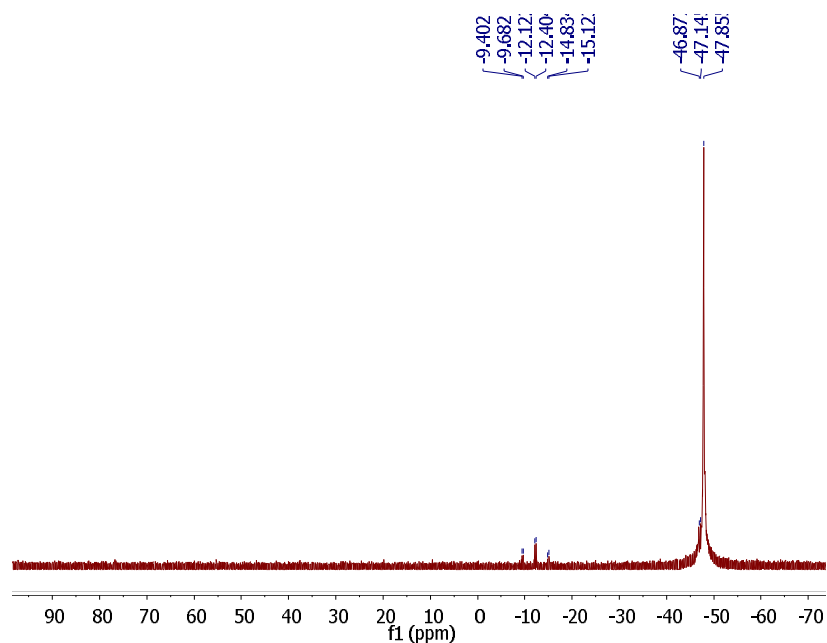


**Figure A2.20.**  $\{^1\text{H}\}^{31}\text{P}$  NMR spectrum of **3.3** obtained in  $\text{CD}_2\text{Cl}_2$  at ambient temperature with a 500 MHz spectrometer. The signal at  $\sim -48$  ppm is consistent with free dmpe in dichloromethane. The resonances centered around  $-12$  ppm are not free dmpe.

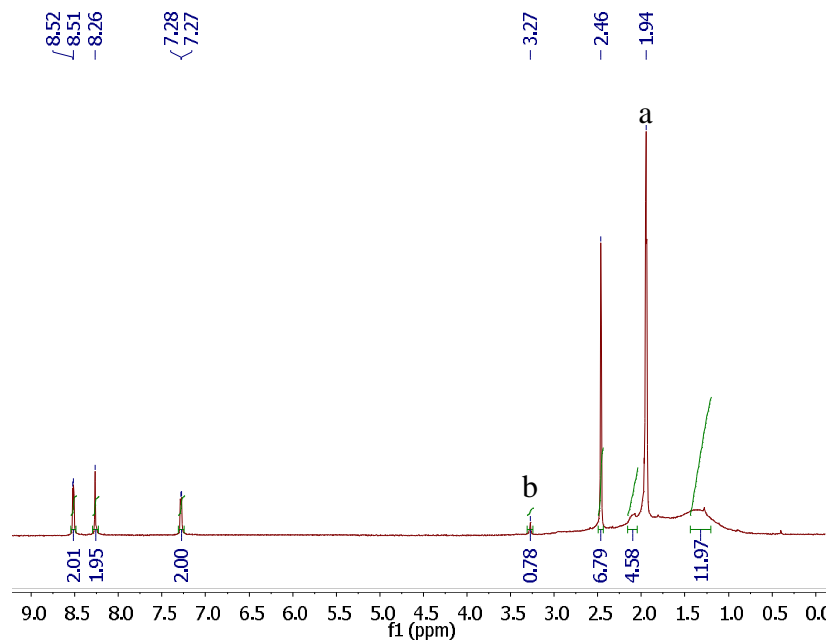


**Figure A2.21.**  $^1\text{H}$  NMR spectrum of **3.4** obtained in  $\text{CD}_3\text{CN}$  at ambient temperature with a 500 MHz spectrometer; (a) is residual solvent peaks for  $\text{CD}_3\text{CN}$  and (b) is residual methanol. For comparison,  $^1\text{H}$  NMR spectra of free dmpe and dmbpy were obtained in  $\text{CD}_3\text{CN}$  at ambient temperature with a 300 MHz spectrometer (dmpe:  $^1\text{H}$  NMR (293 K,  $\text{CD}_3\text{CN}$ ):  $\delta$  0.98 (s, 12 H,  $\text{PCH}_3$ ), 1.39 ppm (t ( $j_{12} = 3.6$  Hz and  $j_{23} = 3.4$  Hz), 4 H,  $\text{PCH}_2$ ) and dmbpy:  $^1\text{H}$  NMR (293 K,  $\text{CD}_3\text{CN}$ ):  $\delta$  8.51 (s, 2 H, Aryl), 8.26 (s, 2 H, Aryl), 7.22 (s, 2 H, Aryl), 2.44 (s, 6 H,  $\text{CH}_3$ ). We conclude that free dmbpy is present in the acetonitrile solution, but dmpe is interacting with the U(IV) ion in solution.

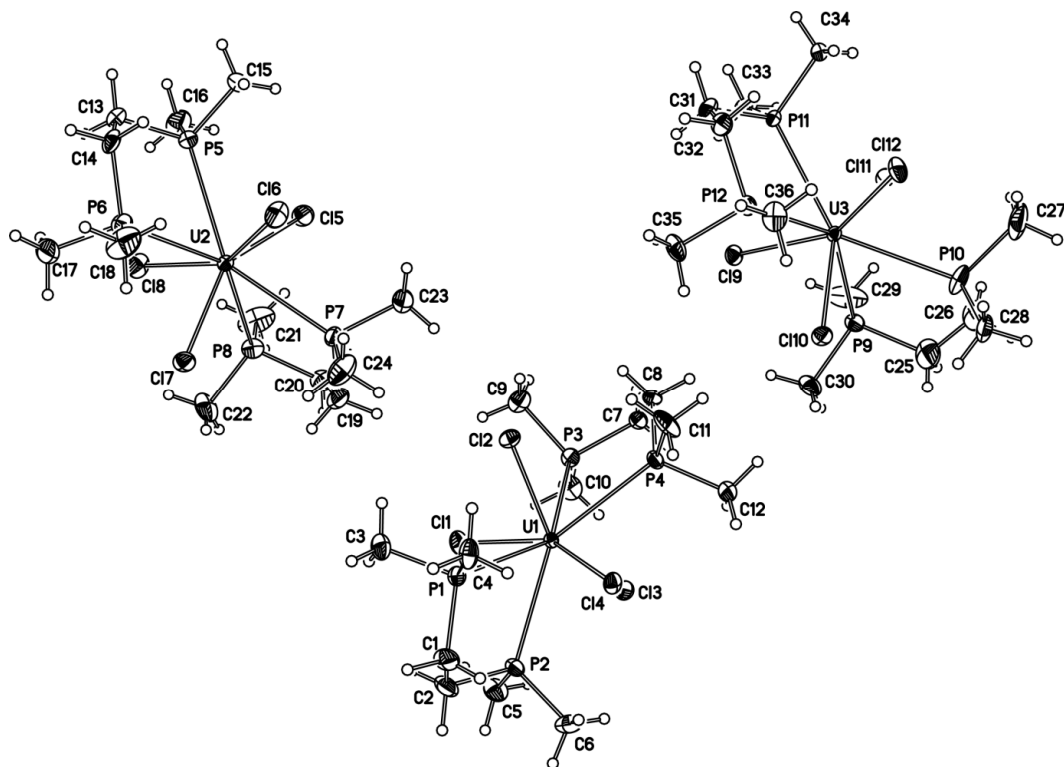


**Figure A2.22.** The U-containing complexes in the crystal structure of **3.1**, rendered with 40% ellipsoids.

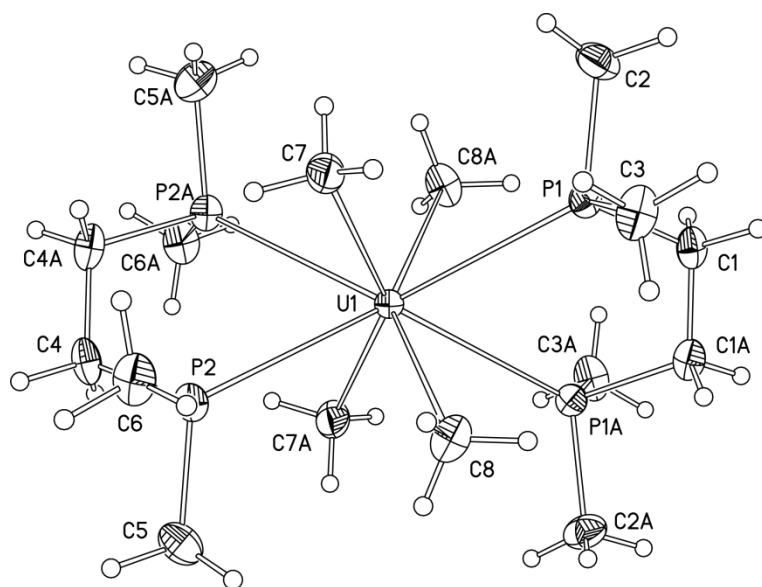


**Figure A2.23.** The U-containing complex in the crystal structure of **3.2**, rendered with 40% ellipsoids. The uranium complex in compound **3.2** sits on a crystallographic inversion center.

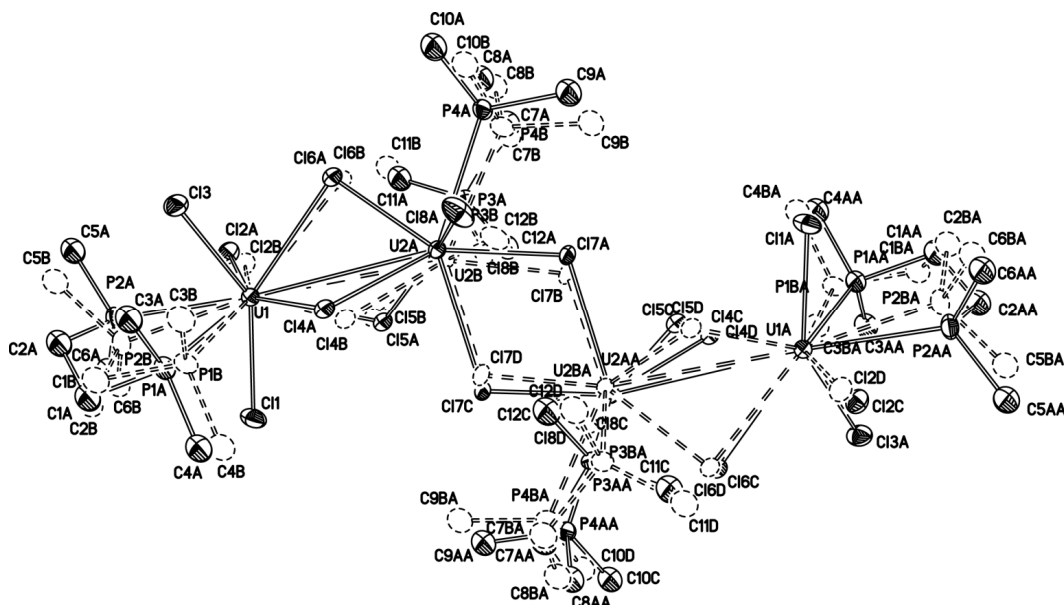


**Figure A2.24.** The U-containing complex in the crystal structure of  $3.3 \cdot 2\text{CH}_2\text{Cl}_2$  at 120 K rendered with 40% ellipsoids. The hydrogen atoms and solvent molecules have been omitted for clarity. There are several groups disordered over two positions and the disordered parts appear as dashed circles in the figure. The uranium complex in  $3.3 \cdot 2\text{CH}_2\text{Cl}_2$  sits on a crystallographic two-fold axis.

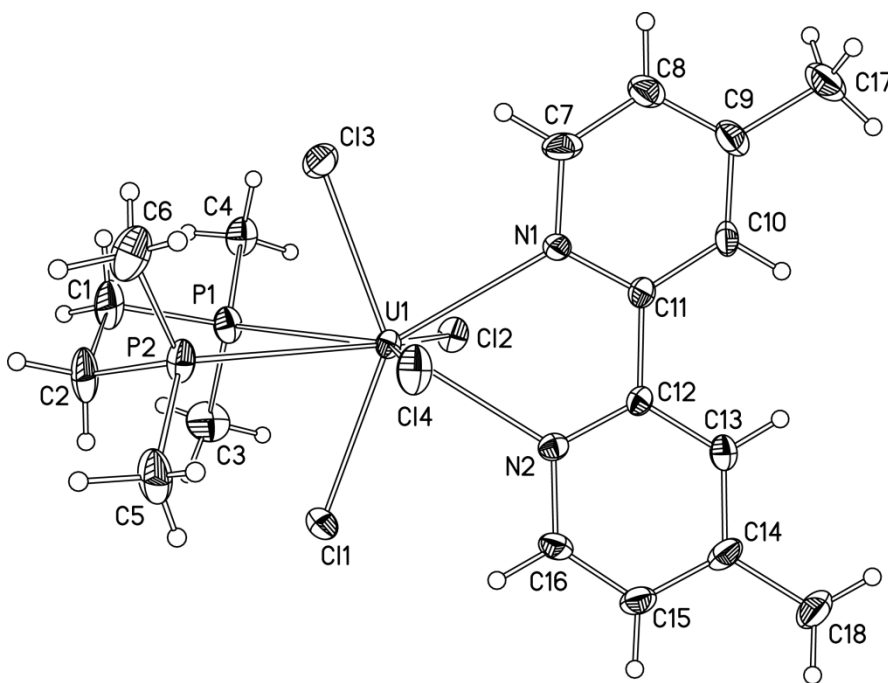


**Figure A2.25.** The U-containing complex in the crystal structure of **3.4**, rendered with 40% ellipsoids.

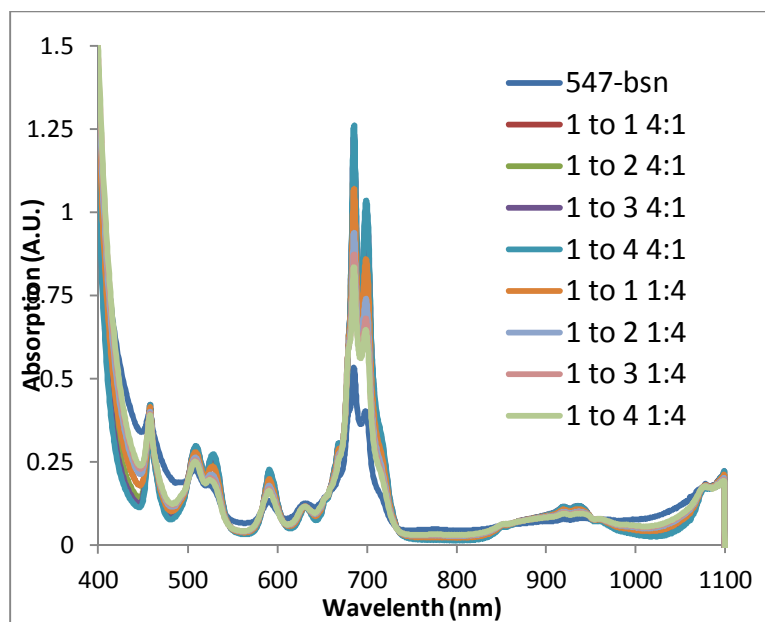


**Figure A2.26.** Electronic absorption spectrum for the product of mixing **3.1** with one equivalent of dmbpy (547-bsn). For comparison the spectrum of **3.1** and **3.4** has been combined in various ratios, the raw data has been multiplied by a constant to match the absorbance of the peak at 457 nm.

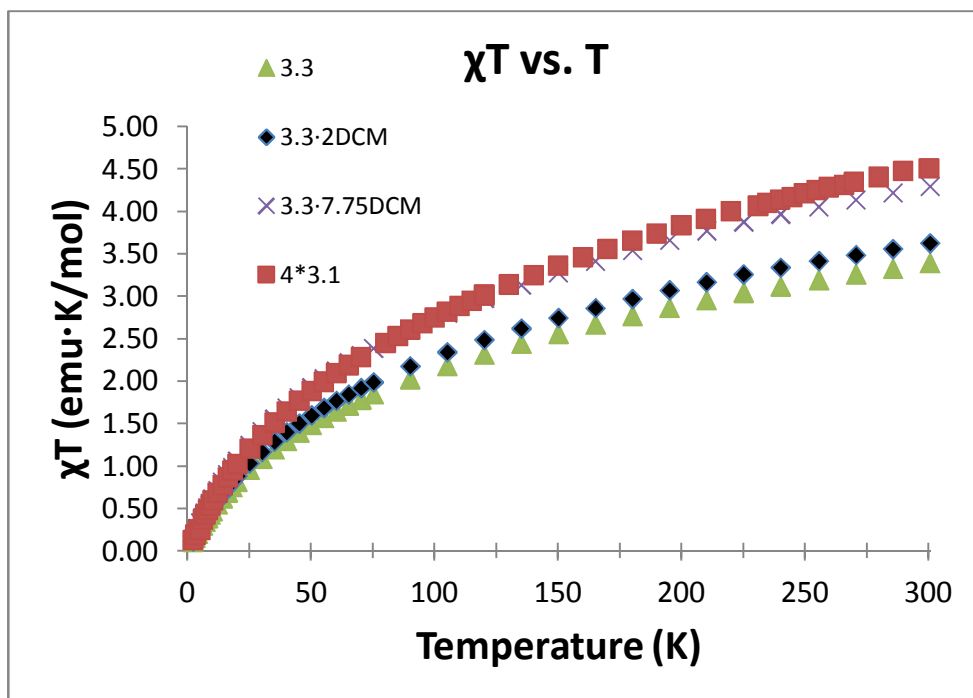


**Figure A2.27.** Temperature dependence of  $\chi_M T$  for compound **3.3** assuming various amounts of  $\text{CH}_2\text{Cl}_2$  solvate (considering scenarios with 0, 2, and 7.75 equivalents of  $\text{CH}_2\text{Cl}_2$ ). The raw data is identical for each plot; only the formula weight has been changed. For comparison, four times  $\chi_M T$  for mononuclear **3.1** is also plotted.

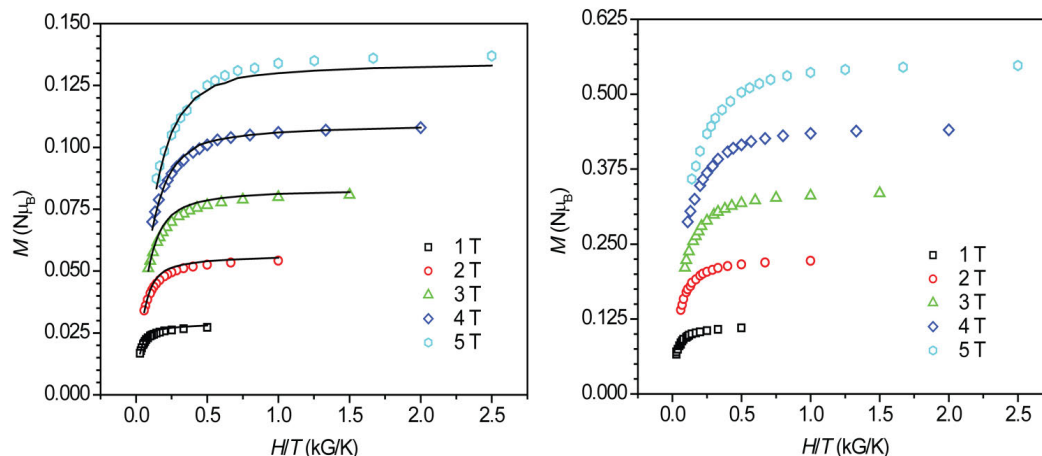


**Figure A2.28.** Magnetization for compounds **3.1** (left) and **3.3** (right), obtained at measuring fields of 1, 2, 3, 4, and 5 T from 2-35 K. The solid black lines in the magnetization plot for compound **3.1** represent fits to the data using ANISOFIT 2.0.<sup>a</sup> For compound **3.1**, fitting with Anisofit afforded values of  $g = 1.65$ ,  $D = -235 \text{ cm}^{-1}$ ,  $E = -38 \text{ cm}^{-1}$ , and  $f = 2.54 \times 10^{-4}$ . Fits using Anisofit for **3.3** have not been obtained, likely owing to the lack of a well defined ground state. We note that these results are not consistent with a purely diamagnetic ground state.

<sup>a</sup> Shores, M. P.; Sokol, J. J.; Long, J. R., *J. Am. Chem. Soc.* **2002**, *124*, 2279.

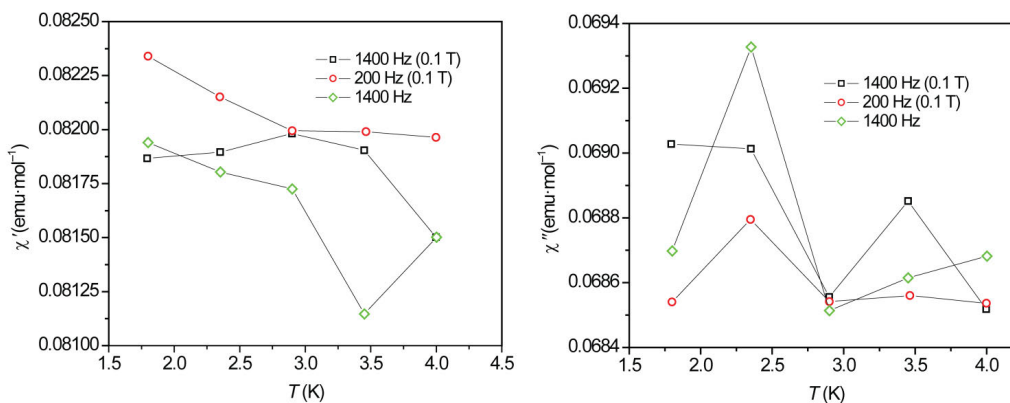


**Figure A2.29.** Temperature dependence of the in-phase ( $\chi'$ , left) and out-of-phase ( $\chi''$ , right) components of the AC susceptibility under 0 or 1000 Oe applied DC field collected at various AC frequencies for **3.3** encased in Eicosane.

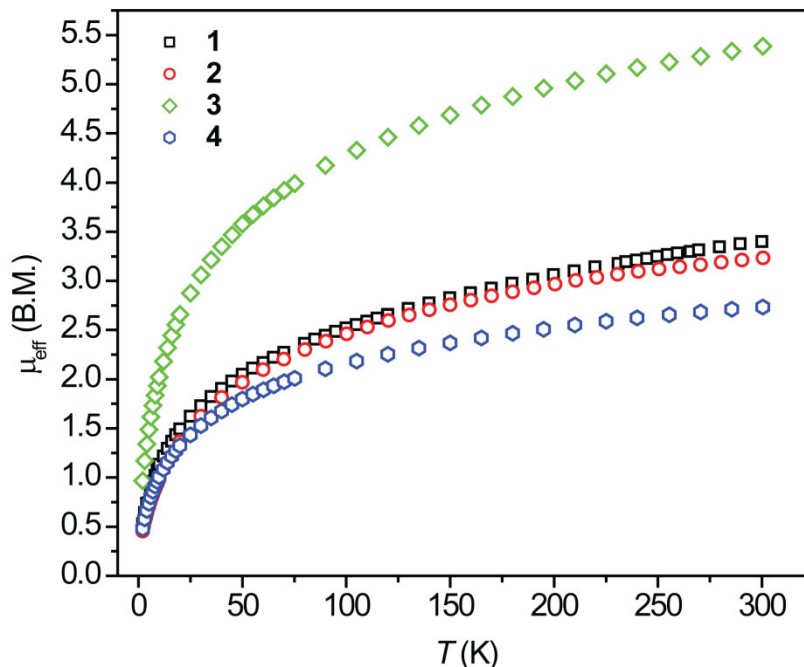


**Figure A2.30.** Temperature dependence of  $\mu_{\text{eff}}$  for compounds **3.1–3.4**; B.M. = Bohr magneton.

**Calculations for the determination of elemental analysis results on compound **3.3**·2CH<sub>2</sub>Cl<sub>2</sub>.** Initial values of U and C were chosen based on calculated values of 10 mg sample of **3.3**. Assuming all of the uranium reacted to form UC, the amount of carbon should be 11.54% (this is below the value of 12.83% obtained from EA). Next, the value found from EA was used to determine the amount of UC that may have been formed.

Using calculated values:

$$\frac{4.158 \text{ mg U}}{10 \text{ mg sample}} \times \frac{1 \text{ mmol U}}{238.03 \text{ mg U}} = 0.00175 \text{ mmol U}$$

$$\frac{1.364 \text{ mg C}}{10 \text{ mg sample}} \times \frac{1 \text{ mmol C}}{12.01 \text{ mg C}} = 0.01136 \text{ mmol C}$$

If all U reacts to form UC:

$$0.1136 \text{ mmol} - 0.00175 \text{ mmol} = 0.00961 \text{ mmol C left}$$

$$0.00961 \text{ mmol C} \times \frac{12.01 \text{ mg C}}{1 \text{ mmol C}} \times 100 = 11.54\%$$

Using values obtained from EA:

$$\frac{1.283 \text{ mg C}}{10 \text{ mg sample}} \times \frac{1 \text{ mmol C}}{12.01 \text{ mg C}} = 0.01068 \text{ mmol C}$$

$$0.1136 \text{ mmol} - 0.01068 \text{ mmol} = 6.8 \times 10^{-4} \text{ mmol C reacted to form UC:}$$

$$6.8 \times 10^{-4} \text{ mmol C} \times \frac{1 \text{ mmol UC}}{1 \text{ mmol C}} \times \frac{250.04 \text{ mg UC}}{1 \text{ mmol UC}} = 0.17 \text{ mg UC}$$

**Table A2.1.** Cross referenced collection of notebook and crystal structure data sets for relevant compounds. Notebook IDs originate from the notebooks belonging to Dr. Wesley Hoffert (WH) and Brian Newell (BSN).

Compound	Dissertation ID	Relevant Notebook IDs	Crystal ID
$[(\text{NN}'_3)\text{U}(\text{CCPh})_2(\text{Li}\cdot\text{Et}_2\text{O})]$	<b>2.1</b>	105-bsn 116-bsn 122-bsn 126-bsn 133-bsn	msn121 msn130
$[(\text{NN}'_3)_2\text{U}_2(p\text{-DEB})(\text{THF})]$	<b>2.2</b>	103-bsn 124-bsn 141-bsn 142-bsn 201-bsn	msn119
$[(\text{NN}'_3)\text{U}(\text{CCPh})]$	<b>2.3</b>	179-bsn 221-bsn	msn145
$[(\text{NN}'_3)_2\text{U}_2(m\text{-DEB})]$	<b>2.4</b>	227-bsn	msn159
$[(\text{NN}'_3)_2\text{U}_2(p\text{-DEB})]$	<b>2.5</b>	229-bsn 240-bsn	msn174
$[(\text{NN}'_3)_3\text{U}_3(\text{TEB})]$	<b>2.6</b>	230-bsn	msn170
$[(\text{dmpe})_2\text{UCl}_4]$	<b>3.1</b>	254-bsn 283-bsn 504-bsn 539-bsn	msn175
$[(\text{dmpe})_2\text{UMe}_4]$	<b>3.2</b>	542-bsn	msn236
$[(\text{dmpe})_4\text{U}_4\text{Cl}_{16}] \cdot 2\text{CH}_2\text{Cl}_2$	<b>3.3</b> ·2CH <sub>2</sub> Cl <sub>2</sub>	503-bsn	msn175r
$[(\text{dmpe})(\text{dmbpy})\text{UCl}_4]$	<b>3.4</b>	526-bsn 535-bsn 545-bsn	msn270
$[(\text{dmpe})_2\text{U}(\text{CCPh})_4]$	<b>4.1</b>	457-bsn 509-bsn 534-bsn 546-bsn	msn219
$[(\text{dmpe})_2\text{U}(\text{CCPh})_5(\text{Li}\cdot\text{Et}_2\text{O})]$	<b>4.2</b>	537-bsn 541-bsn 551-bsn	msn191r
$[(\text{dmpe})_2\text{FeCl}(\text{}^i\text{Pr}_3\text{SiDEB})]$	<b>6.1</b>	WH9-145	N/A
$[(\text{dmpe})_2\text{FeCl}(p\text{-DEBH})]$	<b>6.2</b>	WH9-145	N/A
$[(\text{NN}'_3)_2\text{U}(p\text{-DEB})\text{FeCl}(\text{dmpe})_2]$	<b>6.2</b>	441-bsn 446-bsn 449-bsn 506-bsn 519-bsn	msn220